

DOE/NASA/0330-3
NASA CR-182204
SwRI-8966

The Effect of Insulated Combustion Chamber Surfaces on Direct-Injected Diesel Engine Performance, Emissions, and Combustion

Daniel W. Dickey and Shannon Vinyard
Southwest Research Institute
San Antonio, Texas 78284

and

Rifat Keribar
Integral Technologies Incorporated
Westmont, Illinois 60559

September 1988

Prepared for
National Aeronautics and Space Administration
Lewis Research Center
Cleveland, Ohio 44135
Under Contract DEN3-330

for
U.S. DEPARTMENT OF ENERGY
Conservation and Renewable Energy
Office of Vehicle and Engine R&D
Washington, D.C. 20545
Under Interagency Agreement DE-AI01-86CE50162

TABLE OF CONTENTS

<u>Section</u>	<u>Page</u>
LIST OF ILLUSTRATIONS	iii
LIST OF TABLES	vii
SUMMARY	1
I. INTRODUCTION	3
II. EXPERIMENTAL SETUP	5
A. Engine Installation	5
B. SwRI LHR Engine Support Systems	8
1. Intake Air System	8
2. Fuel System	8
3. Lubricating Oil System	8
4. Cooling System	8
5. Instrumentation System	12
6. Exhaust System	12
C. Insulated Engine Components	12
III. TEST PROCEDURE	23
A. Baseline Engine Tests	23
B. Insulated Engine Tests	23
C. Test Fuel and Oil	25
IV. EXPERIMENTAL RESULTS	27
A. Performance and Emissions	27
B. Temperatures	36
C. Combustion Analysis	36
D. Combustion Analysis Results	40
E. Effects on Cylinder Pressure	50
F. Insulated Engine Durability	50
V. ANALYTICAL INVESTIGATION	61
A. Engine Simulation	61
B. Model Description	61
C. Baseline Engine Simulations	61
D. Insulated Engine Simulations	68
1. Engine Component Temperatures	68
2. Cyclic Variation of Relevant Parameters	83
E. Effect of Insulation and Heat Release on Engine Performance	83

TABLE OF CONTENTS, Cont'd.

<u>Section</u>	<u>Page</u>
VI. DISCUSSION OF RESULTS	91
A. Combustion	91
B. Peak Pressures	95
C. Thermal Efficiency	96
D. Emissions	97
VII. CONCLUSIONS	101
VIII. RECOMMENDATIONS FOR FURTHER RESEARCH	103
LIST OF REFERENCES	105
APPENDICES	
A. Engineering Drawing for Piston Modification	107
B. Fuel Specification and Distillation Curve	111
C. Experimental Performance and Emissions Data	115
D. Combustion Analysis Summary	129
E. High Speed Combustion Plots	135

LIST OF ILLUSTRATIONS

<u>Figure</u>	<u>Page</u>
1. Schematic of Engine and Dynamometer Installed in Test Cell	6
2. Photograph of Single Cylinder, Direct-Injected Diesel Test Engine	7
3. Intake Air System Schematic	9
4. Oil and Fuel System Schematics	10
5. Cooling System Schematic	11
6. Engine Instrumentation Schematic	13
7. Cylinder Liner Thermocouple Locations	14
8. Firedeck Thermocouple Locations	15
9. Exhaust System Schematic	16
10. Photograph of Steel Piston Crown Before Coating With Ceramic Material	18
11. Bolts and Support Plate Used To Attach Steel Piston Crown View From Piston Bottom	19
12. Comparison Between Stock Aluminum Piston (Left) and Modified Ceramic Coated Piston (Right)	20
13. Ceramic Coated Firedeck, Intake Valves, and Exhaust Valves	21
14. Data Points Used For Engine Performance Tests	24
15. Performance and Emissions Results, 2000 rpm	28
16. Performance and Emissions Results, 1700 rpm	29
17. Performance and Emissions Results, 1400 rpm	30
18. Gaseous Emissions Results, 2000 rpm	31
19. Gaseous Emissions Results, 1700 rpm	32
20. Gaseous Emissions Results, 1400 rpm	33
21. Particulate and ISFC Versus ISNO _x Emissions, 2000 rpm, Full Load	34
22. Particulate, ISNO _x , ITE Versus Fire Deck Temperature, 2000 rpm, Full Load	35
23. Firedeck, Top Ring Reversal, and Exhaust Gas Temperatures Versus Indicated Power, 2000 rpm	37

LIST OF ILLUSTRATIONS, Cont'd.

<u>Figure</u>	<u>Page</u>
24. Firedeck, Top Ring Reversal, and Exhaust Gas Temperatures Versus Indicated Power, 1700 rpm	38
25. Firedeck, Top Ring Reversal, and Exhaust Gas Temperatures Versus Indicated Power, 1400 rpm	39
26. Heat Release Rate Versus Crankangle Plot Showing Definition of Combustion Parameters	41
27. Heat Release Rate Versus Crankangle For Baseline Metal and Baseline Ceramic Test Conditions, 2000 rpm, Full Load	42
28. Heat Release Rate Versus Crankangle For Baseline Ceramic and Hot Ceramic Test Conditions, 2000 rpm, Full Load	43
29. Fuel-Injection Pressure Versus Crankangle For Baseline Metal and Baseline Ceramic Test Conditions, 2000 rpm, Full Load	45
30. Fuel-Injection Pressure Versus Crankangle For Baseline Ceramic and Hot Ceramic Test Conditions, 2000 rpm, Full Load	46
31. Fuel-Injection Duration, Ignition Delay, Combustion Duration Versus Indicated Power, 2000 rpm	47
32. Combustion Duration, Peak Cylinder Pressure, Peak Rate of Pressure Rise Versus Indicated Power, 2000 rpm	48
33. Combustion Duration, Premix/Total Combustion, ITE Versus Indicated Power, 2000 rpm	49
34. Comparison Between Baseline Metal, Baseline Ceramic, Hot Ceramic Engine Firing Cylinder Pressure, 2000 rpm, Full Load	51
35. Comparison Between Baseline Metal, Baseline Ceramic, Hot Ceramic Engine Motoring Cylinder Pressure, 2000 rpm, Full Load	52
36. Photograph Showing Ceramic-Coated Firedeck, Intake Valves, and Exhaust Valves After 95 Hours of LHR Engine Tests	53
37. Photograph Showing Ceramic-Coated Piston Crown (Side View) After 95 Hours of LHR Engine Tests	54
38. Photograph Showing Ceramic-Coated Piston Crown (Top View) After 95 Hours of LHR Engine Tests	55
39. Photograph Showing Top Portion of Cylinder Liner Coated with Ceramic Material After 95 Hours of LHR Engine Tests	56
40. Photograph Showing Melted Fuel Injector Holder O-Ring Gasket After 95 Hours of LHR Operation	58
41. Comparison Between Measured and Predicted Air Flow Rate	62

LIST OF ILLUSTRATIONS, Cont'd.

<u>Figure</u>	<u>Page</u>
42. Comparison Between Measured and Predicted Indicated Mean Effective Pressure	63
43. Comparison Between Measured and Predicted Peak Cylinder Pressure	64
44. Comparison Between Measured and Predicted Cylinder Liner Temperature	65
45. Comparison Between Measured and Predicted Firedeck Center Temperature	66
46. Comparison Between Measured and Predicted Exhaust Gas Temperature	67
47. Comparison Between Measured and Predicted Liner Top Ring Reversal Temperature, Baseline Metal Engine	69
48. Comparison Between Measured and Predicted Firedeck Center Temperature, Baseline Metal Engine	70
49. Predicted Piston Bowl Average Temperature, Baseline Metal Engine	71
50. Predicted Average Surface Temperature for Ceramic-Coated Liner Top Ring Reversal Location, Baseline Ceramic Engine	72
51. Predicted Average Surface Temperature for Ceramic-Coated Firedeck, Baseline Ceramic Engine	73
52. Predicted Average Surface Temperature for Ceramic-Coated Exhaust Valve, Baseline Ceramic Engine	74
53. Predicted Average Surface Temperature for Ceramic-Coated Intake Valve, Baseline Ceramic Engine	75
54. Predicted Average Surface Temperature for Ceramic-Coated Liner Top Ring Reversal Location, Hot Ceramic Engine	76
55. Predicted Average Surface Temperature for Ceramic-Coated Fire Deck, Hot Ceramic Engine	77
56. Predicted Average Surface Temperature for Ceramic-Coated Piston Bowl, Hot Ceramic Engine	78
57. Comparison Between Measured and Predicted Ceramic-Coated Liner Top Ring Reversal Temperature, Hot Ceramic Engine	79
58. Comparison Between Measured and Predicted Ceramic-Coated Firedeck Temperature, Hot Ceramic Engine	80
59. Predicted Average Surface Temperature for Ceramic-Coated Exhaust Valve, Hot Ceramic Engine	81

LIST OF ILLUSTRATIONS, Cont'd.

<u>Figure</u>	<u>Page</u>
60. Predicted Average Surface Temperature for Ceramic-Coated Intake Valve, Hot Ceramic Engine	82
61. Comparison Between Predicted Cyclic Variation of Intake Air Mass Flow for Baseline Metal and Hot Ceramic Engines, 2000 rpm, Full Load	84
62. Comparison Between Predicted Cyclic Variation of Cylinder Pressure for Baseline Metal and Hot Ceramic Engines, 2000 rpm, Full Load	85
63. Comparison Between Predicted Cyclic Variation of Heat Transfer Rate for Baseline Metal and Hot Ceramic Engines, 2000 rpm, Full Load	86
64. Predicted Cyclic Temperature Variation of Piston Surfaces for Baseline Metal Engine, 2000 rpm, Full Load	87
65. Predicted Cyclic Temperature Variation of Piston Surfaces for Hot Ceramic Engine, 2000 rpm, Full Load	88
66. Heat Release Rate Versus Crankangle for Baseline Metal and Hot Ceramic Test Conditions, 2000 rpm, Full-Load	93
67. Fuel-Injection Pressure Versus Crankangle for Baseline Metal and Hot Ceramic Test Conditions, 2000 rpm, Full-Load	94

LIST OF TABLES

<u>Table</u>		<u>Page</u>
1	Caterpillar 1Y-540 Single-Cylinder Engine Specifications	5
2	Engine Test Conditions	26
3	Combustion Analysis Parameters	40
4	Combustion Analysis 2000 rpm, Full Load	50
5	Engine Oil Analysis	59
6	SwRI Measurements and IRIS Simulation Results for Baseline Metal Engine and Hot Ceramic Engine With and Without the Adverse Effects on Combustion (2000 rpm, Full Load)	90
7	Organic Soluble Extraction, 2000 rpm, Full Load	98

SUMMARY

The combustion chamber of a single-cylinder, direct injected, diesel engine was insulated to determine the effect of low heat rejection (LHR) operation on engine performance, emissions, and combustion.

The insulated engine was assembled using a ceramic-coated fire deck, intake valves, exhaust valves, piston crown, and top portion of the cylinder liner. The stock aluminum piston was modified so a steel piston crown could be bolted to the piston for coating with ceramic material. The fire deck, intake valves, exhaust valves, and piston crown were coated with a 0.762 mm (0.030 inch) thick coating of yttria stabilized zirconia (7% Y_2O_3 , 93% ZrO_2). The top 21.6 mm (0.85-inch) of the cylinder liner (above top ring reversal location) was coated with 0.635 mm (0.025 inch) of the yttria stabilized zirconia and then 0.254 mm (0.010 inch) of chrome oxide coating to resist piston-liner scuffing.

The engine was installed in a test cell and connected to an eddy-current motoring dynamometer. Two Roots blowers mounted in series were connected to the intake air system to maintain baseline air flow rates during LHR engine tests. The engine coolant system was modified to incorporate separate cylinder head and cylinder block cooling circuits. Thermocouples were mounted in the tip of the fuel injector holder and just below the cylinder liner surface to measure fire deck and cylinder liner surface temperatures, respectively. Gaseous emissions measurements were made using a 13-Mode emissions cart. Gaseous emissions included unburned hydrocarbons (HC), carbon monoxide (CO), and nitrogen oxides (NO_x). The particulate emissions were measured using an exhaust gas dilution tunnel.

Engine tests were conducted at speeds of 1400, 1700, and 2000 rpm for loads of 33%, 66%, and 100% of full power. The all-metal engine was first baseline tested with 82°C and 104°C coolant temperatures at the standard injection timing of 24.0 degrees before top dead center. The engine was then insulated and tested at baseline conditions. High temperature LHR engine tests were then conducted with the insulated engine by replacing the cylinder head coolant with a regulated supply of compressed air. The cylinder liner remained cooled with ethylene glycol at 121°C. LHR engine tests were performed at standard, retarded, and advanced fuel injection timings. The LHR engine tests were conducted by repeating the baseline data points using the same fuel flow and adjusting the boost pressure to maintain the baseline air-fuel ratios. The full-load air-fuel ratio was 25:1. The exhaust gas back pressure was adjusted to maintain a constant pressure ratio across the cylinder head of 1.0. The intake air temperature was held constant at 82°C for all engine tests.

Analytical work was subcontracted to Integral Technologies Incorporated (ITI). ITI modeled the engine to predict engine component surface temperatures and assist in analyzing the experimental performance data.

The experimental results showed that the addition of ceramic insulation and subsequent reduction of heat transfer to the coolant did not improve engine performance relative to the Baseline Metal engine. At 2000 rpm full load, the indicated thermal efficiency was reduced by 3.4 percentage points for (7.4 percent) the LHR engine compared to the Baseline Metal engine. In general, the LHR engine had higher full load smoke and particulate emissions, lower full load NO_x emissions, higher full load CO emissions, and lower unburned hydrocarbon emissions across the load range compared to the Baseline Metal engine. The LHR engine's reduced thermal efficiency and change in exhaust emissions was attributed to degraded combustion. The LHR engine combustion had less premixed burning, lower peak heat release rates, and longer combustion duration compared to the Baseline Metal engine. The degraded LHR engine combustion was thought to be the result of poor fuel-air mixing.

ITI simulated the insulated engine assuming baseline combustion and predicted an increase in indicated thermal efficiency of 0.9 percentage points (2.0 percent) with a 30 percent reduction in heat transfer to the coolant.

I. INTRODUCTION

Insulating the combustion chamber of an internal combustion engine theoretically results in improved thermal efficiency according to the Second Law of Thermodynamics. The Second Law of Thermodynamics stipulates that all heat engines operating on continuous cycles require a heat rejection process as part of the cycle. In typical internal combustion engines, the heat rejection process involves an energy loss that is larger than theoretically required by the reservoir temperatures. The quantity of heat rejected from the working fluid is larger than required due to the engine's limited expansion stroke and thermal limitations of current materials and lubricants. Insulating an engine's combustion chamber represents an effort to recover more of the heat energy in the working fluid rather than rejecting such a large portion (approximately 30 percent of the fuel energy) to the coolant system.

The terms adiabatic, insulated, ceramic, uncooled, and low heat rejection have all been applied to engines designed to minimize the heat rejected to the coolant. The term adiabatic however is incorrectly used to describe these engines because by definition adiabatic means that no heat is transferred to or from the working fluid. A true adiabatic engine is impossible to achieve because it requires perfect insulation and an engine material with infinitely small heat capacity to keep the combustion chamber surfaces the same temperature as the working fluid during the cycle. An adiabatic engine is theoretically impossible because heat must be transferred to and from the working fluid to complete the thermodynamic cycle. The so called "adiabatic" engines therefore are engines designed to reduce heat transfer to the coolant not to and from the working fluid. The increased energy of the working fluid in these engines does not result in significant thermal efficiency gains because of the piston engine's limited expansion stroke. Thermal efficiency gains can perhaps be achieved by expanding the hotter exhaust gases through a bottoming cycle device such as compounded turbine.

The U. S. Army initiated the development of the low heat rejection engine. The Army's objective was to eliminate the engine's conventional cooling system to reduce engine maintenance and reduce combat vehicle vulnerability. The Army was willing to sacrifice other engine qualities such as engine life to obtain this objective.

Cummins Engine Company (ref. 1-6) has been working on low heat rejection engines since 1975. Cummins was selected by the U. S. Army to design and demonstrate a low heat rejection engine. Cummins made extensive use of ceramic materials to insulate the engine's combustion chamber. Ceramics were chosen as an insulating material because certain ceramic materials have low thermal conductivity. Unfortunately, the low thermal conductivity ceramic materials are also very brittle. Because of the extensive use of ceramics in the Army/Cummins program, the terms ceramic and adiabatic became synonymous when describing low heat rejection engines.

The results of the Army/Cummins program showed that there are two major problems with low heat rejection engines. The first problem was maintaining an oil film on the cylinder liner for suitable lubrication at high temperature. Both Cummins and SwRI (ref. 7) have shown that 320°C top ring reversal temperature is about the upper limit for current liquid lubricants. SwRI showed that lower volatility lubricating oils produce troublesome oil deposits while more volatile lubricants cause excessive oil consumption. The second problem was poor durability of the ceramic insulation material. Quality control of ceramics is a major problem. Ceramics have a high probability of failure that increases with increasing part size. Ceramic component failures in low heat rejection engines are common and often lead to catastrophic engine failures. Ceramic failures are attributed to the brittleness of most insulating ceramic materials due to the small flaw size that can initiate brittle fracture. The two most common forms of ceramics in LHR engines include monolithic ceramic components and ceramic coatings which are applied to existing engine components. In recent years, partially-stabilized zirconia has become a popular ceramic material for use in LHR engines because it provides good insulation and has a thermal expansion coefficient and elastic modulus similar to iron and steel. LHR engines can also be designed using conventional metal materials and air gaps to provide insulation. However, even if engine durability is improved using conventional metal materials, the lubrication problem in LHR engines still exists.

The development of LHR engine technology has occurred in such a way that the combustion and emissions aspects of these engines have not been adequately investigated. The reasons for the deficiency in emissions and combustion data stems from the fact that much of the LHR engine development effort has, by necessity, been devoted to the development of ceramic materials and coating technologies (ref. 8-18).

To date, there have been conflicting results published concerning the effect of LHR engine operation on engine performance, emissions, and combustion. Both efficiency gains (ref. 6, 19, 20, 21, 22) and losses (ref. 4, 23, 24) have been reported. In practice it is difficult to realize improvements in thermal efficiency due to the complex nature of diesel combustion systems and the thermal limitations of current materials and lubrication. Conflicting data has also been published concerning the effects of LHR engine operation on engine emissions and combustion (ref. 4, 6, 23, 25, 26) The conflicting results are probably due to the infinite number of possible LHR engine configurations, test conditions, and analysis techniques used.

The objective of this investigation is not to end the debate on how LHR engine operation affects engine performance, emissions, and combustion, but simply to add the test results for a specific direct-injected diesel engine to the LHR engine database.

This report covers the results of LHR engine experiments conducted at Southwest Research Institute (SwRI). SwRI insulated and tested a single-cylinder, direct-injected diesel engine that was representative of a heavy duty truck engine. The SwRI LHR engine was assembled using a ceramic coated fire deck, intake valves, exhaust valves, piston crown, and top portion of the cylinder liner. The engine coolant system was modified to incorporate separate cylinder head and cylinder block cooling circuits. LHR engine tests were conducted by replacing the cylinder head coolant with a regulated supply of compressed air. The cylinder liner remained cooled with ethylene glycol at 121°C. An intake air blower was used to maintain baseline airflow rates during LHR engine tests. Baseline tests were first conducted with the cooled engine. LHR engine tests were then performed to determine the effect of LHR engine operation on engine performance, emissions, and combustion.

II. EXPERIMENTAL SETUP

In this section, the SwRI Low Heat Rejection (LHR) Engine Test Facility and its supporting systems will be described. The supporting systems include the intake air system, cooling system, oil system, fuel system, and exhaust system with all relevant instrumentation.

A. Engine Installation

A Caterpillar 1Y-540 single-cylinder engine was selected as the test engine. The Caterpillar engine was selected because it was considered to be representative of an on highway, heavy-duty, truck engine. The Caterpillar 1Y-540 engine is essentially one cylinder of a Caterpillar 3406 truck engine. The test engine was installed in Test Cell No. 3 located in SwRI's Engine and Vehicle Research Division. The engine specifications are given in Table 1.

Table 1. Caterpillar 1Y-540 Single-Cylinder Engine Specifications

Bore Diameter	137 mm
Stroke	165 mm
Displacement Volume	2.4 liter
No. of Intake Valves	2
No. of Exhaust Valves	2
Diameter of Intake Valve	45.0 mm
Diameter of Exhaust Valve	41.9 mm
Fuel Injection System	Jerk Pump, 6 hole nozzle .27 mm Diameter crack pressure = 15,170 Kpa
Length of Connecting Rod	262 mm
Piston Pin Diameter	50.8 mm
Rod Journal Diameter	97 mm
Main Bearing Diameter	108.2 mm

The engine and dynamometer were mounted in the test cell as shown in Figure 1. Figure 2 is a photograph of the engine installed in the test cell. The engine was rigidly mounted on a 4,800 kg concrete inertia block. The concrete block was mounted on tunable spring pads to isolate vibration. The spring pads were bolted to the test cell floor. The concrete block weight and stiffness of the spring pads were selected so that the resonant vibration frequency of the inertia block and engine was located outside the engine operating speed range. A driveshaft and two flexible couplings were used to connect the engine to an eddy current motoring dynamometer. The two flexible couplings consisted of a universal joint that connected the driveshaft to the dynamometer and a thermoid disk used to connect the other end of the driveshaft to the engine. The dynamometer was mounted on a dynamometer base so that the engine crankshaft and dynamometer driveshaft could be properly aligned.

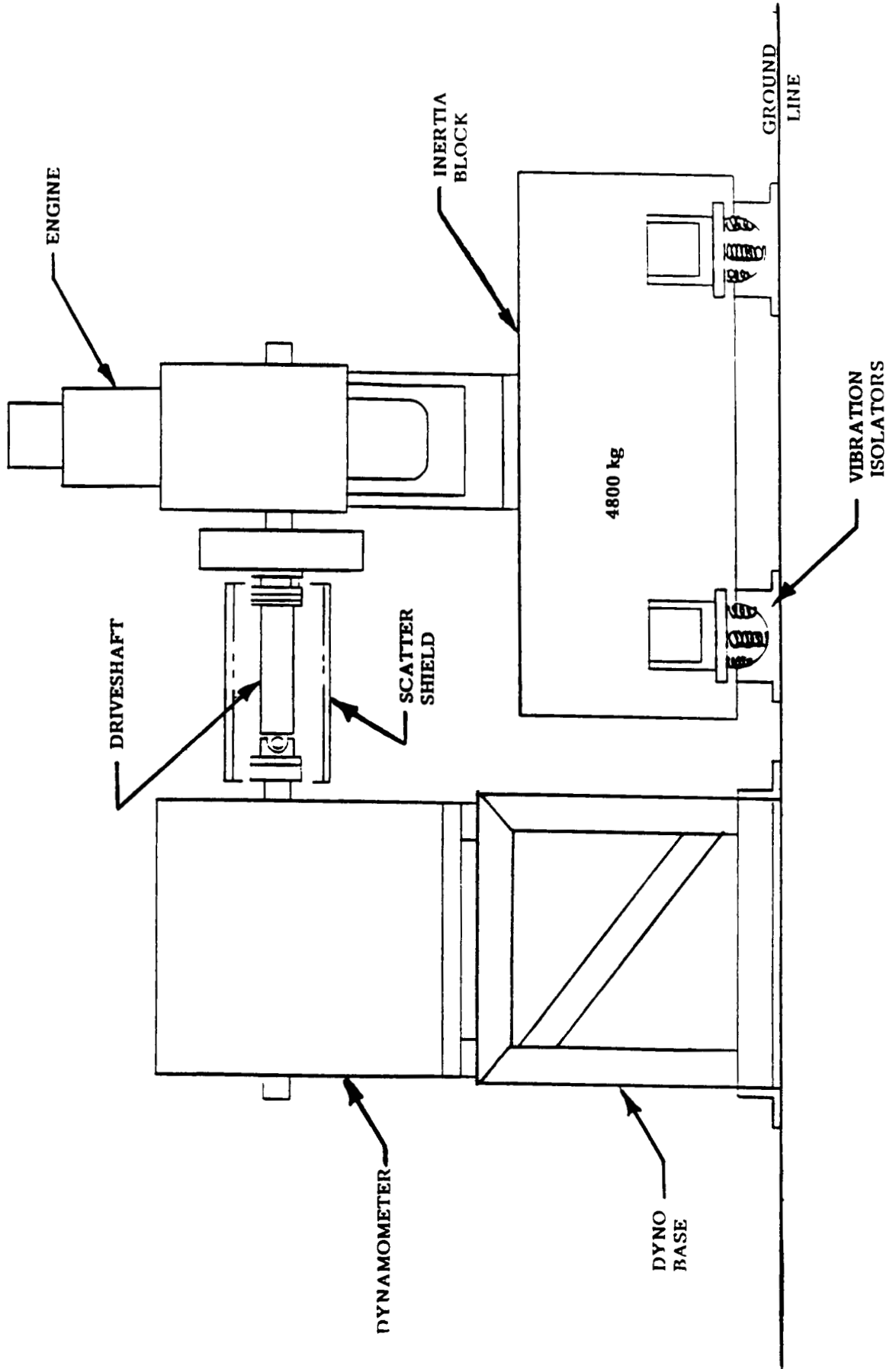


FIGURE 1. ENGINE AND DYNAMOMETER INSTALLED IN TEST CELL

ORIGINAL PAGE IS
OF POOR QUALITY

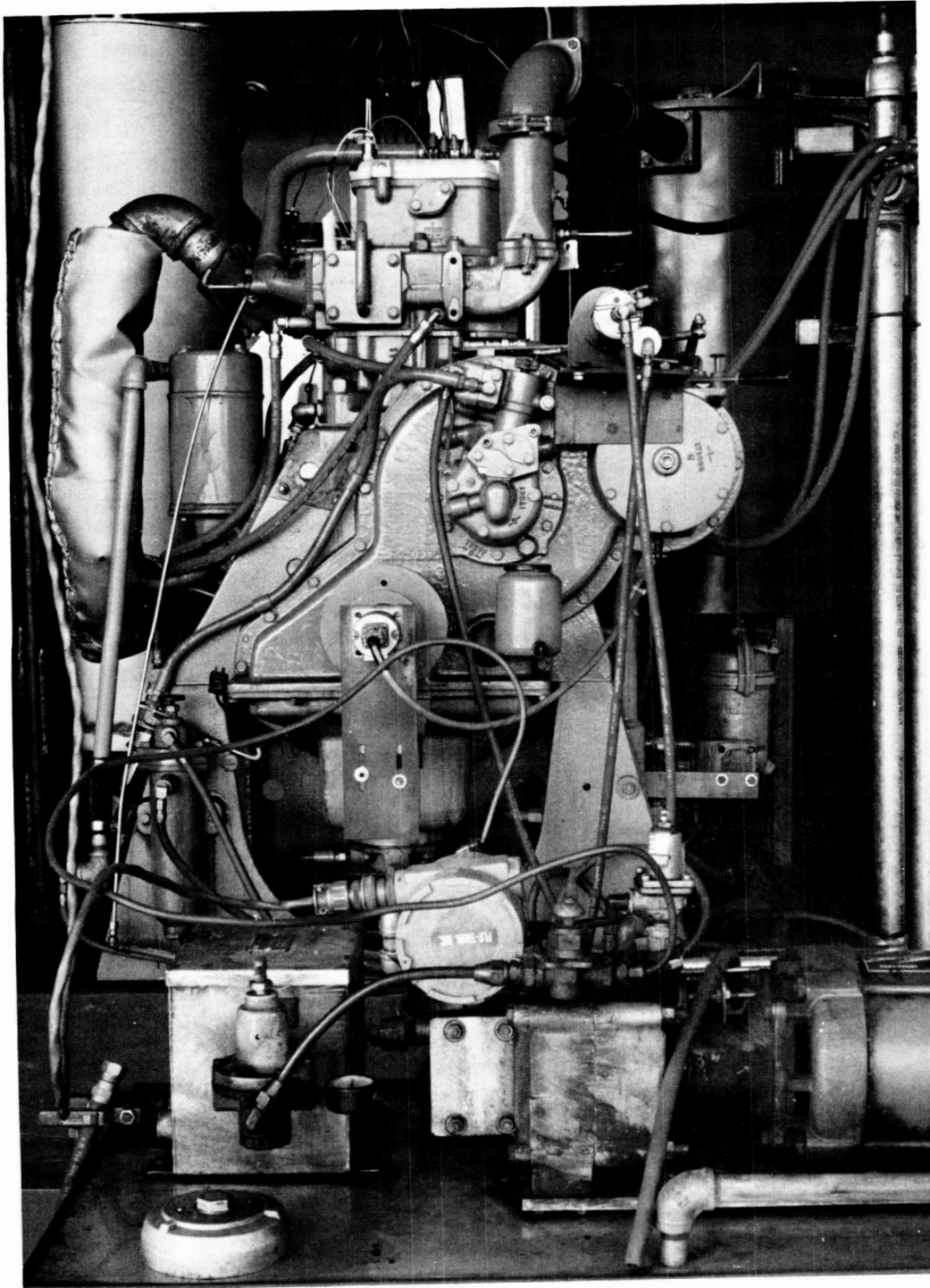


FIGURE 2. PHOTOGRAPH OF SINGLE CYLINDER,
DIRECT-INJECTED DIESEL TEST ENGINE

B. SwRI LHR Engine Support Systems

A detailed description of the six engine support systems is as follows.

1. Intake Air System

The schematic for the engine intake air system is shown in Figure 3. Air entered the intake system through a paper element air filter. A 400 CFM laminar flow element (LFE), was used to measure air flow. The pressure drop across the LFE and the LFE static pressure were measured using inclined manometers and electric pressure transducers. Air then entered a series of two roots blowers. The two roots blowers were used to simulate turbocharged engine conditions and also to maintain baseline air flow rates during LHR engine tests. An exhaust back pressure valve was used to maintain a constant pressure ratio of 1.0 across the cylinder head during boosted conditions. Each blower had a capacity of 200 kPa at a flow rate of 7.0 m³/min. A heat exchanger was used between the blowers to reduce the inlet air temperature to the second blower. A heat exchanger was also used after the second blower to further reduce the inlet air temperature if required. A pneumatic control valve regulated the boost pressure. The valve served as a bypass valve and allowed excess air to return to the inlet of the first blower. Pressurized air then entered the intake air surge tank. Twelve 15-kW electric heating elements were installed inside the surge tank to preheat the intake air before it reached the engine. A temperature controller regulated the intake air temperature. Thermocouples were used to measure the air temperature before the laminar flow element, after each heat exchanger, and in the intake air manifold. The intake air boost pressure was measured using an electric pressure transducer and gages mounted in the engine control console. The output signals from the electric pressure transducers and thermocouples were recorded by the data acquisition computer.

2. Fuel System

The fuel system is shown in Figure 4. Fuel was pumped from the fuel supply tank to a mass fuel flow meter. The fuel then entered a pressure regulator which reduced the fuel pressure to 40 kPa before it entered the day tank. The fuel passed through the fuel filter and into the injection pump. Excess fuel that did not pass to the fuel injector returned to the day tank as shown in Figure 4. An air cylinder was used to control the fuel injection pump rack position. An air control valve regulated the pressure to the air cylinder. A fuel injector from a Caterpillar 3406 truck engine with six 0.27 mm diameter holes was used to inject the fuel.

3. Lubricating Oil System

The lubricating oil system is also shown in Figure 4. The engine oil pump circulated oil from the oil sump through an oil filter and into a heat exchanger. The heat exchanger was used to cool the lubricating oil. The oil then passed through another oil filter and back to the engine. Oil filters were installed before and after the heat exchanger to eliminate the possibility of contaminating the heat exchanger with foreign particles in the event of an engine failure. Oil pressure and temperature were recorded with the computer data acquisition system.

4. Cooling System

The test engine cooling system was modified to incorporate separate cylinder head and cylinder block cooling circuits as shown in Figure 5. The cylinder head cooling circuit was connected to a compressed air supply during LHR engine tests. Air was flowed through the cylinder head cooling circuit to achieve higher cylinder head temperatures during LHR operation. Two centrifugal water pumps circulated the coolant through each cooling circuit. Shell-and-tube heat exchangers provided heat rejection for each coolant circuit. Pneumatic control valves regulated the flow of cooling water through each heat exchanger to independently control the temperature of the head and block cooling circuits.

INTAKE SYSTEM

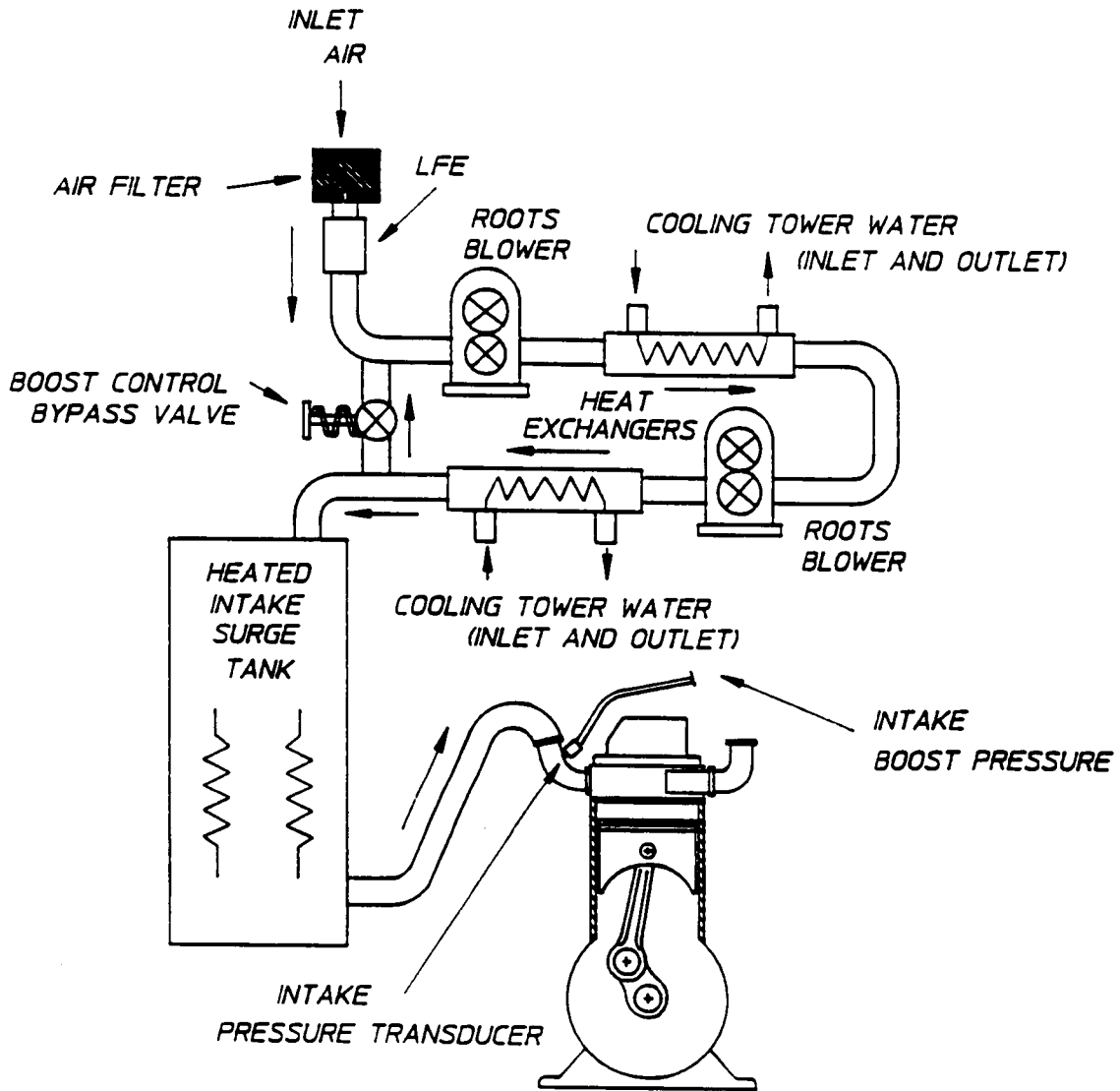


FIGURE 3. INTAKE AIR SYSTEM SCHEMATIC

OIL AND FUEL SYSTEMS

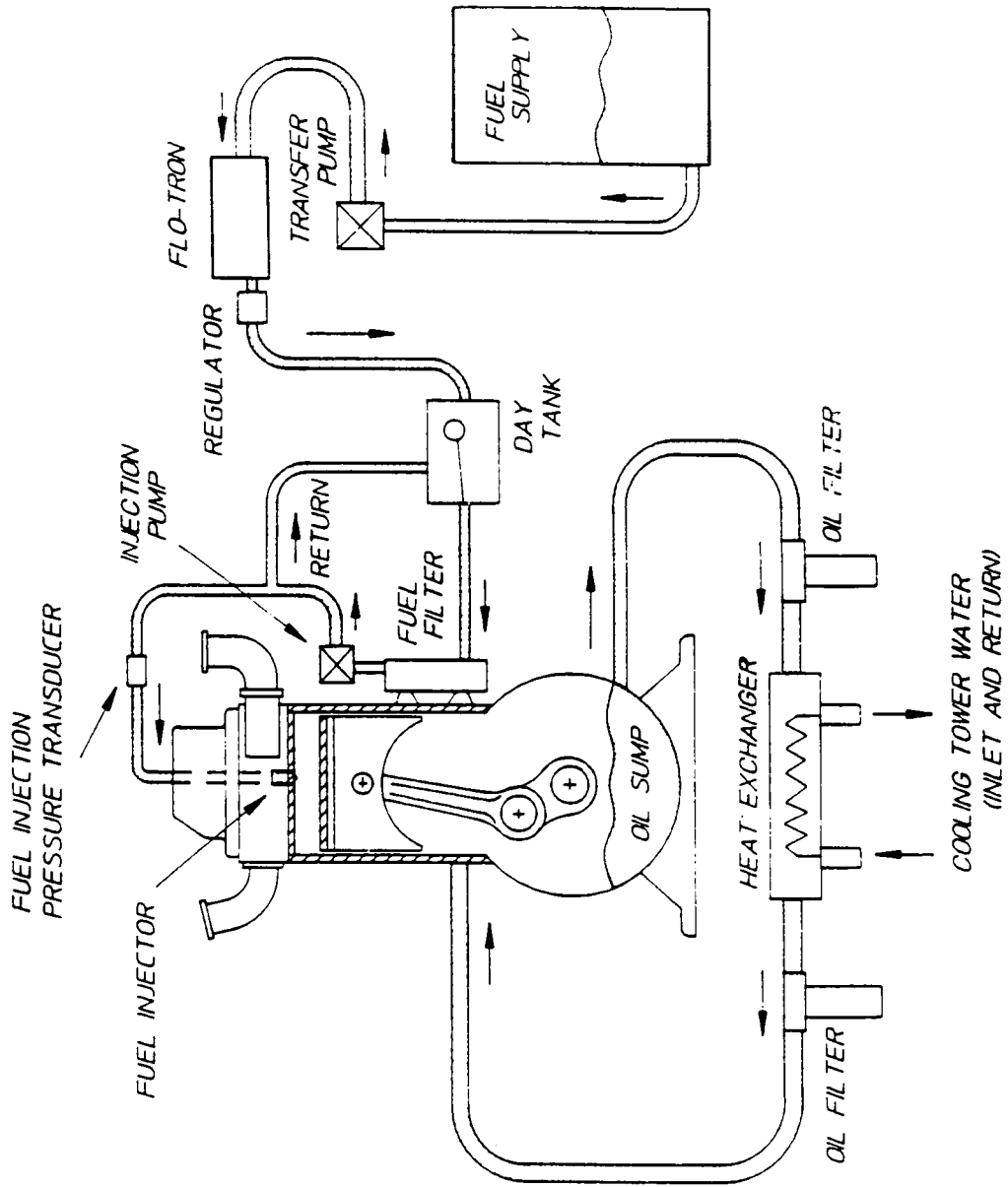
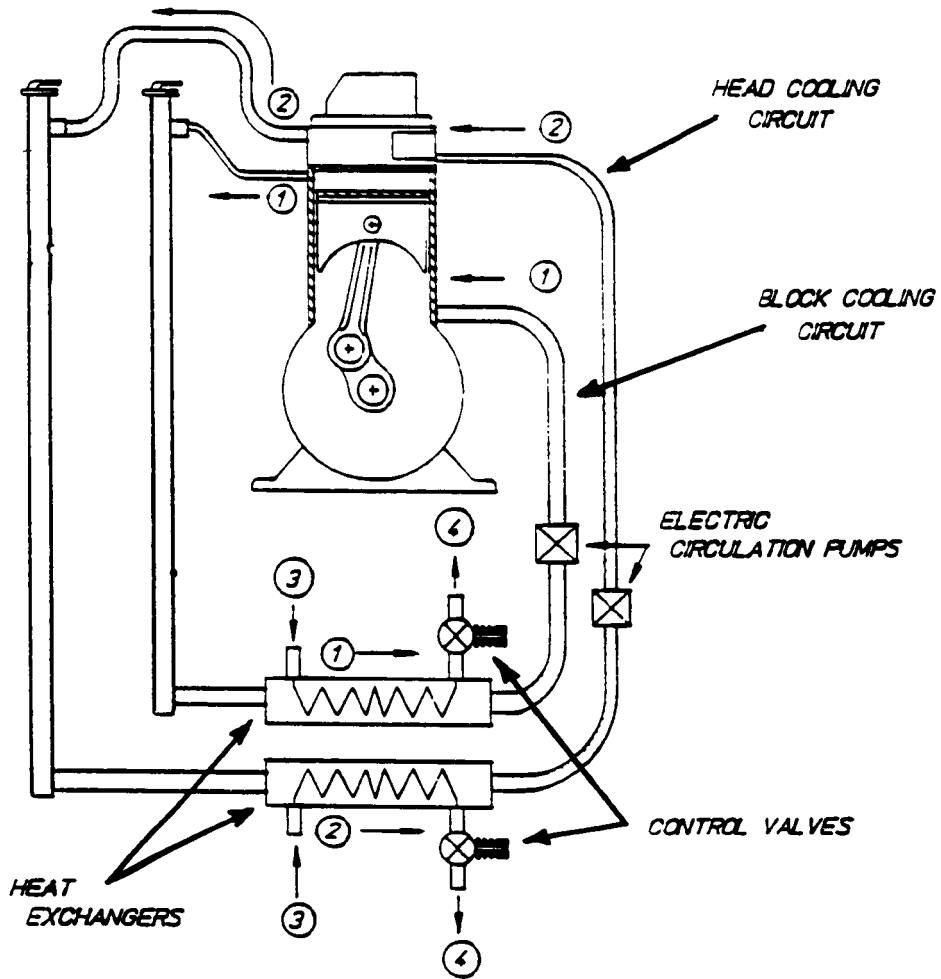


FIGURE 4. OIL AND FUEL SYSTEM SCHEMATICS

COOLING SYSTEM



- 1 — BLOCK COOLANT FLOW PATH
- 2 — HEAD COOLANT FLOW PATH
- 3 — COOLING TOWER WATER INLET
- 4 — COOLING TOWER WATER RETURN

FIGURE 5. COOLING SYSTEM SCHEMATIC

5. Instrumentation System

A schematic of the engine instrumentation is shown in Figure 6. Piezoelectric pressure transducers were used to monitor cylinder and fuel injection pressures. A shaft encoder was connected to the engine crankshaft to detect crank angle position. The shaft encoder used a light source and photo diodes to produce two signals. One signal was a Z pulse which occurred every revolution and was aligned with engine top dead center. The other signal generated 720 pulses per revolution, which provided a time base for the high-speed data acquisition system. High-speed data which included cylinder pressure and fuel injection pressure were recorded for each pulse or every one-half degree crank angle. The fuel injector needle lift position was not recorded because a reliable needle lift probe could not be found that would work with the engine's unique fuel injector.

The cylinder liner temperature was measured at six locations as shown in Figure 7. K-type thermocouples using 0.127 mm diameter wires were mounted at the top ring reversal location, at the bottom ring reversal location, and at the middle of the cylinder liner on the thrust side. These thermocouples were mounted 0.381 mm away from the inside of the liner. Identical thermocouples were also mounted on the outside of the liner surface in these three locations so the temperature gradient through the cylinder liner could be determined. Two K-type thermocouples were also installed in the tip of the fuel injector holder to measure the fire deck temperature as shown in Figure 8.

The oil pressure and fuel supply pressure were measured using gauges mounted in the control panel. Both of these pressures were also recorded using electric pressure transducers connected to the computer. All gaseous emissions and exhaust opacity measurements were recorded using the data acquisition computer.

6. Exhaust System

The exhaust system for the engine is shown in Figure 9. The exhaust gases exited from the exhaust manifold and entered a steel surge tank through 7.6 cm diameter exhaust tubing. A pneumatic control valve was used after the surge tank to regulate exhaust gas back pressure. The exhaust back pressure valve was required to maintain a constant pressure ratio of 1.0 across the cylinder head during boosted conditions. Just after the back pressure valve, a line was inserted into the exhaust system for sampling the gaseous exhaust emissions. Gaseous emissions measurements were made using a 13-mode emissions cart. Gaseous emissions included HC, CO, and NO_x . The exhaust gases then passed through an in-line smoke meter which measured exhaust gas opacity. Two control valves were located after the smoke meter. One valve allowed the exhaust gases to pass out to the environment; the other valve directed the exhaust gases to pass into an exhaust gas dilution tunnel for particulate measurements.

C. Insulated Engine Components

The insulated engine was assembled using a ceramic coated fire deck, intake valves, exhaust valves, piston crown, and top portion of the cylinder liner. A 0.127 mm super alloy bond coating (NiCrAlY) was first applied to these engine components. The fire deck, intake valves, exhaust valves, and piston crown were then coated with a 0.762 mm thick coating of yttria stabilized zirconia (which is 7 percent Y_2O_3 and 93 percent ZrO_2). The top 21.6 mm of the cylinder liner was coated with 0.635 mm of the yttria stabilized zirconia and then 0.254 mm of chrome oxide coating to resist piston liner scuffing. Only the top 21.6 mm of the cylinder liner was coated with ceramic material to improve engine durability by preventing the piston ring from traveling on the ceramic coating. The 21.6 mm distance from the top of the liner corresponds to approximately 35 degrees crank angle after top dead center which should insure that the combustion gases are surrounded by ceramic coated surfaces during most of the combustion period. The entire engine liner was not coated because SwRI decided to cool the cylinder liner during LHR engine tests.

The stock aluminum piston could not be coated with ceramic material due to the difference in thermal expansion between aluminum and zirconia. Initially SwRI investigated using a ductile iron piston because ductile iron has the same coefficient of thermal expansion as zirconia. Upon further investigation, however, it was found that the quotes to procure a ductile iron piston were excessive.

ENGINE INSTRUMENTATION

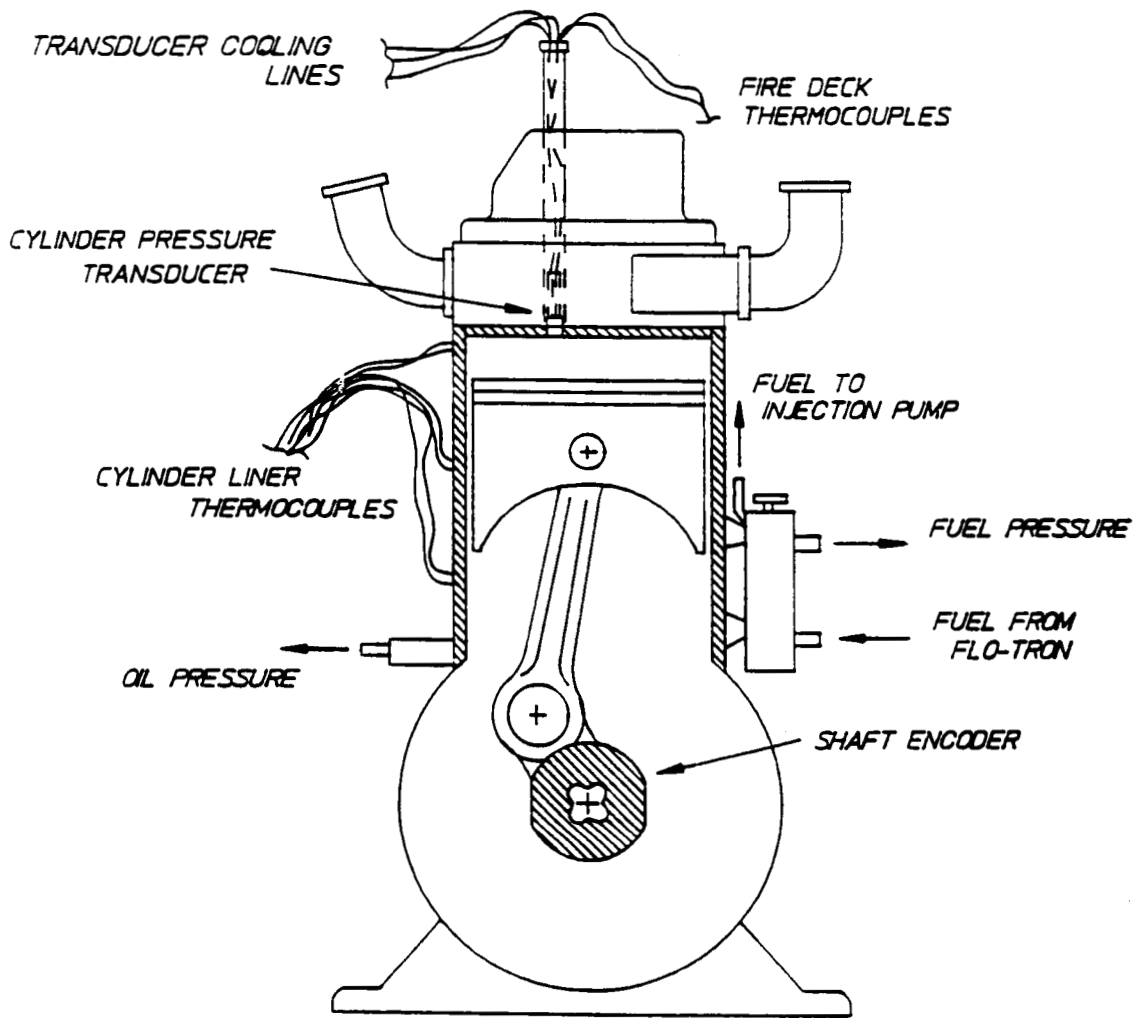


FIGURE 6. ENGINE INSTRUMENTATION SCHEMATIC

CYLINDER LINER THERMOCOUPLE LOCATIONS

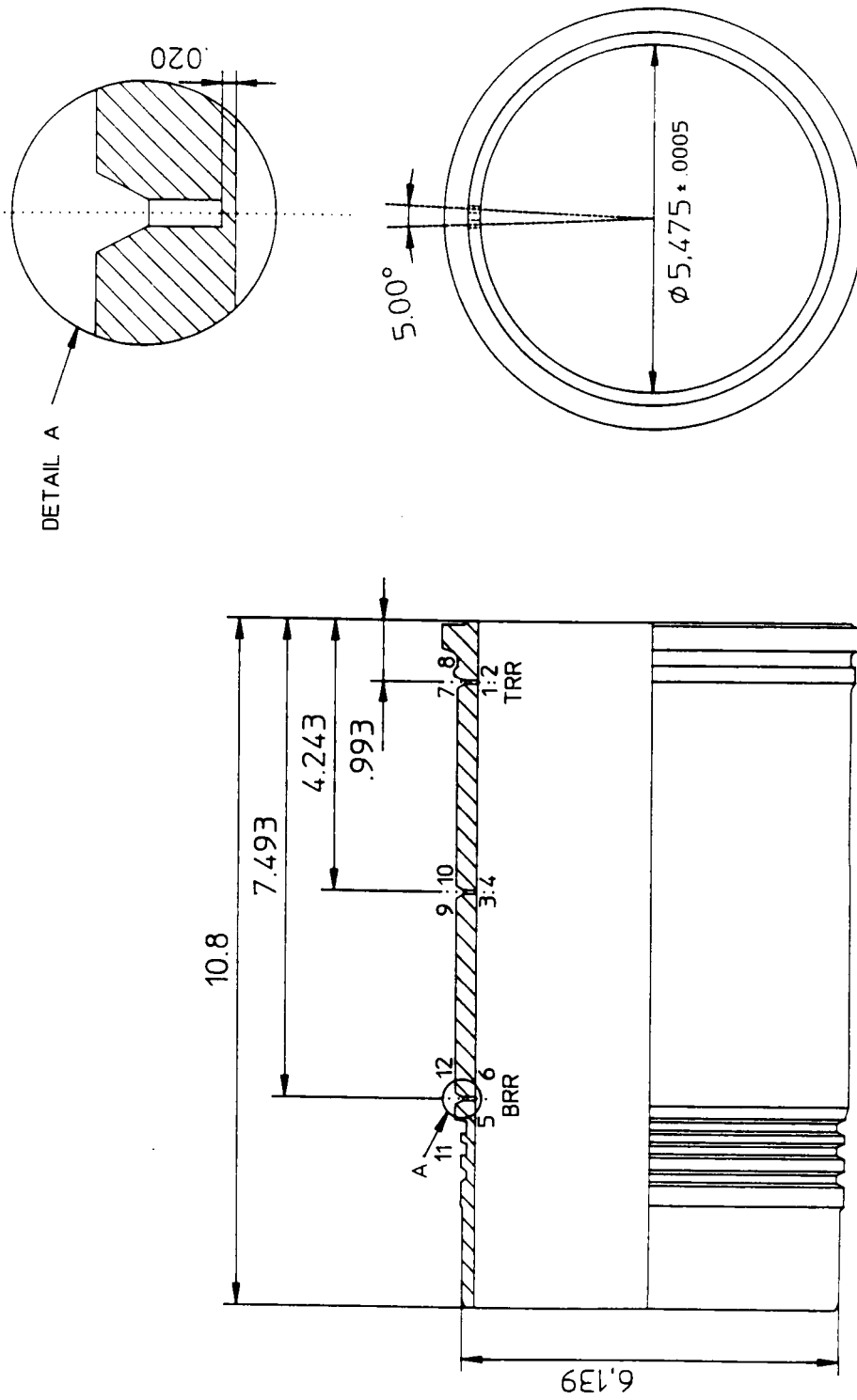


FIGURE 7. CYLINDER LINER THERMOCOUPLE LOCATIONS

FUEL INJECTOR HOLDER SHOWING FIRE DECK THERMOCOUPLE LOCATIONS

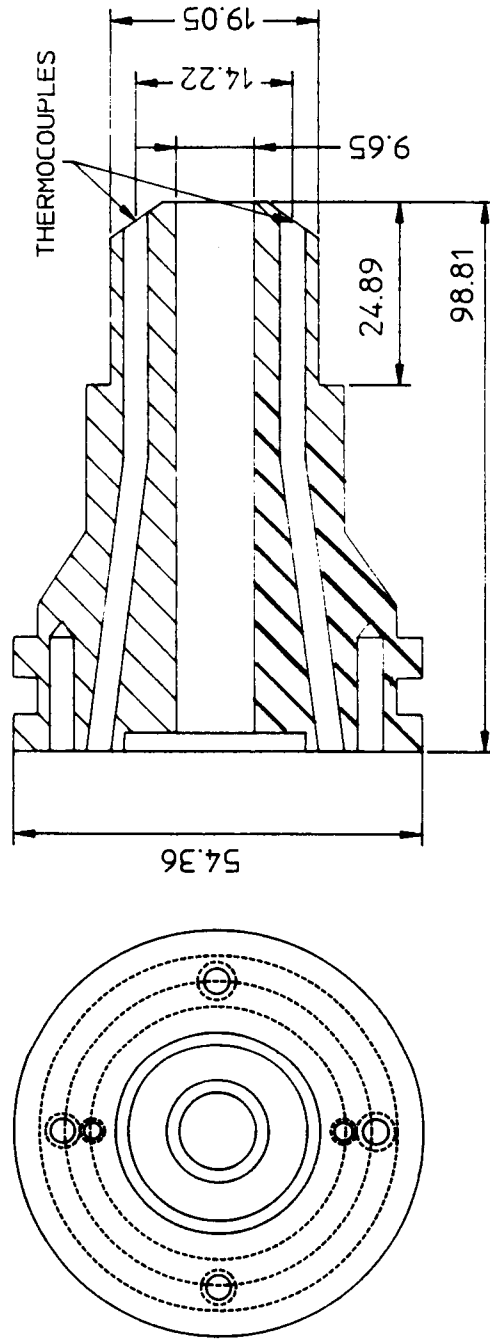


FIGURE 8. FIREDECK THERMOCOUPLE LOCATIONS

EXHAUST SYSTEM

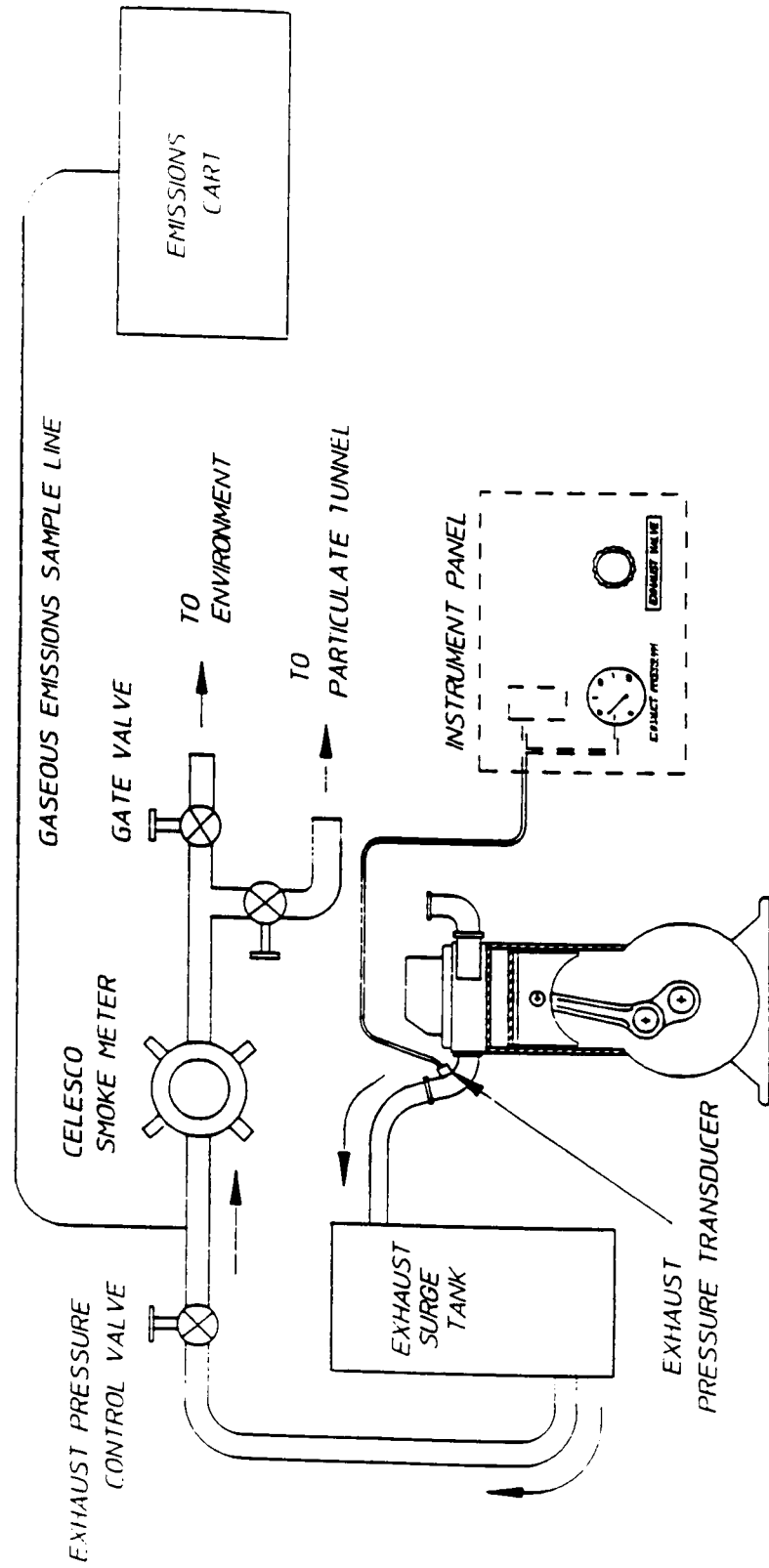


FIGURE 9. EXHAUST SYSTEM SCHEMATIC

As an alternative to a ductile iron piston, SwRI designed a composite piston using a stainless steel cap bolted to a modified stock piston using the stock piston aluminum skirt and piston pin bosses. The stainless steel cap was then sprayed with partially stabilized zirconia to provide insulation. The composite piston was designed and fabricated with a compression ratio, ring height, and bowl volume equivalent to the stock aluminum piston. The steel cap was bolted to the piston using six counter sunk socket head cap screws located around the circumference of the piston bowl. The counter sunk socket head cap screws were then welded over and the piston crown was machined flat as shown in Figure 10. Two large bolts and a support plate were also used to hold the steel cap on from underneath the piston. The two large bolts and support plate are shown in Figure 11. Copies of the engineering drawings for these piston modifications are shown in Appendix A. The composite piston was then stress tested in the engine by motoring the engine at 2500 rpm without a cylinder head to maximize the piston mechanical stress loading. After passing the stress test, the SwRI designed composite piston crown was coated with ceramic material. The stock aluminum piston (left) and modified coated piston (right) are shown in Figure 12. The plasma sprayed zirconia coated fire deck, intake, and exhaust valves are shown in Figure 13.

ORIGINAL PAGE IS
OF POOR QUALITY

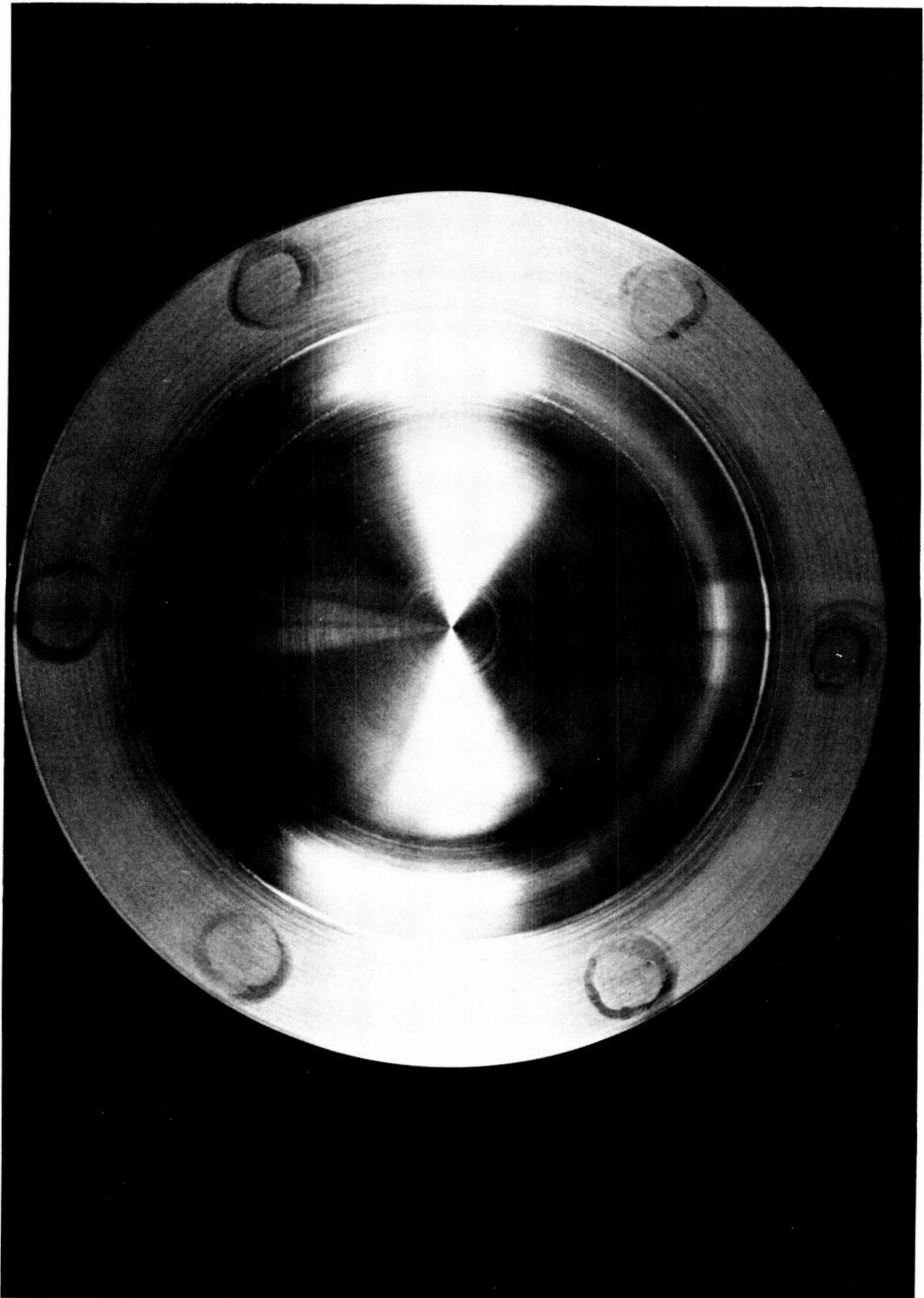
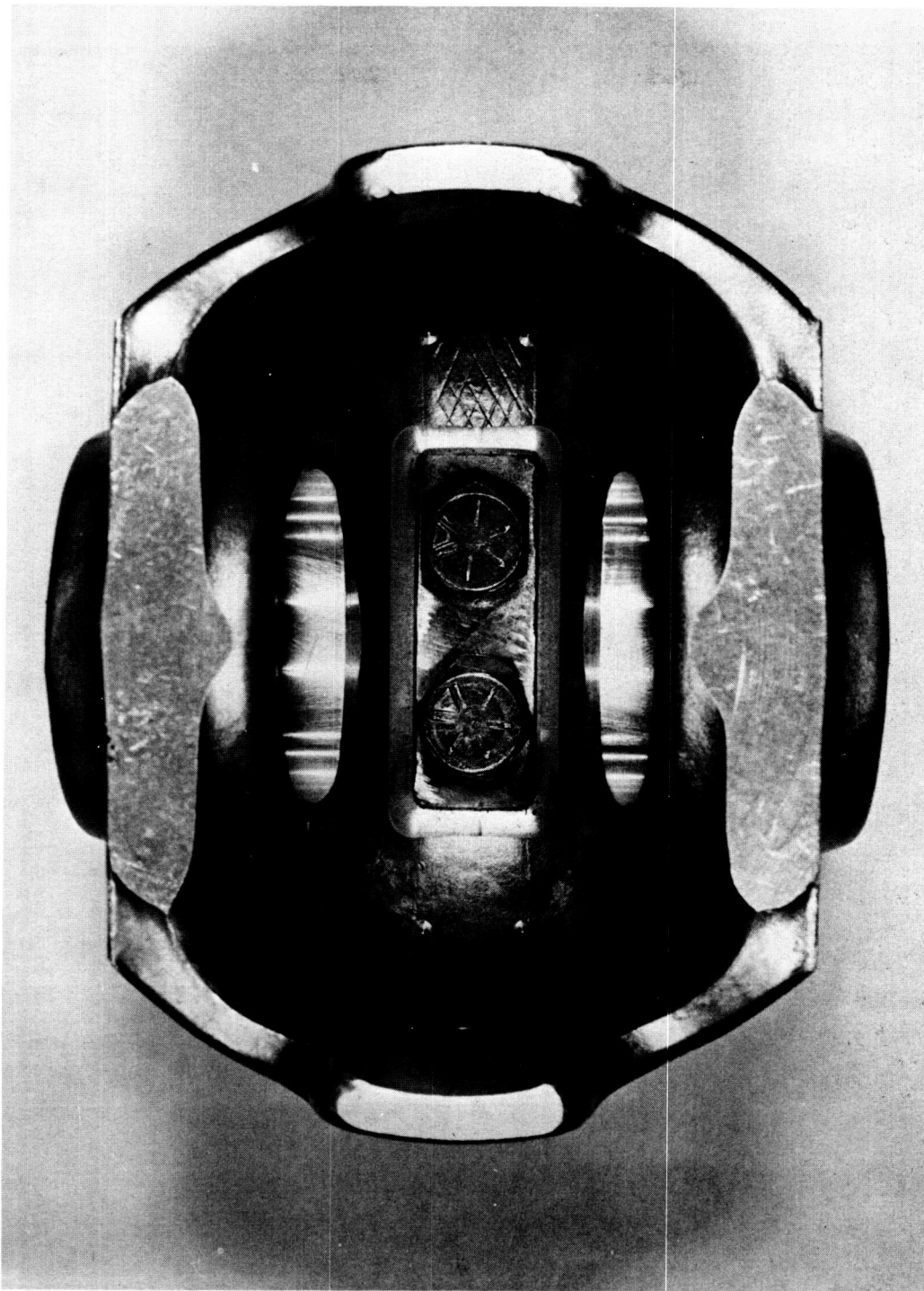


FIGURE 10. PHOTOGRAPH OF STEEL PISTON CROWN
BEFORE COATING WITH CERAMIC MATERIAL

ORIGINAL PAGE IS
OF POOR QUALITY



**FIGURE 11. BOLTS AND SUPPORT PLATE USED TO ATTACH
STEEL PISTON CROWN VIEW FROM PISTON BOTTOM**

ORIGINAL PAGE IS
OF POOR QUALITY

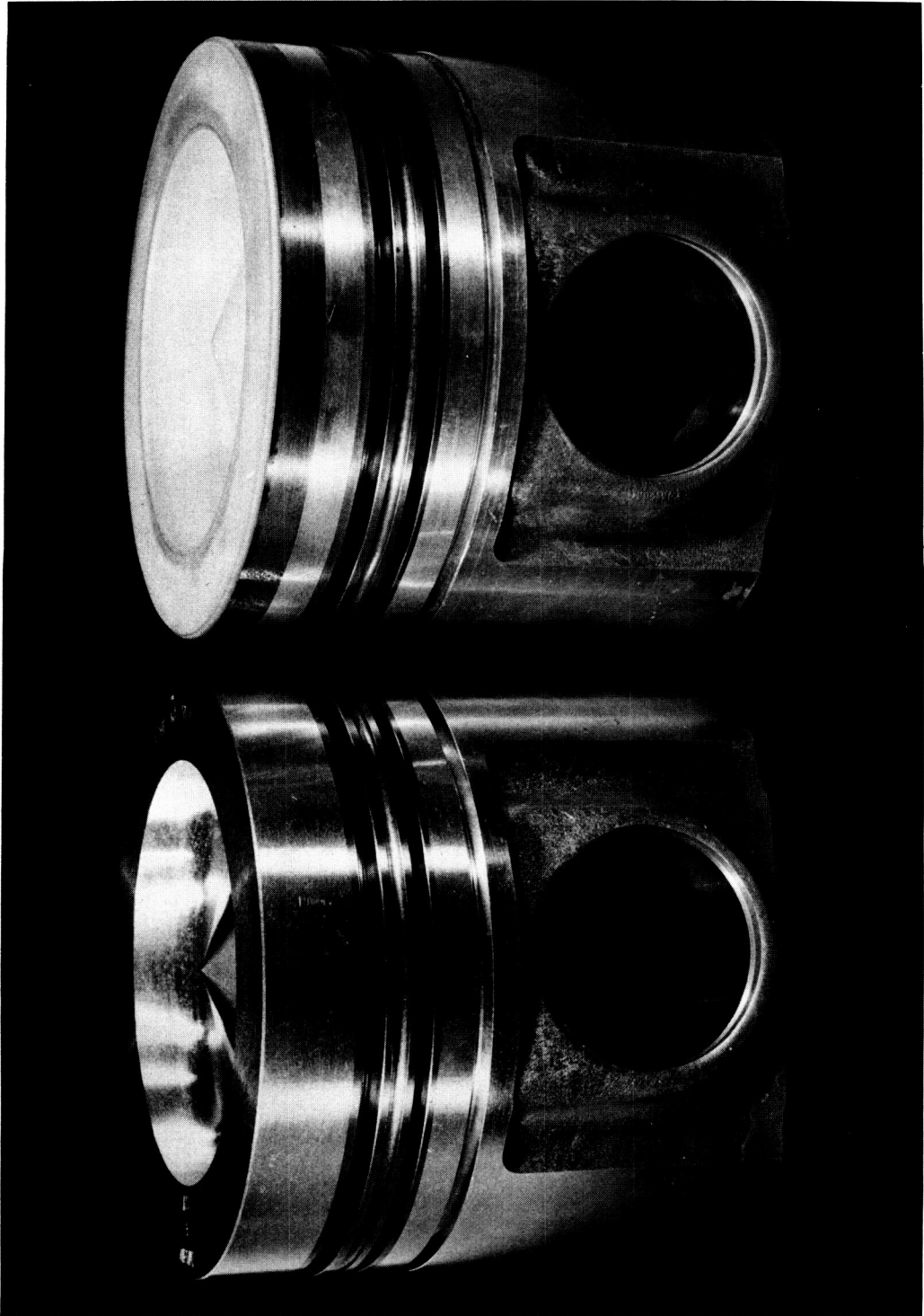


FIGURE 12. COMPARISON BETWEEN STOCK ALUMINUM
PISTON (LEFT) AND MODIFIED CERAMIC-COATED
PISTON (RIGHT)

ORIGINAL PAGE IS
OF POOR QUALITY

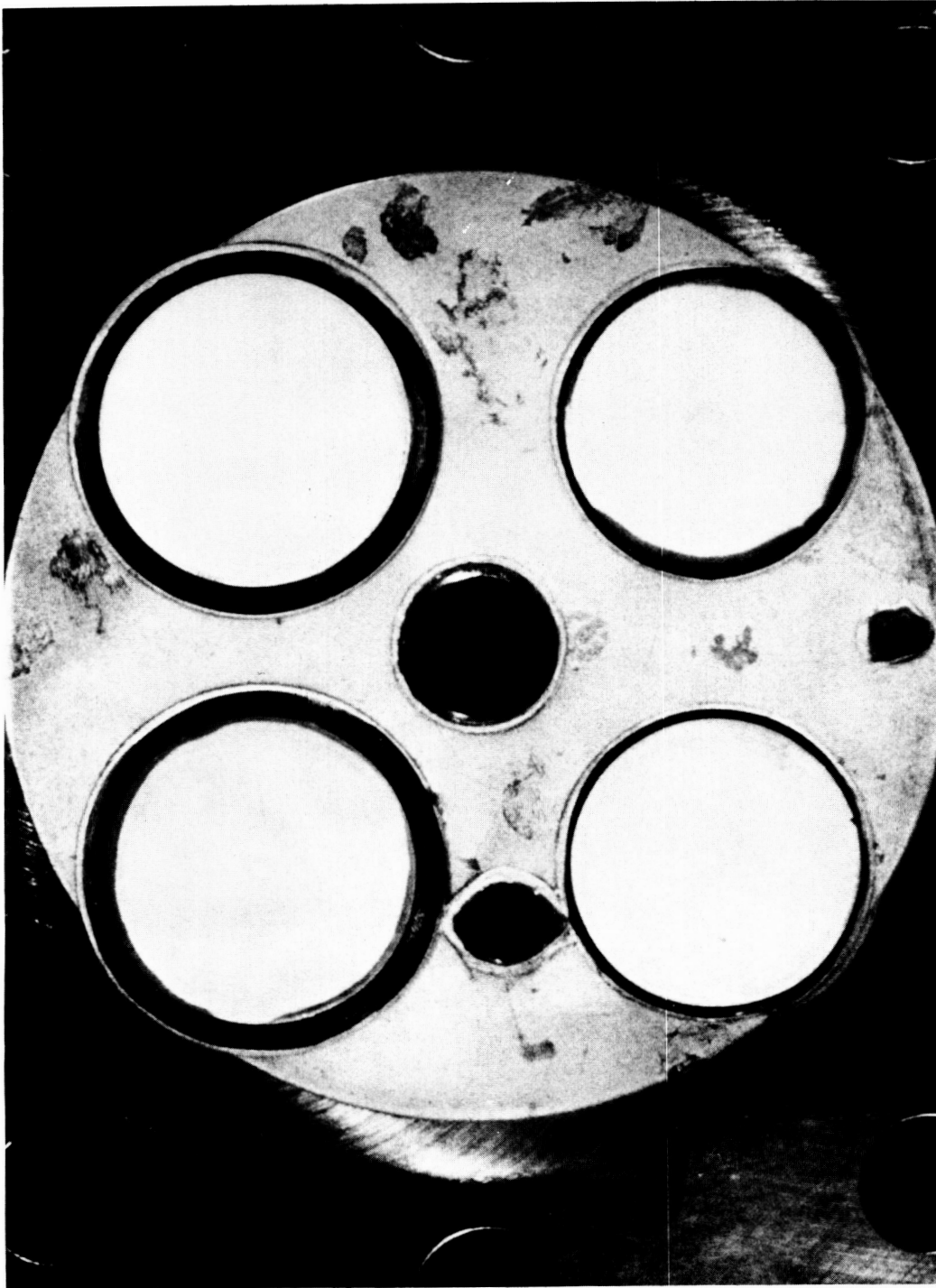


FIGURE 13. CERAMIC-COATED FIREDECK, INTAKE
VALVES (LEFT), AND EXHAUST VALVES (RIGHT)

III. TEST PROCEDURE

A. Baseline Engine Tests

Baseline engine tests were first conducted with the all metal (uninsulated) engine. Data points were recorded at speeds of 1400, 1700, 2000 rpm for loads of 33, 66, and 100 percent of full power as shown in Figure 14. The boost pressure was adjusted to obtain an air/fuel ratio of 25 to 1 at the 100 percent load conditions. The exhaust gas back pressure was adjusted to maintain an intake air manifold to exhaust manifold pressure ratio of 1.0. The intake air, cylinder block coolant, and head coolant temperatures were held constant at 82°C. The oil sump temperature was not allowed to exceed 121°C and was lower than this value at lower engine speeds and loads. The baseline fuel injection timing was 26.0 degrees before top dead center at 2000 rpm, 100 percent load.

Engine temperatures, pressures, speed, load, air flow, fuel flow, exhaust opacity and gaseous emissions measurements were recorded at each test point using a low-speed data acquisition computer. A high-speed analog-to-digital converter in conjunction with a digital computer was used to record cylinder and fuel injection pressures every one-half crank angle degree for 100 engine cycles. The 100 engine cycles were then averaged to provide one cycle for combustion analysis. The fuel injector needle lift position was not monitored with a needle lift sensor because a reliable needle lift sensor could not be found that would work well with the engine's unique fuel injector. The high-speed cylinder pressure and fuel injection pressure data were used for combustion analysis. The SwRI pressure analysis program (PANAL) was used to calculate the combustion parameters that are presented in the results section of this report. Gaseous emissions measurements were made with a 13 mode emissions cart. The emissions included hydrocarbons, carbon monoxide, oxides of nitrogen, oxygen, and carbon dioxide. The particulate emissions were measured using an exhaust gas dilution tunnel.

After completing the baseline data points (designated Baseline Metal test condition), the all metal engine was tested using an elevated cylinder head and cylinder block coolant temperature of 104°C. These increased temperature tests were conducted to see the effect of increased coolant temperature on engine performance, emissions, and combustion without the additional variable of ceramic insulation. The baseline fuel flow and air fuel ratio were held constant for all subsequent tests.

Three data points were also collected at 2000 rpm, 100, 66, 33 percent load with 180°F coolant and 140°F intake air. These data points were collected to simulate air-to-air after-cooling.

B. Insulated Engine Tests

The ceramic coated fire deck, intake valves, exhaust valves, cylinder liner, and piston were then installed in the engine. The compression ratio was checked by measuring the piston-to-head clearance and observing the log pressure versus log volume motoring diagram to insure that the insulated engine compression ratio was equivalent to the Baseline Metal engine compression ratio. The baseline data points were then repeated with the insulated engine to see the effect of insulated engine surfaces on engine performance, emissions, and combustion without the added variable of increased coolant temperature. These tests were referred to as the "Baseline Ceramic" test condition.

High temperature engine experiments were then conducted with the insulated engine to determine the maximum coolant and engine component temperatures that could be obtained. The maximum head coolant temperature that could be achieved at 2000 rpm, 100 percent load was 142°C using pure ethylene glycol. The measured maximum fire deck temperature at this condition was 343°C. The ethylene glycol was then drained from the cylinder head coolant circuit and replaced with a regulated supply of compressed air to achieve higher fire deck temperatures. Air flow through the cylinder head was adjusted to maintain a measured maximum fire deck temperature of 482°C. The fire deck temperature was measured with thermocouples mounted in the tip of the fuel injector holder on the surface exposed to the combustion chamber. The 482°C fire deck temperature could not be achieved at some part load conditions. The cylinder liner coolant temperature was increased

DATA POINTS

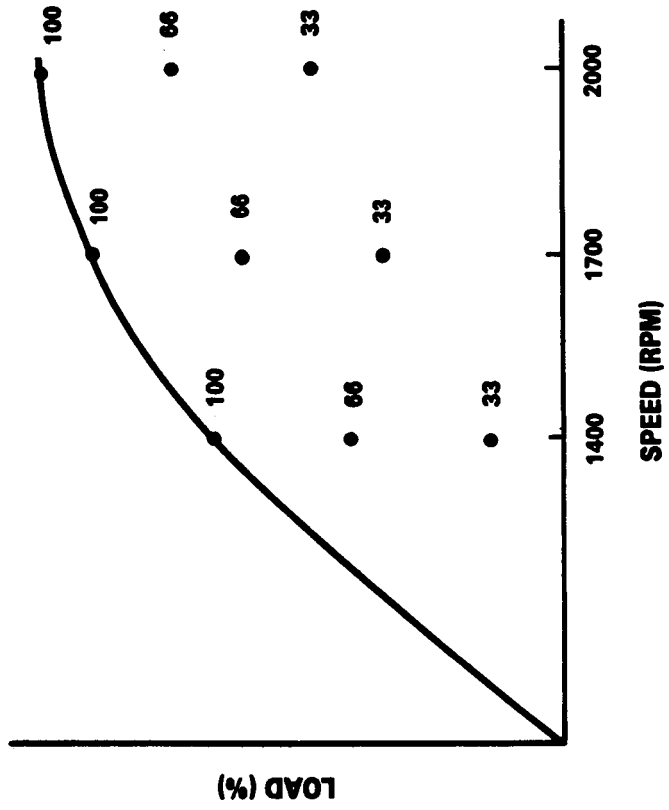


FIGURE 14. DATA POINTS USED FOR ENGINE PERFORMANCE TESTS

to 121°C which resulted in a measured maximum top ring reversal temperature of approximately 204°C. The cylinder liner remained cooled with pure ethylene glycol at 121°C for three reasons:

- Cooling the cylinder liner resulted in improved engine durability by maintaining an oil film on the cylinder liner.
- Previous studies at SwRI (ref. 26) have shown that increased cylinder liner temperature has no beneficial effect on indicated specific fuel consumption.
- It was assumed that a cooled cylinder liner would help to reduce the problem of increased particulate and unburned hydrocarbon emissions due to burning oil on the cylinder wall of LHR engines.

The LHR engine tests conducted with compressed air as the cylinder head coolant and 121°C ethylene glycol block coolant were referred to as the "Hot Ceramic" test condition. The Hot Ceramic engine tests were conducted at standard, retarded, and advanced fuel injection timings. The Hot Ceramic engine tests were conducted at 1400, 1700, and 2000 rpm 100 percent load. The 67 and 33 percent load points were also recorded at 2000 rpm. The part load data points were not recorded at some 1400 and 1700 rpm test conditions to reduce the total number of Hot Ceramic engine data points. This abbreviated test procedure still showed the effect of engine speed and load while reducing the total number of data points. The total number of Hot Ceramic engine data points was reduced to ensure getting the most useful data at various timings during the suspected short life of the insulated engine operating at increased temperature.

The Hot Ceramic engine tests were stopped during the advanced timing test at 1400 and 1700 rpm when it was noticed that engine blowby increased. It was suspected that the increased blowby was due to a scuffed piston and liner. However, upon engine disassembly, it was found that the fuel injector holder O-ring gasket had melted and was allowing the cylinder head coolant (compressed air) to leak into the engine crankcase resulting in an apparent increase in engine blowby. Engine tests were stopped after this tear-down because it was noticed that some of the ceramic coatings had come off of the engine piston and valves.

The engine test conditions are summarized in Table 2.

C. Test Fuel and Oil

A reference grade diesel fuel was used for all engine tests. The fuel specifications and distillation curve are given in Appendix B.

The lubricating oil used for this investigation was Valvoline Turboguard 5. High temperature lubrication requirements were discussed with personnel from the Belvoir Fuels and Lubricants Research Facility (BFLRF) at SwRI concerning the latest information available on lubricants for LHR engines. Lubricant recommendations were made based upon an SwRI report entitled "High-Temperature Lubricants for Minimum-Cooled Diesel Engines," (ref. 7). The BFLRF personnel stated that there are three problems with selecting a lubricant for LHR engines:

- Oil thickening
- Oil consumption
- Oil deposits, which cause ring sticking.

According to the BFLRF personnel there is currently no commercial oil that solves all three problems. The recommendations for the best commercially available oil at the time of these experiments included Mobil No. 245 (a turbine engine oil with no diesel additive package and no API rating for diesels), and Valvoline turboguard 5. The Valvoline turboguard 5 oil was selected because it has an API rating of CD and was thought to provide the best overall cost effective performance for the LHR engine. The Valvoline oil was also representative of oils with wide spread commercial availability. The Valvoline oil, however, has a tendency toward oil thickening and may require frequent changes.

The replacement intervals for the oil were determined by oil sampling to monitor the increased oil viscosity and increased acid number. The Valvoline turboguard 5 oil specifications and sample oil analyses are included in Table 5, found in Section IV of this report. The oil analyses results are discussed in Section IV.

Table 2. Engine Test Conditions

	Block Coolant °C	Head Coolant °C	Injection Timing (°CABTDC)	Intake Air °C
Baseline Metal	82	82	26.0	82
Baseline Metal	104	104	26.0	82
Baseline Ceramic	82	82	26.0	82
Hot Ceramic Standard	121	Air	26.0	82
Hot Ceramic Retarded	121	Air	26.0	82
Hot Ceramic Advanced	121	Air	28.0	82

IV. EXPERIMENTAL RESULTS

The engine test results are discussed in terms of engine performance, emissions, temperatures, and combustion. For reference purposes, the six engine test conditions are listed in Table 2. All of the engine performance and emissions data are included in Appendix C.

A. Performance and Emissions

The performance and emissions results for the three engine test speeds of 2000, 1700, and 1400 rpm are shown in Figures 15 through 20. All curves with dashed lines correspond to insulated engine tests.

The performance and emissions results at 2000 rpm are shown in Figure 15. Figure 15 is a plot of indicated thermal efficiency (ITE), smoke opacity, and particulates versus indicated power. Increasing the Baseline Metal engine coolant temperature from 82°C to 104°C had no measurable effect on indicated thermal efficiency while slightly increasing the low load smoke and full load particulate emissions. The insulated engine at baseline conditions (Baseline Ceramic) had significantly lower ITE, with higher smoke and particulate emissions, especially at full load, compared to the Baseline Metal engine. Increasing the coolant temperature of the ceramic insulated engine (Hot Ceramic) slightly reduced the ITE at full load, and increased the lowest load particulate emissions compared to the Baseline Ceramic engine. Advancing the fuel injection timing 2 degrees for the Hot Ceramic engine had no measurable effect on ITE while slightly reducing the smoke and particulate emissions compared to the Hot Ceramic engine at standard injection timing. Retarding the fuel injection timing by 6 degrees reduced the ITE and significantly increased smoke and particulate emissions. The most significant result of these tests is that the addition of ceramic insulation and subsequent reduction of heat transfer to the coolant did not improve engine performance relative to the Baseline Metal engine.

The performance and emissions results at 1700 and 1400 rpm are shown in Figures 16 and 17. In general, the same trends were observed at these two lower engine speeds.

The gaseous emissions results at 2000 rpm are shown in Figure 18. In general, insulating the engine and then increasing the coolant temperature reduced the HC emissions across the load range while slightly reducing the CO emissions at part-load. The CO emissions increased at the full-load condition. The NO_x emissions for the Baseline Ceramic engine were the same as the Baseline Metal engine at low load and were slightly reduced at the full load condition. The NO_x emissions were higher across the entire load range for the advanced fuel injection timing. The NO_x emissions were significantly reduced at retarded fuel injection timings but only at the expense of increased particulate emissions as shown in Figure 15.

The gaseous emissions results at 1700 and 1400 rpm are shown in Figures 19 and 20. In general, the same gaseous emission trends observed at 2000 rpm were preserved at the lower engine speeds. The NO_x emissions were significantly reduced at retarded fuel injection timings but only at the expense of increased particulate emissions. The trade off between the particulate and NO_x emissions for the three fuel injection timings at 2000 rpm is shown in Figure 21.

Figure 21 is a plot of particulates and indicated specific fuel consumption (ISFC) versus NO_x emissions for the Hot Ceramic engine at 2000 rpm full load. The curves in Figure 21 show that retarding the fuel injection timing significantly increased the particulate emissions and ISFC while reducing the NO_x emissions. Advancing the fuel injection timing slightly reduced the particulate emissions and ISFC while significantly increasing the NO_x emissions. The curves in Figure 21 are significant because they show that the Baseline Metal engine particulate and NO_x emission levels of 0.12 and 6.6 (g/ihp-hr), respectively, could not be reached in the Hot Ceramic engine by advancing or retarding the fuel injection timing.

The effect of reducing heat transfer to the engine coolant on engine performance is shown in Figure 22. Figure 22 is a plot of indicated thermal efficiency, NO_x and particulate emissions versus

PERFORMANCE AND EMISSIONS, 2000 RPM

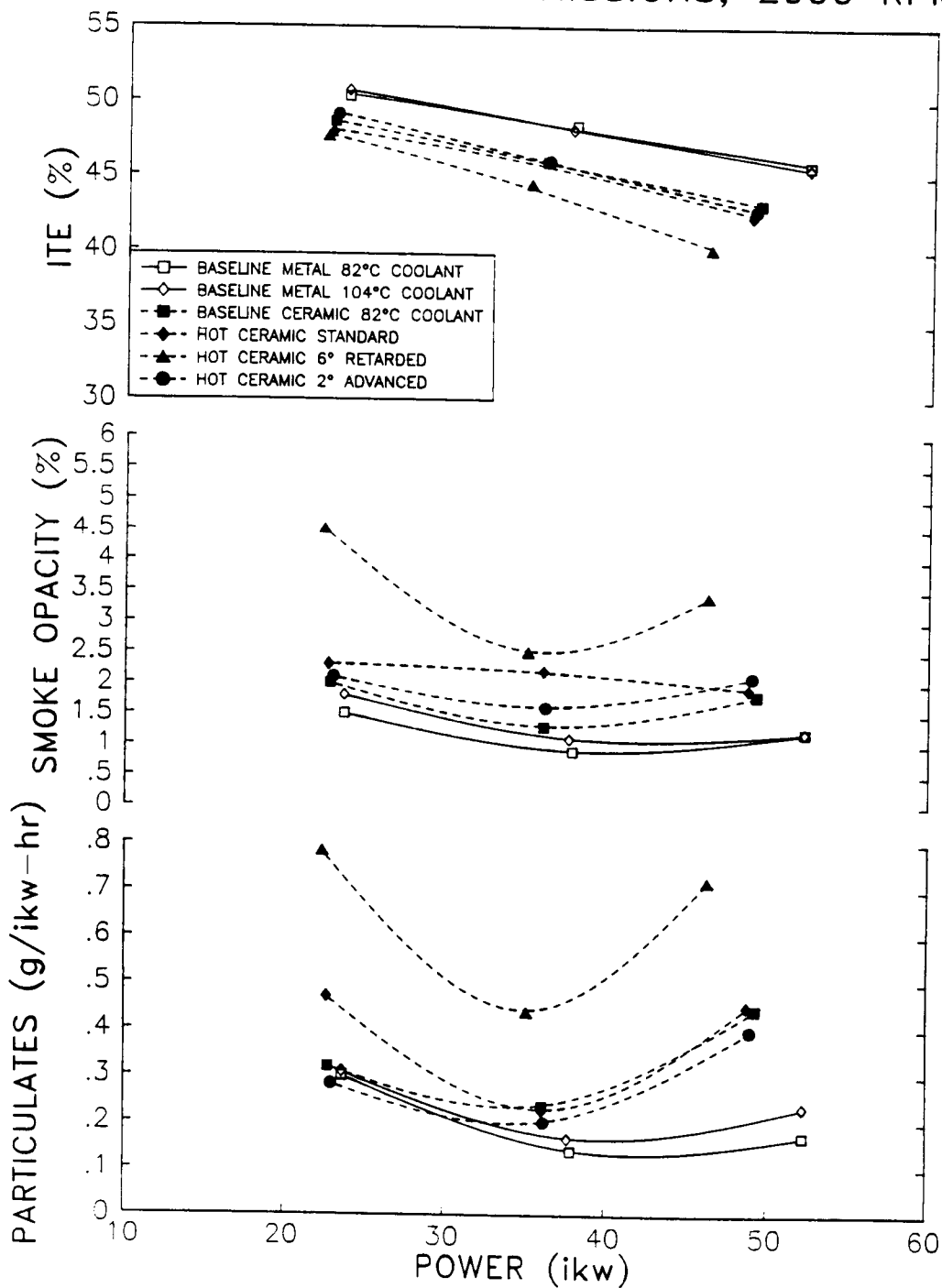


FIGURE 15. PERFORMANCE AND EMISSIONS RESULTS, 2000 RPM

PERFORMANCE AND EMISSIONS, 1700 RPM

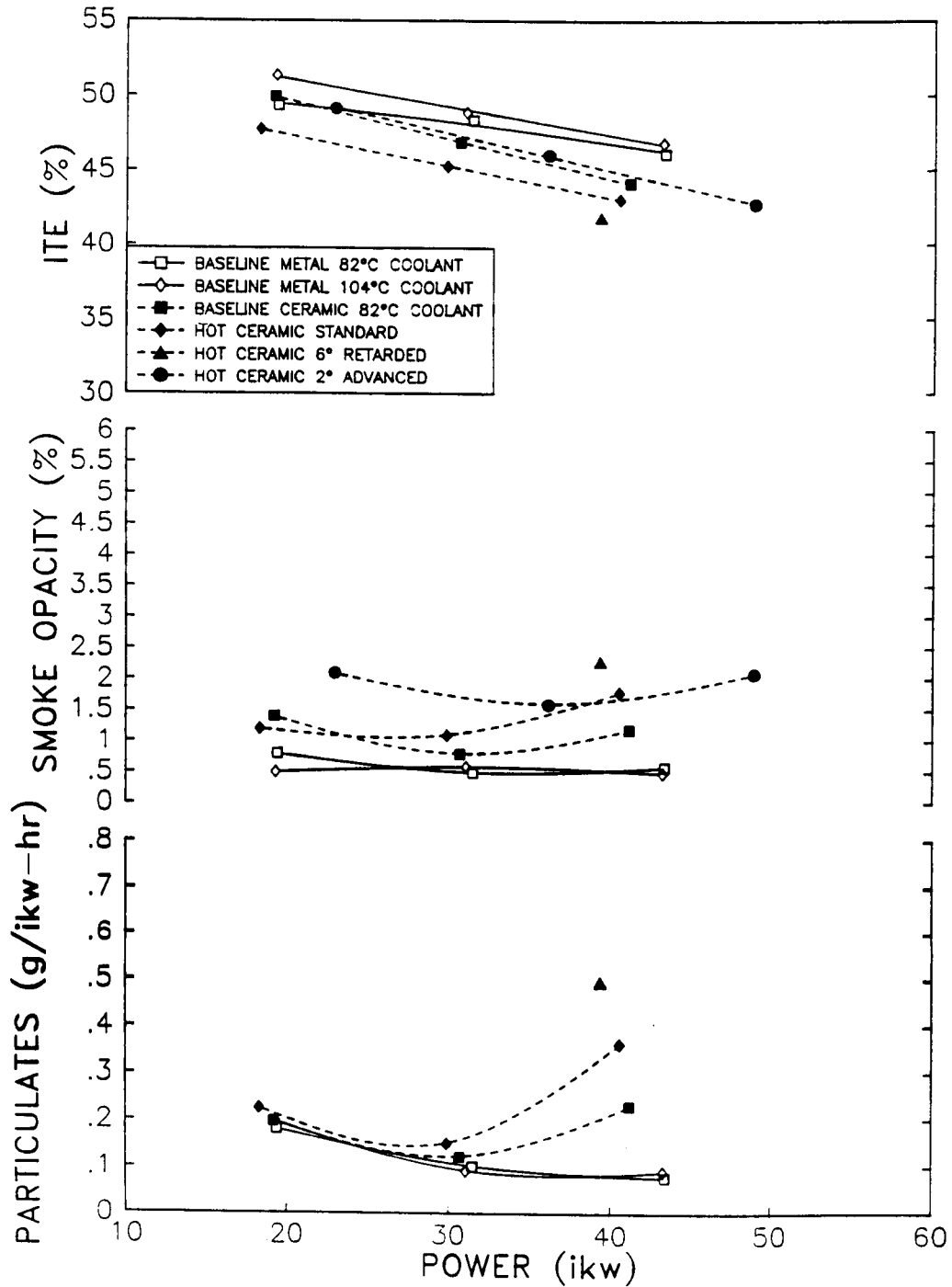


FIGURE 16. PERFORMANCE AND EMISSIONS RESULTS, 1700 RPM

PERFORMANCE AND EMISSIONS, 1400 RPM

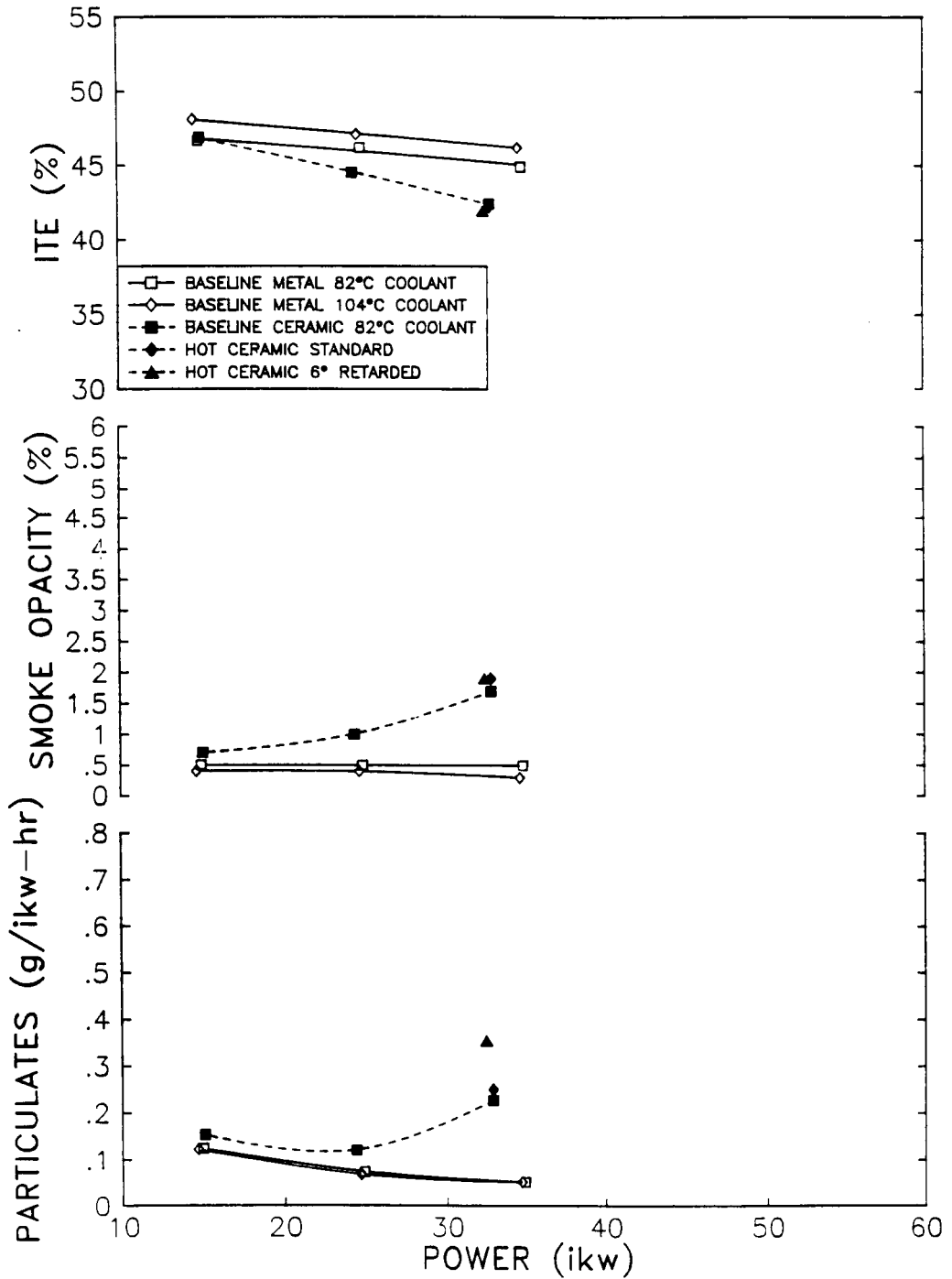


FIGURE 17. PERFORMANCE AND EMISSIONS RESULTS, 1400 RPM

GASEOUS EMISSIONS, 2000 RPM

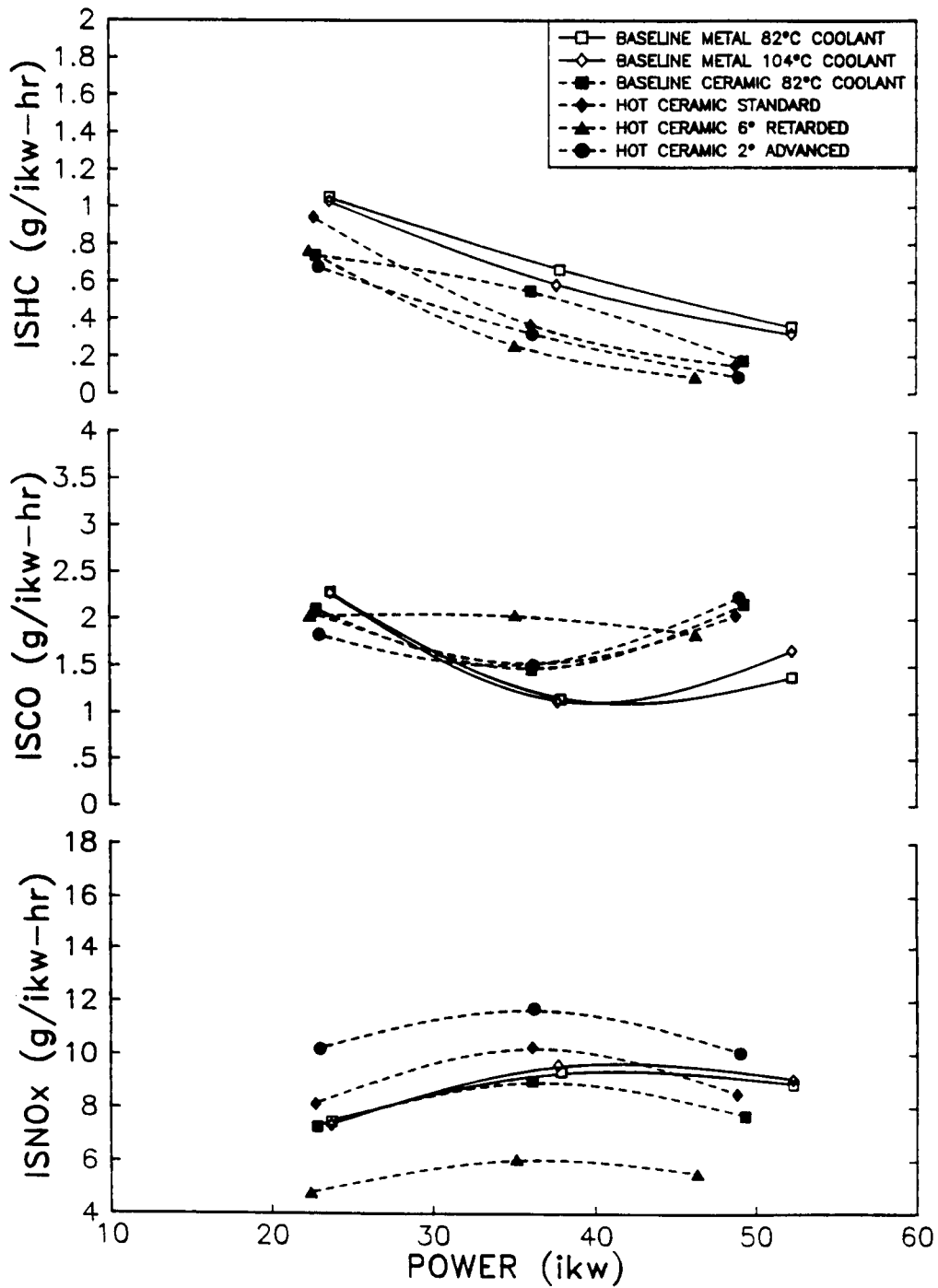


FIGURE 18. GASEOUS EMISSIONS RESULTS, 2000 RPM

GASEOUS EMISSIONS, 1700 RPM

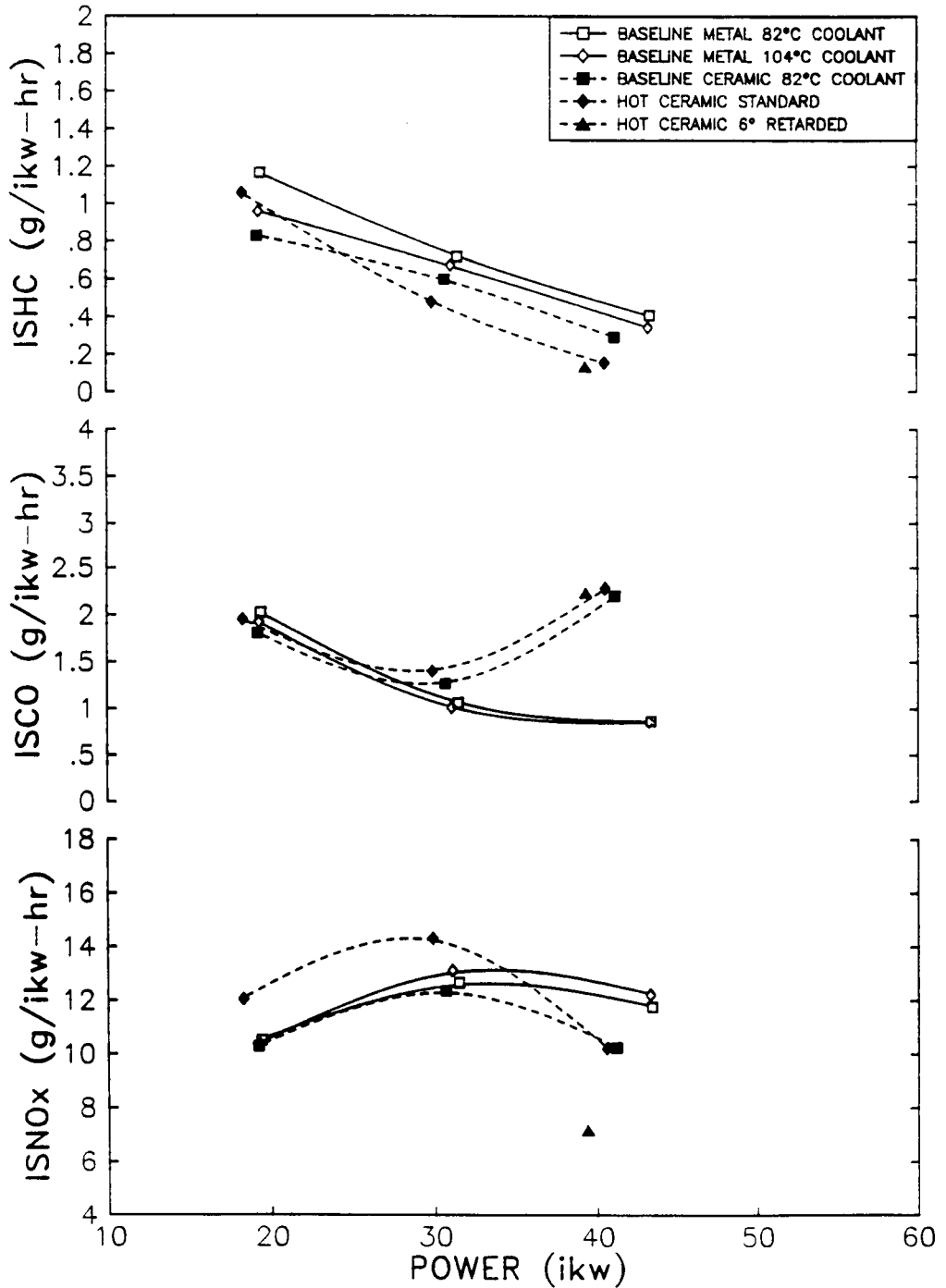


FIGURE 19. GASEOUS EMISSIONS RESULTS, 1700 RPM

GASEOUS EMISSIONS, 1400 RPM

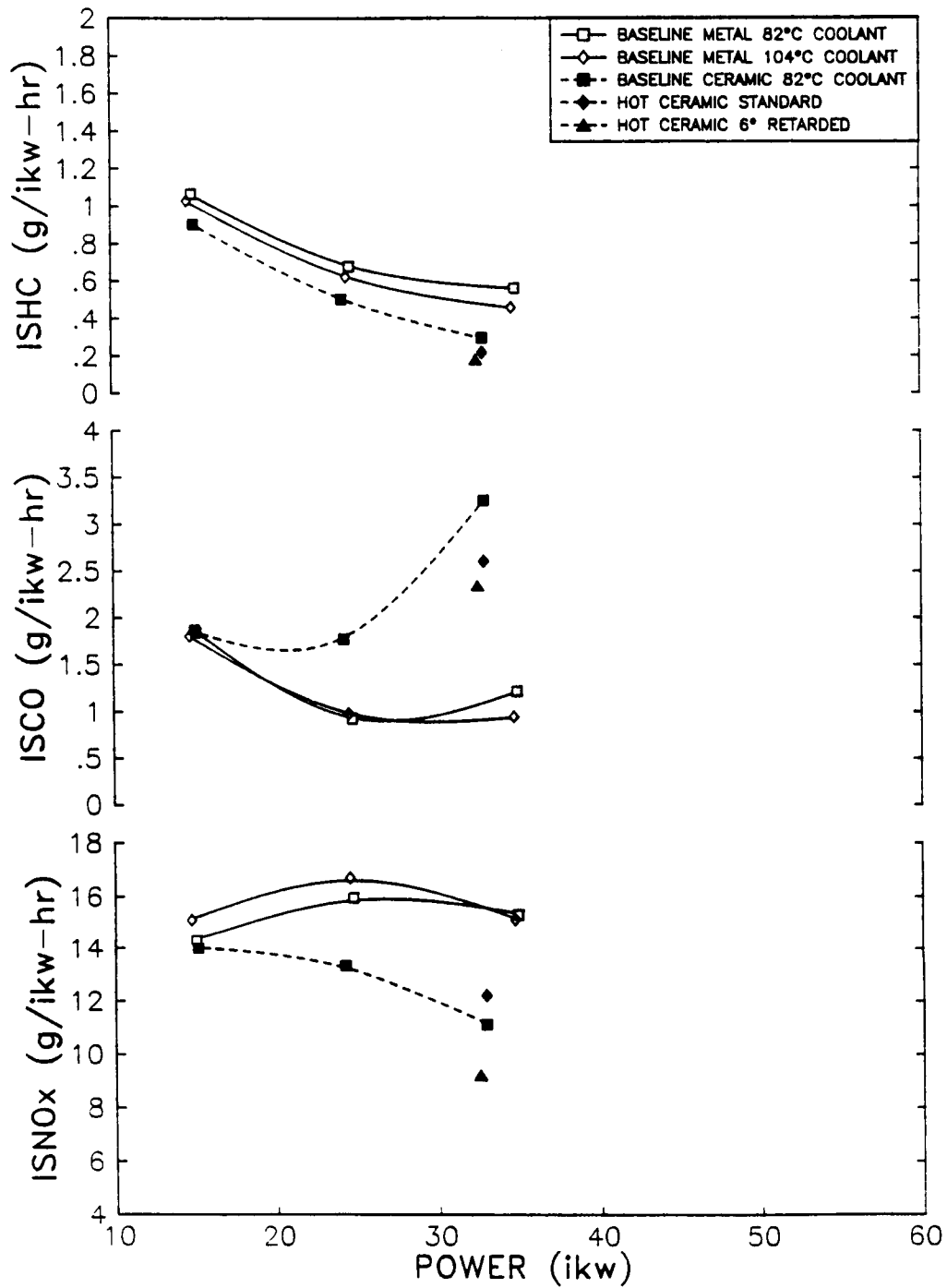


FIGURE 20. GASEOUS EMISSIONS RESULTS, 1400 RPM

INSULATED ENGINE 2000 RPM, FULL LOAD

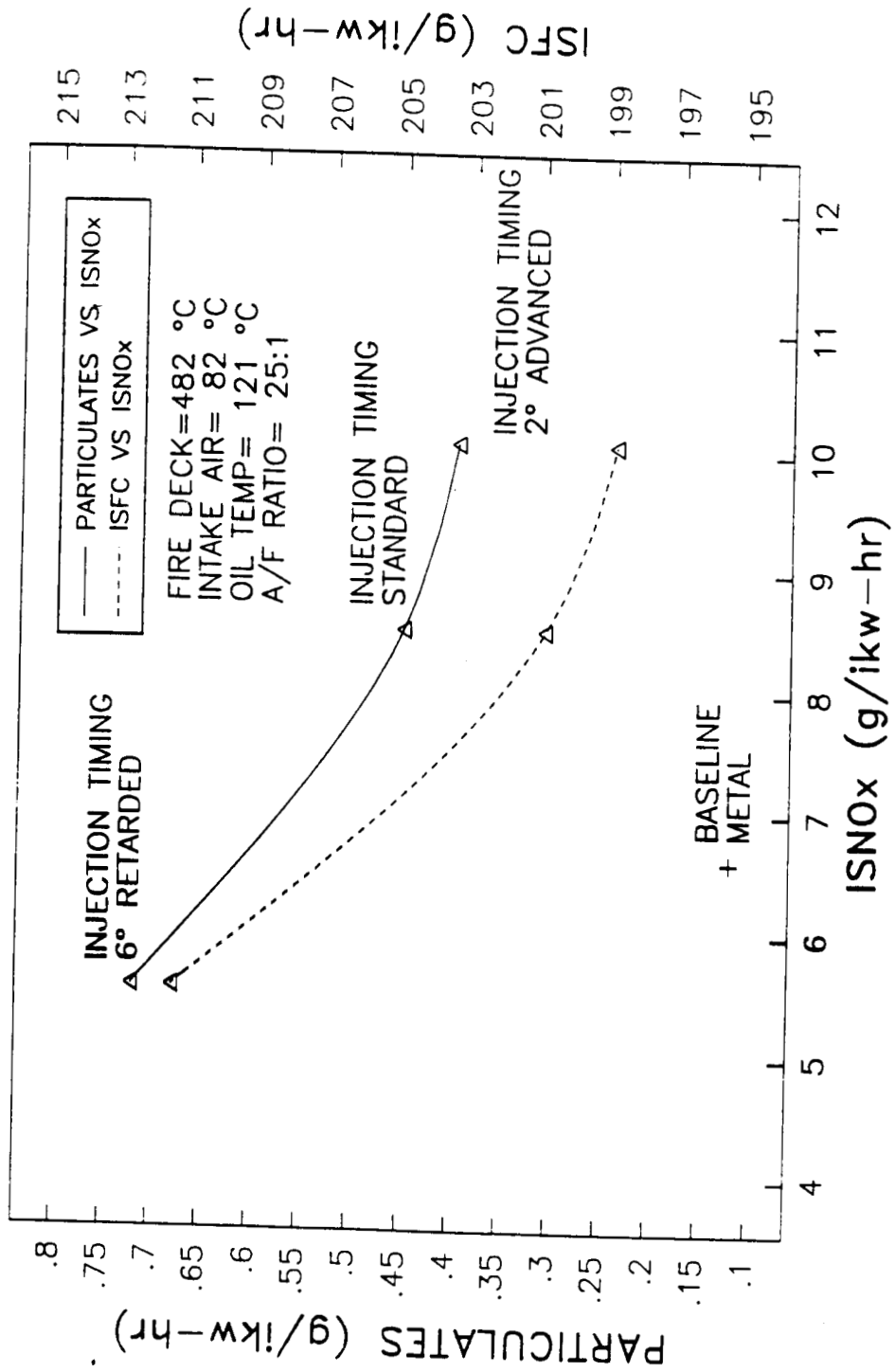


FIGURE 21. PARTICULATE AND ISFC VERSUS ISNO_x EMISSIONS, 2000 RPM, FULL LOAD

INSULATED ENGINE 2000 RPM, FULL LOAD

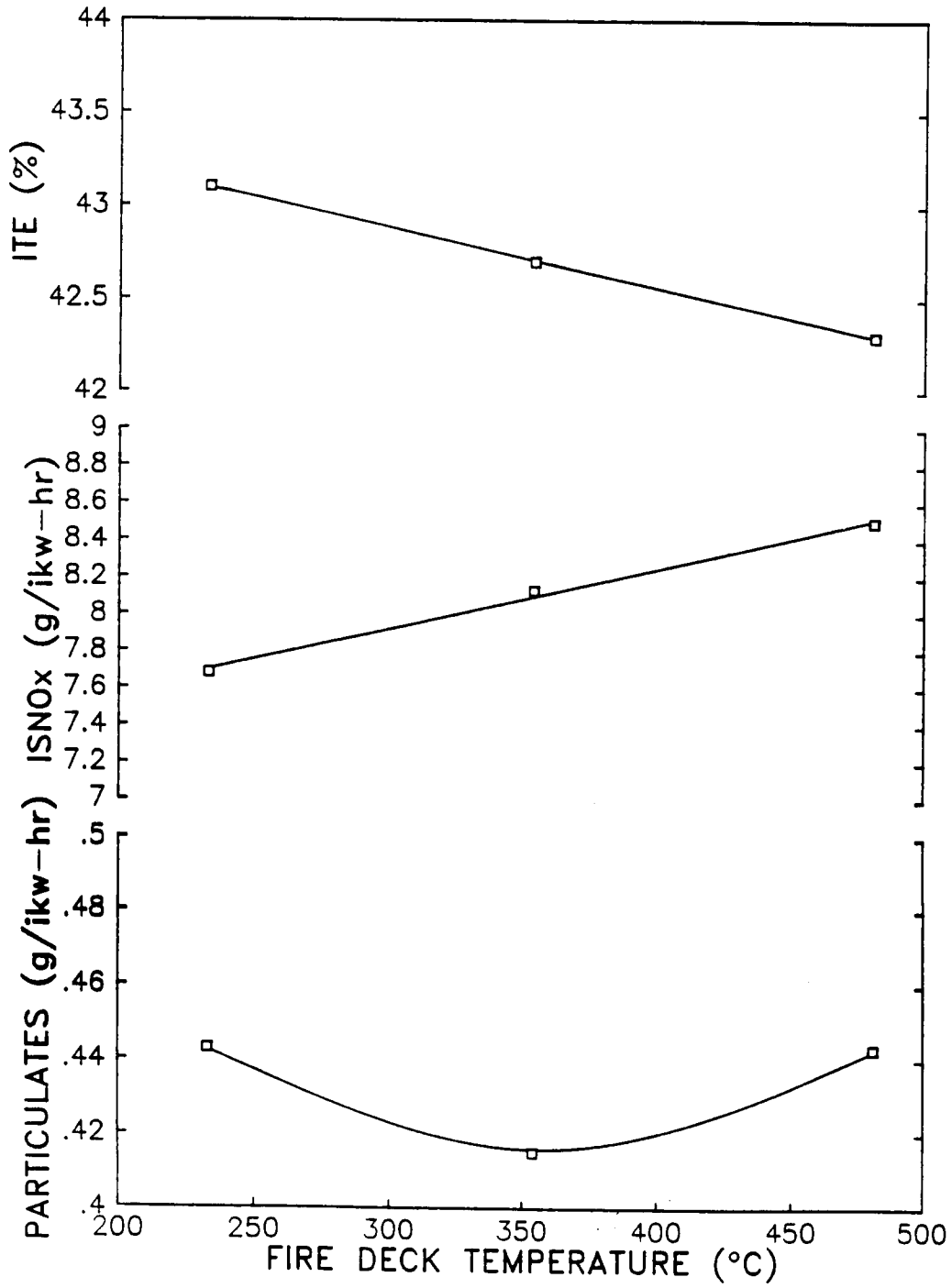


FIGURE 22. PARTICULATE, ISNO_x, ITE VERSUS FIRDECK TEMPERATURE, 2000 RPM, FULL LOAD

measured fire deck temperature for the insulated engine at 2000 rpm full load. The fire deck temperatures of approximately 230 and 480°C corresponded to the Baseline Ceramic and Hot Ceramic engine test conditions, respectively. The curves in Figure 22 show that, as the heat rejection to the coolant was reduced and as the fire deck temperature increased, the ITE was reduced, NO_x emissions increased, and the particulate emissions remained about the same.

B. Temperatures

The measured fire deck, top ring reversal, and exhaust gas temperatures versus indicated power are shown in Figures 23 through 25 for the 2000, 1700, and 1400 rpm test conditions respectively. All three temperatures increased with indicated power. At 2000 rpm increasing the Baseline Metal engine coolant temperature from 82°C to 104°C increased the top ring reversal temperature by approximately 17°C and had little effect on the fire deck and exhaust gas temperatures. Insulating the engine with ceramic coatings reduced the fire deck and top ring reversal temperatures while significantly increasing exhaust gas temperature. The fire deck and top ring reversal temperatures were reduced due to the Baseline Ceramic engine's degraded combustion as explained in the next section. The exhaust gas temperature increased due to reduced heat transfer to the coolant and also because of combustion occurring late in the cycle.

All three temperatures increased for the Hot Ceramic engine as shown in Figure 23. At 2000 rpm, the fire deck temperature increased by approximately 167°C for the Hot Ceramic engine compared to the Baseline Metal engine. The increased temperatures were attributed to the removal of liquid coolant from the cylinder head. Changing the fuel injection timing had little effect on these three temperatures except at the full load condition where the exhaust gas temperature increased for the retarded fuel injection timing. These same temperature trends were observed at the lower engine speeds of 1700 and 1400 rpm as shown in Figures 24 and 25.

Integral Technologies Incorporated IRIS engine model was used to predict average engine component surface temperatures based on thermocouple, engine performance, and combustion data. The IRIS model predicted an average fire deck temperature of approximately 650°C, an exhaust valve temperature of 730 °C, piston bowl temperature of 480°C, and a top ring reversal temperature greater than 343°C for the Hot Ceramic engine at 2000 rpm, full load.

C. Combustion Analysis

Combustion in a direct injected diesel engine is a complex process involving fuel injection, atomization, evaporation, and auto-ignition. The premixed fuel auto-ignites after the ignition delay period and initiates diffusion burning of the injected fuel. It is expected that the LHR engine's higher component and gas temperatures will have a significant effect on fuel spray penetration, atomization, and combustion. High speed combustion data were collected and analyzed to interpret the LHR engine performance and emissions trends.

The combustion analysis was based upon the acquisition of cylinder pressure and fuel injection pressure data every one-half crank angle degree for one-hundred engine cycles. The one-hundred cycles were then averaged to obtain one cycle for analysis.

The cylinder and fuel-injection pressure data were reduced using the SwRI Pressure Analysis Program (PANAL). The output of the PANAL code included the calculation of the parameters shown in Table 3.

The start of fuel injection and fuel injection duration were defined by the crank angle where the fuel injection pressure equaled the fuel injector crack pressure. While this method of measuring injection duration was not completely accurate (because the needle crack pressure is not equal to the closing pressure), it was a reliable and repeatable substitute in the absence of needle lift data. The point of ignition was defined as the crank angle where the heat release rate curve became positive after a brief negative excursion due to fuel vaporization. The ignition delay period was the difference between the start of fuel injection and point of ignition. The end of combustion was defined as the crank - angle where 95 percent of the peak cumulative heat release occurred. The combustion duration was

TEMPERATURES, 2000 RPM

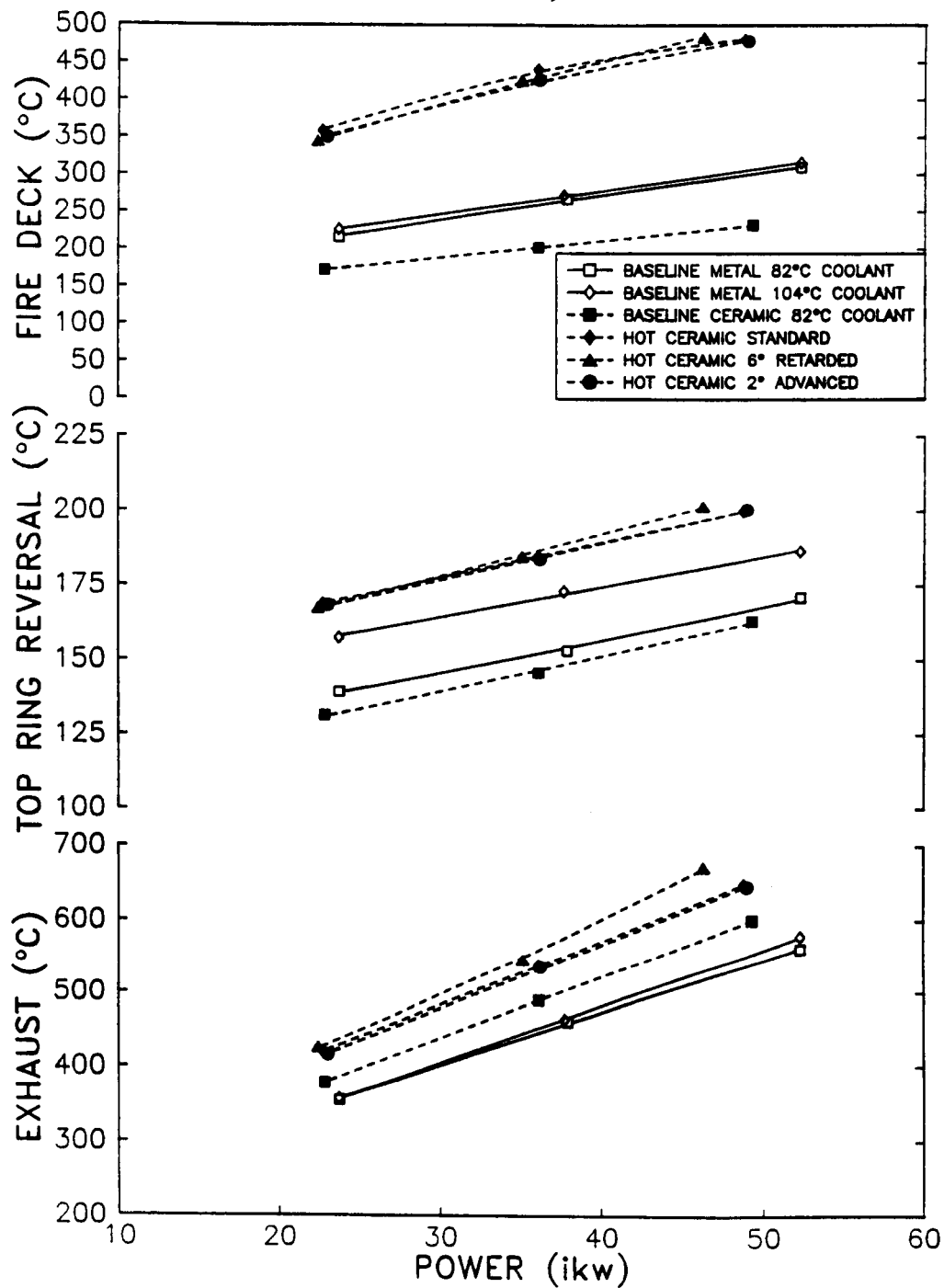
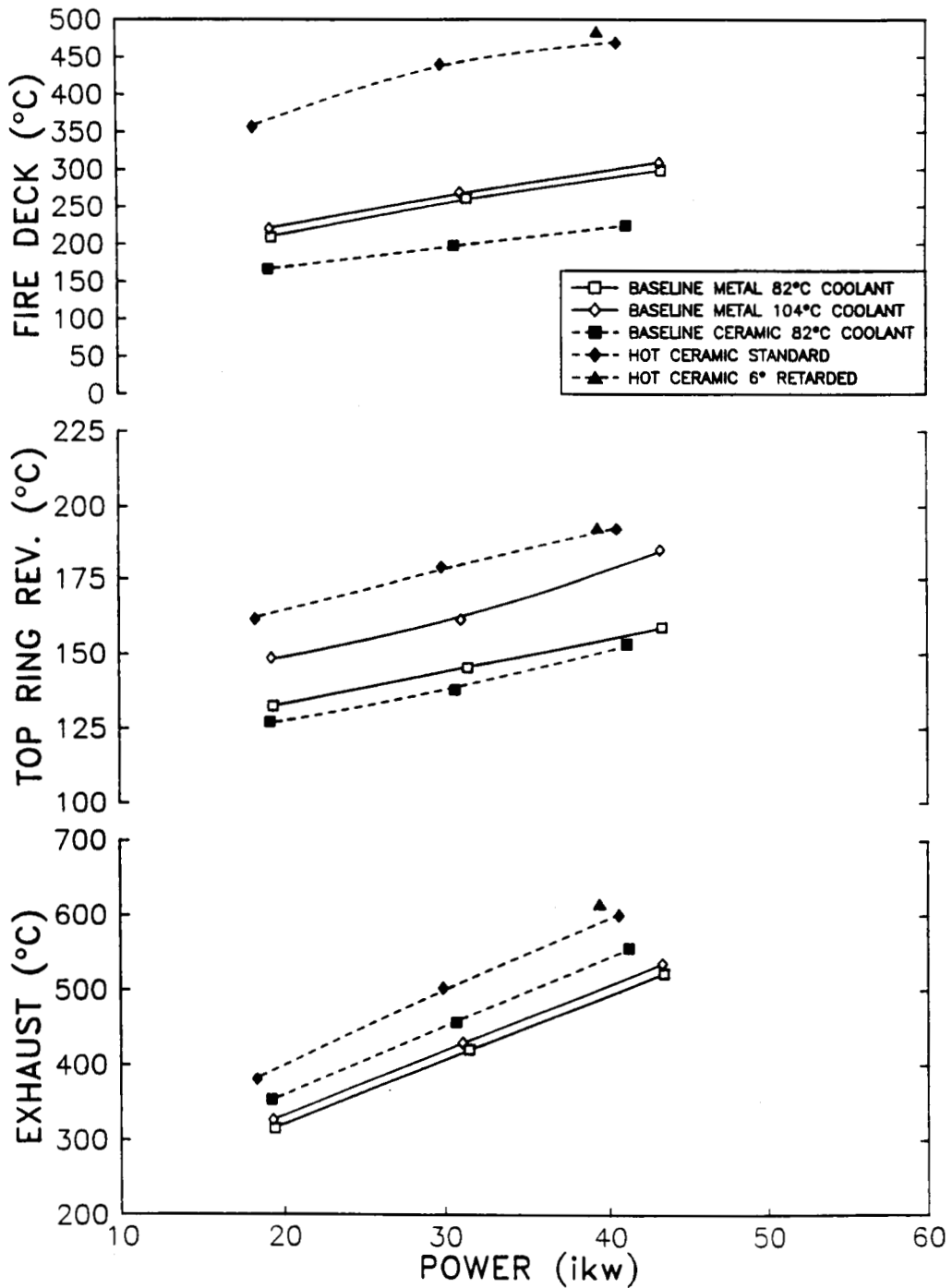


FIGURE 23. FIREDECK, TOP RING REVERSAL, AND EXHAUST GAS TEMPERATURES VERSUS INDICATED POWER, 2000 RPM

TEMPERATURES, 1700 RPM



**FIGURE 24. FIREDECK, TOP RING REVERSAL, AND EXHAUST GAS TEMPERATURES
VERSUS INDICATED POWER, 1700 RPM**

TEMPERATURES, 1400 RPM

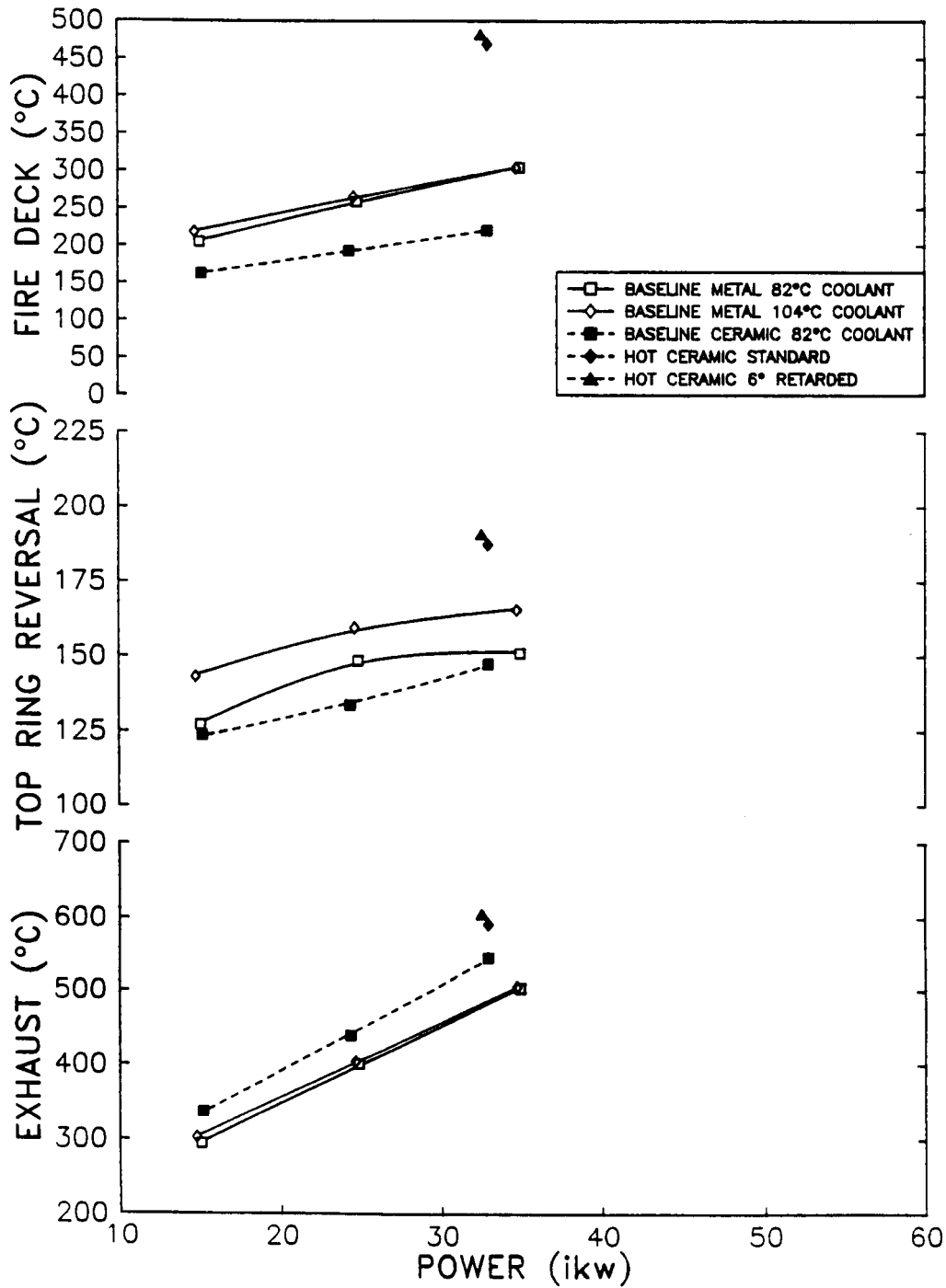


FIGURE 25. FIREDECK, TOP RING REVERSAL, AND EXHAUST GAS TEMPERATURES VERSUS INDICATED POWER, 1400 RPM

the difference between the point of ignition and end of combustion. The premixed combustion fraction was calculated by determining the magnitude of the cumulative heat release (or area under the heat release rate curve) at the crank angle corresponding to the end of the premixed spike as shown in Figure 26. The crank angle corresponding to the end of the premixed spike was determined by the point where the derivative of the heat release rate crossed the abscissa for the second time after the point of ignition. The diffusion burn fraction was the difference between the peak cumulative heat release and the premixed burn fraction.

Table 3. Combustion Analysis Parameters

Parameter	Units
Indicated Power	kW
Injection Timing	degrees
Injection Duration	degrees
Point of Ignition	degrees
Ignition Delay	degrees
Combustion Duration	degrees
Total Heat Release	J
Premixed/Total Heat Release Ratio	
Peak Cylinder Pressure	MPa
Peak Rate of Pressure Rise	kPa/deg
Angle where Peak Cylinder Pressure Occurs	degrees
Angle where Peak Rate of Pressure Rise Occurs	degrees

High speed combustion data were recorded for all test conditions except for the Hot Ceramic engine at advanced and retarded fuel-injection timings (Test Conditions numbers 5 and 6) where an instrumentation failure occurred. The combustion analysis parameters shown in Table 3 are included in Appendix D. High-speed data plots showing fuel injection pressure, cylinder pressure, heat release rate, and cumulative heat release versus crank angle for all the high speed data points are included in Appendix E.

D. Combustion Analysis Results

The poor LHR engine performance and emissions were attributed to degraded combustion. Figure 27 is a plot of apparent heat release rate versus crank angle comparing the Baseline Metal engine with the Baseline Ceramic engine results at 2000 rpm, full load. Combustion in the LHR engine was characterized by less premixed burning, lower heat release rates, and longer combustion duration compared to the Baseline Metal engine. This same combustion trend was preserved when the coolant temperature was increased in the LHR engine as shown in Figure 28.

Figure 28 is a plot comparing the apparent heat release rates of the Baseline Ceramic engine with the Hot Ceramic engine at 2000 rpm, full load. The + and * symbols in Figures 27 and 28 designate the heat release rate centroids for the different test conditions as shown in the Figures. The centroid for the Baseline Ceramic engine in Figure 27 shifted to the right due to the reduced premixed burning and longer combustion duration. The centroid for the Hot Ceramic engine in Figure 28 was also shifted to the right compared to the Baseline Ceramic engine centroid. Studies (ref. 28) have shown that engine efficiency is maximized when the heat release rate centroid corresponds to engine top dead center. A shift in the heat release rate centroid away from top dead center, therefore results in an efficiency reduction. The longer combustion duration for the LHR engine also resulted in reduced thermal efficiency because engine thermal efficiency is reduced as the heat release process (heat addition to the system) deviates from the ideal constant volume process.

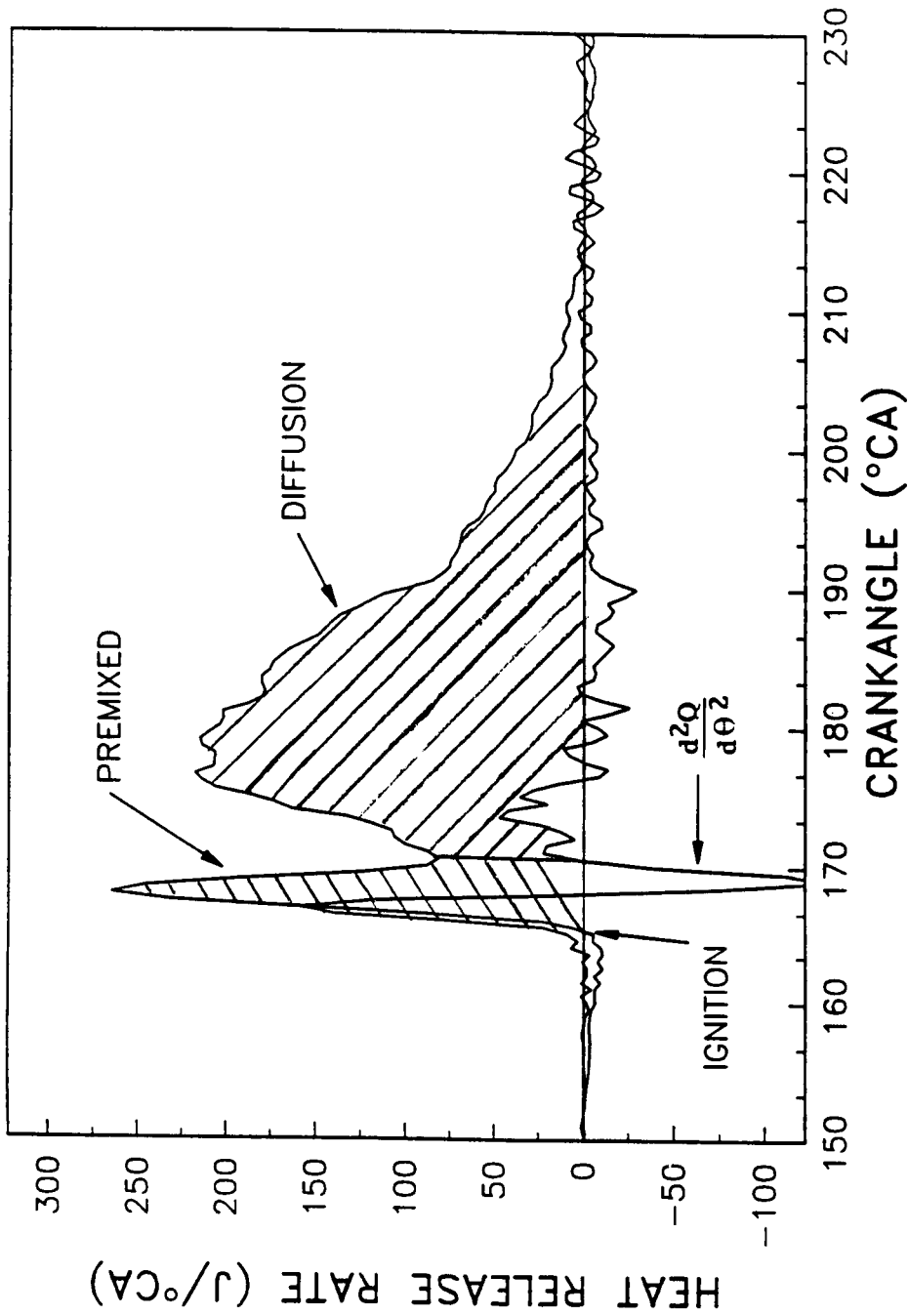


FIGURE 26. HEAT RELEASE RATE VERSUS CRANKANGLE PLOT SHOWING DEFINITION OF COMBUSTION PARAMETERS

COMBUSTION RESULTS, 2000 RPM FULL LOAD

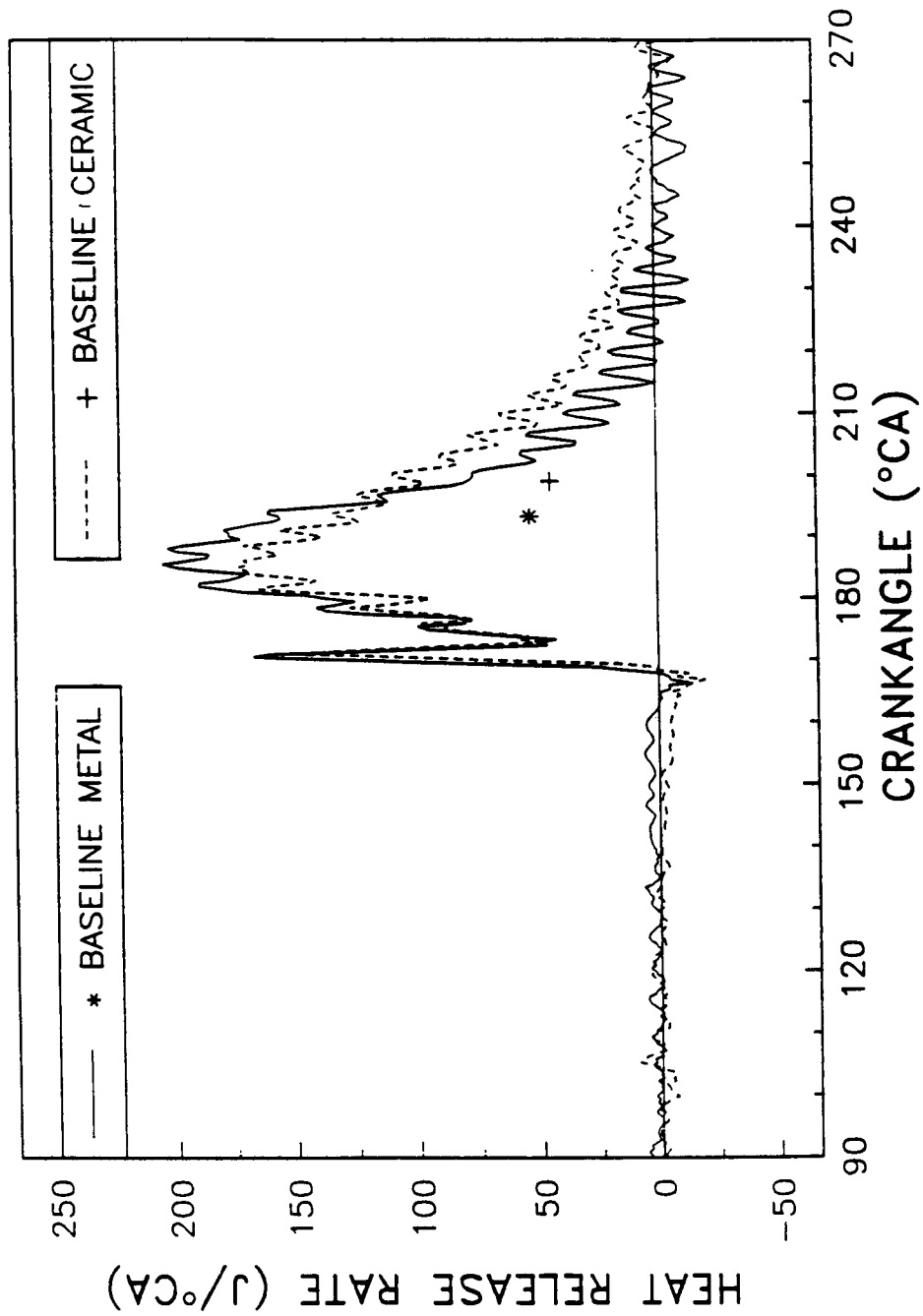


FIGURE 27. HEAT RELEASE RATE VERSUS CRANKANGLE FOR BASELINE METAL AND BASELINE CERAMIC TEST CONDITIONS, 2000 RPM, FULL LOAD

COMBUSTION RESULTS, 2000 RPM FULL LOAD

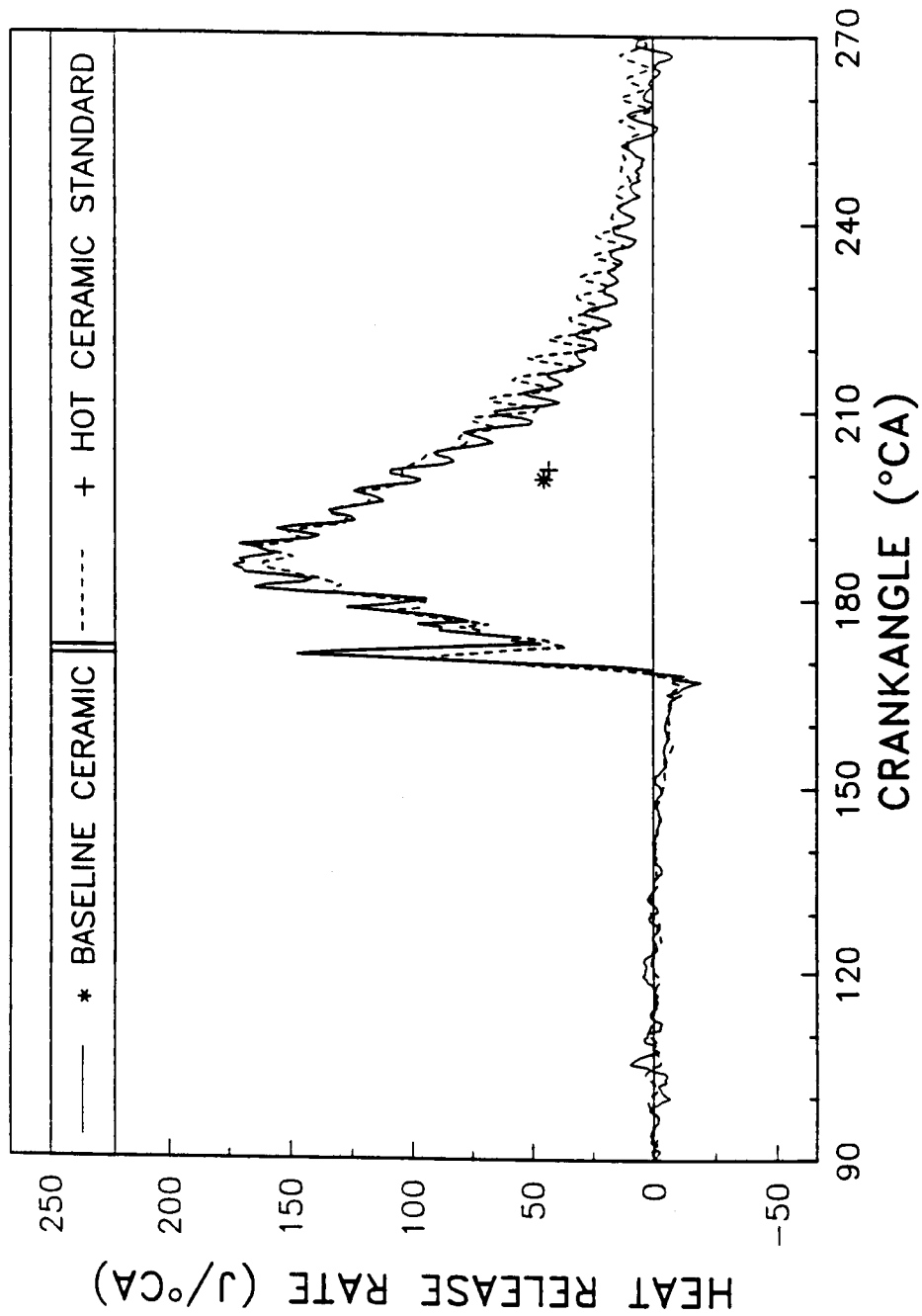


FIGURE 28. HEAT RELEASE RATE VERSUS CRANKANGLE FOR BASELINE CERAMIC AND HOT CERAMIC TEST CONDITIONS, 2000 RPM, FULL LOAD

The obvious question is, why does the LHR engine have prolonged combustion? One might first suspect that the prolonged combustion is the result of increased fuel injection duration. The fuel injection pressure versus crank angle curves corresponding to the heat release rate curves shown in Figures 27 and 28 are shown in Figures 29 and 30, respectively. Figure 29 is a plot of fuel injection pressure versus crank angle for the Baseline Metal and Baseline Ceramic engines at 2000 rpm, full load. The fuel injection curves are essentially identical for the two test conditions. The fuel rate was held constant for the two test conditions shown in Figure 29 so the increased LHR combustion duration can not be attributed to increased fueling.

A comparison between the Baseline Ceramic and Hot Ceramic fuel injection pressure curves is shown in Figure 30. The cracking pressure for the fuel injector was approximately 16 MPa; therefore, the start of fuel injection was the same for both engine configurations. The fuel injection pressure curve was shifted to the right and peak pressure was reduced slightly for the Hot Ceramic engine compared to the Baseline Ceramic engine as shown in Figure 30. The change in fuel injection pressure characteristics was attributed to changes in fuel viscosity with temperature. The fuel temperature at the point of fuel injection was not measured; however, the temperature at the tip of the fuel injector holder increased by approximately 250°C for the Hot Ceramic engine compared to the Baseline Ceramic engine. This increase in holder temperature should be indicative of the increase in fuel temperature since the engine does not have a recirculating fuel system. At 2000 rpm, full-load, the fuel injector holder temperature increased from 233°C for the Baseline Ceramic engine to 481°C for the Hot Ceramic engine. After completing the LHR engine tests, the fuel injector was bench-tested. The cracking pressure was 16 MPa (the same as Baseline) and no visual degradation in fuel spray formation was observed.

The shift in the Hot Ceramic engine fuel injection pressure curve resulted in a slight increase in fuel injection duration of approximately 3 degrees crank angle at 2000 rpm full load. The increase in fuel injection duration partially explains the increase in combustion duration for the Hot Ceramic engine compared to the Baseline Ceramic engine. The increase in combustion duration will be discussed further in Section VII.

A summary of the combustion analysis results for the three test conditions of Baseline Metal, Baseline Ceramic, and Hot Ceramic at 2000 rpm, full load are shown in Table 4. As shown earlier, the fuel-injection duration was unchanged between the Baseline Metal and Baseline Ceramic engines. The fuel-injection duration increased by 3 degrees for the Hot Ceramic engine as shown in Table 4.

The ignition delay was reduced only slightly for the insulated engines because the intake air temperature was held constant at 82°C for all test conditions. Further analysis using the IRIS engine model showed that the unburned gas temperature during the ignition delay period was only 10°C higher for the Hot Ceramic engine compared to the Baseline Metal engine. The premixed burning was reduced and the combustion duration increased as the engine was insulated and the coolant temperature increased. The longer combustion duration resulted in lower peak cylinder pressures and lower indicated thermal efficiencies as shown in Table 4.

Selected results of the high-speed data analysis for all three load conditions are shown in Figures 31 through 33. Figure 31 is a plot of fuel injection duration, ignition delay period, and combustion duration versus indicated power for the engine at 2000 rpm. The results in Figure 31 show that the fuel-injection duration for the Baseline Metal and Baseline Ceramic engines were identical. The fuel-injection duration increased slightly for the Hot Ceramic engine with a maximum increase of 3 degrees occurring at full-load. The longer fuel-injection duration for the Hot Ceramic engine was attributed to changes in fuel viscosity with temperature. The increased fuel-injection duration was not attributed to increased fueling since the fuel flow was held constant at each load setting for all three test conditions.

The ignition delay period was identical for all three test conditions at the lowest load condition. The ignition delay period was reduced at the full load conditions for the insulated engine test conditions as shown in Figure 31 and Table 4. The change in ignition delay period among the three test conditions were small because the intake air temperature was held constant at 82°C.

COMBUSTION RESULTS, 2000 RPM FULL LOAD

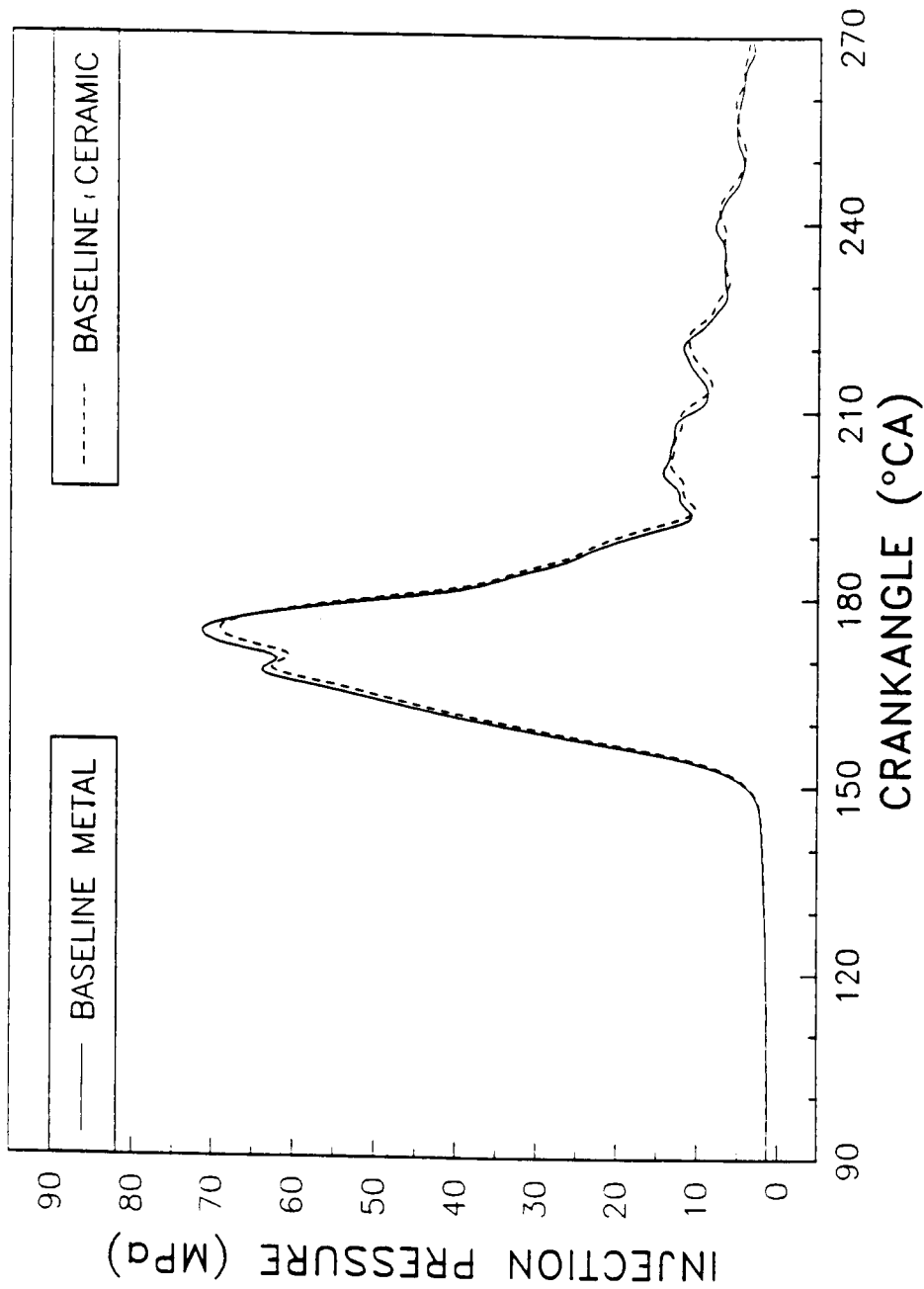


FIGURE 29. FUEL-INJECTION PRESSURE VERSUS CRANKANGLE FOR BASELINE METAL AND BASELINE CERAMIC TEST CONDITIONS, 2000 RPM, FULL LOAD

COMBUSTION RESULTS, 2000 RPM FULL LOAD

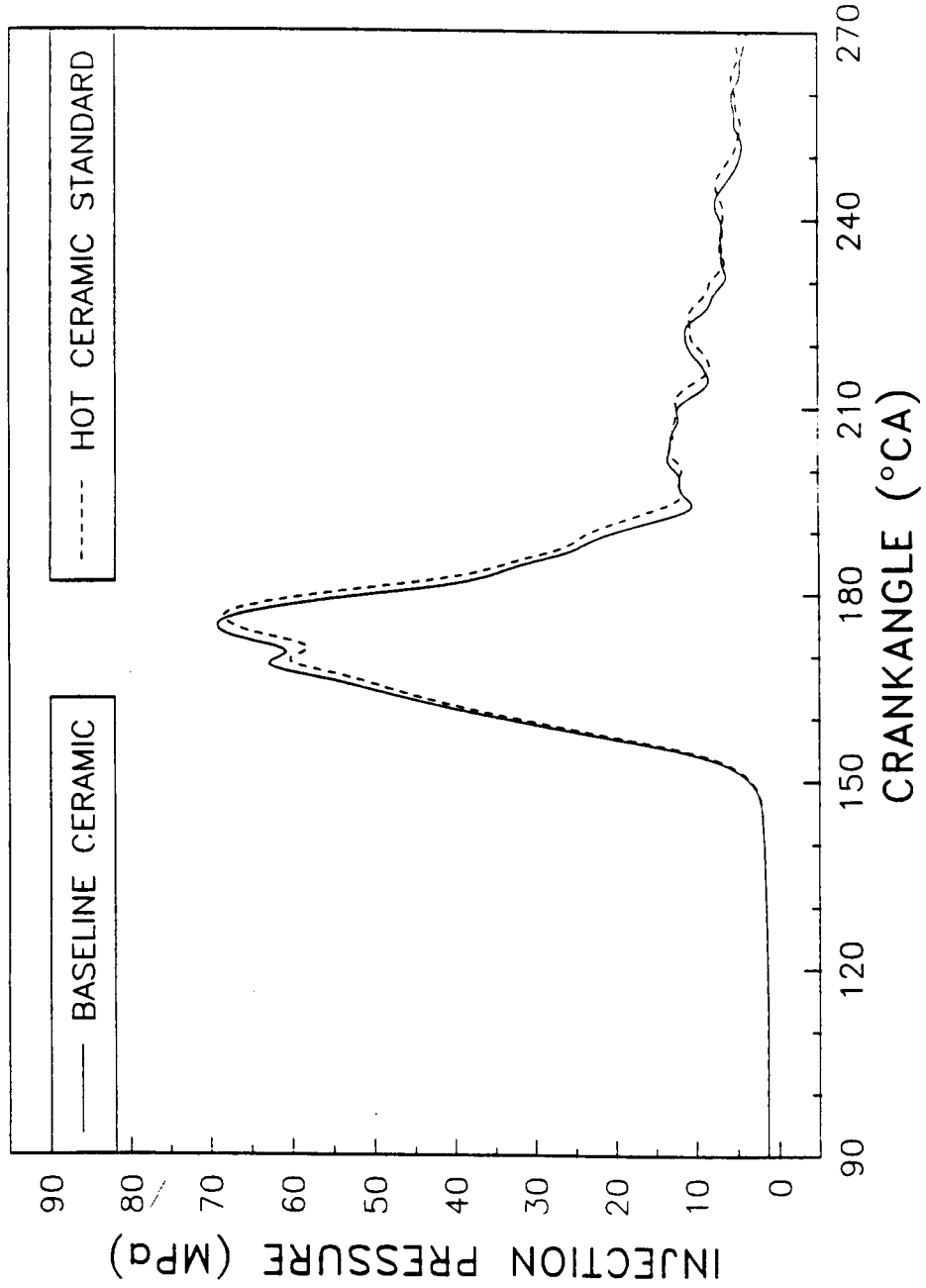


FIGURE 30. FUEL-INJECTION PRESSURE VERSUS CRANKANGLE FOR BASELINE CERAMIC AND HOT CERAMIC TEST CONDITIONS, 2000 RPM, FULL LOAD

COMBUSTION RESULTS, 2000 RPM

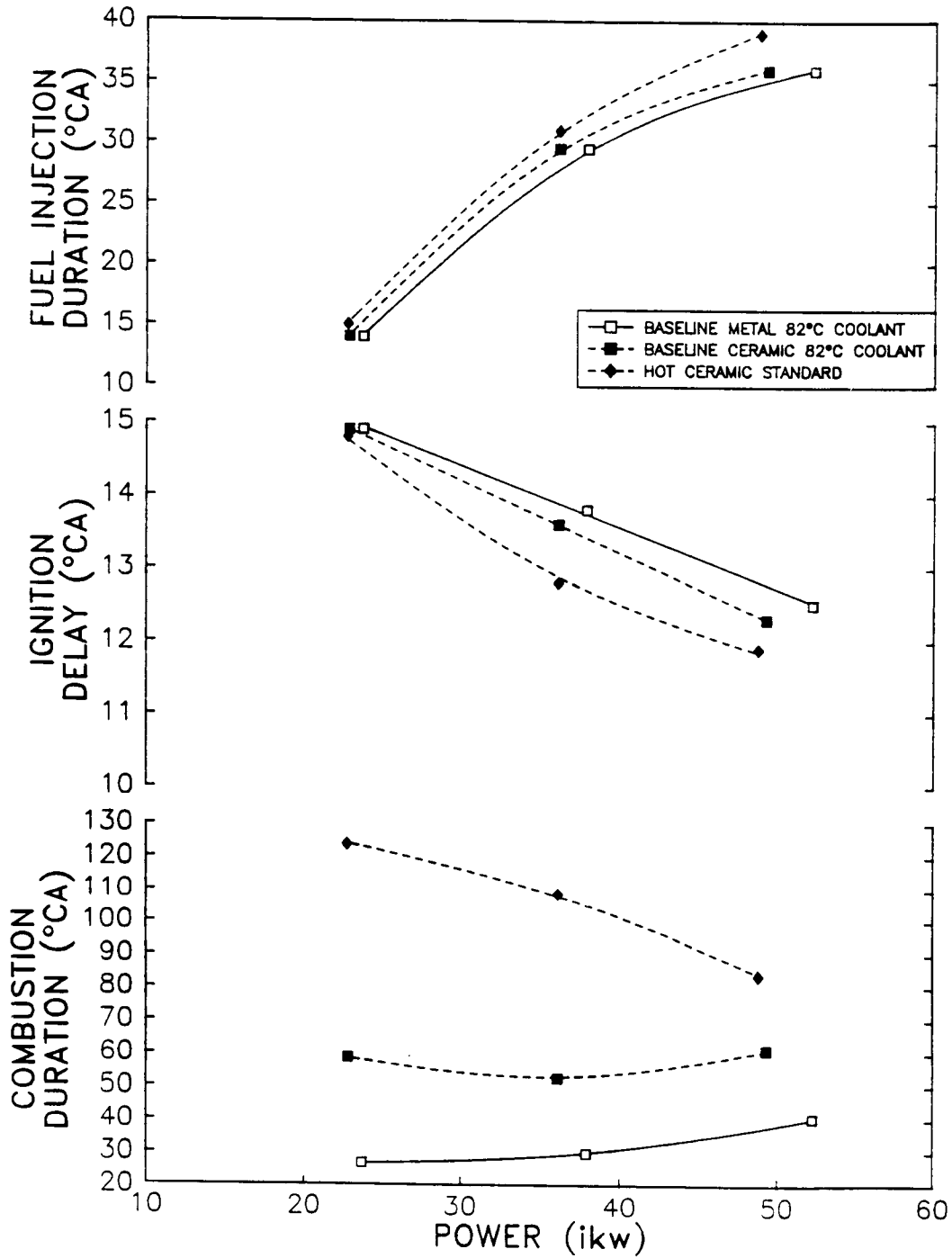


FIGURE 31. FUEL-INJECTION DURATION, IGNITION DELAY, COMBUSTION DURATION VERSUS INDICATED POWER, 2000 RPM

COMBUSTION RESULTS, 2000 RPM

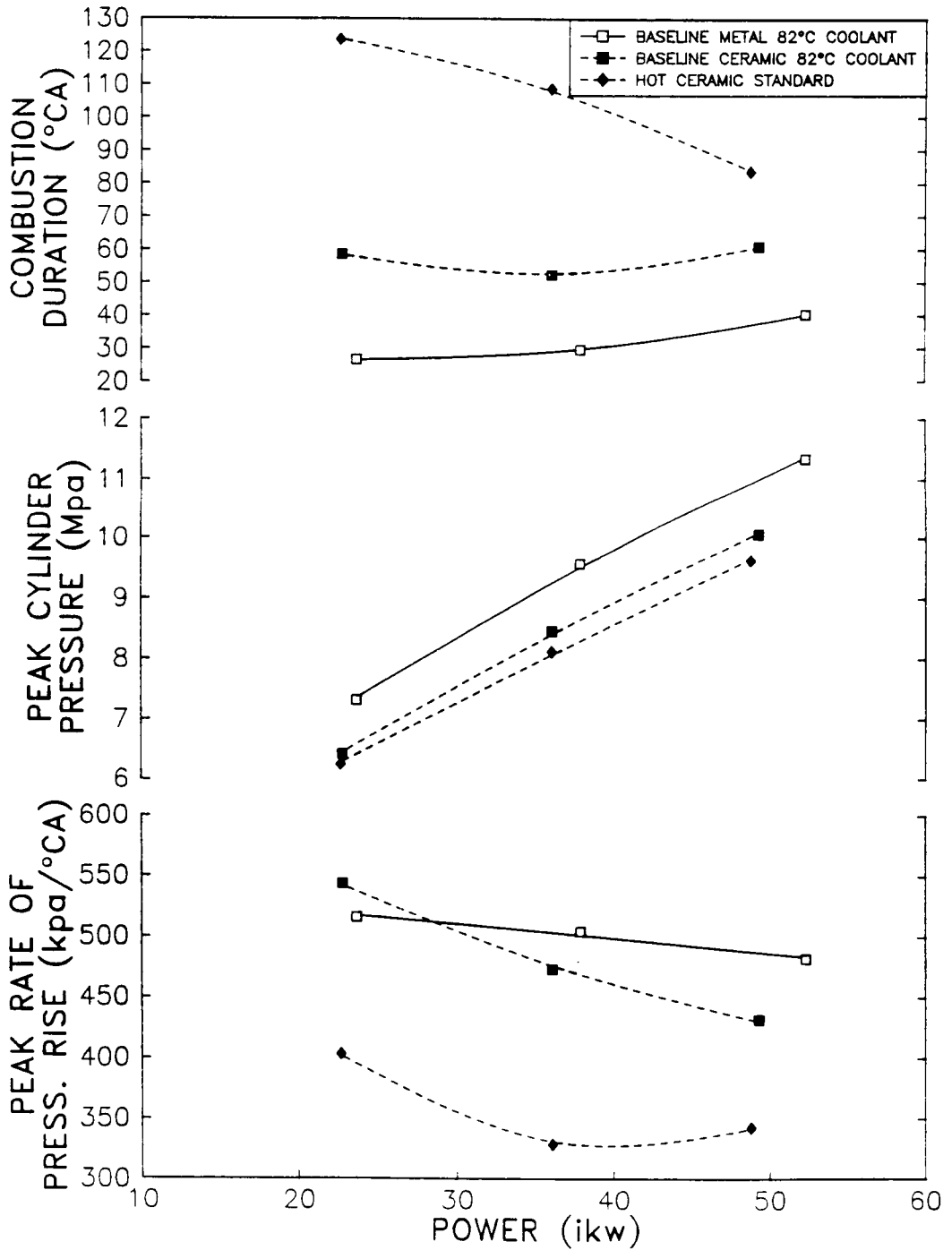


FIGURE 32. COMBUSTION DURATION, PEAK CYLINDER PRESSURE, PEAK RATE OF PRESSURE RISE VERSUS INDICATED POWER, 2000 RPM

COMBUSTION RESULTS, 2000 RPM

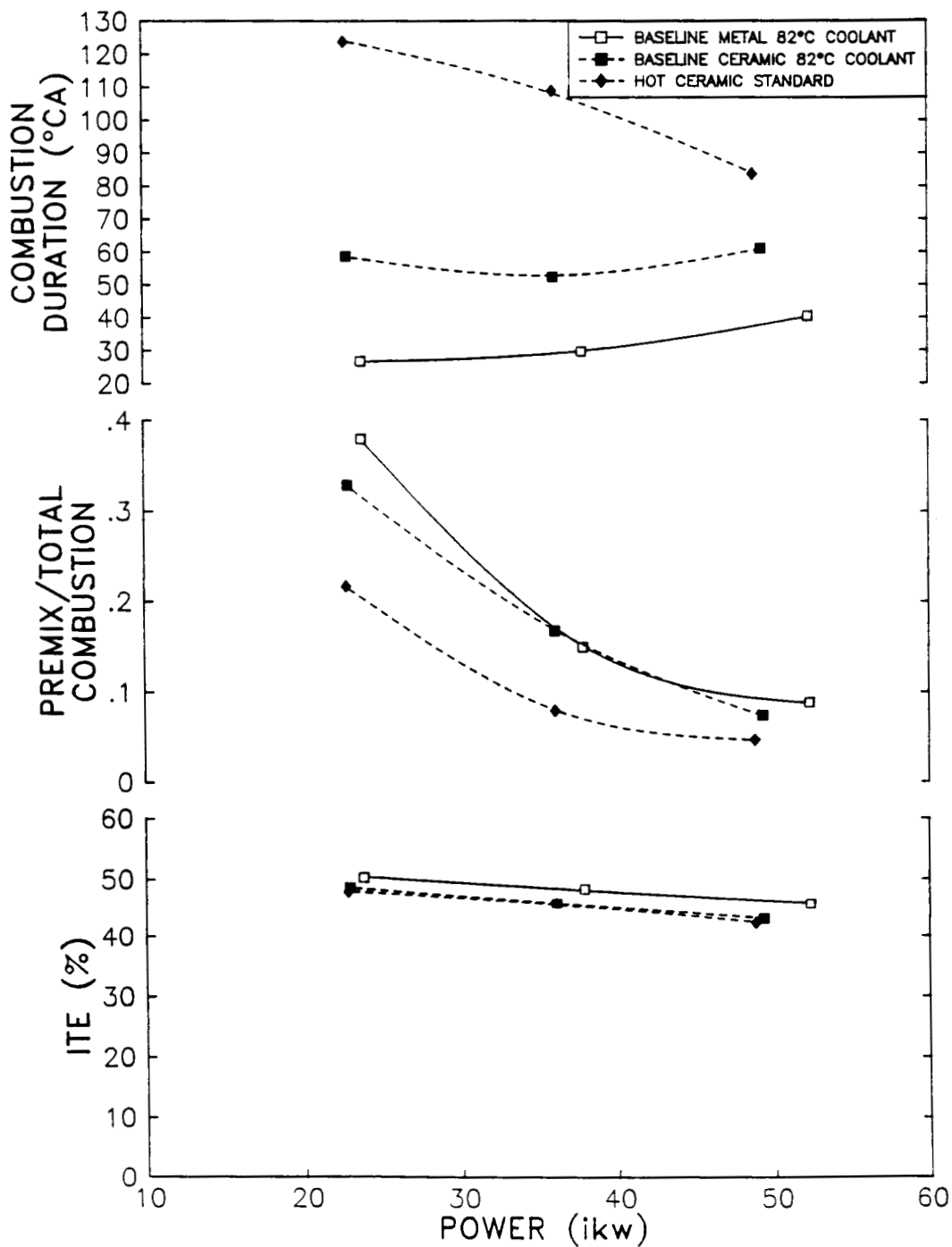


FIGURE 33. COMBUSTION DURATION, PREMIX/TOTAL COMBUSTION, ITE VERSUS INDICATED POWER, 2000 RPM

Table 4. Combustion Analysis 2000 rpm, Full Load

Engine Test Condition	Inject. Duration (Degree)	Fuel Ignition Delay (Degree)	Combust. Duration (Degree)	Premix/Total Heat Release	Peak Cylinder Pressure (MPa)	Indicated Thermal Efficiency
Baseline Metal	36.0	12.5	40.5	0.09	11.34	45.7
Baseline Ceramic	36.0	12.3	61.2	0.07	10.06	43.1
Hot Ceramic	39.0	11.9	83.6	0.05	9.63	42.3

The combustion duration increased when the engine was insulated and run at Baseline conditions as shown in Figure 31. The combustion duration increased even more for the Hot Ceramic engine. Other researchers (ref. 6, 19, 20, 26, 28, 29) have observed prolonged combustion duration in LHR engines. One researcher (ref. 26) hypothesized that the prolonged combustion was due to an increase in the fuel-injection duration although there was no evidence to support this theory since the fuel-injection period was not measured. SwRI, however, has shown that in this case, only a very small portion of the prolonged combustion duration is due to increased fuel-injection duration.

The effect of prolonged combustion duration on the peak cylinder pressure and peak rate of pressure rise is shown in Figure 32. The insulated engine's reduced premixed burning and longer combustion duration resulted in lower peak cylinder pressures and lower pressure rise rates compared to the Baseline Metal engine.

The effect of the prolonged combustion duration on the premixed/total heat release ratio and indicated thermal efficiency (ITE) is shown in Figure 33. The LHR engine's reduced premixed burning and longer combustion duration resulted in a lower premix/total heat release ratio and lower ITE. Engine thermal efficiency is reduced as the combustion period deviates from the ideal constant volume process.

E. Effects on Cylinder Pressure

The peak firing pressure was reduced for the LHR engine compared to the Baseline Metal engine as shown in Figure 34. This reduction in peak cylinder pressure can be partially attributed to the LHR engine's reduced premixed combustion and longer combustion duration. However, a reduction in peak cylinder pressure was also observed for the insulated engine during motoring tests, as shown in Figure 35. There are several possible explanations for the observed reduction in peak cylinder pressure that will be presented in the Discussion section (Section VII) of this report.

F. Insulated Engine Durability

The objective of this project was to determine the effect of LHR engine operation on engine performance, emissions, and combustion. The objective was not to develop an LHR engine but simply to construct one that would have sufficient durability to complete engine testing.

The LHR engine was constructed using a ceramic coated fire deck, intake valves, exhaust valves, piston crown, and top portion of the cylinder liner. Figures 36 through 39 are photographs of these components after 95 hours of insulated engine tests. Figure 36 shows the fire deck, intake valves,

FIRING ENGINE 2000 RPM, FULL LOAD

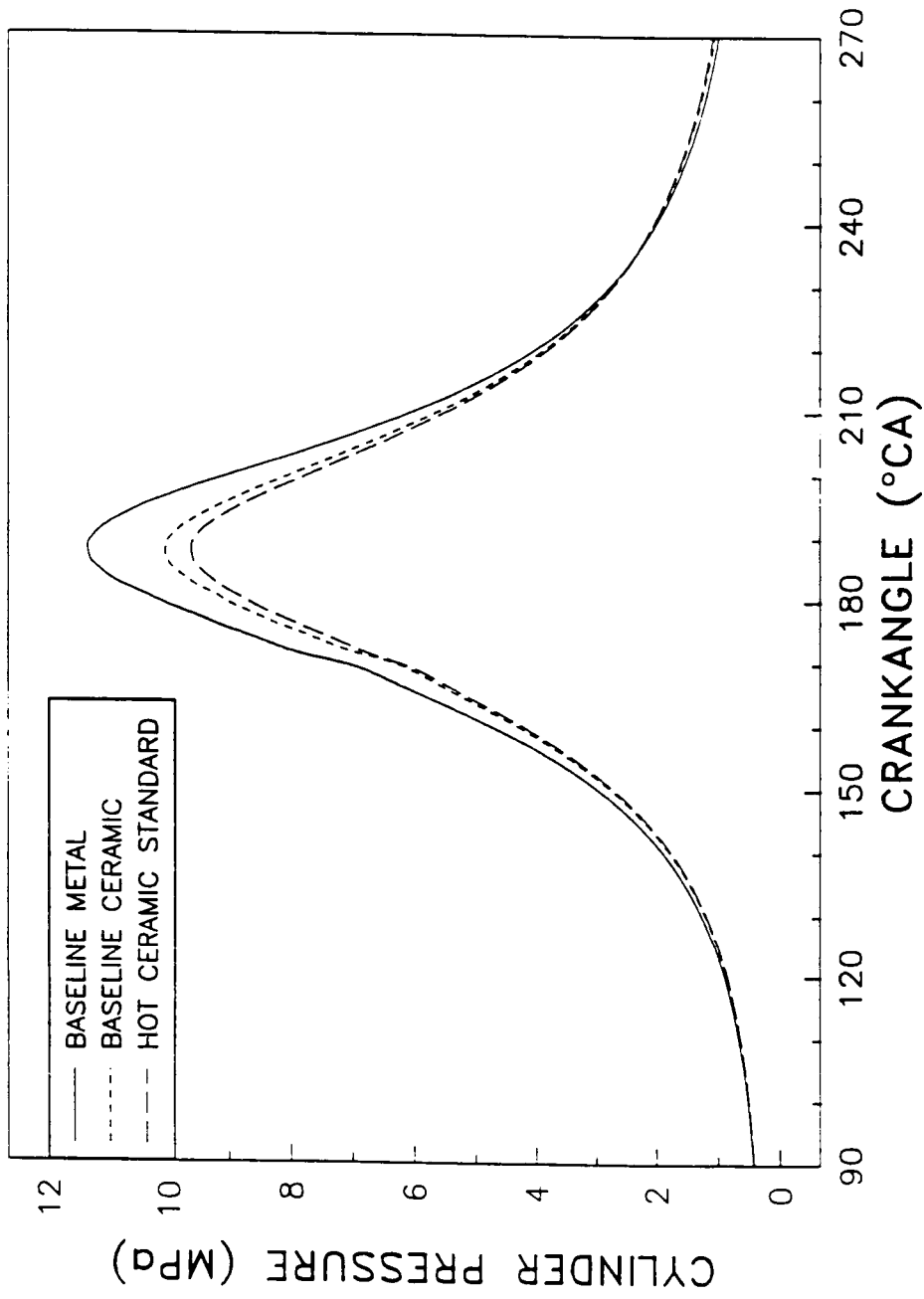


FIGURE 34. COMPARISON BETWEEN BASELINE METAL, BASELINE CERAMIC, HOT CERAMIC ENGINE FIRING CYLINDER PRESSURE, 2000 RPM, FULL LOAD

MOTORING ENGINE 2000 RPM

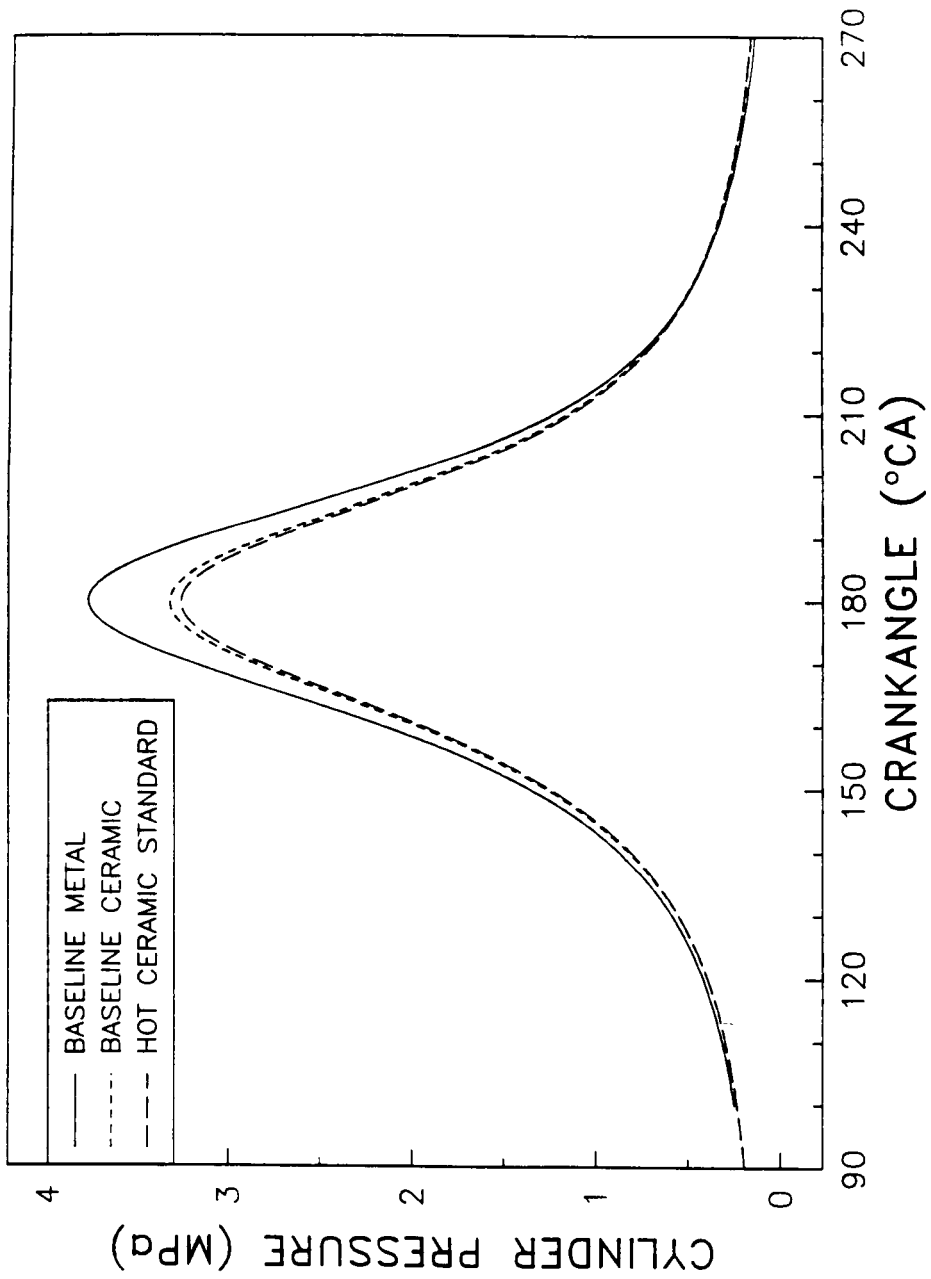


FIGURE 35. COMPARISON BETWEEN BASELINE METAL, BASELINE CERAMIC, HOT CERAMIC ENGINE MOTORING CYLINDER PRESSURE, 2000 RPM, FULL LOAD

ORIGINAL PAGE IS
OF POOR QUALITY

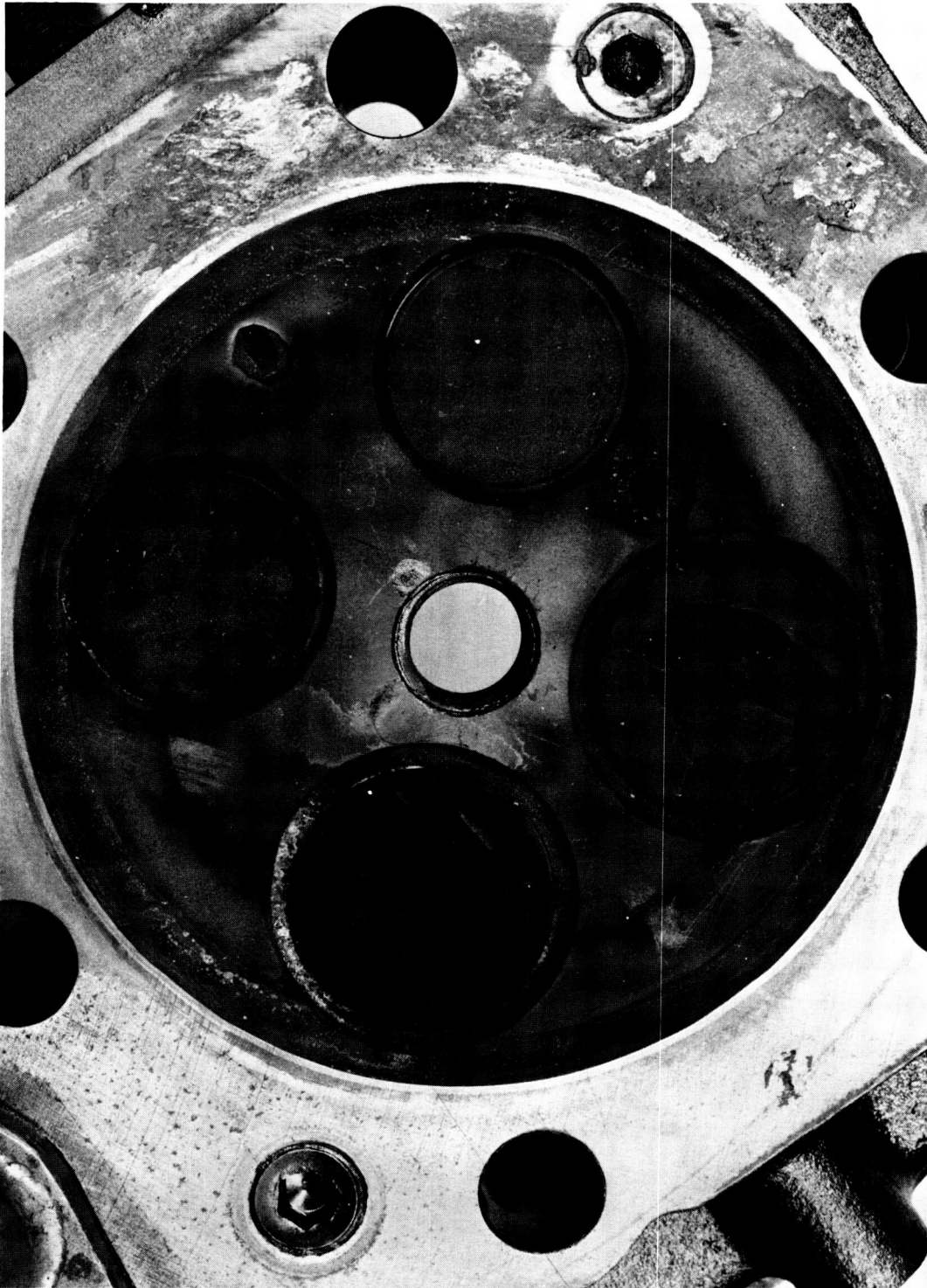


FIGURE 36. PHOTOGRAPH SHOWING CERAMIC-COATED
FIREDECK, INTAKE VALVES, AND EXHAUST VALVES
AFTER 95 HOURS OF LHR ENGINE TESTS

ORIGINAL PAGE IS
OF POOR QUALITY

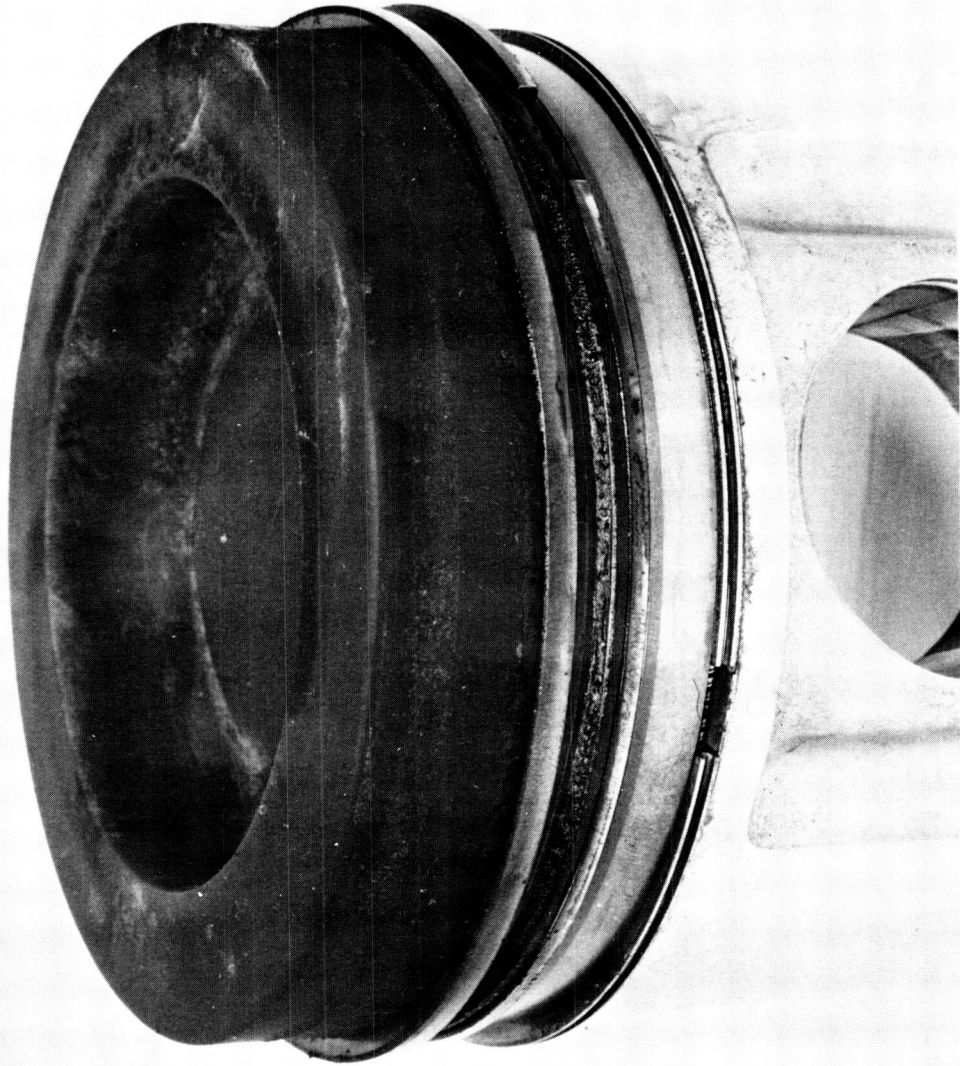


FIGURE 37. PHOTOGRAPH SHOWING CERAMIC-COATED
PISTON CROWN (SIDE VIEW) AFTER 95 HOURS OF LHR
ENGINE TESTS

ORIGINAL PAGE IS
OF POOR QUALITY



FIGURE 38. PHOTOGRAPH SHOWING CERAMIC-COATED
PISTON CROWN (TOP VIEW) AFTER 95 HOURS OF LHR
ENGINE TESTS

ORIGINAL PAGE IS
OF POOR QUALITY

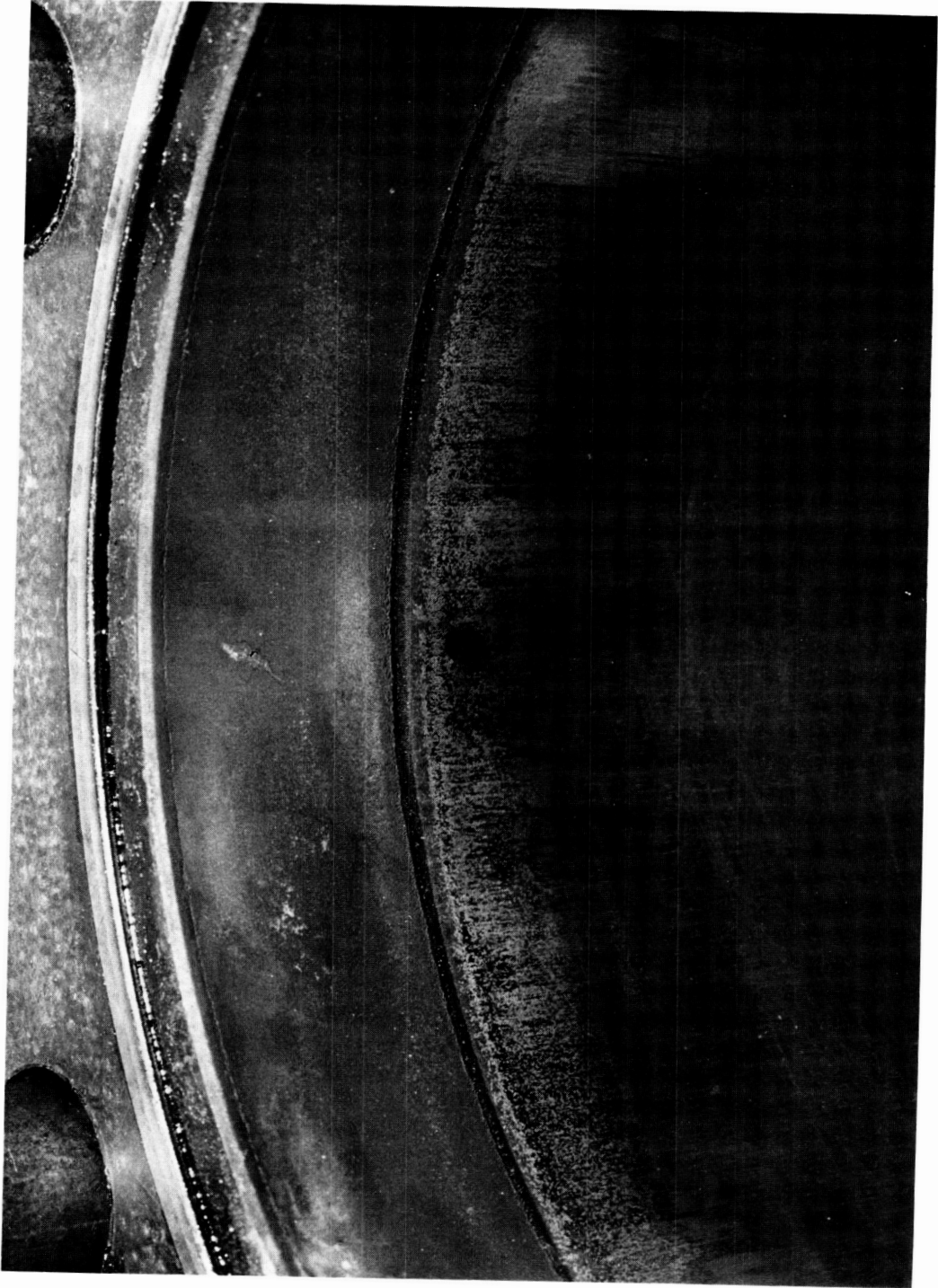


FIGURE 39. PHOTOGRAPH SHOWING TOP PORTION OF
CYLINDER LINER COATED WITH CERAMIC MATERIAL
AFTER 95 HOURS OF LHR ENGINE TESTS

and exhaust valves. Ceramic material was missing from both exhaust valves, one intake valve, and from 75 percent of the second intake valve. The fire deck ceramic coating remained intact. The piston crown is shown in Figures 37 and 38. After 95 hours of operation, ceramic material was missing from the piston bowl and from one thumb sized spot on the piston top as shown in Figure 38. The top portion of the cylinder liner is shown in Figure 39. Only the top 21.6 mm of the liner was coated with ceramic material and a 0.254 mm thick coating of chrome oxide. No ceramic material was missing from the top portion of the liner as shown in Figure 39. The chrome oxide coating may have improved the durability of the ceramic coating.

After 95 hours of insulated engine operation, the engine tests were stopped because of an apparent increase in blowby. The increased blowby was thought to be the result of a scuffed liner or blown head gasket. The engine was torn down and inspected. The head gasket and cylinder liner were both in good condition. The cause of the increased blowby turned out to be a melted fuel injector holder O-ring gasket as shown in Figure 40. The melted O-ring gasket allowed compressed air (used as the cylinder head coolant for the Hot Ceramic engine tests) to leak from the cylinder head and pressurize the engine crank case causing the apparent increase in blowby. The two thermocouples shown in Figure 40 were mounted in the tip of the fuel injector holder to measure fire deck temperature.

The time(s) that the ceramic material was lost from the combustion chamber is (are) not known. It appears that the ceramic coating broke off in large chunks although an in-depth failure analysis was not conducted.

G. Oil Analysis

Valvoline Turboguard 5 oil was used for all engine tests. The engine oil capacity including heat exchanger and filters was approximately 10 liters. Oil was sampled and analyzed before each oil change. The results are shown in Table 5. The zero hour test (Column 1) was conducted with new oil. Baseline Ceramic engine tests were conducted before the oil changes that occurred at 41.3 and 62.9 hours of operation. Hot Ceramic engine tests were conducted between the 62.9 and 94.7 hour oil changes. As shown in Table 5, the oil properties did not change significantly during the 31.8 hours of Hot Ceramic engine tests. Oil viscosity was reduced only 1 or 2 percent during this period. The small change in oil properties was probably the result of frequent oil changes, large oil capacity, and the relatively low oil temperature that was not allowed to exceed 121°C.

ORIGINAL PAGE IS
OF POOR QUALITY

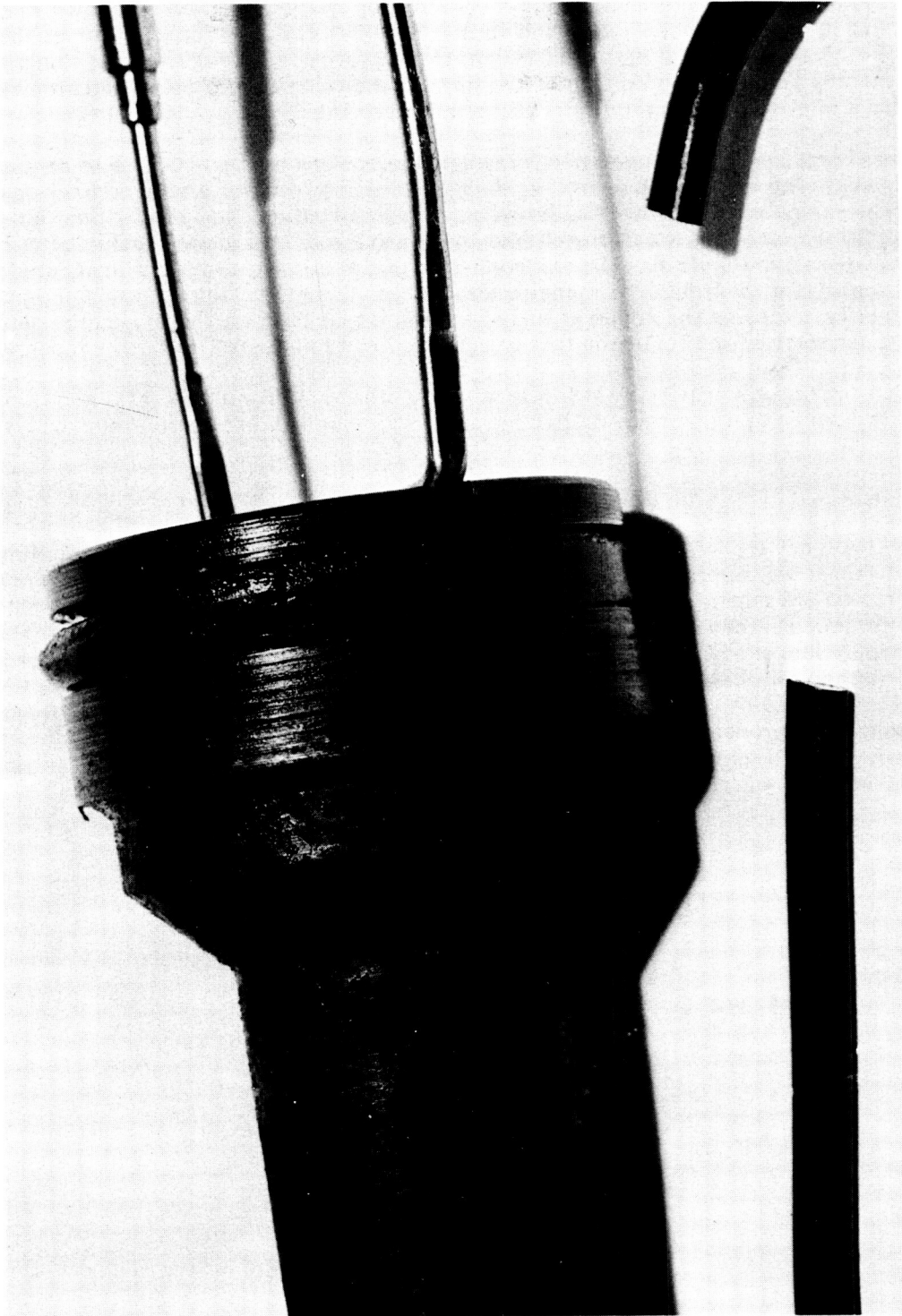


FIGURE 40. PHOTOGRAPH SHOWING MELTED FUEL
INJECTOR HOLDER O-RING GASKET AFTER 95
HOURS OF LHR OPERATION

Table 5. Engine Oil Analysis

	New Oil	Baseline Ceramic Tests		Hot Ceramic Tests
Engine Hours	<u>0</u>	<u>41.3</u>	<u>62.9</u>	<u>94.7</u>
TAN	1.96	1.86	1.73	1.14
TBN	7.27	5.82	5.66	4.54
V 40°C, cSt	104.04	100.82	98.92	102.13
Vis 100°C, cSt	11.93	11.96	11.71	11.79
C-Pentane Insols, % wt	0.03	0.04	0.05	0.04
Yttrium, ppm	1	1	1	1
Iron, ppm	4	24	17	1
Chromium, ppm	1	2	1	1
Lead, ppm	1	1	1	1
Copper, ppm	1	10	23	22
Tin, ppm	17	15	22	23
Aluminum, ppm	1	1	1	1
Nickel	1	1	1	1
Silver	1	4	1	1
Manganese	1	1	1	1
Silicon	5	8	7	9
Boron	1	1	1	1
Molybdenum	2	5	1	1
Magnesium	456	423	441	437
Barium	2	2	2	2
Phosphorous	1121	1030	1061	1002
Zinc	1344	1109	1247	1226
Antimony	1	1	1	1

V. ANALYTICAL INVESTIGATION

A. Engine Stimulation

Analytical work for this project was subcontracted to Integral Technologies Incorporated (ITI). The objective of the subcontract was to use ITI's IRIS code to predict combustion chamber surface temperatures for the metal and ceramic insulated engines. A joint objective of the ITI subcontract was to use the IRIS code to interpret the SwRI experimental data concerning the effect of insulated surfaces on engine performance.

B. Model Description

The ITI IRIS code is an engine performance and thermal analysis model that includes the following features pertinent to calculation of component temperatures:

- Two zone combustion and thermodynamic simulations
- A zonal radiation model that accounts for the effects of temperature, soot particle concentration, percent burned volume, and instantaneous view factors.
- A spatially resolved flow/convection model that accounts for local effective velocities due to squish, swirl, and turbulence.
- A structural heat conduction model that employs a thermal resistance network with programmable dimensions, properties, and insulation strategy.
- A cylinder friction model based on hydrodynamic and boundary layer lubrication for the ring-liner and piston skirt-liner interfaces.

The input data required for the IRIS code includes engine design, performance, and temperature data. The input design data used for this project is included in Appendix F.

C. Baseline Engine Simulations

Baseline Metal engine performance data at 2000, 1700, and 1400 rpm for 100, 67, and 33 percent load was supplied to ITI for calibration of the IRIS engine model. The initial Baseline simulations were carried out with constant intake manifold pressure assuming no significant pressure dynamics between the plenums and the cylinder head. The initial simulation results showed that the predicted airflow rates and peak cylinder pressures were consistently lower than the SwRI measured values. The predicted exhaust gas temperature was also higher than the measured exhaust temperature. The discrepancy between predicted and measured quantities was attributed to pulsations in the intake piping that resulted in higher effective pressures in the intake port at the time of intake valve closure. The engine intake system was then modeled to predict the effective intake pressure. Engine simulations were then carried out with the IRIS code using the adjusted intake air manifold pressure. The results of the corrected simulation, presented in Figures 41 through 46, compare the measured and predicted air flow rate, IMEP, peak cylinder pressure, surface temperatures, and exhaust gas temperature. The agreement between measured and predicted values was quite good. The predicted exhaust gas temperature was slightly higher than the measured values, but considered within the range of experimental accuracy of exhaust gas temperature measurement. Measured exhaust temperatures tend to be lower than predicted values because of radiative heat loss from the hot thermocouple to the exhaust port walls.

The agreement between the IRIS and SwRI experimental results for the Baseline Metal engine was considered sufficiently accurate to provide confidence in predictions of temperature, heat transfer, and performance of the insulated engine.

AIR FLOW RESULTS

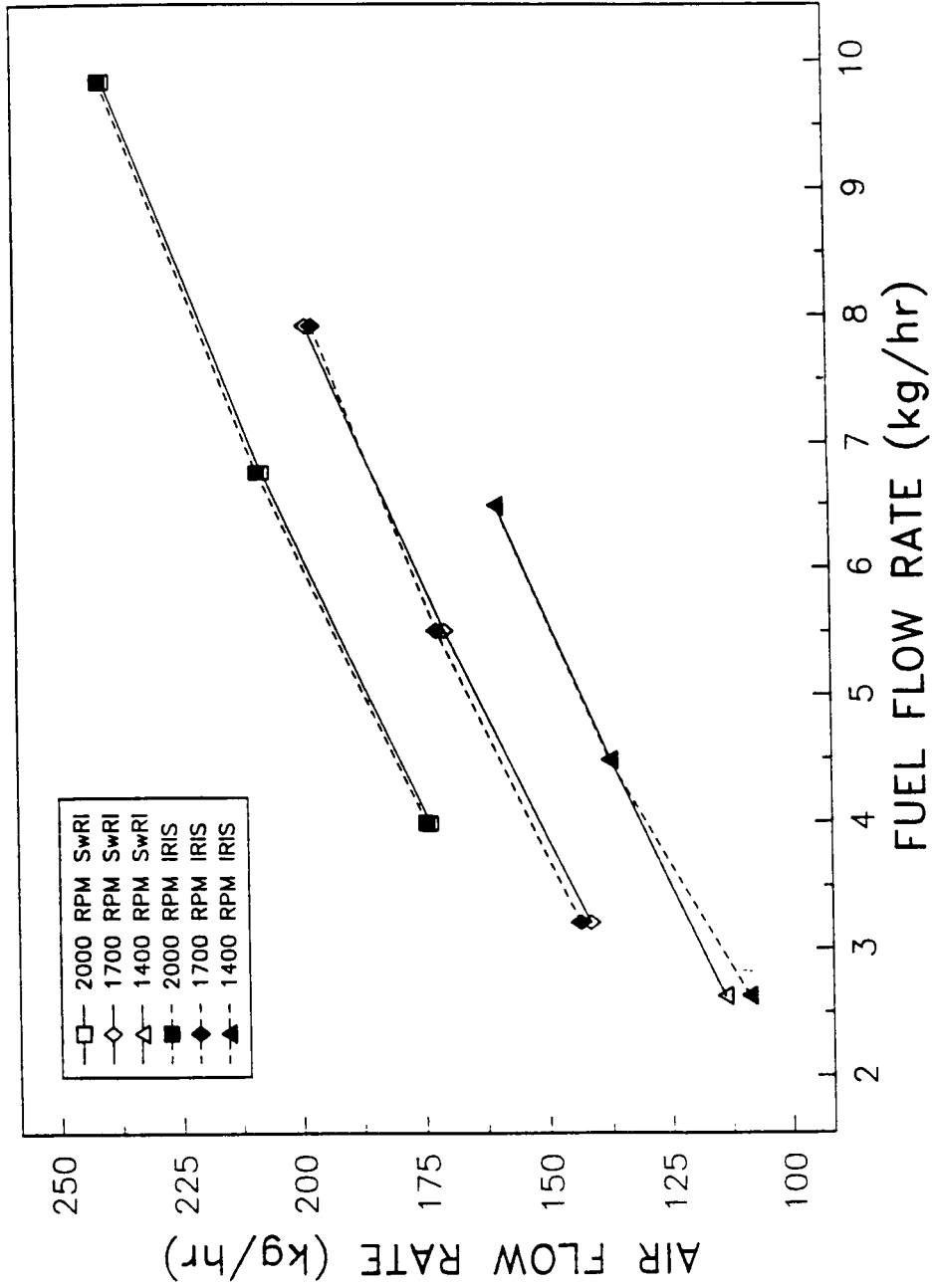


FIGURE 41. COMPARISON BETWEEN MEASURED AND PREDICTED AIR FLOW RATE

INDICATED MEAN EFFECTIVE PRESSURE RESULTS

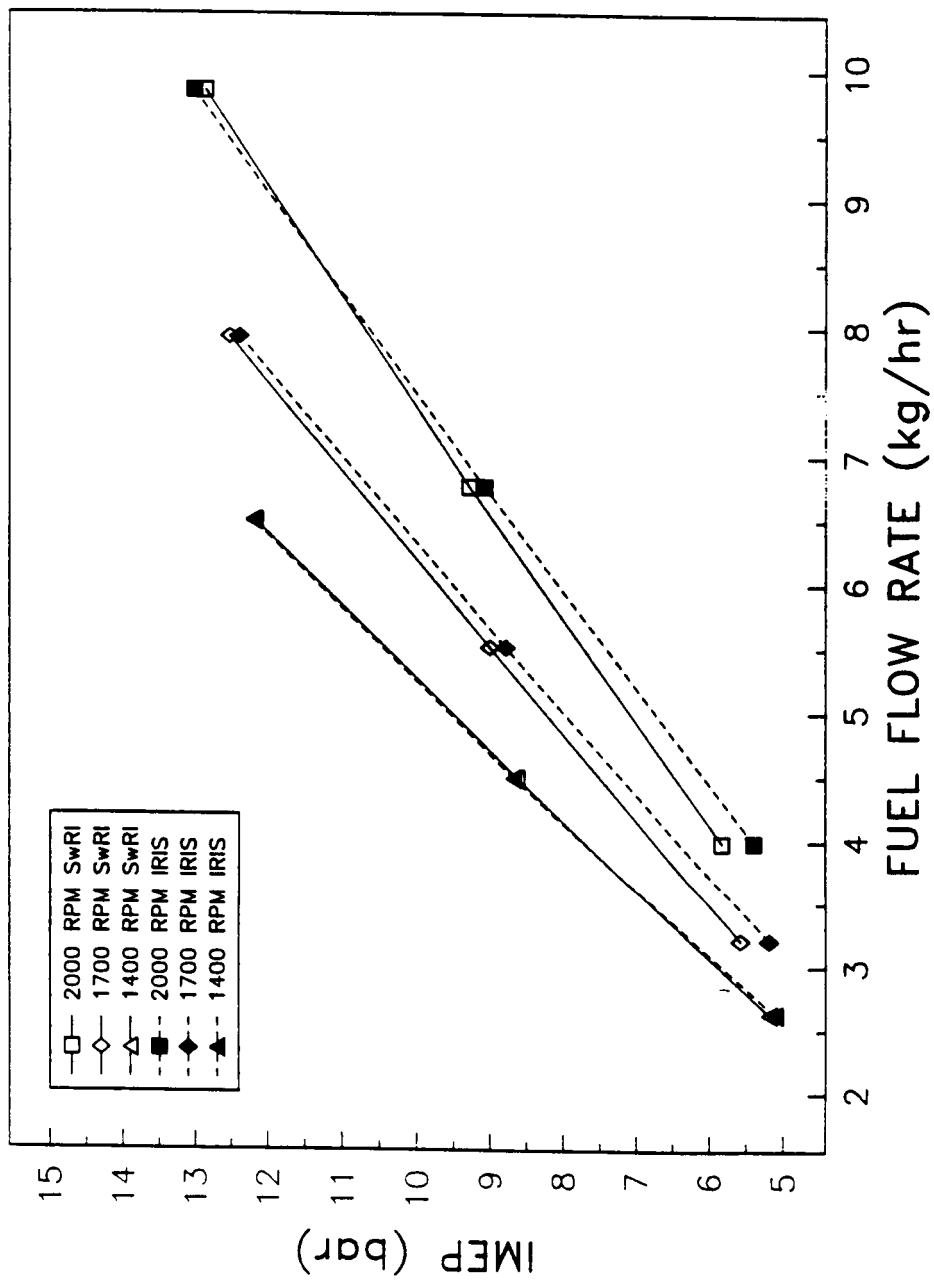


FIGURE 42. COMPARISON BETWEEN MEASURED AND PREDICTED INDICATED MEAN EFFECTIVE PRESSURE

PEAK CYLINDER PRESSURE RESULTS

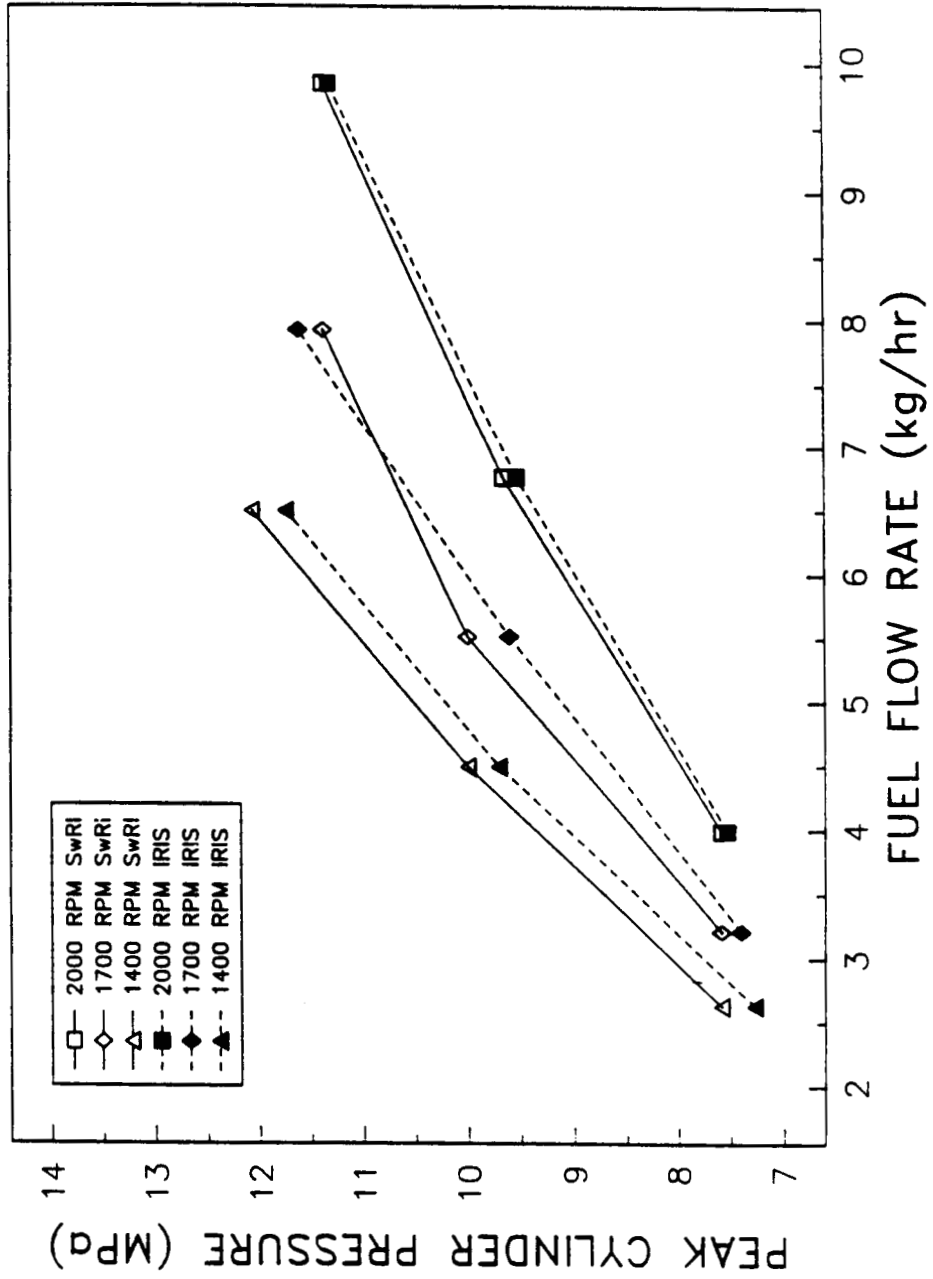


FIGURE 43. COMPARISON BETWEEN MEASURED AND PREDICTED PEAK CYLINDER PRESSURE

CYLINDER LINER TEMPERATURE RESULTS

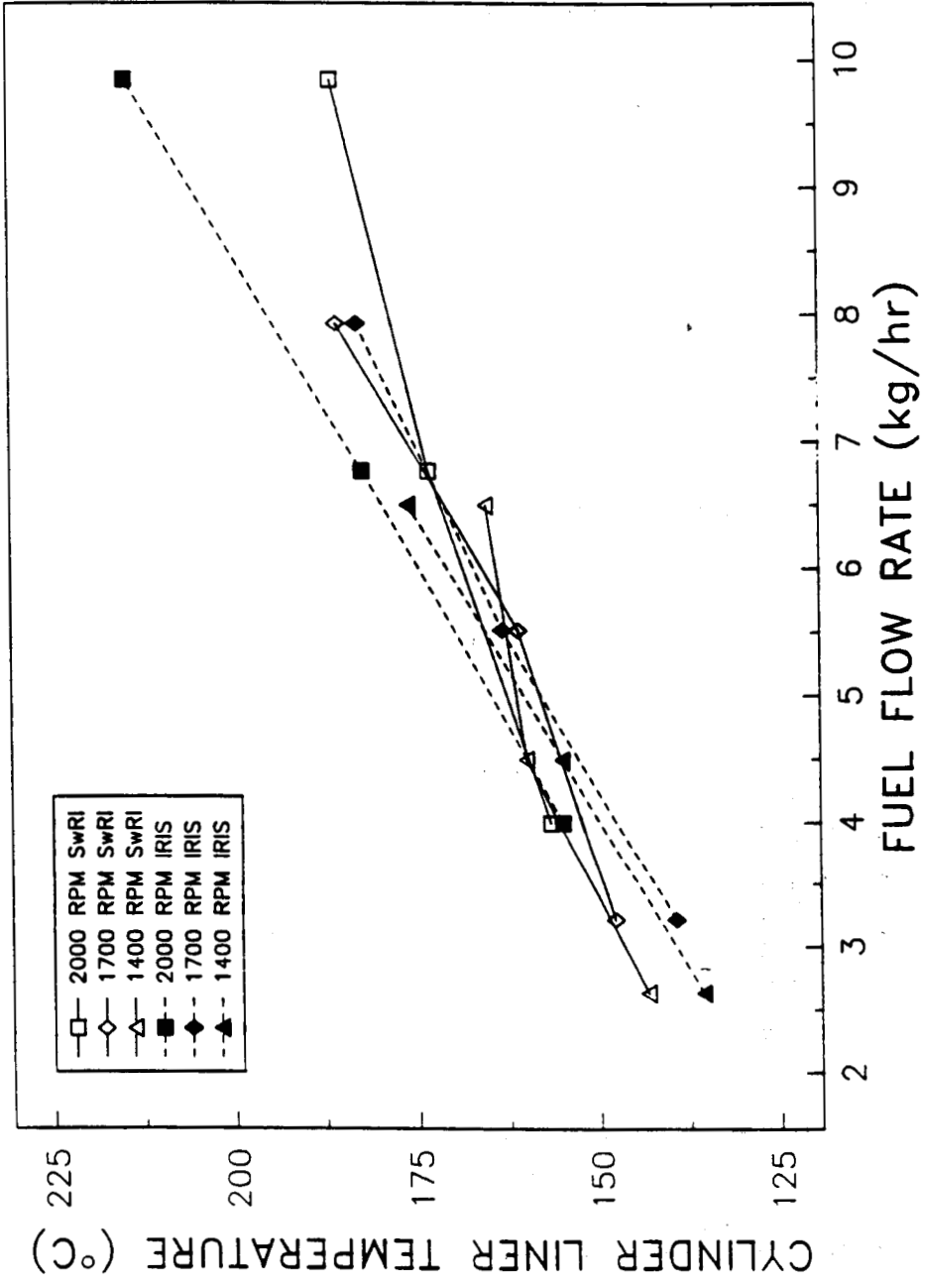


FIGURE 44. COMPARISON BETWEEN MEASURED AND PREDICTED CYLINDER LINER TEMPERATURE

FIREDECK CENTER TEMPERATURE RESULTS

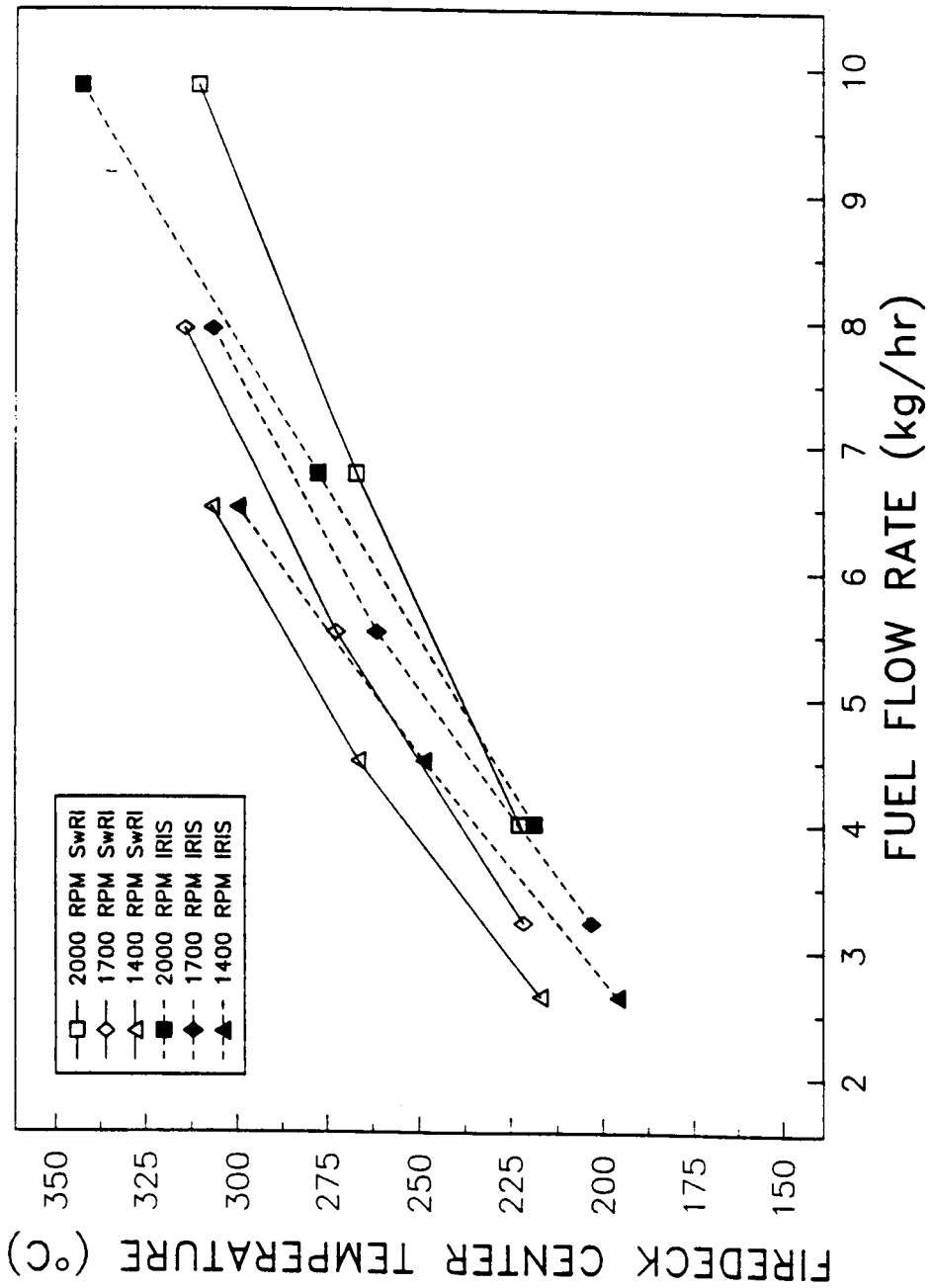


FIGURE 45. COMPARISON BETWEEN MEASURED AND PREDICTED FIREDECK CENTER TEMPERATURE

EXHAUST TEMPERATURE RESULTS

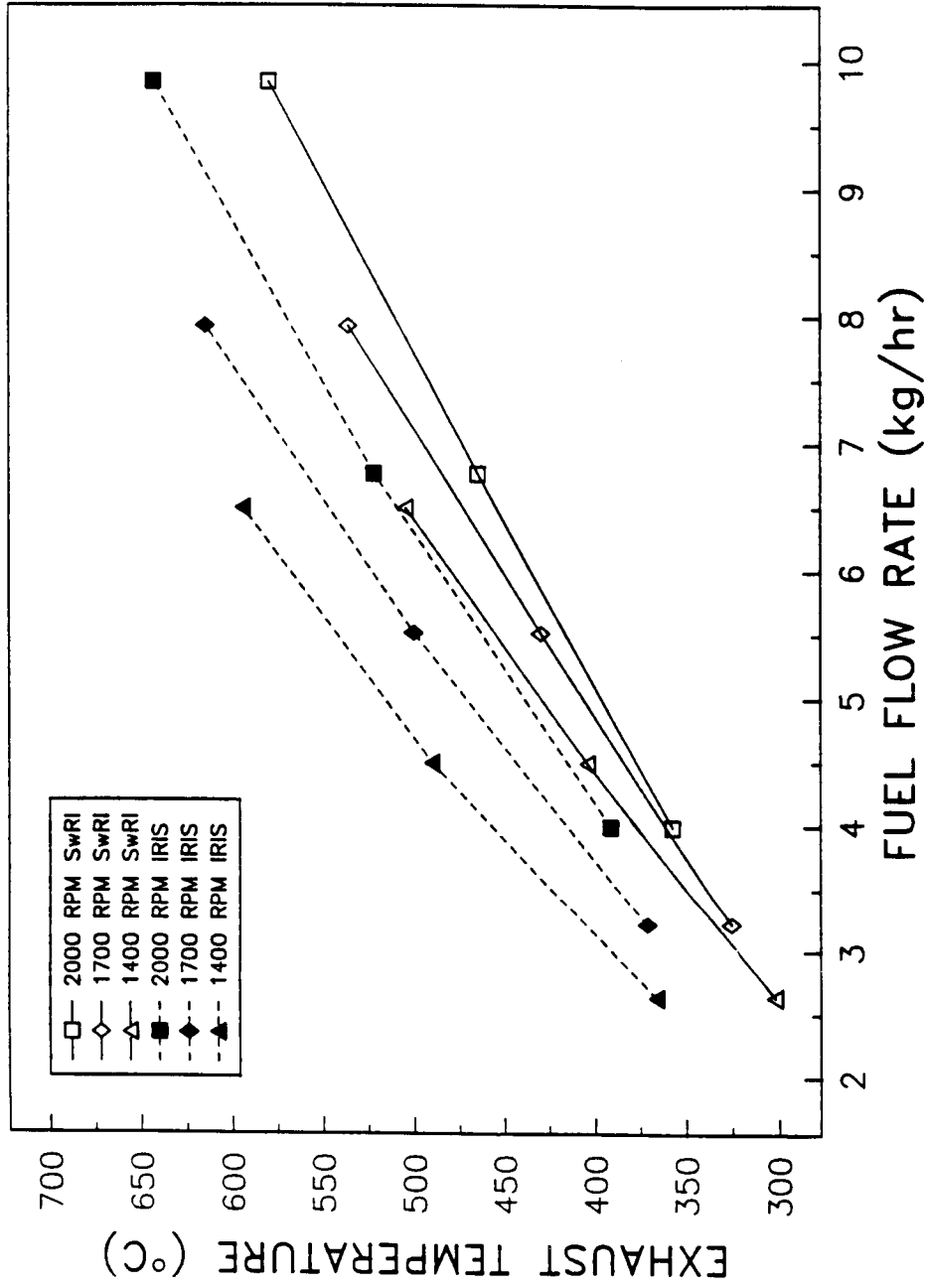


FIGURE 46. COMPARISON BETWEEN MEASURED AND PREDICTED EXHAUST GAS TEMPERATURE

D. Insulated Engine Simulations

The SwRI insulated engine data, supplied to ITI, included engine performance, temperature, and combustion results from the insulated engine test conditions. ITI used this data in conjunction with the IRIS code to predict ceramic coated combustion chamber surface temperatures, cyclic component temperatures, heat transfer rates, and engine performance parameters.

1. Engine Component Temperatures

Two engine test configurations were simulated to predict ceramic and metal combustion chamber surface temperatures. The first engine configuration simulated corresponds to SwRI run numbers 87 through 96 (Test condition No. 4 found in Appendix C) for the insulated engine with 82°C intake air and coolant temperatures. The second engine configuration simulated corresponds to SwRI run numbers 103 through 112 (Test condition No. 7 found in Appendix C) for the increased temperature insulated engine with 121°C coolant in block and no coolant in the head. The network heat conduction model used during the Baseline Metal calculations was used again with the following physical properties for the Zirconia ceramic coating:

$$\begin{aligned}k &= 0.87 \quad \text{W/mK} \\C_p &= 2.4 \times 10^6 \text{ J/m}^3\text{K}\end{aligned}$$

Figures 47 and 48 show a comparison between the ITI predicted and SwRI measured top ring reversal and fire deck center temperatures, respectively, for the Baseline Metal engine configuration. The fire deck center temperature was measured with thermocouples mounted on the exposed surface of the fuel injector holder. As shown in Figures 47 and 48 there is good agreement between predicted and measured results.

Ceramic coated surface temperatures at the piston bowl, top portion of the cylinder liner (between the top ring reversal location and top of the cylinder liner), fire deck, exhaust valve, and intake valve, not measured with thermocouples, were predicted for the same run numbers 87 through 96 (test condition No. 4). The results are shown in Figures 49 through 53.

A comparison between the predicted and measured top ring reversal and fire deck temperatures for the Hot Ceramic insulated engine configuration are shown in Figures 54 and 55 respectively. There was good agreement in liner top ring reversal temperature as shown in Figure 54. The predicted fire deck center temperature was lower than the measured value which appeared to show no sensitivity to engine speed. The predicted combustion chamber surface temperatures at the piston bowl, top portion of cylinder liner, fire deck, intake, and exhaust valves locations for the Hot Ceramic engine configurations are shown in Figures 56 through 60. The effect of the higher block coolant temperature and absence of coolant in the cylinder head had the most pronounced effect on the ceramic fire deck surface temperature which increased by 177°C at 2000 rpm, full load. The ceramic coated valve, liner, and piston temperatures were affected less by the increased coolant temperature, but also rose by 35°C to 95°C. These temperature changes can be seen by comparing Figures 49 through 53 (run numbers 87 through 96) with Figures 56 through 60 (run numbers 103 through 112).

In general, the predictions showed that the target wall temperatures of 700°C and 350°C (for fire deck and top ring reversal location, respectively) were approached for the Hot Ceramic engine (run numbers 103 through 112) at high speed and load. These temperatures were achieved because of the absence of head coolant and relatively low air-fuel ratio of 25:1. The peak combustion chamber surface temperature, occurred at the exhaust valve with a peak temperature greater than 700°C for the 2000 rpm, full load condition.

BASELINE METAL 82°C LINER TEMPERATURE

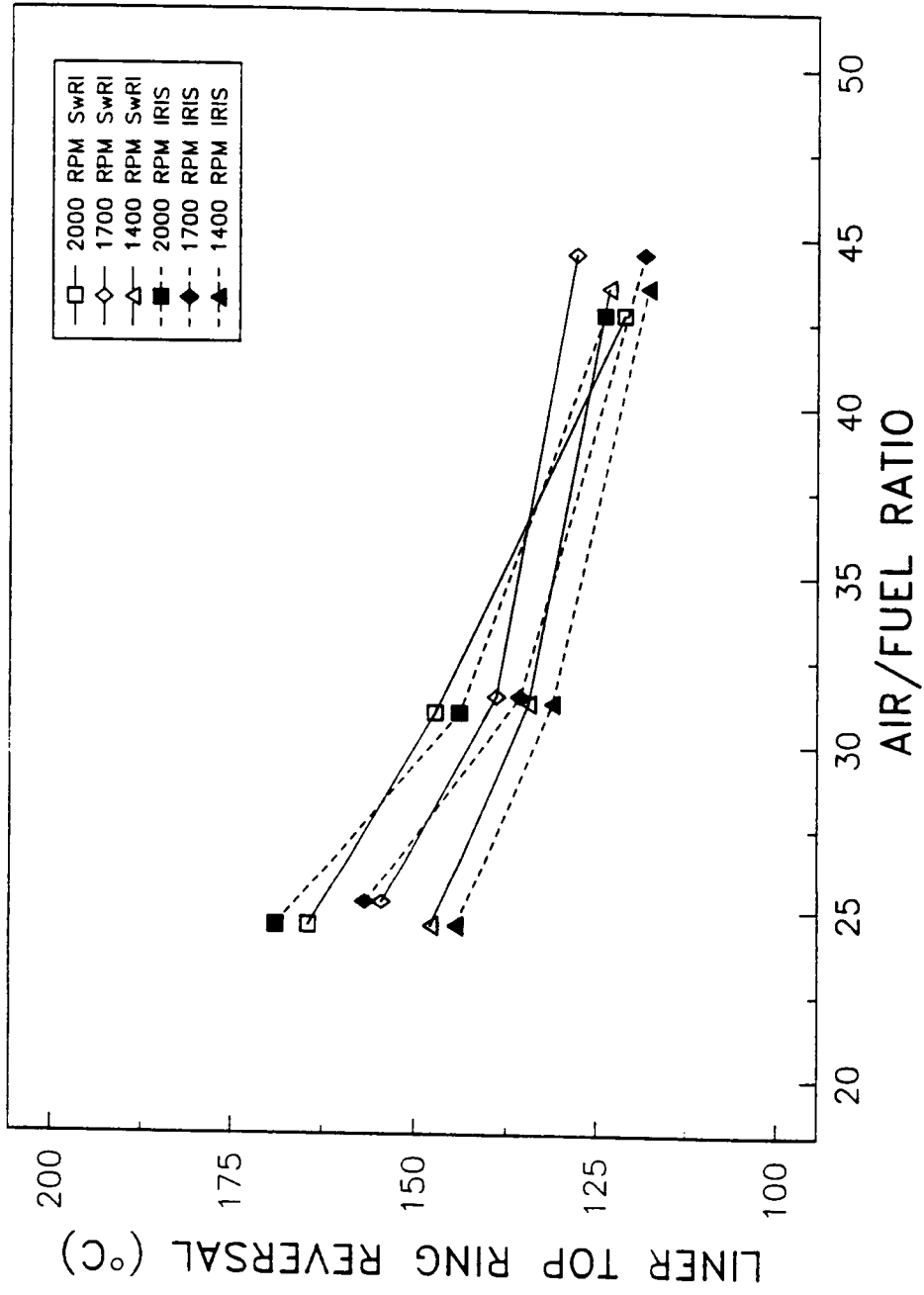


FIGURE 47. COMPARISON BETWEEN MEASURED AND PREDICTED LINER TOP RING REVERSAL TEMPERATURE, BASELINE METAL ENGINE

BASELINE METAL 82°C FIREDECK TEMPERATURE

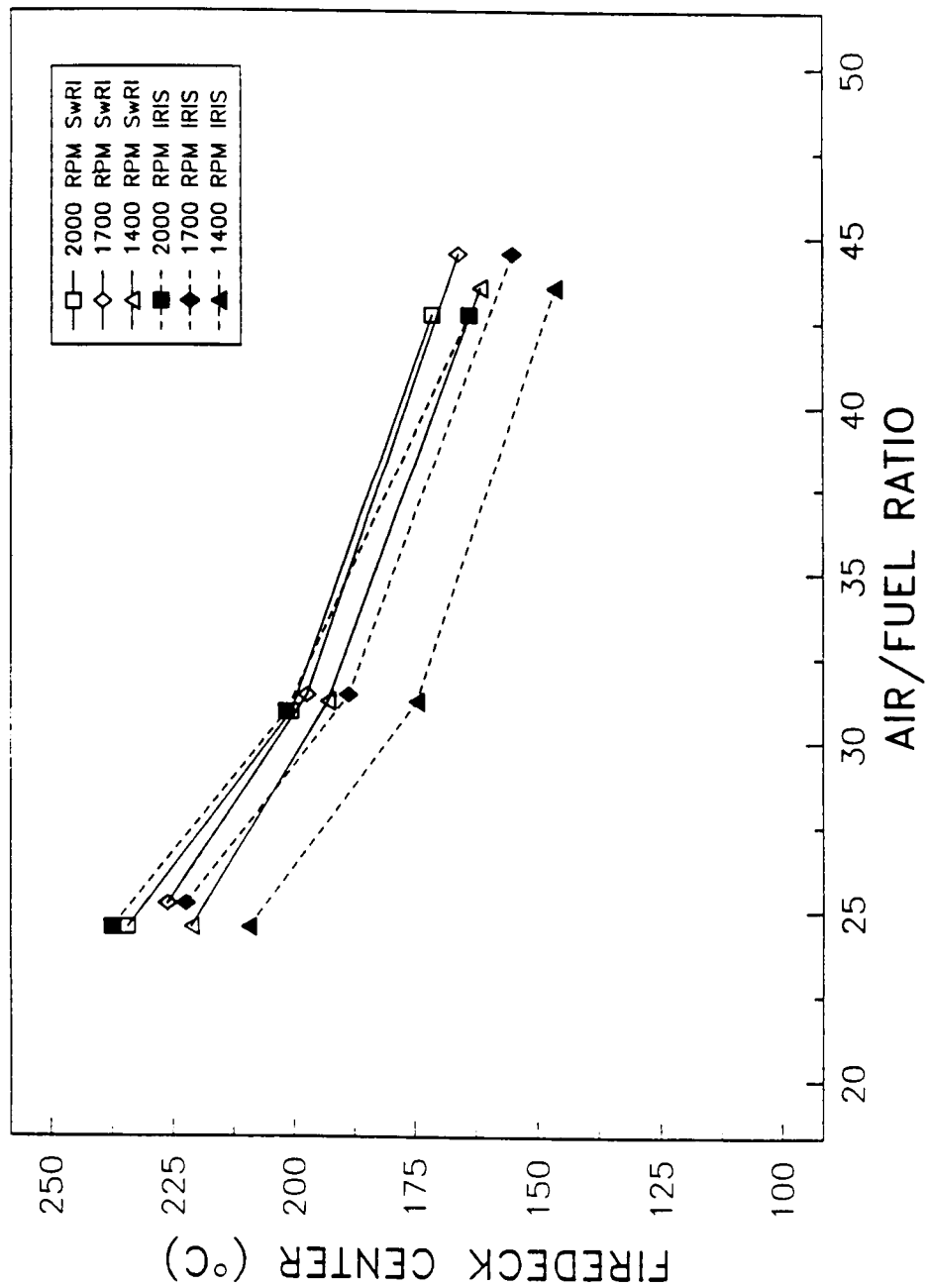


FIGURE 48. COMPARISON BETWEEN MEASURED AND PREDICTED FIREDECK CENTER TEMPERATURE, BASELINE METAL ENGINE

BASELINE CERAMIC 82°C
PISTON BOWL AVERAGE TEMPERATURE

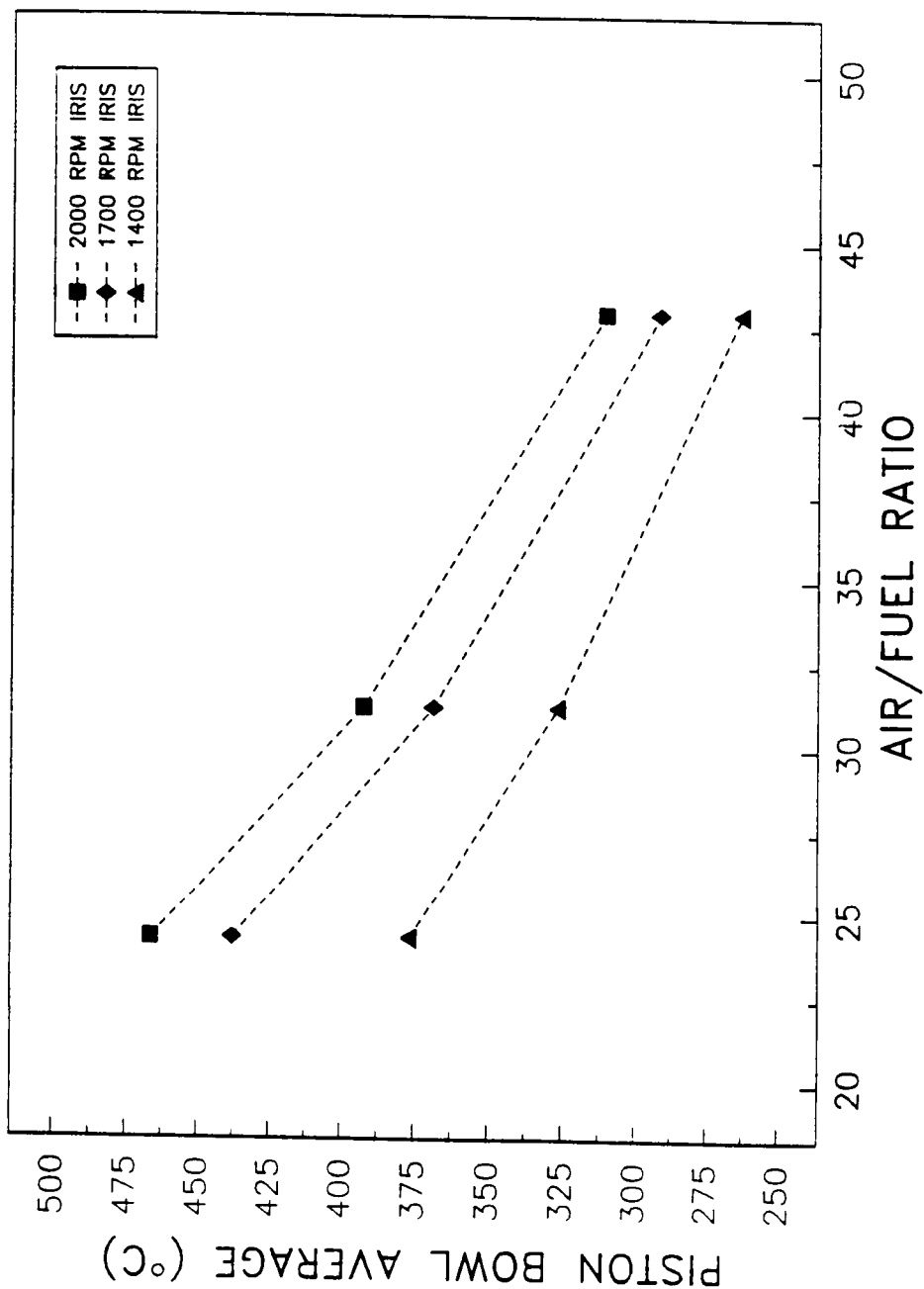


FIGURE 49. PREDICTED PISTON BOWL AVERAGE TEMPERATURE, BASELINE METAL ENGINE

BASELINE CERAMIC 82°C
LINER CERAMIC TOP AVERAGE TEMPERATURE

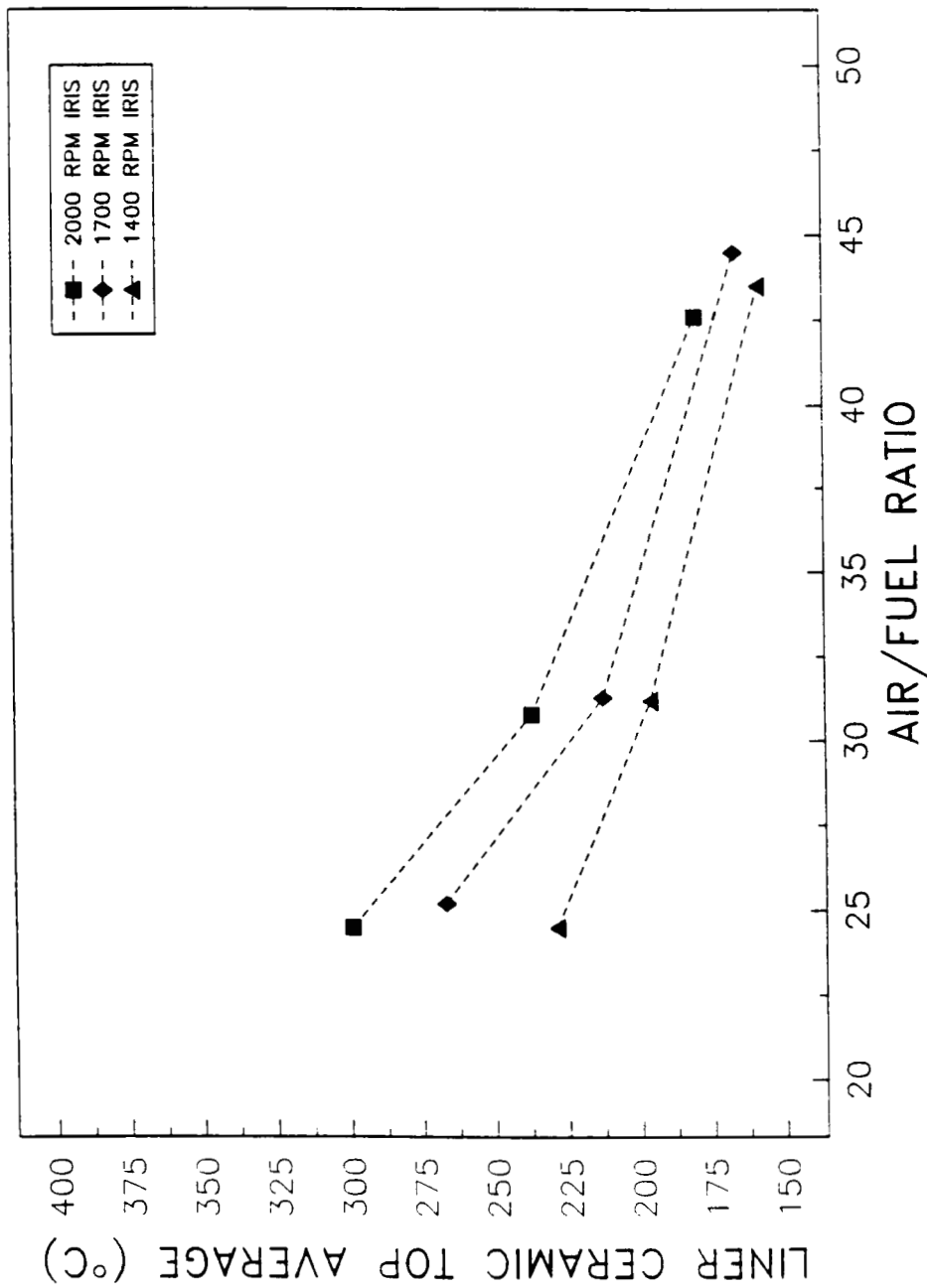


FIGURE 50. PREDICTED AVERAGE SURFACE TEMPERATURE FOR CERAMIC-COATED LINER TOP RING REVERSAL LOCATION, BASELINE CERAMIC ENGINE

BASELINE CERAMIC 82°C
 FIREDECK CERAMIC AVERAGE TEMPERATURE

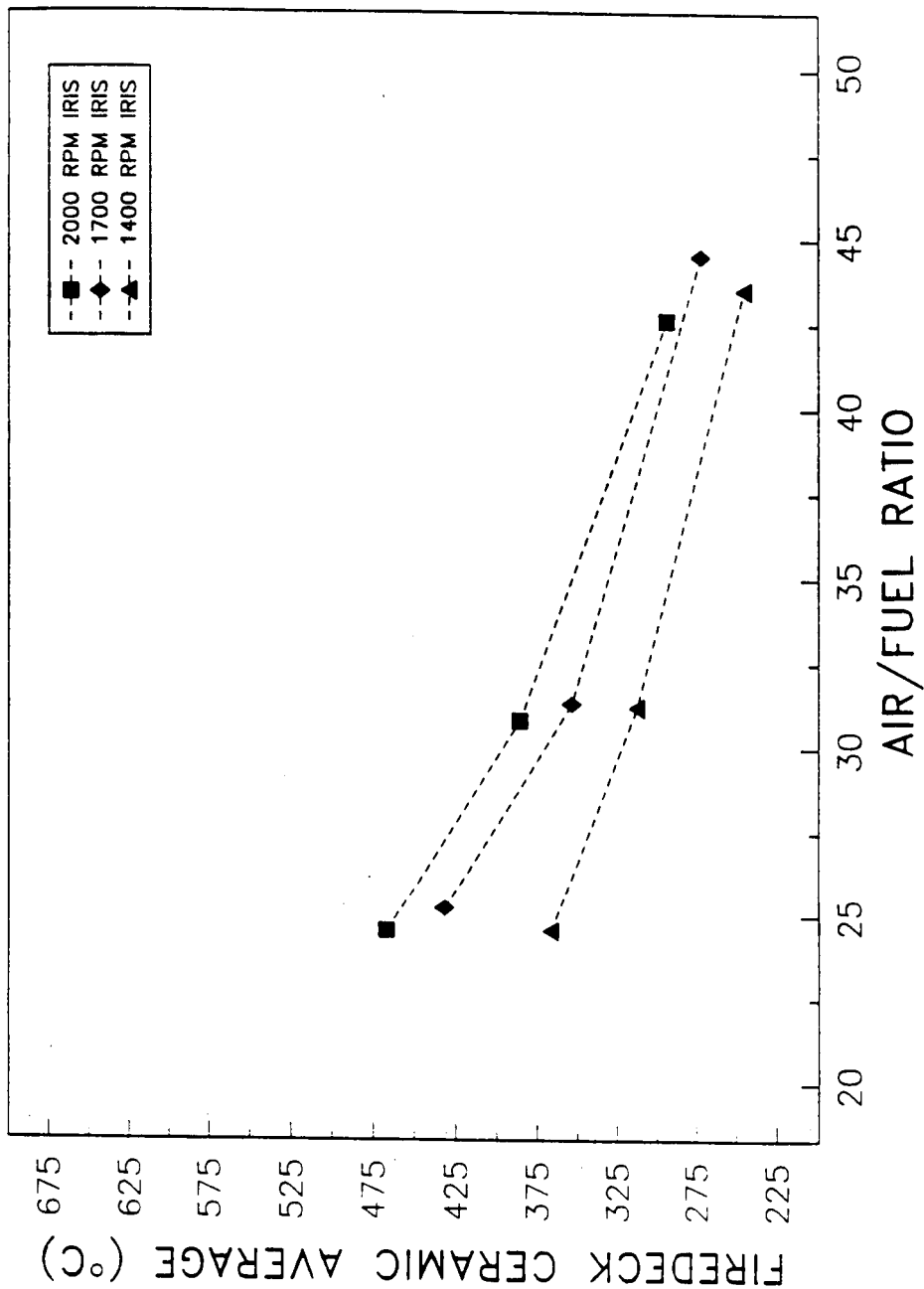


FIGURE 51. PREDICTED AVERAGE SURFACE TEMPERATURE FOR CERAMIC-COATED FIREDECK, BASELINE CERAMIC ENGINE

BASELINE CERAMIC 82°C
CERAMIC COATED EXHAUST VALVE TEMPERATURE

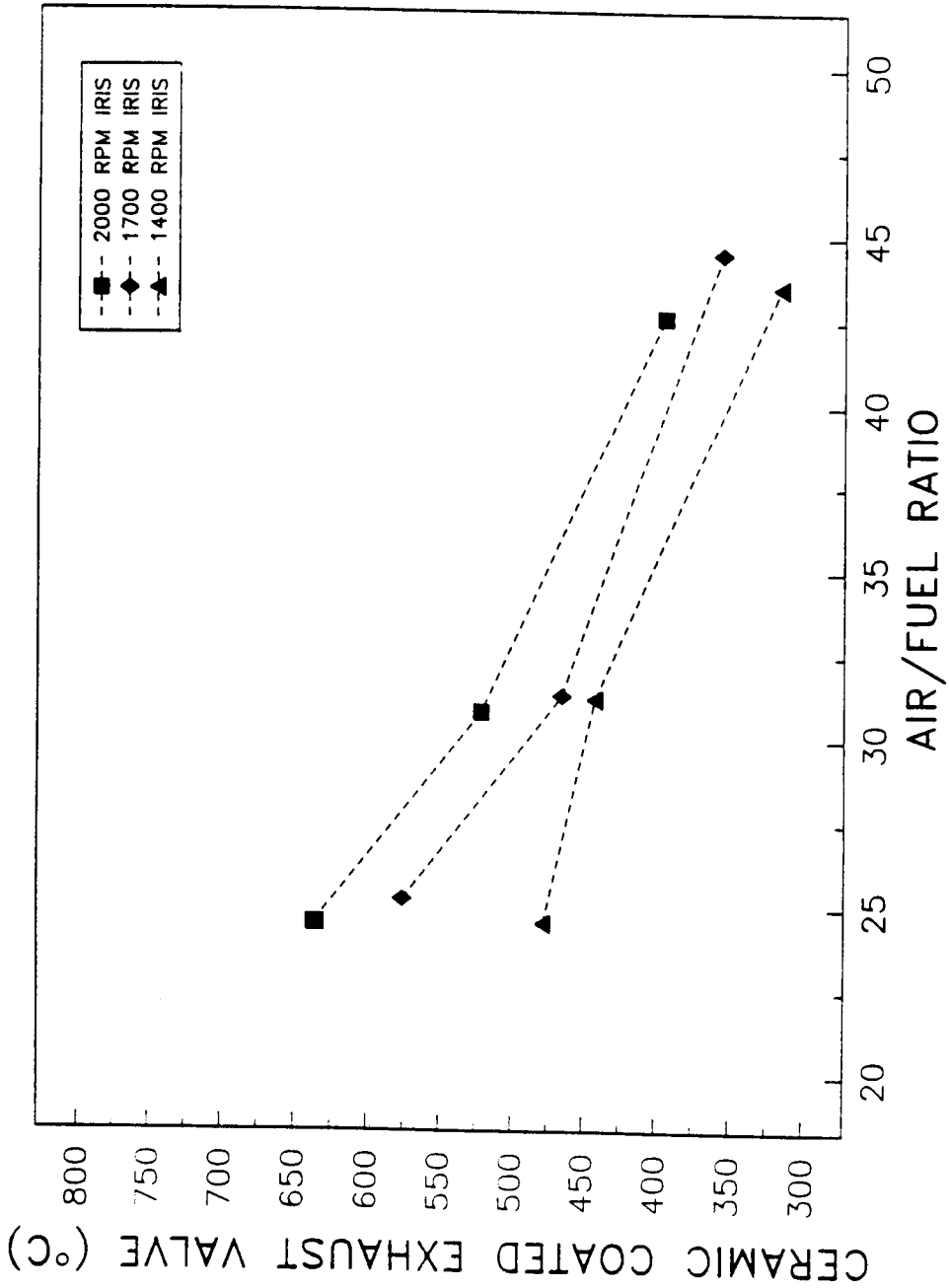


FIGURE 52. PREDICTED AVERAGE SURFACE TEMPERATURE FOR CERAMIC-COATED EXHAUST VALVE, BASELINE CERAMIC ENGINE

BASELINE CERAMIC 82°C
CERAMIC COATED INTAKE VALVE TEMPERATURE

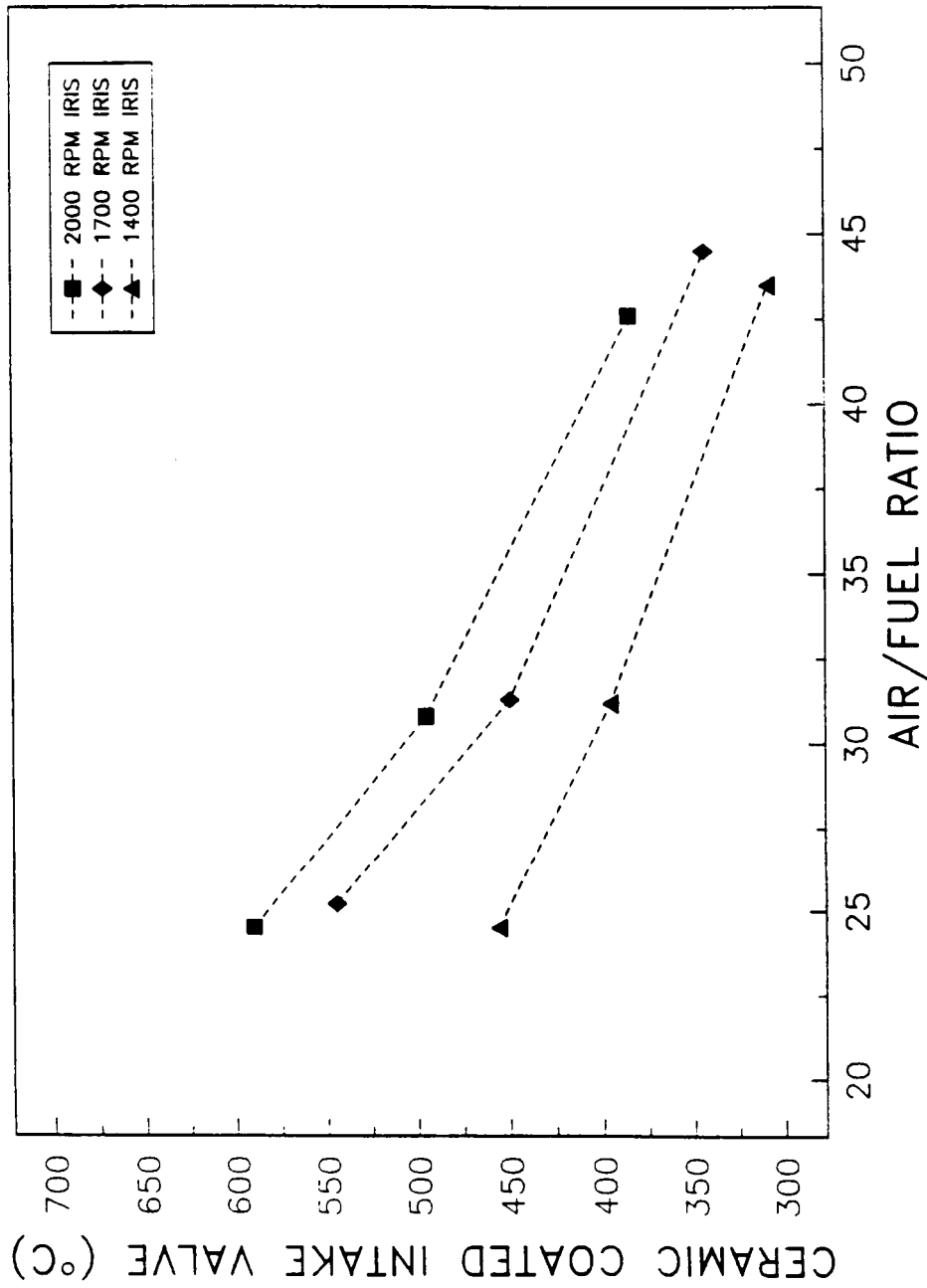


FIGURE 53. PREDICTED AVERAGE SURFACE TEMPERATURE FOR CERAMIC-COATED INTAKE VALVE, BASELINE CERAMIC ENGINE

HOT CERAMIC
LINER CERAMIC TOP AVERAGE TEMPERATURE

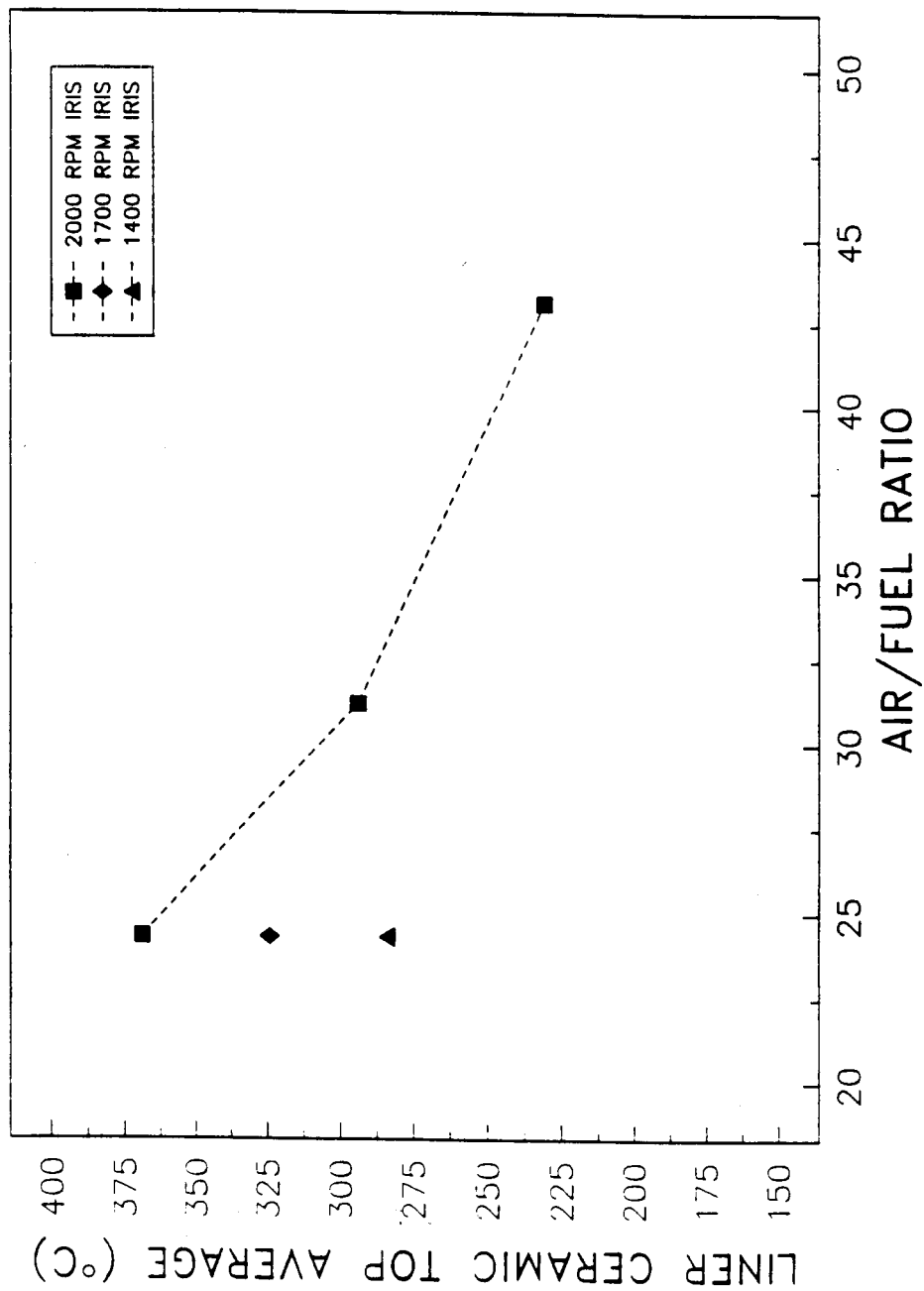


FIGURE 54. PREDICTED AVERAGE SURFACE TEMPERATURE FOR CERAMIC-COATED LINER TOP RING REVERSAL LOCATION, HOT CERAMIC ENGINE

HOT CERAMIC FIREDECK CERAMIC AVERAGE TEMPERATURE

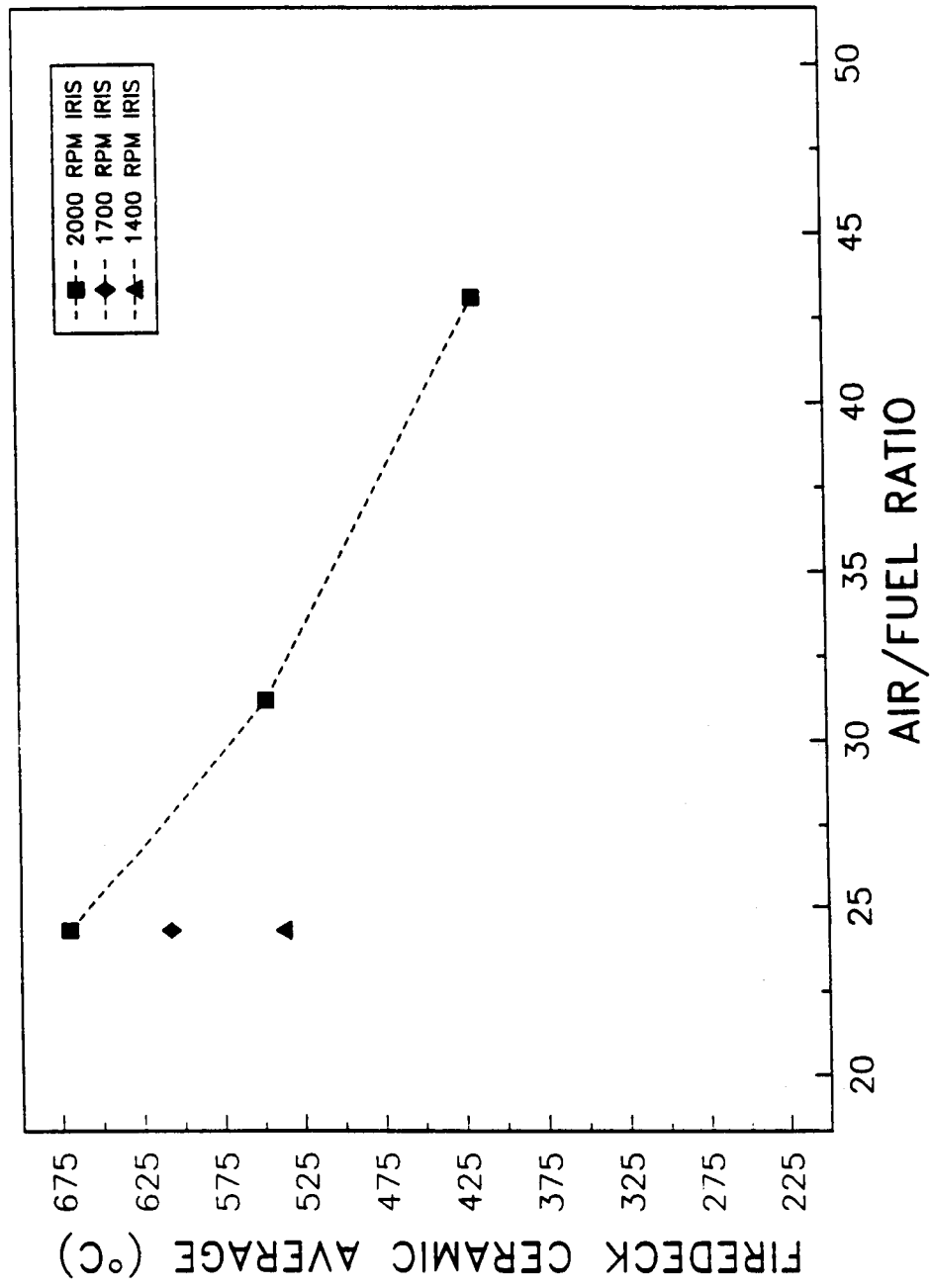


FIGURE 55. PREDICTED AVERAGE SURFACE TEMPERATURE FOR CERAMIC-COATED FIREDECK, HOT CERAMIC ENGINE

HOT CERAMIC PISTON BOWL AVERAGE TEMPERATURE

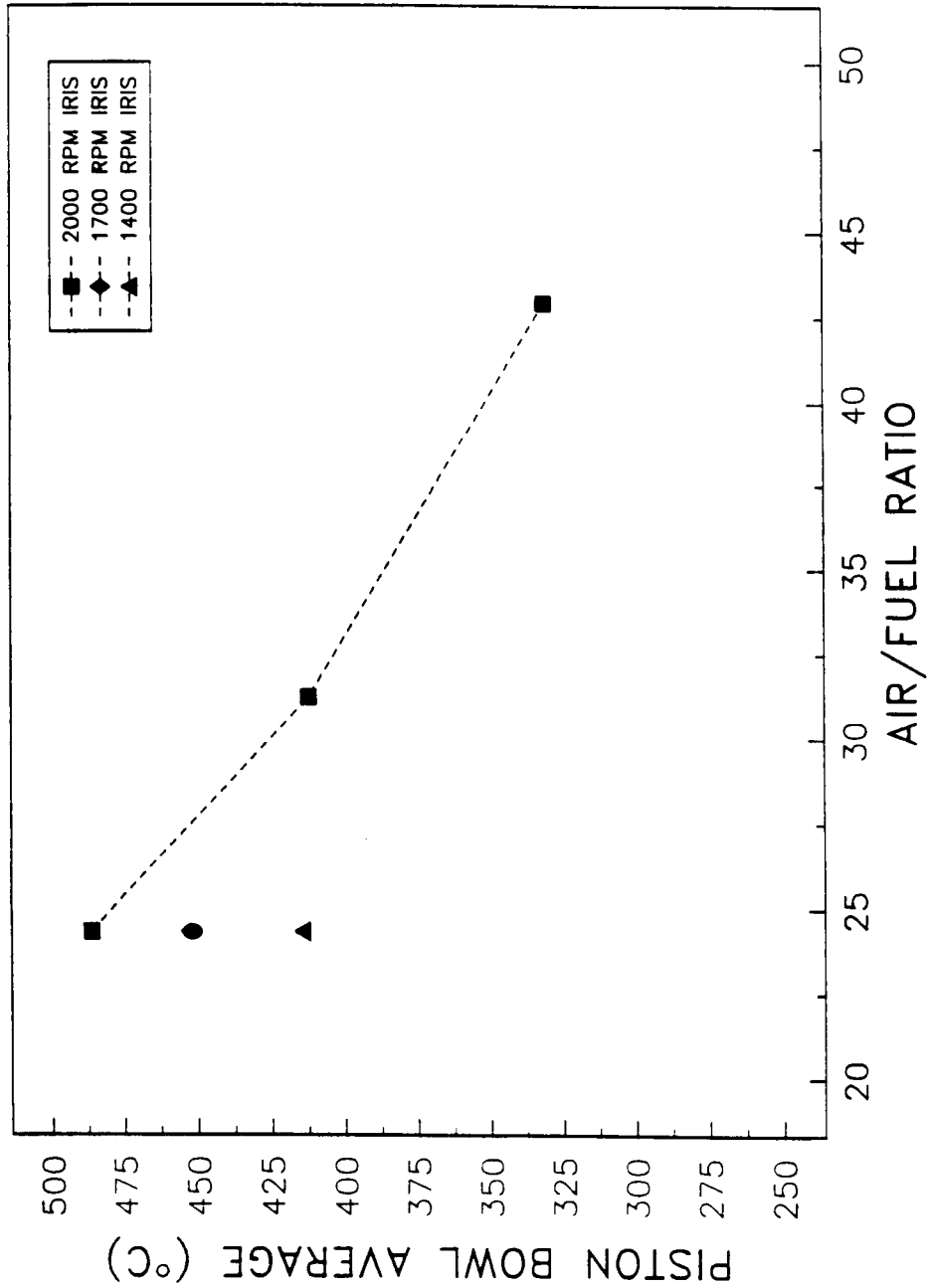


FIGURE 56. PREDICTED AVERAGE SURFACE TEMPERATURE FOR CERAMIC-COATED PISTON BOWL,
HOT CERAMIC ENGINE

HOT CERAMIC LINER TEMPERATURE

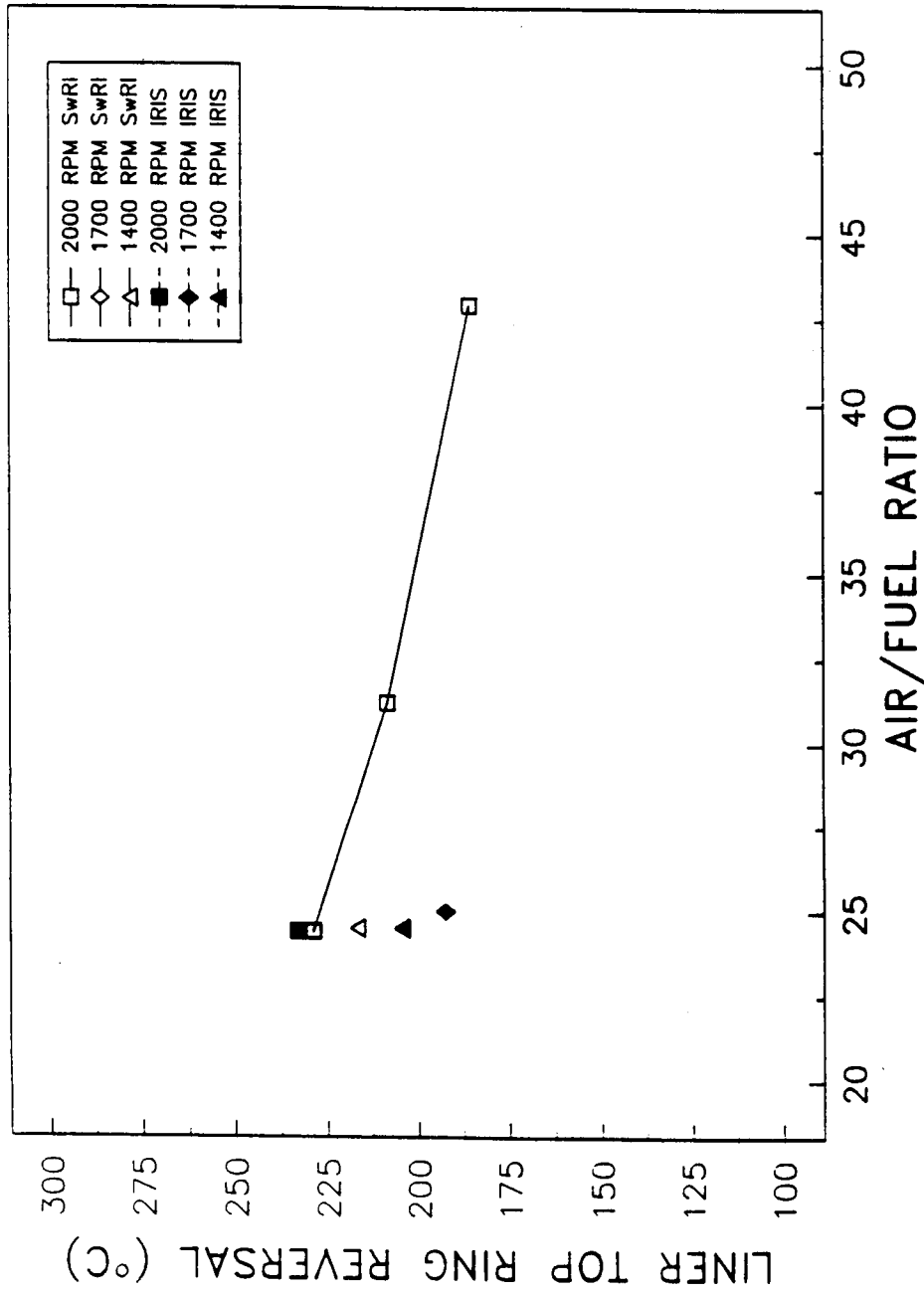


FIGURE 57. COMPARISON BETWEEN MEASURED AND PREDICTED CERAMIC-COATED LINER TOP RING REVERSAL TEMPERATURE, HOT CERAMIC ENGINE

HOT CERAMIC FIREDECK TEMPERATURE

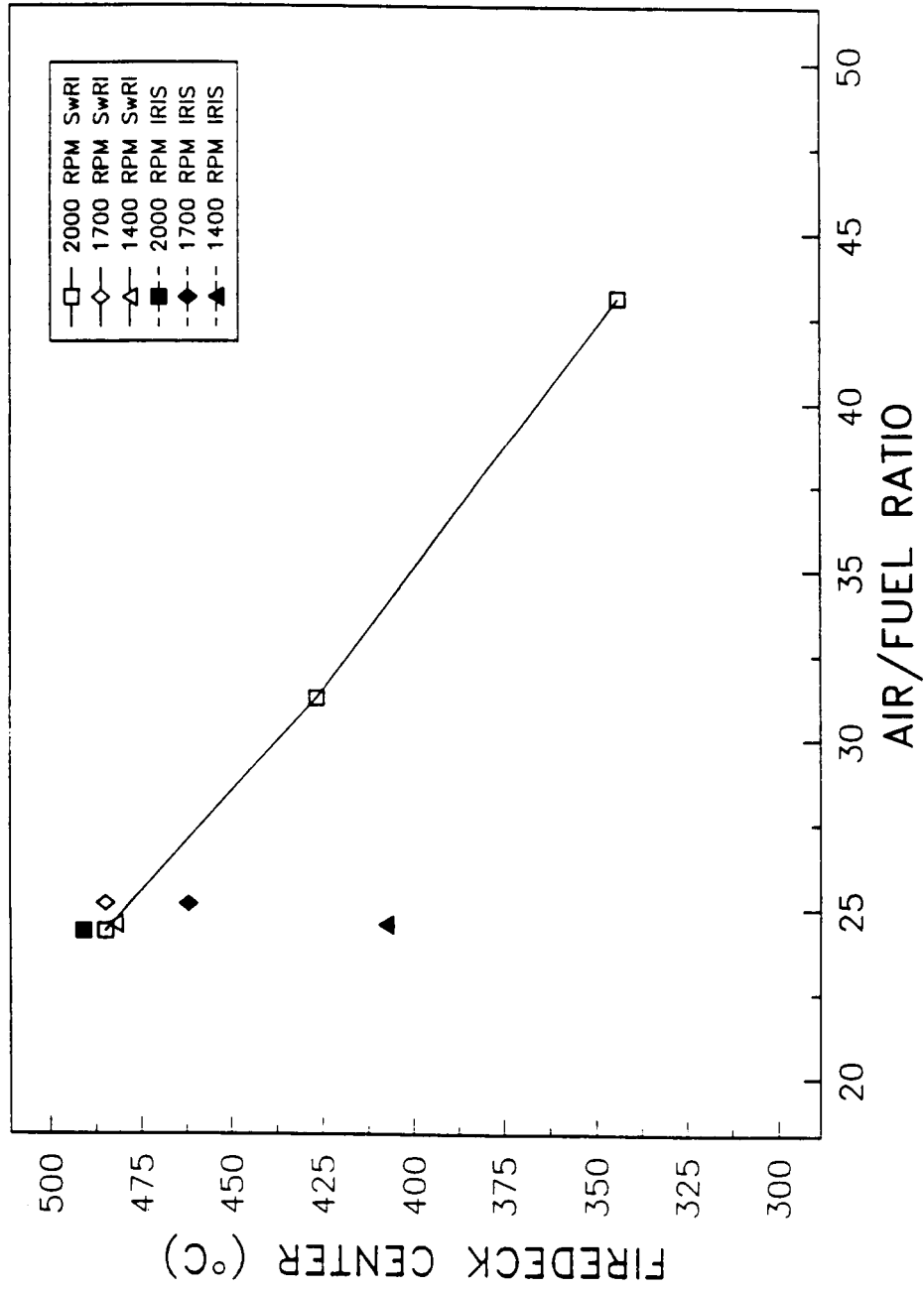


FIGURE 58. COMPARISON BETWEEN MEASURED AND PREDICTED CERAMIC-COATED FIREDECK TEMPERATURE, HOT CERAMIC ENGINE

HOT CERAMIC
CERAMIC COATED EXHAUST VALVE TEMPERATURE

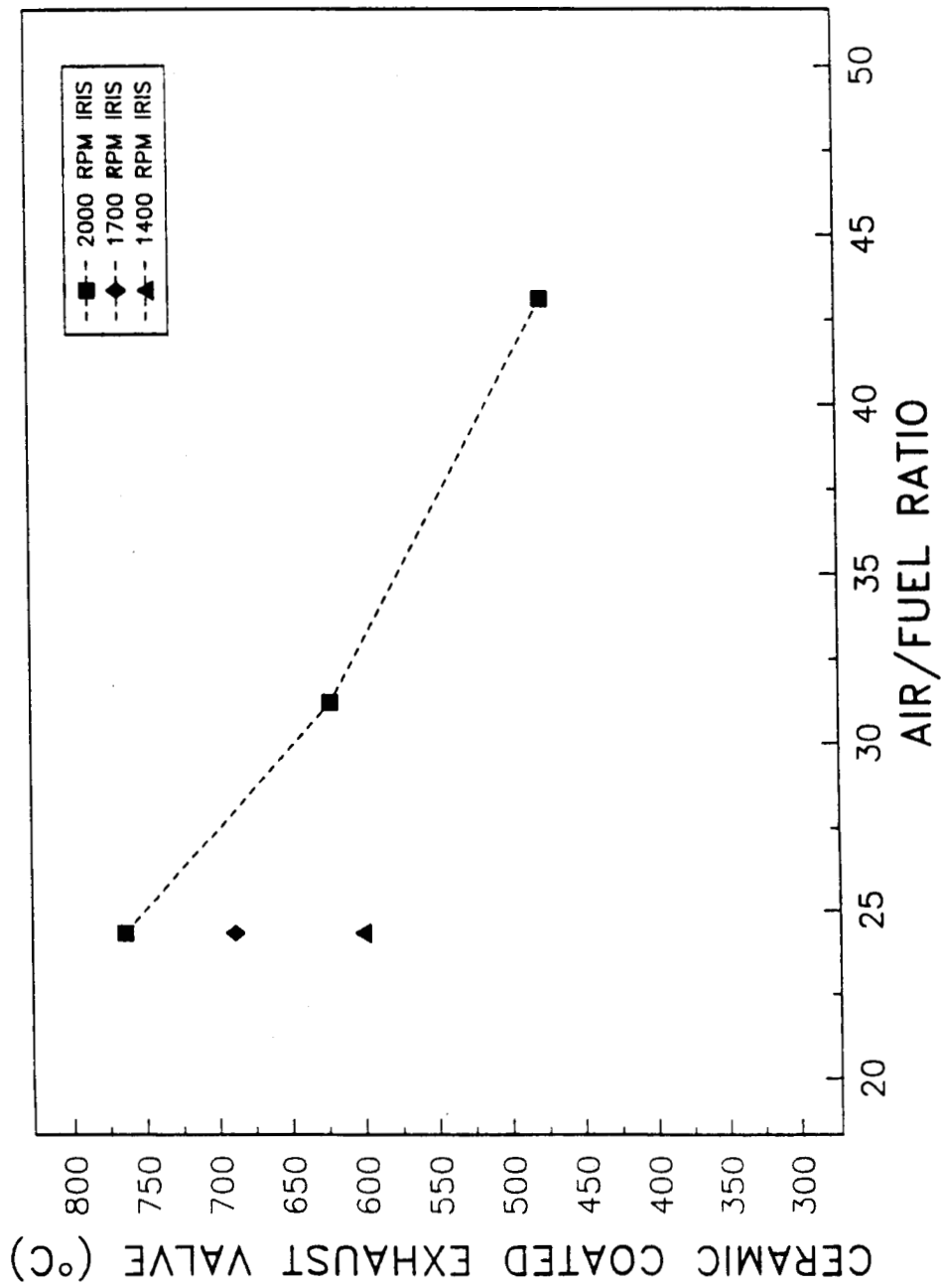


FIGURE 59. PREDICTED AVERAGE SURFACE TEMPERATURE FOR CERAMIC-COATED EXHAUST VALVE, HOT CERAMIC ENGINE

HOT CERAMIC CERAMIC COATED INTAKE VALVE TEMPERATURE

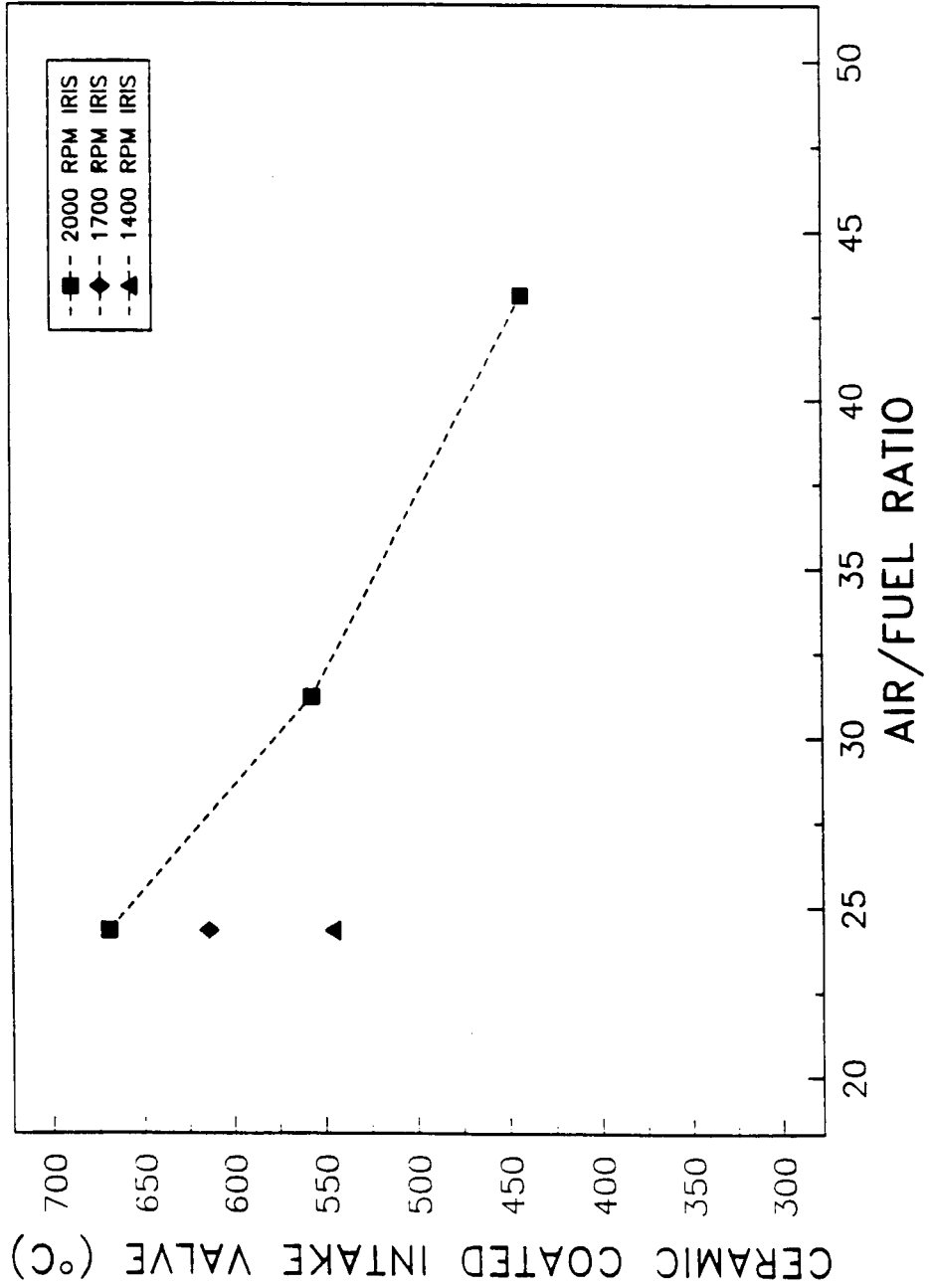


FIGURE 60. PREDICTED AVERAGE SURFACE TEMPERATURE FOR CERAMIC-COATED INTAKE VALVE, HOT CERAMIC ENGINE

2. Cyclic Variation of Relevant Parameters

Adding ceramic insulation to the engine combustion chamber affects both the mean and transient parameters such as intake air flow rate, cylinder pressure, heat transfer rate, and component temperatures. The crank-angle by crank-angle (or cyclic) variation of intake air mass flow rate, cylinder pressure, heat transfer rate, and component temperatures for the 2000 rpm, 100 percent load condition are shown in Figures 61 through 65. In each figure two curves are included, one for the Baseline Metal engine (test condition No. 1) and another for the insulated engine with 121°C block coolant and no coolant in head (test condition No. 7). The intake air mass flow rate over the engine cycle was the same for both test conditions as shown in Figure 61. This was achieved by slightly increasing the boost pressure for the hot insulated engine in order to maintain Baseline Metal engine air flow rates.

A comparison between the cylinder pressures of the two simulated test conditions is shown in Figure 62. The peak cylinder pressure in the insulated engine was considerably lower than in the Baseline engine due to less premixed burning and longer combustion duration in the insulated engine. However, in contrast to the experimental results, the decrease in cylinder pressure occurs only after the beginning of combustion. Further, during the compression stroke there is a small increase in pressure due to the increased heat transfer from the hot cylinder walls to the gas. The cyclic variation of heat transfer rate for the two test conditions is shown in Figure 63.

The effect of ceramic insulation on predicted piston surface temperature transients is shown in Figures 64 and 65. The heat transfer predictions (shown in Figure 63) included the calculation of cyclic surface temperature transients (transient heat conduction in the coating). By comparing Figures 64 and 65, it can be seen that the predicted piston surface temperature transients (temperature swing) were substantially higher for the ceramic surfaces compared to the metal surface. Despite the larger negative excursions from the mean surface temperature during the compression stroke, the ceramic wall temperatures were at all times much higher than the metal surface temperatures which resulted in heat transfer from the hot wall to the cylinder gas. These results suggest that the measured lower pressure during the compression stroke of the test engine (assuming the same trapped mass, compression ratio, and blowby) cannot be caused by the ceramic insulation and its direct effects on transient heat transfer.

E. Effect of Insulation and Heat Release on Engine Performance

The IRIS code was used to predict engine performance parameters based on input data from SwRI engine tests. The experimental data showed that engine performance was reduced when the engine was insulated and then operated at increased coolant temperatures. The reduced engine performance was attributed to degraded combustion but engine performance must also have been influenced by the ceramic insulation. By analyzing the experimental data, we were unable to separate the effects of combustion and insulation on engine performance. However, it is possible through simulation to differentiate between combustion and insulation effects on engine performance by inputting the experimentally obtained heat release rates into the IRIS code. The effect of insulation alone can be observed by inputting the Baseline Metal engine heat release rate into the IRIS code used to simulate the insulated engine. The result of this simulation allows the calculation of insulated engine performance assuming no combustion degradation.

The IRIS code was used to predict engine performance at 2000 rpm, full load for the following three conditions:

- 1) Baseline Metal engine using heat release rate extracted from the Baseline Metal engine pressure data (test condition number 1, run number 59).
- 2) Hot Ceramic engine using heat release rate extracted from the Hot Ceramic engine pressure data (test condition number 7, run number 110).

INTAKE MASS FLOW, METAL vs. "HOT"-INSULATED ENGINE, 2000 RPM, FULL LOAD
 MASS FLOXES
 INTAKE (←→).
 11-SEP-87
 10,06,19
 ITI/IRISPLT 103

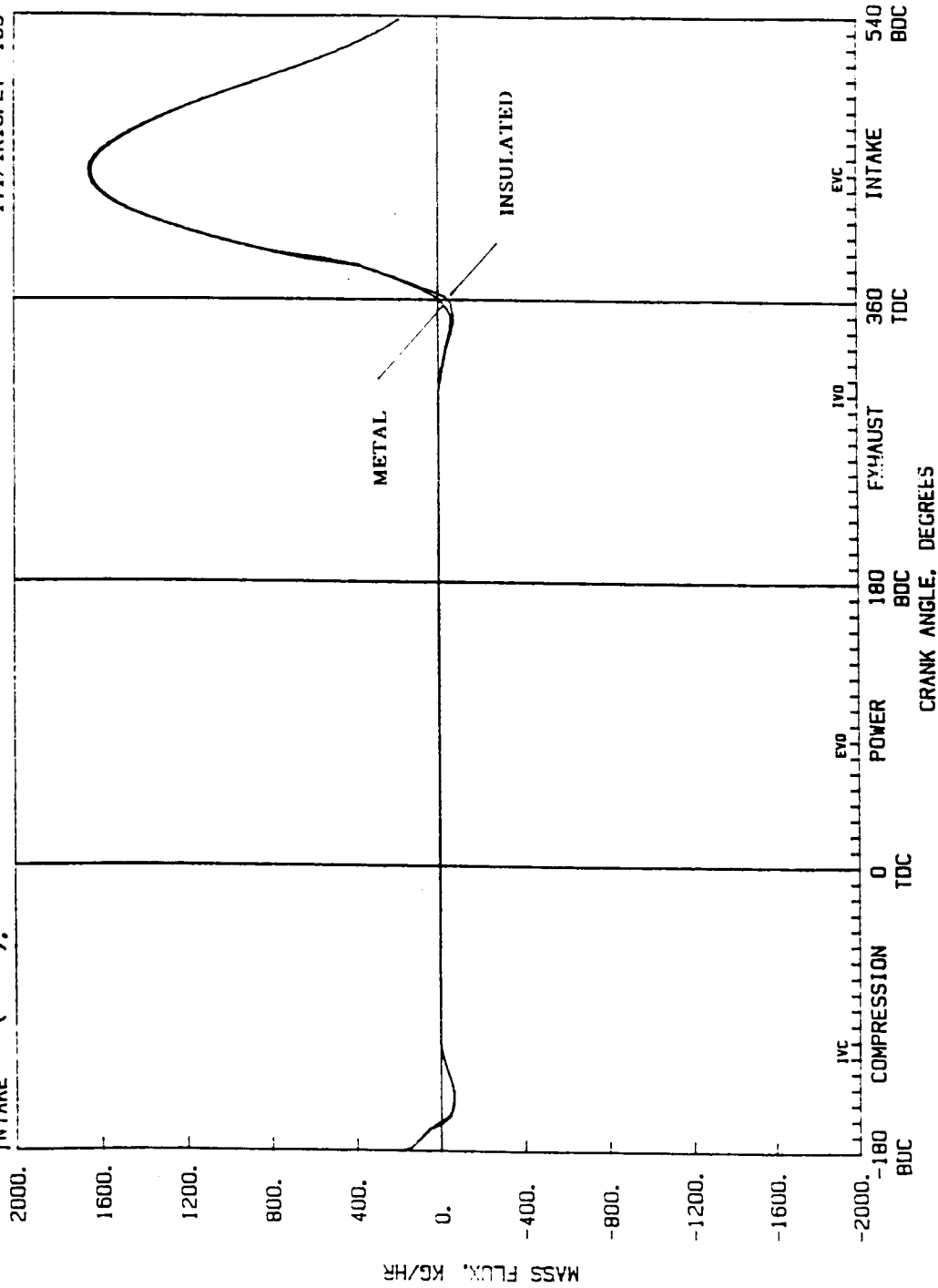


FIGURE 61. COMPARISON BETWEEN PREDICTED CYCLIC VARIATION OF INTAKE AIR MASS FLOW FOR BASELINE METAL AND HOT CERAMIC ENGINES, 2000 RPM, FULL LOAD

ORIGINAL PAGE IS
OF POOR QUALITY

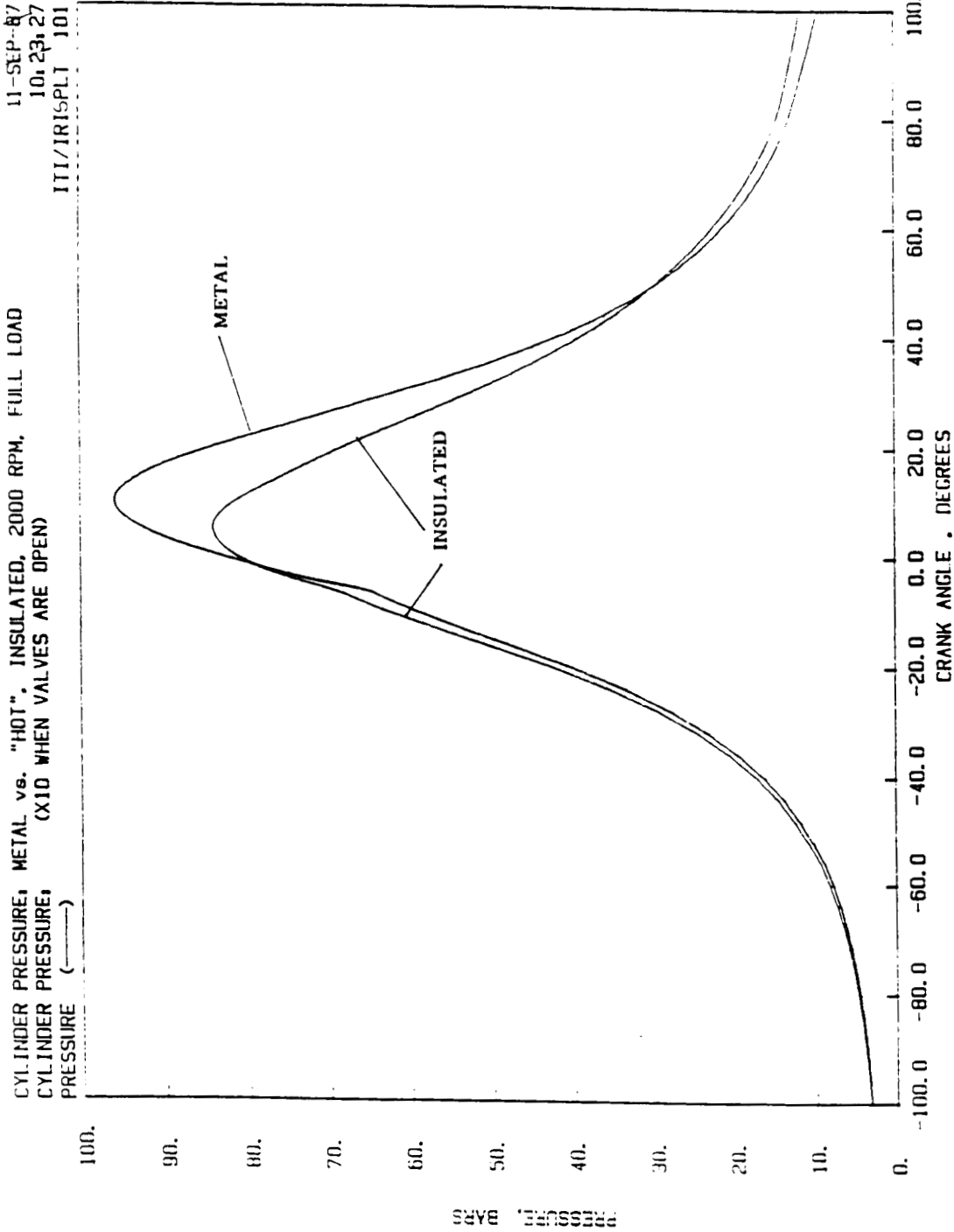


FIGURE 62. COMPARISON BETWEEN PREDICTED CYCLIC VARIATION OF CYLINDER PRESSURE FOR
BASELINE METAL AND HOT CERAMIC ENGINE, 2000 RPM, FULL LOAD

ORIGINAL PAGE IS
OF POOR QUALITY

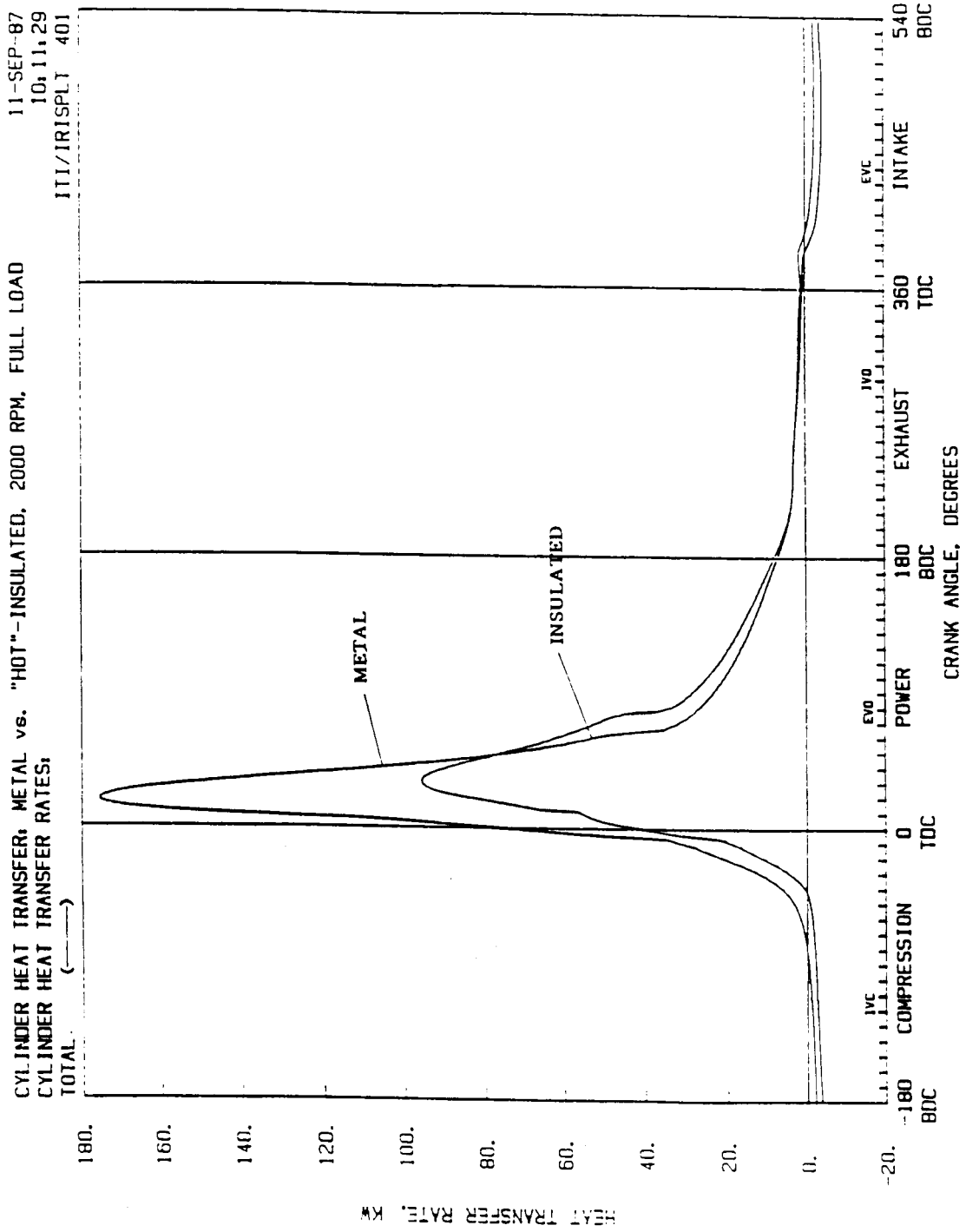


FIGURE 63. COMPARISON BETWEEN PREDICTED CYCLIC VARIATION OF HEAT TRANSFER RATE FOR BASELINE METAL AND HOT CERAMIC ENGINES, 2000 RPM, FULL LOAD

9-SEP-87
10:46:59
ITI/IRISPLT 451

RUN #59, 2000 RPM - 100% LOAD - 180F COOLANT TEMPERATURE
PISTON WALL TEMPERATURE SWINGS
CUP. BOT (-----), P. CROWN (-----)

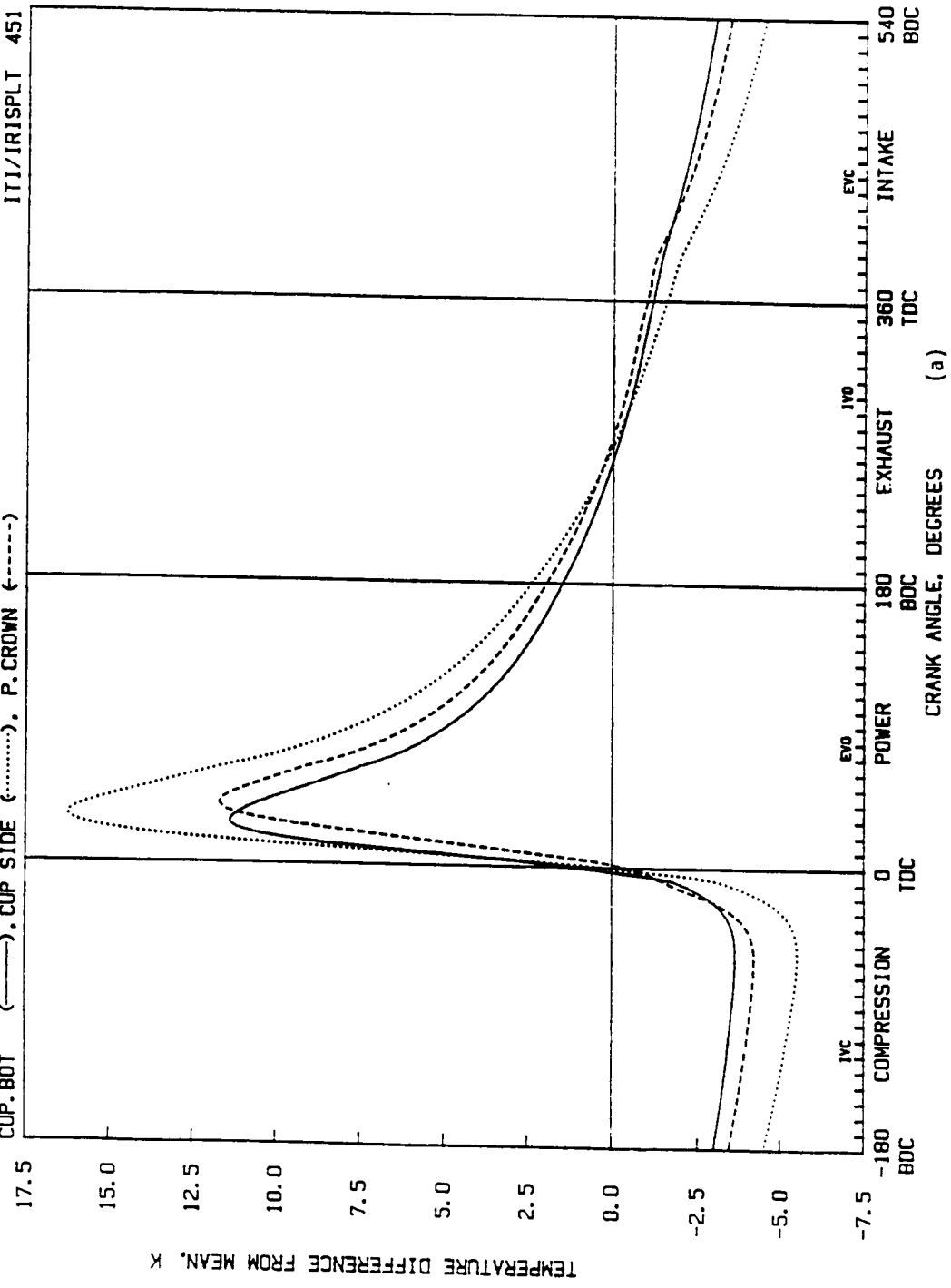
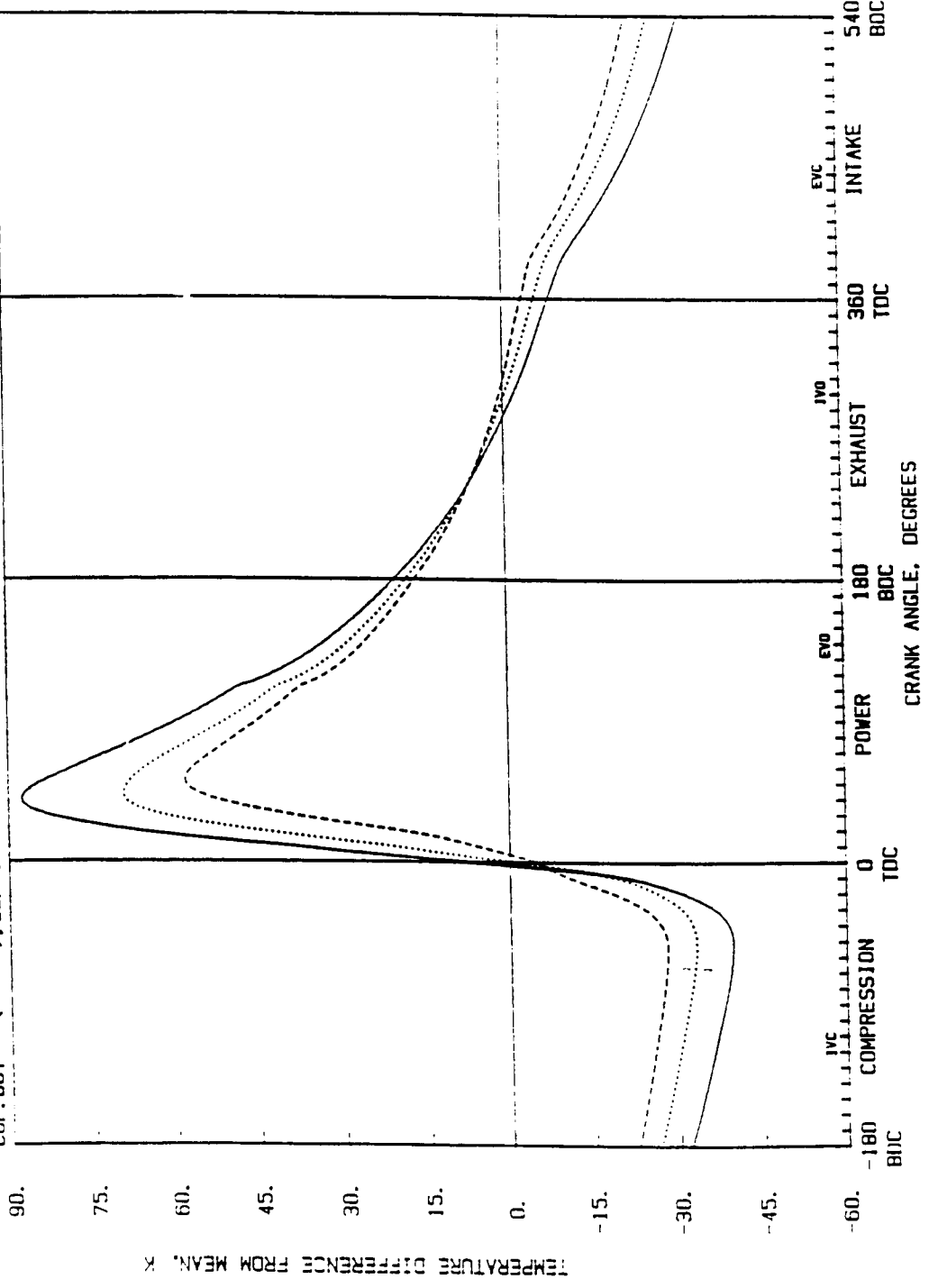


FIGURE 64. PREDICTED CYCLIC TEMPERATURE VARIATION OF PISTON SURFACES FOR BASELINE METAL ENGINE, 2000 RPM, FULL LOAD

RUN #119, 2000 RPM - 100% LOAD - INSULATED, AIR-COOLED HEAD
 PISTON WALL TEMPERATURE SWINGS
 CUP, BOT (————), CUP SIDE (.....), P. CROWN (-----)

9-SEP-87
 10,50,11
 ITI/IRISPLT 451



(b)

FIGURE 65. PREDICTED CYCLIC TEMPERATURE VARIATION OF PISTON SURFACES FOR HOT CERAMIC ENGINE, 2000 RPM, FULL LOAD

3) Hot Ceramic engine using heat release rate extracted from the Baseline Metal engine pressure data (test condition number 1, run number 59).

Simulation numbers 1 and 2 above were carried out to establish a good correlation between predicted and measured results. The experimental apparent heat release rate curves used in the above analysis are shown in Appendix E. The apparent heat release rate curves were smoothed and corrected for heat transfer before being entered into the IRIS code. Simulation No. 3 was carried out to see the effect of insulation alone on engine performance assuming no combustion degradation. A comparison between the predicted and measured results at 2000 rpm, full load is shown in Table 6.

The predicted results were obtained by inputting actual heat release data (as measured from cylinder pressure data) into the IRIS engine model. The measured results were obtained from actual engine tests. The first two columns in Table 6 show a comparison between the SwRI measured results and the IRIS predicted results for the Baseline Metal engine. The measured and predicted results show good agreement in indicated horsepower (IHP), indicated thermal efficiency (ITE), top ring reversal temperature (TRR), and fire deck temperature. The percent heat transfer was calculated by the IRIS engine model and corresponds to the percent of fuel energy transferred to the coolant by the combustion chamber surfaces. The third and fourth columns in Table 6 correspond to the Hot Ceramic engine test. Again there was good agreement between measured and predicted results. The IRIS model predicted a decrease in indicated thermal efficiency of 3.6 (8.0 percent) percentage points for the Hot Ceramic engine compared to the SwRI measured decrease of 3.4 percentage points (7.4 percent). The IRIS model also predicted a 30 percent reduction in heat transfer to the coolant for the Hot Ceramic engine compared to the Baseline Metal engine. Experimental heat transfer measurements were not made to compare with this predicted reduction in heat transfer. The baseline heat release was then input into the insulated engine model to simulate Hot Ceramic engine performance with no degradation in combustion, as shown in the last column of Table 6. The result was a predicted increase in ITE of 0.9 percentage points, with a 28 percent reduction in heat transfer to the coolant.

Table 6. SwRI Measurements and IRIS Simulation Results for Baseline Metal Engine and Hot Ceramic Engine With and Without the Adverse Effects on Combustion (2000 rpm, Full Load)

	Baseline Metal Baseline Combustion		Hot Ceramic Degraded Combustion		Hot Ceramic Baseline Combustion
	<u>SwRI</u>	<u>IRIS</u>	<u>SwRI</u>	<u>IRIS</u>	<u>IRIS</u>
Indicated Power (kW)	52.3	52.2	48.8	48.4	53.6
ITE %	45.7	45.1	42.3	41.5	46.0
Brake Power (kW)	42.8	44.3	39.4	39.5	45.7
Air Flow (kg/hr)	239.0	238.5	241.7	235.8	238.5
A/F	24.6	24.6	24.6	23.8	24.1
% Heat Transfer	---	12.92	---	9.0	9.27
Exhaust Temperature (°C)	562	654	649	760	722
TRR Temperature (°C)	171	161	200	202	200
Firedeck Temperature (°C)	310	299	481	493	471

VI. DISCUSSION OF RESULTS

The experimental results of this investigation showed that, under the given test conditions, the addition of ceramic insulation and subsequent reduction of heat transfer to the coolant did not improve engine performance relative to the Baseline Metal engine. The reduction in thermal efficiency and change in exhaust emissions was attributed to the LHR engine's degraded combustion.

The experimental results presented in Section IV raised two important questions:

- 1) Why is the insulated engine combustion characterized by less premixed burning and longer combustion duration compared with the Baseline Metal engine?
- 2) Why is the compression pressure lower for the insulated engine?

In this section, an attempt will be made to answer these two questions and to discuss the impact of insulation engine performance and emissions.

A. Combustion

Combustion in a diesel engine is the mechanism by which the fuel chemical energy is converted into heat energy or what is commonly referred to as heat release. Before discussing the combustion or heat release (the two terms will be considered synonymous in this section) characteristics of the LHR engine compared to the Baseline Metal engine, it is important to define the different stages of combustion. During the combustion period there are three distinct stages of combustion (ref. 30). In the first stage, the fuel that is premixed during the ignition delay period ignites resulting in a very high rate of heat release. This "premixed" stage of combustion lasts for approximately 5 degrees crank angle and results in rapid cylinder pressure rise. The second stage of combustion results from diffusion flame combustion and is characterized by lower rates of heat release. The second stage of combustion lasts approximately 40 degrees crank angle. The third stage of combustion corresponds to the "tail" of the heat release rate curve. This stage of combustion results in small rates of heat release that occur during the expansion stroke. Approximately 10 to 20 percent of the total heat is released during the third stage of combustion (ref. 27). The three phases of combustion will be referred to as premixed combustion (stage 1), diffusion combustion (stage 2) and combustion tail (stage 3).

Combustion in a direct-injected diesel engine is controlled by the rate and quality of fuel air mixing. The fuel-air mixing is controlled by the fuel injection characteristics and air motion within the combustion chamber. Since the test engine uses a quiescent combustion chamber, the fuel-air mixing is primarily controlled by the fuel injection characteristics such as fuel injection timing, duration, and fuel spray parameters. A fuel spray can be described in terms of the following parameters:

- Break-up length
- Spray angle
- Spray tip penetration
- Droplet size distribution

The break-up length is the length of the fuel-spray before it begins to break-up or disintegrate. The spray angle is the included angle formed by the edges of the spray. The spray tip penetration is the furthest distance reached by the spray. The droplet size distribution is usually described by the Sauter Mean Diameter which describes the fuel droplet size. All of these spray parameters are a function of the difference between the cylinder gas and fuel injection pressures, the density of the fuel and air during injection, and nozzle geometry. Fuel spray penetration is reduced with increasing gas temperature, lower fuel pressure, shorter injection duration, and smaller nozzle hole diameters.

A comparison between the combustion characteristics of the Baseline Metal and Hot Ceramic engine test conditions is shown in Figure 66. Figure 66 is a plot of heat release rate versus crank angle at 2000 rpm, full load. As shown in Figure 66, the Hot Ceramic engine had less premixed burning as evidenced by the smaller premixed combustion spike. The reduced premixed burning can be attributed to the Hot Ceramic engine's 0.6 degree (5 percent) shorter ignition delay. Less fuel accumulated in the Hot Ceramic engine combustion chamber during the shorter ignition delay which resulted in less premixed burning and the smaller premixed spike as shown in Figure 66. The reduced premixed combustion in LHR engines has been well documented (ref. 6, 14, 26, 31).

The Hot Ceramic engine also had lower rates of heat release during the second stage of combustion (which occurs between crank angles of approximately 175-210 degrees) and a longer heat release "tail." The Hot Ceramic engine's lower rates of heat release are probably the result of poor fuel-air mixing. The Hot Ceramic engine's increased gas and fuel temperatures had an adverse effect on the fuel spray penetration. In Section IV it was mentioned that the fuel injector holder temperature increased by 250°C which is an indication of the increase in fuel temperature for the Hot Ceramic engine compared to the Baseline Metal engine because the test engine does not have a recirculating fuel system. The fuel temperature increase lowers the fuel viscosity and density which causes reduced fuel spray penetration. The Hot Ceramic engine's higher fuel and air temperatures cause shorter fuel spray break-up length, larger spray cone angles, and smaller droplet sizes all which contribute to reduced fuel spray penetration and poorer fuel-air mixing. The poor fuel-air mixing for the Hot Ceramic engine also resulted in a longer combustion "tail" since the fuel that did not burn during the second stage of combustion burned later in the cycle as shown in Figure 66.

The Hot Ceramic engine's increased wall and gas temperatures also contribute to the prolonged combustion. The increased gas temperature causes faster droplet evaporation and burning of fuel closer to the injector. Burning fuel close to the injector reduces fuel spray penetration and air utilization resulting in prolonged combustion.

The prolonged combustion duration for the Hot Ceramic engine versus the Baseline Metal engine is partially due to the Hot Ceramic engine's increased fuel injection duration as shown in Figure 67 and Table 4. However, the change in fuel injection duration of 3 degrees is small compared to the change in combustion duration of 43.1 degrees. An increase in combustion duration was also observed where the fuel injection duration remained constant. The combustion duration increased by 20.7 degrees for the Baseline Ceramic engine versus Baseline Metal engine while there was no change in fuel injection duration.

The combustion duration increase of 43.1 degrees or 106 percent for the Hot Ceramic engine compared to the Baseline Metal engine appears to be dramatic. While this combustion duration increase is substantial, the increase occurs mainly during the third stage of combustion where only 10 to 20 percent of the fuel is burned. The combustion duration was defined as the crank angle increment between the start of combustion and the crank angle where 95 percent of the peak cumulative heat release occurred. The cumulative heat release curve (as shown in Appendix E) approaches its maximum value asymptotically. Therefore, a small change in the slope of the cumulative heat release curve results in a large increase in combustion duration.

In summary, the LHR engine's reduced premixed combustion was attributed to shorter ignition delays. The prolonged combustion was primarily the result of poor fuel-air mixing due to degradation of the fuel spray. A small portion of the Hot Ceramic engine's increased combustion duration was due to a 3° increase in fuel injection duration. It is obvious from these combustion results that the fuel injection system must be optimized for LHR engine operation.

COMBUSTION RESULTS, 2000 RPM FULL LOAD

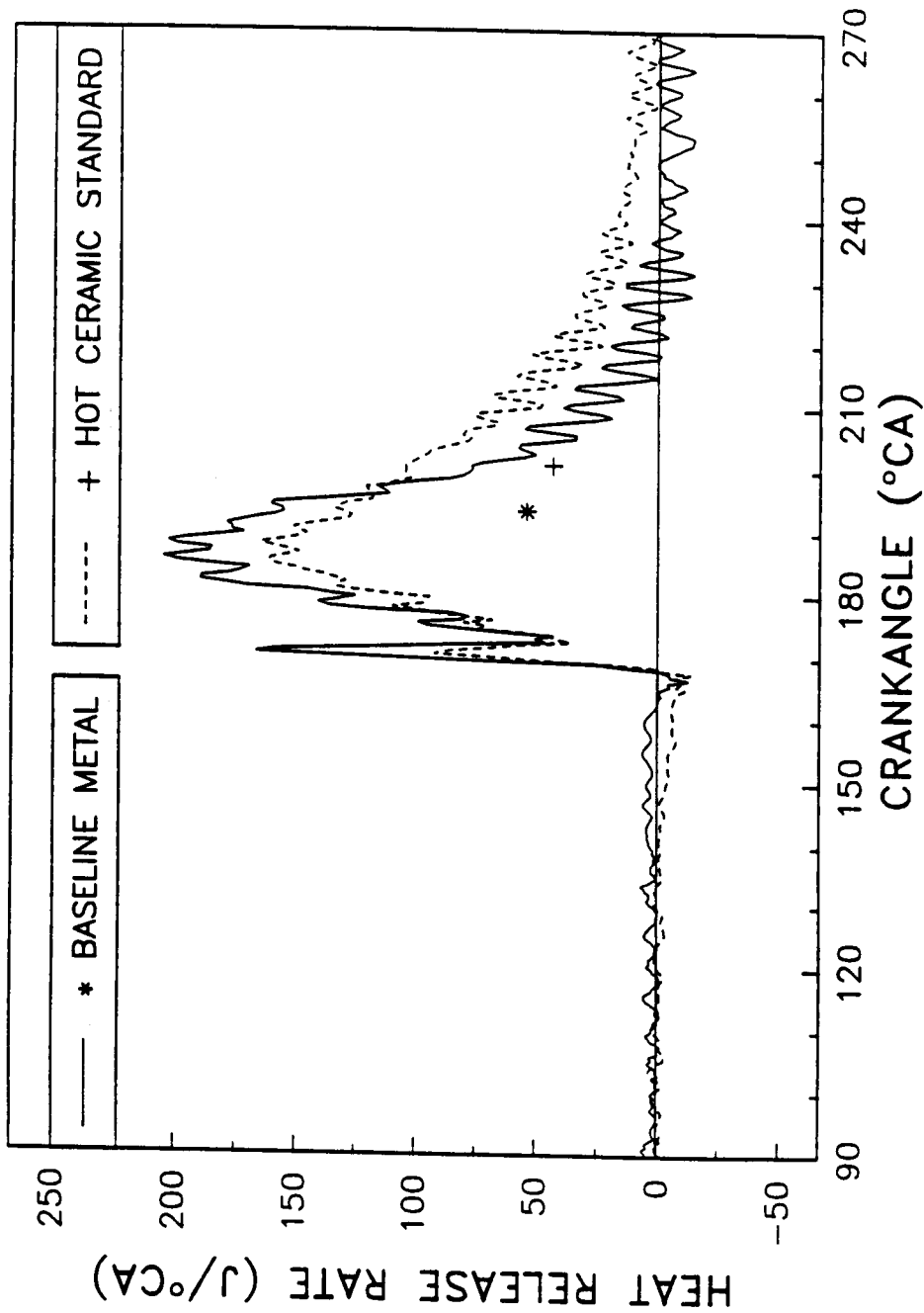


FIGURE 66. HEAT RELEASE RATE VERSUS CRANKANGLE FOR BASELINE METAL AND HOT CERAMIC TEST CONDITIONS, 2000 RPM, FULL LOAD

COMBUSTION RESULTS, 2000 RPM FULL LOAD

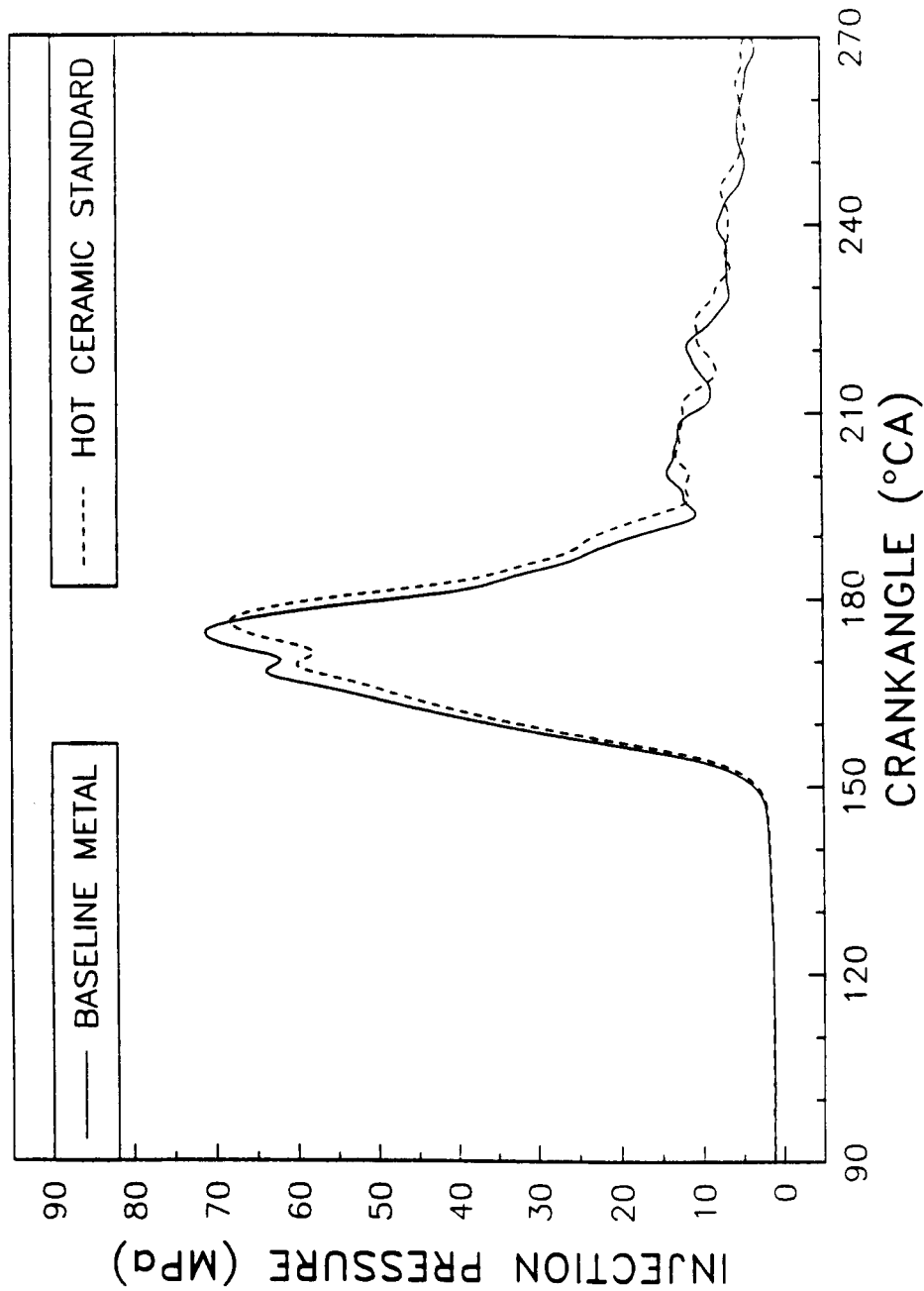


FIGURE 67. FUEL INJECTION PRESSURE VERSUS CRANKANGLE FOR BASELINE METAL AND HOT CERAMIC TEST CONDITIONS, 2000 RPM, FULL LOAD

B. Peak Pressures

The second question resulting from the experimental data is; why is the compression pressure lower for the insulated engine? The compression pressure and peak cylinder pressure were lower for both the firing and motoring LHR engine test conditions, as shown in Figures 34 and 35 respectively.

Figure 35 is a plot of cylinder pressure versus crank angle for the motored engine at 2000 rpm. Each motoring trace was recorded immediately after the firing engine test condition. The intake air blowers were bypassed and the engine was motored in the naturally-aspirated mode. As shown in Figure 35, the peak cylinder pressure of 3.33 MPa for the Baseline Ceramic engine was 12 percent lower than the Baseline Metal engine peak pressure of 3.78 MPa. The Hot Ceramic engine peak motoring pressure of 3.24 MPa was 14 percent lower than the Baseline Ceramic engine pressure.

The peak cylinder pressure may have been reduced due to changes in engine:

- compression ratio
- blowby
- heat transfer

The change in peak pressure for the Baseline Metal and Baseline Ceramic engine conditions corresponds to a compression ratio reduction of approximately 1.3 assuming the polytropic exponent remains constant at 1.353. The peak motoring pressure for the Hot Ceramic engine test was 3.24 MPa which corresponded to a compression ratio reduction of 1.6 compared to the Baseline Metal engine.

When the insulated engine was assembled, every effort was made to assemble the engine with the Baseline Metal engine compression ratio of 14.5. The piston bowl volume and deck height were measured and found to agree with the Baseline engine. At the conclusion of the insulated engine tests, the engine was disassembled and inspected. Ceramic material was missing from both exhaust valves, one intake valve, 75 percent of the second intake valve, and from a portion of the piston bowl. Unfortunately, the time the ceramic material was lost from the combustion chamber is not known. The volume of ceramic material missing was determined by measuring the volume of the piston bowl and by measuring the area where the ceramic material had flaked off. The total volume of missing ceramic material increased the engine clearance volume by approximately 8 cc. The 8 cc change in clearance volume reduced the engine compression ratio from 14.5 to 13.9. This change in compression ratio of 0.6 partially explains the reduced peak pressures for the insulated engine.

No evidence was found to explain the remaining difference in peak motoring pressure. Unfortunately, blowby was not recorded during motoring conditions. Blowby was recorded during firing conditions and was actually lower for the Hot Ceramic engine compared to the Baseline Metal engine. The calibration of the cylinder pressure transducer was also checked to see if a change in calibration could explain the reduced peak pressures. The cylinder pressure transducer calibration was checked during the project and only changed by 1.2 percent from the beginning of Baseline Metal to end of Hot Ceramic engine tests. The effect of the ceramic insulation on heat transfer should have resulted in a slight increase in peak motoring pressure for the insulated engine. The only other possible explanation for a change in peak pressures may have been a change in valve timing resulting from the higher engine temperature. Although valve lash was not measured immediately following a Hot Ceramic engine test, valve lash effects should not have been significant during motoring tests or during Baseline Ceramic engine tests where engine component temperatures were not significantly higher than Baseline Metal engine temperature. Airflow was not recorded during motoring tests to verify that the trapped air mass was the same for the Baseline Metal and insulated engine motoring tests.

Figure 34 is a plot of cylinder pressure versus crank angle for the firing engine at 2000 rpm, full load. The three curves in Figure 34 correspond to the three motoring test conditions shown in Figure 35. As shown in Figure 34, the cylinder pressure during the compression stroke was lower for the insulated engine. The change in engine compression ratio partially explains this difference, but the remaining difference in compression pressures is currently unexplained. An increase in engine blowby for the insulated engine could explain the reduced compression pressure, but the blowby for the insulated engine was not significantly different from the baseline engine, as shown in Appendix C by comparing Run Nos. 59, 94, and 110. At 2000 rpm, full load, the blowby for the Baseline Metal, Baseline Ceramic and Hot Ceramic engine test conditions were 11.8, 12.4, and 11.5 m³/hr respectively. The intake air flow rate and pressure ratio across the cylinder head were also held constant for all three test conditions as shown in Appendix C. The trapped air mass for all three test conditions should therefore be the same. The remaining variable among the three test conditions shown in Figure 34 is the ceramic insulation. The insulated engine should have a slightly higher cylinder pressure during the compression stroke due to heat transfer from the Hot cylinder walls to the intake charge. However, the insulated engine had a lower compression pressure. Integral Technologies Incorporated simulated the Baseline engine and Hot Ceramic test conditions using the IRIS engine simulation code. The result shown in Figure 62 shows that the pressure during the compression stroke should be higher for the insulated engine.

The peak firing pressure was also reduced for the insulated engine. The lower insulated engine peak firing pressure was due to less premixed burning, longer combustion duration, and lower compression ratio due to lost ceramic material from the combustion chamber.

The insulated engine's lower peak firing pressure may also be the result of increased heat transfer from the gas to the wall. Woschni et al. (ref. 24) contend that the heat transfer increases during the first stage of combustion according to the "convection vive" heat transfer phenomenon. The "convection vive" phenomenon is described as follows. A flame or combustion chemical reaction will come closer to the cylinder wall as wall temperature increases. When the flame comes closer to the wall the temperature gradient across the thin boundary layer increases and the heat transfer increases. Woschni claims that insulating a combustion chamber under certain high temperature conditions will actually increase the heat transfer from the gas to the wall. The effect of reducing the temperature gradient from the gas to the wall by insulation is overcome by the effect of increased heat transfer as described by the "convection vive" phenomenon. A modified combustion term has been added to an equation for heat transfer in internal combustion engines to account for the "convection vive" phenomenon (ref. 32).

No direct evidence from the SwRI experimental results exists to support the "convection vive" phenomenon in explaining the reduced LHR engine peak firing pressures. The insulated engine's lower peak firing pressure was attributed to shorter ignition delays, poorer fuel-air mixing with degraded combustion, and a lower compression ratio due to lost ceramic material. Approximately 40 percent of the reduced insulated engine motoring pressure was the result of the lower compression ratio. The remaining cause for the LHR engine reduced motoring pressure remains unexplained.

C. Thermal Efficiency

Insulating the combustion chamber of an internal combustion engine theoretically results in improved thermal efficiency according to the second law of Thermodynamics. However; the addition of ceramic insulation and subsequent reduction of heat transfer to the coolant did not improve engine efficiency relative to the Baseline Metal engine. The experimental results showed that the indicated thermal efficiency (ITE) for the Baseline Metal, Baseline Ceramic, and Hot Ceramic test conditions at 2000 rpm, full load were 45.7, 43.1 and 42.3 respectively. The reduction in ITE was attributed to the insulated engine's degraded combustion and lower compression ratio due to lost ceramic material. The degraded combustion was due to poor fuel-air mixing that resulted in less premixed burning and longer combustion duration. Engine thermal efficiency is reduced as the heat release period deviates from the ideal

constant volume process. The effect of combustion duration on indicated thermal efficiency was investigated by Lyn (ref. 27) using a heat release simulation model. Lyn showed that a significant loss in thermal efficiency results when the heat release duration is extended beyond 50 degrees crank angle. For example, Lyn calculated a reduction in ITE of 3.8 percentage points when the heat release period was increased from 30 to 50 degrees crank angle. These results were obtained assuming a right triangular heat release shape and a 15:1 compression ratio. Lyn was also able to show that engine cycle efficiency is maximized when the centroid of the heat release diagram coincides with top dead center. The LHR engine's prolonged combustion caused the heat release diagram centroid to shift away from top dead center resulting in a loss of engine efficiency for the insulated engine compared to the Baseline Metal engine.

The insulated engine's lower compression ratio also helps to explain the reduced thermal efficiency. During the insulated engine tests approximately 8cc of ceramic material was lost from the combustion chamber. The loss of ceramic material caused the compression ratio to decrease from 14.5 to 13.9 or a 4.1 percent. Using an engine model, Lyn (ref. 27) estimated that thermal efficiency is reduced by .7 percent per ratio in a compression ratio range of 15:1 to 20:1.

Other researchers have reported efficiency gains (ref. 6, 19, 20, 21, 22) and losses (ref. 4, 23, 24) in LHR engines. The conflicting results are probably due to the large number of possible LHR engine configurations, test conditions, and analysis techniques used. A comprehensive review of the literature concerning the effect of LHR operation on engine thermal efficiency can be found in reference 26.

During engine test runs, no attempt was made to optimize the combustion system for LHR engine performance. The fuel-injection timing and spray penetration could perhaps have been modified to obtain Baseline Metal engine combustion in the insulated engine. As mentioned in Section V, ITI simulated the case of Baseline combustion in the Hot Ceramic engine and predicted an increase in ITE of .9 percentage points or 2 percent.

The extra exhaust gas energy (due to an increase in exhaust gas temperature) was not accounted for in the efficiency calculation. The higher exhaust gas temperature would have resulted in improved thermal efficiency for a direct-injected diesel engine with a bottoming cycle device such as turbo compounding. The higher exhaust gas temperature was partially due to insulating the combustion chamber and partially due to combustion occurring later in the cycle.

D. Emissions

The emissions results presented in Section IV show that the insulated engine had significantly higher smoke and particulate emissions compared to the Baseline Metal engine. The full-load exhaust smoke opacity and particulate emissions increased by as much as 300 and 500 percent respectively for the Hot Ceramic engine compared to the Baseline Metal engine. Although the exact mechanism for the formation of smoke and particulate emissions is unknown, it is expected that the LHR engine's higher component and gas temperatures will have a significant effect on smoke and particulate emissions. It is expected that exhaust soot should increase in the LHR engines because exhaust soot is formed at high temperature in the absence of oxygen where pyrolysis of the fuel vapor takes place. Conversely, less smoke and particulates may be formed in an LHR engine where the high gas temperature delays quenching of the flame reaction which allows more carbon particles to be oxidized resulting in less smoke and particulates. It is the authors opinion that the increase in smoke and particulates emissions was due to poor fuel air mixing and higher gas temperatures which increased pyrolysis of the fuel.

The increased smoke emissions may also be attributed to the LHR engines prolonged combustion duration. Hiroyasu et. al. (ref. 33) reported a correlation between increased diesel engine smoke emissions and combustion occurring late in the cycle.

A soluble extraction was conducted on the particulate samples for the 2000 rpm, full-load test conditions. The results of the extraction for the Baseline Metal, Baseline Ceramic, and Hot Ceramic test conditions are shown in Table 7. These results show that the soluble organic fraction (SOF) was low which means that most of the particulate consisted of insoluble fuel or dry soot. The particulate level for the Hot Ceramic engine increased significantly compared to the Baseline Metal engine while the SOF was reduced. Therefore, the increase in particulate emission for the Hot Ceramic engine is attributed to insoluble fuel or dry soot formation. The particulate level of the Baseline Ceramic engine increased by 161 percent while the SOF increased by only 14 percent.

Table 7. Organic Soluble Extraction, 2000 rpm, Full-Load

<u>Run Number</u>	<u>Test Condition</u>	<u>Particulate (g/IKW-HR)</u>	<u>Soluble Organic Fraction %</u>
59	Baseline Metal	.1697	14
94	Baseline Ceramic	.443	16
110	Hot Ceramic	.450	9

Increased smoke and particulate emissions in LHR engines is often attributed to increased oil consumption due to oil burning on the hot cylinder walls and leakage caused by liner distortion. Although oil consumption was not measured during these tests, the soluble organic fraction results in Table 7 suggest that the particulate increase for the insulated engine was fuel rather than oil derived. During the Hot Ceramic engine tests, the block coolant temperature was maintained at 121°C to minimize the contribution of oil to the total particulate emissions.

The gaseous emissions results presented in Section IV showed the following trends for the insulated engine compared to the Baseline Metal engine. The insulated engine had:

- 1) reduced full-load ISNO_x with a slight increase at low loads
- 2) increased full-load ISCO
- 3) reduced ISHC across the load range

NO_x emissions are formed in a diesel engine when nitrogen and oxygen in the air react at high temperature. NO_x emissions are a strong function of gas temperature. It is expected that LHR engines should produce higher NO_x emissions due to increased in-cylinder gas temperatures. The experimental results, however; showed that the full load (25:1 air-fuel ratio) NO_x emissions were lower for the insulated engine compared to the Baseline Metal engine. The reduction in NO_x may actually be due to lower full-load gas temperatures in the insulated engine. Just because the engine component temperatures are higher, it doesn't mean that the peak in-cylinder gas temperature is significantly higher in the insulated engine. The lower insulated engine gas temperature may be the result of lower initial rates of heat release and the increased combustion duration. The peak firing pressure was consistently lower for the insulated engine which means that with the same trapped air mass the peak gas temperature must also be lower. Kamo et al. (ref. 4) measured a distinct increase in NO_x emissions for an LHR engine across the load range except at the highest load condition corresponding to a fuel-air ratio of approximately 23:1. Thring (ref. 26) also showed that NO_x emissions are sensitive to air-fuel ratio in an LHR engine as liner temperature is increased. At air-fuel ratios in the range from 33 to 32:1 the NO_x emissions began to decrease instead of increase with increasing liner temperature. However; Thring concluded that there were no clear trends in NO_x emissions since the results were not consistent at other engine speeds. Bryzik et al. (ref. 6) found that the NO_x emissions from an LHR engine were lower than the standard engine when the injection timing was retarded to obtain the same fuel economy. Alkidas (ref. 26) also showed that the LHR engine NO_x emissions were about

the same as the standard engine emissions at full-load. Alkidas attributed the low NO_x emissions to combustion occurring later in the cycle for the LHR engine.

The experimental results showed that the carbon monoxide emissions increased at full-load (25:1 air-fuel ratio) for the insulated engine compared to the Baseline Metal engine. Carbon monoxide is oxidized to carbon dioxide at high temperature in the presence of oxygen. The increase in full-load CO emissions is the result of poor fuel-air mixing and lower peak gas temperatures for the LHR engine due to degraded combustion.

The LHR engine unburned hydrocarbons were reduced across the entire load range compared to the Baseline Metal engine. The LHR engine's higher fire deck and piston crown temperatures may have reduced quenching of the oxidation reactions near the combustion chamber surfaces resulting in reduced hydrocarbon emissions. The LHR engine's increased exhaust gas temperature may also have contributed to the oxidation of hydrocarbons. Alkidas (ref. 26) measured an increase in LHR engine unburned hydrocarbons that was attributed to oil burning on the hot cylinder walls. This was not a problem with the SwRI experiment, as shown by the soluble organic fractions particulate results because the liner was cooled during LHR engine tests. Kamo (ref. 4) measured no consistent differences in HC or CO emissions from insulated and cooled engines. Cole et al. (ref. 25) using an air gap insulated piston measured HC reductions from 0 to 40 percent depending on the test conditions.

VII. CONCLUSIONS

The following conclusions were drawn from this investigation that used a single-cylinder, direct-injected diesel engine:

1. Adding ceramic coatings to the combustion chamber significantly reduced heat transfer to the engine coolant. The IRIS engine model predicted a 30 percent reduction in heat transfer to the coolant for the Hot Ceramic engine compared to the Baseline Metal engine at 2000 rpm, full-load conditions (25:1 air-fuel ratio). Experimental heat transfer measurements were not made.
2. Insulating the combustion chamber reduced the engine's ITE. An ITE decrease of 3.4 percentage points (7.4 percent) was measured at 2000 rpm, full-load for the Hot Ceramic engine compared to the Baseline Metal engine.
3. The full load smoke and particulate emissions were higher for the LHR engine compared to the Baseline Metal engine. The full load smoke and particulate emissions increased by as much as 300 and 500 percent respectively for the Hot Ceramic engine compared to the Baseline Metal engine.
4. The LHR engine hydrocarbon emissions were lower across the load range, the CO emissions increased at full load and NO_x emissions were reduced slightly at the full-load condition compared to the Baseline Metal engine.
5. The NO_x and particulate emissions were very sensitive to fuel injection timing. The lower baseline particulate and NO_x emission levels could not be reached in the Hot Ceramic engine at 2000 rpm, full-load by advancing or retarding the fuel injection timing.
6. The Hot Ceramic engine had significantly higher engine component and exhaust gas temperatures compared to the Baseline Metal engine. The increase in exhaust gas temperature was partially due to the insulation and combustion occurring later in the cycle.
7. The LHR engine combustion was characterized by less premixed burning, lower peak heat release rates, and longer combustion duration compared to the Baseline Metal engine. The combustion duration increased by 51 percent for the Baseline Ceramic engine and 106 percent for the Hot Ceramic engine compared to the Baseline Metal engine combustion at 2000 rpm full load. A small portion (3 degrees crank angle) of the increased combustion duration in the Hot Ceramic engine was attributed to longer fuel injection duration.
8. The LHR engine's reduced thermal efficiency and changed exhaust emissions were attributed to degraded combustion. The degraded combustion was thought to be the result of an unoptimized LHR engine fuel injection system that resulted in poor fuel air mixing.
9. The Hot Ceramic engine fuel injection duration increased and the peak fuel injection pressure was reduced compared to the Baseline Metal engine. The change in fuel injection pressure characteristics was attributed to changes in fuel viscosity with temperature.
10. Volumetric efficiency was reduced in the LHR engine. The boost pressure had to be increased during LHR engine tests to maintain Baseline Metal engine air flow rates.

PRECEDING PAGE BLANK NOT FILMED

VII. RECOMMENDATIONS FOR FURTHER RESEARCH

- 1) The LHR engine combustion system should be optimized to see if baseline metal engine combustion and emissions can be obtained. Specific combustion system modifications should include the following components:
 - a) High pressure fuel injection pump
 - b) Fuel injection nozzles with different hole diameters
 - c) New piston bowl
- 2) Conduct LHR engine tests to see if combustion degradation is due to high combustion chamber temperatures or surface composition effects. The porous ceramic coatings may have a catalytic effect on combustion, change wall wetting characteristics, or influence radiative heat transfer. The LHR engine combustion chamber surface composition may be changed by:
 - a) Constructing an air-gap insulated engine with smooth metal combustion chamber surfaces
 - b) Coating the ceramic coated parts with a layer of chrome oxide

A comparison between the two surface finishes at the same temperature should help to determine if surface finish (smoothness, roughness, porosity, etc.) has an effect on LHR engine performance, emissions, and combustion.

- 3) An experimental energy balance should be conducted on the engine to verify the analytical heat transfer predictions.
- 4) Investigate the combustion and emissions characteristics of synthetic fuels and water/oil emulsions in LHR engines. The high temperatures should help to reduce these fuel's longer ignition delays.

PRECEDING PAGE BLANK NOT FILMED

REFERENCES

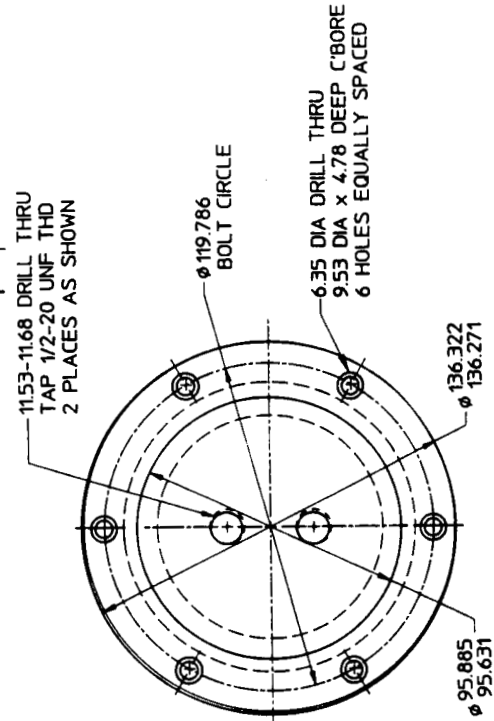
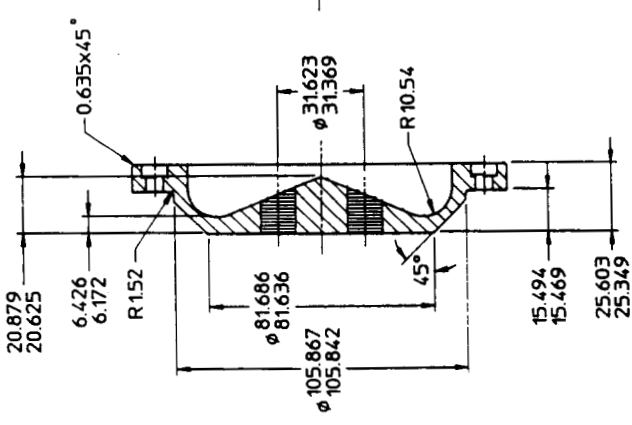
1. Bryzik, W., "Adiabatic Diesel Engine," Research/Development, January 1978, pp. 34-40.
2. Kamo, R., Bryzik, W., "Adiabatic Turbocompound Engine Performance Prediction," SAE Paper 780068, February 1978.
3. Kamo, R., Bryzik, W., "Ceramics in Heat Engines," SAE Paper 790645, June 1979.
4. Kamo, R., Woods, M., Yamada, T., Mori, M., "Thermal Barrier Coating for Diesel Engine Piston," ASME Paper 80-DGP-14, February 1980.
5. Brands, M., Werner, J., Hoehne, J., Kramer, S., "Vehicle Testing of Cummins Turbocompound Diesel Engine," SAE Paper 810073, February 1981.
6. Bryzik, W., Kamo, R., "TACOM/Cummins Adiabatic Engine Program," SAE Paper 830314, February 1983.
7. Frame, E. A., "High-Temperature Lubricants For Minimum-Cooled Diesel Engines," Army Fuels Report, November 1983.
8. Marmach, M., Servant, D., Hannink, R.H.J., Murray, M. J., Swain, M. V., "Toughened PSZ Ceramics - Their Role as Advanced Engine Components," SAE Paper 830318, 1983.
9. Matsuoka, H., Kawamura, H., Toeda, S., "Development of Ceramic Pre-Combustion Chamber for the Automotive Diesel Engine," SAE Paper 840426, 1984.
10. Carr, J., Jones, J., "Post Densified Cr₂O₃ Coatings for Adiabatic Engine," SAE Paper 840432, 1984.
11. Timoney, S. G., "Engine Rig for Screening Ceramic Materials," SAE Paper 840433, 1984.
12. Shimauchi, T., Murakami, T., Nakagaki, T., Tsuya, Y., Umeda, K., "Tribology at High Temperature for Uncooled Heat Insulated Engine," SAE Paper 840429, 1984.
13. Timoney, S. G., Farmer, M. H., "Hoop Stress Effects on Thick Ceramic Cylinders for Diesel Engines," SAE Paper 860449, 1986.
14. Havstad, P. H., Garwin, I. J., Wade, W. R., "A Ceramic Insert Uncooled Diesel Engine," SAE Paper 860447, 1986.
15. Matsuoka, H., Kawamura, H., Matsuda, R., "New Connection System Between Ceramic and Metal for Adiabatic Piston Head," SAE Paper 860441, 1986.
16. Booker, M. K., "Ceramic Technology for Advanced Heat Engines Program Data Base," SAE Publication P-209, Proceedings of the Twenty-Fifth Automotive Technology Development Contractors' Coordination Meeting, pp. 219-224, October 26-29, 1987.
17. Rossi, G. A., Blum, J. B., Knapp, C. E., "Zirconia Toughened Ceramics for Heat Engine Applications," SAE Publication P-209, Proceedings of the Twenty-Fifth Automotive Technology Development Contractors' Coordination Meeting, pp. 225-232, October 26-29, 1987.
18. French, C. C., "Ceramics in Reciprocating Internal Combustion Engines," SAE Paper 841135, September 1984.

19. Yoshimitsu, T., Toyama, K., Sata, F., Yamaguchi, H., "Capabilities of Heat Insulated Diesel Engine," ASME Paper 80-DGP-14.
20. Toyama, K., Yoshimitsu, T., Nishiyama, T., Shimauchi, T., Nakagaki, T., "Heat Insulated Turbocompound Engine," SAE Paper 831345, 1983.
21. Wade, W. R., Havstad, P. H., Ounsted, E. J., Trinker, F. H., Garwin, I. J., "Fuel Economy Opportunities with an Uncooled DI Diesel Engine," I. Mech. E. Paper C432/84, 1984.
22. Toyama, K., Yoshimitsu, T., Nishiyama, T., Shimauchi, T., Nakagaki, T., "Heat Insulated Turbocompound Engine," SAE Technical Paper 830314, 1983.
23. Alkidas, A. C., "Experiments with an Uncooled Single-Cylinder Open-Chamber Diesel," SAE Paper 870020, 1987.
24. Woschni, G., Spindler, W., Kolesa, K., "Heat Insulation of Combustion Chamber Walls - A Measure to Decrease the Fuel Consumption of I. C. Engines?," SAE Paper 870339, 1987.
25. Cole, R. M., Alkidas, A. C., "Evaluation of an Air-Gap-Insulated Piston in a Divided-Chamber Diesel engine," SAE Paper 850359, 1985.
26. Thring, R. H., "Low Heat Rejection Engines," SAE Paper 860314, 1986.
27. Lyn, W. T., "Calculations of the Effect of Rate of Heat Release on the Shape of Cylinder-Pressure Diagram and Cycle Efficiency," Proc. Instn. Mech. Engineers (A. D.), No. I. 1960-61.
28. Timoney, S. G., "No Coolant Diesel Engine," E. E. C. Conference on New Ways to Save Energy, Brussels, Belgium, October 1979.
29. Kamo, R., Bryzik, W., "Cummins-TARADCOM Adiabatic Turbocompound Engine Program," SAE Transactions, Vol. 90, pp. 263-274, 1981.
30. Austen, A. E. W., Lyn W. T., "Relation Between Fuel Injection and Heat Release in a Direct-Injection Engine and the Combustion Processes," Proc. Instn. Mech. Engineers (A. D.), No.1, 1960-61.
31. Henningsen, S., "Evaluation of Emissions and Heat-Release Characteristics from a Simulated Low-Heat-Rejection Diesel Engine," SAE Paper 871616, 1987.
32. Woschni G.: Die Berechnung der Wandverluste und der thermischen Belastung 5der Bauteile von Dieselmotoren. MTZ 31, 1970
33. Hiroyasu, H., Arai, M., Nakawishi, K., "Soot Formation and Oxidation in Diesel Engine," SAE Transactions, Vol. 89, pp. 1148-1161, 1980.

APPENDIX A

ENGINEERING DRAWING FOR PISTON MODIFICATION

EXCEPT AS MAY BE OTHERWISE PROVIDED BY CONTRACT THESE DRAWINGS AND SPECIFICATIONS ARE THE PROPERTY OF SOUTHWEST RESEARCH INSTITUTE AND ARE TO BE USED IN STRICT CONFIDENCE AND SHALL NOT BE REPRODUCED OR COPIED OR USED AS THE BASIS FOR THE MANUFACTURE OR SALE OF APPARATUS WITHOUT PERMISSION



ORIGINAL PAGE IS OF POOR QUALITY

ALL DIMENSIONS IN MILLIMETERS
MAT'L: SAE 8645 ALLOY STEEL

ON Dwg	REVISIONS	DATE	APPROVED
	DESCRIPTION		
	LTR		

FIND NO.	QTY. REQ.	MATERIAL	CODE IDENT NO.	PART OR IDENTIFYING NO.	NOMENCLATURE OR DESCRIPTION
PARTS LIST					
UNLESS OTHERWISE SPECIFIED, INCLUDE CHEMICALLY APPLIED OR PLATED FINISHES			CONTRACT DWN D. DICKY 9/7/86		
TOLERANCES			MECH		
BASIC DIMENSION UNDER 6			ELECT		
6-24 INCL			STDS		
OVER 24			SCALE		
ANGLES 1/2°			SIZE CODE IDENT NO. DRAWING NO.		
COML TOL APPLY TO STOCK SIZES			B 26401		
QTY. REQ.			SHEET		
USED ON			APPLICATION		
NEXT ASSY			SHEET		
SIZE			SHEET		

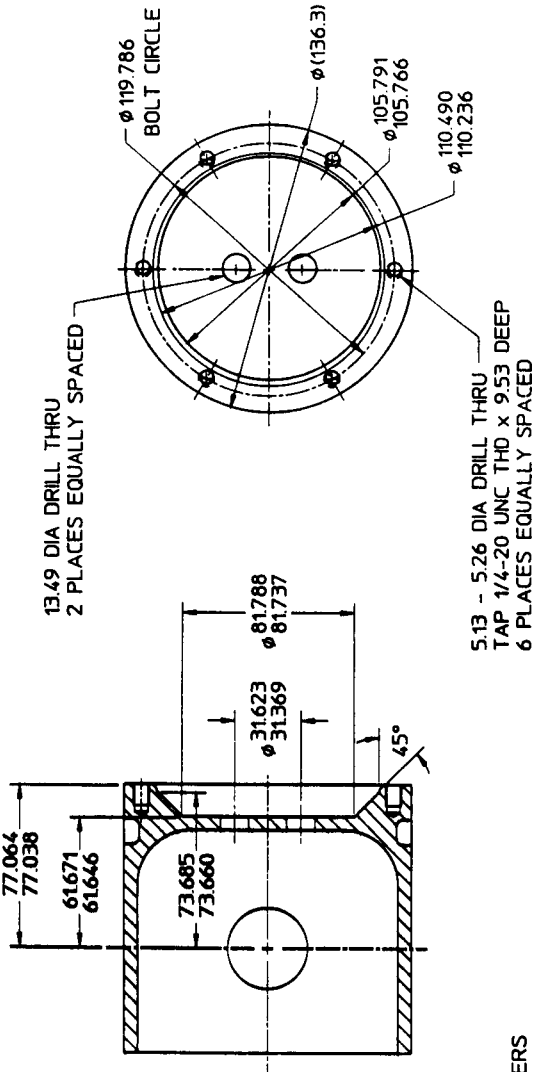
SOUTHWEST RESEARCH INSTITUTE
SAN ANTONIO, TEXAS

PISTON CAP FOR CAT 1Y540 PISTON

SIZE CODE IDENT NO. DRAWING NO.
B 26401

REVISIONS	
DESCRIPTION	DATE
LTR	APPROVED

ORIGINAL PAGE IS
OF POOR QUALITY



13.49 DIA DRILL THRU
2 PLACES EQUALLY SPACED

5.13 - 5.26 DIA DRILL THRU
TAP 1/4-20 UNC THD x 9.53 DEEP
6 PLACES EQUALLY SPACED

ALL DIMENSIONS IN MILLIMETERS
MATERIAL: CAT 1Y540 PISTON

EXCEPT AS MAY BE OTHERWISE PROVIDED BY CONTRACT, THESE DRAWINGS AND SPECIFICATIONS ARE THE PROPERTY OF SOUTHWEST RESEARCH INSTITUTE AND SHALL NOT BE REPRODUCED OR COPIED OR USED AS THE BASIS FOR THE MANUFACTURE OR SALE OF APPARATUS WITHOUT PERMISSION.

FIND NO.		QTY. REQ.	CODE IDENT NO.	PART OR IDENTIFYING NO.	NOMENCLATURE OR DESCRIPTION
PARTS LIST					
UNLESS OTHERWISE SPECIFIED DIMENSIONS ARE IN INCHES AND INCLUDING UNLESS INDICATED PLATED FINISHES		CONTRACT			
TOLERANCES		DWN D. DICKEY 9/7/88			
BASIC DIMENSION	DECIMALS	3 PLACE	FRAC. TIONS		
UNDER 6	± .02	7 .005	± 1/64		
6-24 INCL	± .03	7 .010	± 1/32		
OVER 24	± .06	7 .015	± 1/16		
ANGLES: 1/2°					
MATERIAL					
FINISH					
COML TOL. APPLY TO STOCK SIZES					
QTY. REQ.	USED ON				
APPLICATION					
NEXT ASSY					
SIZE					
SOUTHWEST RESEARCH INSTITUTE SAN ANTONIO, TEXAS					
PISTON MODIFICATION TO ACCEPT PISTON CAP FOR CAT 1Y540 ENGINE					
SIZE		CODE IDENT NO		DRAWING NO	
B		26401			
SCALE		SHEET			

APPENDIX B
FUEL SPECIFICATION AND DISTILLATION CURVE

FUEL SPECIFICATIONS

FUEL TYPE: DF-2

API GRAVITY = 34.00 AT 60°F

SPECIFIC GRAVITY = 0.8550 AT 60°F

CETANE NUMBER = 41.3

CETANE INDEX = 43.7

40°C VISCOSITY = 2.50 CST.

PERCENT SATURATES = 60.8

PERCENT AROMATICS = 39.2

PERCENT SULFUR = 0.12

MONO PERCENT AROMATICS = 8.34

DI PERCENT AROMATICS = 5.69

TRI PERCENT AROMATICS = 1.21

PERCENT CARBON = 86.99 ± .18

PERCENT HYDROGEN = 12.70 ± .00

GROSS HEAT OF COMBUSTION = 19384, BTU/LB

NET HEAT OF COMBUSTION = 18227, BTU/LB

STEAM GUM = 2.2 mg/100 ml

FLASH POINT = 134°F/57°C

PRECEDING PAGE BLANK NOT FILMED

DISTILLATION CURVE

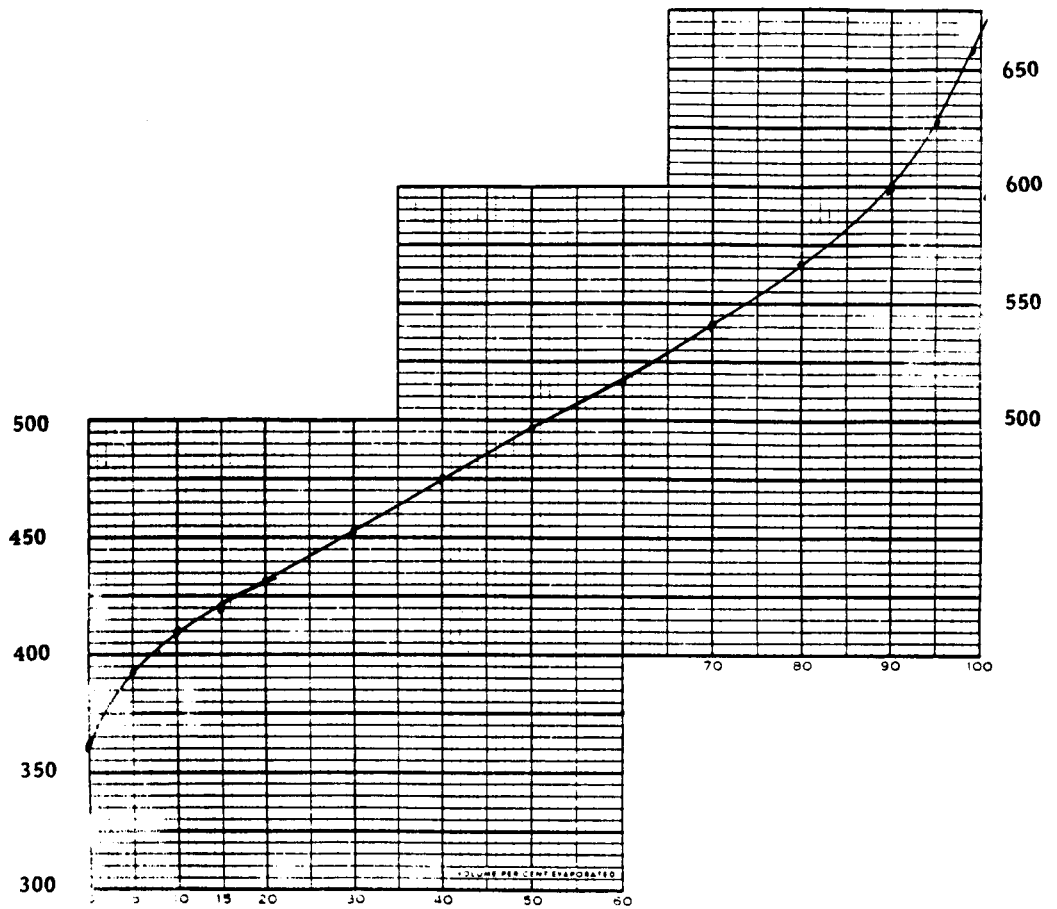
<u>%</u>	<u>IBP</u>	<u>5</u>	<u>10</u>	<u>15</u>	<u>20</u>	<u>30</u>	<u>40</u>	<u>50</u>	<u>60</u>	<u>70</u>	<u>80</u>	<u>90</u>	<u>95</u>	<u>EP</u>
COND. F	360	391	407	418	430	450	473	494	514	538	564	597	624	658
COND.* F	362	393	409	420	432	452	475	497	517	541	567	600	627	658
EVAP.* F	362	393	409	420	432	452	475	497	517	541	567	600	627	658

TIME **

*CORRECT TO 29.92" Hg

** SUCCESSIVE INCREMENTS IN MIN. AND SEC.

ROOM TEMPERATURE 73.4°F



APPENDIX C
EXPERIMENTAL PERFORMANCE AND EMISSIONS DATA

<u>Test Number</u>		<u>Condition</u>	<u>Run Numbers</u>
1	Baseline Metal:	82°C Coolant, 82°C Intake Air	53 - 61
2	"	104°C Coolant, 82°C Intake Air	64 - 72
3	"	82°C Coolant, 60°C Intake Air	74 - 76
4	Baseline Ceramic:	82°C Coolant, 82°C Intake Air	87 - 96
5	"	104°C Coolant, 82°C Intake Air	97 - 99
6	"	82°C Coolant, 60°C Intake Air	100 - 102
7	Hot Ceramic:	121°C Block Coolant, 82°C Intake Air, Coolant Drained From Head	103 - 112
8	"	Same as No. 7 but with retarded fuel-injection timing	117 - 121
9	"	Same as No. 7 but with advanced fuel-injection timing	122 - 124

Three plots are shown for each run number. The top plot is fuel injection pressure versus crankangle. The middle plot is cylinder pressure versus crankangle. The bottom plot displays both heat release rate and cumulative heat release versus crankangle. The cumulative heat release curve is the smoother of the two heat release curves and does not have any spikes.

PRECEDING PAGE BLANK NOT FILMED

****NASA PROJECT 03-8966 ****

TEST #1	53	54	55	56	57	58	59	60	61
RUN NUMBER	53	54	55	56	57	58	59	60	61
DAY (julian)	7083	7083	7083	7084	7084	7084	7085	7085	7085
TIME (military)	1354	1519	1644	1232	1414	1539	1123	1430	1617
ENGINE HOURS	50.9	52.2	53.6	56.9	58.6	59.9	63.3	66.1	67.7
ENGINE PARAMETERS									
ENGINE SPEED (rpm)	1401	1400	1403	1700	1703	1701	2001	2001	2000
TORQUE (N-M)	204.1	135.7	68.2	203.3	136.4	68.3	204.0	135.6	67.8
POWER (kw)	30.0	19.9	10.0	36.2	24.3	12.2	42.8	28.4	14.2
BSFC (g/kw-hr)	220.2	229.5	271.7	220.6	227.9	273.9	227.3	234.2	281.4
BMEP (bar)	10.4	6.9	3.5	10.3	6.9	3.5	10.4	6.9	3.4
BTE (%)	38.6	37.0	31.3	38.5	37.3	31.0	37.4	36.3	30.2
INDICATED PARAMETERS									
POWER (ikw)	34.9	24.8	15.0	43.4	31.5	19.4	52.3	37.9	23.7
ISFC (g/ikw-hr)	189.0	183.9	182.0	184.0	175.8	172.1	186.0	175.6	168.7
IMEP (bar)	12.1	8.6	5.2	12.4	9.0	5.5	12.7	9.2	5.7
ITE, actual (%)	44.9	46.2	46.7	46.1	48.3	49.3	45.7	48.4	50.3
ITE, theoretical (%)	55.8	57.2	58.6	55.9	57.2	58.6	55.8	57.1	58.5
RATIO, actual/theoretical	.806	.808	.796	.825	.844	.842	.819	.847	.860
ENGINE FLOW PARAMETERS									
FUEL FLOW (kg/hr)	6.6	4.6	2.7	8.0	5.5	3.3	9.7	6.7	4.0
AIR FLOW (kg/hr)	161.7	142.9	119.3	200.5	174.3	146.3	239.0	205.6	172.5
AIR FUEL RATIO	24.5	31.3	43.8	25.1	31.4	43.9	24.6	30.9	43.1
CHEMICAL AIR FUEL RATIO	27.1	32.2	46.8	26.5	33.1	46.8	26.1	32.4	44.7
EQUIVALENCE RATIO	.5863	.4594	.3283	.5728	.4576	.3275	.5847	.4658	.3333
APPARENT BLOWBY (m**3/hr)	10.4	8.8	0.0	10.7	8.8	6.9	11.9	11.1	9.3
SMOKE OPACITY (%)	.5	.5	.5	.6	.5	.8	1.2	.9	1.5
TEMPERATURE PARAMETERS (deg.c)									
COOLANT IN BLOCK	80	80	80	79	80	81	79	79	80
COOLANT OUT BLOCK	82	82	82	82	82	82	82	82	82
COOLANT IN HEAD	79	79	79	79	79	80	79	79	79
COOLANT OUT HEAD	82	81	80	82	81	80	82	81	80
OIL TO COOLER	92	93	88	97	96	94	101	104	99
OIL TO ENGINE	91	92	87	93	95	93	100	102	98
FUEL	33	35	35	33	34	34	32	36	36
INTAKE AT PORT	83	81	80	85	83	84	84	84	82
LFE INLET	20	21	22	19	19	19	16	19	20
EXHAUST PORT	503	401	294	523	421	315	562	461	355
LINER INSIDE #1	151	149	127	159	145	132	171	153	139
LINER INSIDE #2	151	148	127	159	146	133	171	153	139
LINER INSIDE #3	120	115	104	124	116	109	128	121	112
LINER INSIDE #4	121	116	105	125	118	110	131	123	114
LINER INSIDE #5	119	117	106	123	117	111	129	124	116
LINER INSIDE #6	118	116	106	122	117	111	128	123	116
LINER OUTSIDE #7	135	132	117	141	130	121	150	136	125
LINER OUTSIDE #8	135	131	117	140	130	121	148	134	125
LINER OUTSIDE #9	106	102	95	108	104	99	111	107	101
LINER OUTSIDE #10	101	98	93	102	99	95	105	101	97
LINER OUTSIDE #11	109	107	99	112	108	103	116	113	108
LINER OUTSIDE #12	108	106	99	110	106	102	114	110	105
FIRE SURFACE #1	307	261	205	303	263	210	315	271	218
FIRE SURFACE #2	302	257	204	295	259	208	305	263	213
PRESSURE PARAMETERS									
OIL (kpa)	37.4	37.2	38.3	41.3	40.4	41.0	44.3	43.0	44.1
FUEL (kpa)	23.1	23.3	23.5	23.6	24.4	25.3	22.6	23.8	24.2
BOOST (kpa)	6.7	4.5	2.3	7.6	5.1	2.6	8.8	5.9	2.9
EXHAUST (kpa)	6.7	4.6	2.3	7.6	5.1	2.6	8.9	5.9	2.9
EMISSION PARAMETERS									
PARTICULATES (g/kw-hr)	.0595	.0908	.1842	.0938	.1307	.2882	.2072	.1836	.5027
BSHC (g/kw-hr)	.6498	.8426	1.5845	.4878	.9281	1.8522	.4422	.8863	1.7577
BSCO (g/kw-hr)	1.4172	1.1526	2.7913	1.0359	1.3712	3.2241	1.6821	1.5185	3.8010
BSNOx (g/kw-hr)	17.857	19.925	21.401	14.102	16.416	16.736	10.837	12.847	12.459
CO2 (%)	8.0	6.7	4.5	8.2	6.5	4.5	8.3	6.6	4.7
O2 (%)	8.8	11.3	14.2	9.3	11.5	14.2	9.2	11.4	13.9
PARTICULATES (g/ikw-hr)	.0511	.0728	.1228	.0782	.1007	.1807	.1697	.1378	.3004
ISHC (g/ikw-hr)	.5579	.6752	1.0614	.4070	.7160	1.1635	.3618	.6644	1.0539
ISCO (g/ikw-hr)	1.2168	.9236	1.8698	.8642	1.0578	2.0253	1.3764	1.1384	2.2789
ISNOx (g/ikw-hr)	15.332	15.968	14.336	11.764	12.664	10.513	8.8682	9.6309	7.4699
AMBIENT PARAMETERS									
BARO. PRESSURE (mm.hg)	734.5	733.9	733.9	738.4	737.5	737.5	739.6	737.9	737.1
RELATIVE HUMIDITY (%)	25.7	30.9	30.4	31.2	35.7	36.7	44.5	42.2	36.9

****NASA PROJECT 03-8966 ****

TEST #2		64	65	66	67	68	69	70	71	72
RUN NUMBER		64	65	66	67	68	69	70	71	72
DAY	(julian)	7089	7089	7089	7089	7089	7089	7090	7090	7090
TIME	(military)	1511	1636	1749	1414	1551	1718	12 9	15 9	1658
ENGINE HOURS		75.3	76.6	77.8	82.9	84.5	85.9	89.5	92.3	94.0
ENGINE PARAMETERS										
ENGINE SPEED	(rpm)	1405	1398	1397	1701	1701	1702	2001	1999	2001
TORQUE	(N-M)	203.8	135.4	68.4	203.6	135.2	68.6	204.3	134.9	67.9
POWER	(kw)	30.0	19.8	10.0	36.3	24.1	12.2	42.8	28.3	14.2
BSFC	(g/kw-hr)	212.8	223.1	259.8	216.8	225.1	261.2	228.0	235.6	279.0
BMEP	(bar)	10.4	6.9	3.5	10.4	6.9	3.5	10.4	6.9	3.5
BTE	(%)	39.9	38.1	32.7	39.2	37.7	32.5	37.2	36.0	30.4
INDICATED PARAMETERS										
POWER	(ikw)	34.7	24.6	14.7	43.3	31.1	19.3	52.3	37.7	23.7
ISFC	(g/ikw-hr)	183.7	180.2	176.5	181.5	174.1	165.6	186.6	176.4	167.3
IMEP	(bar)	12.0	8.5	5.1	12.4	8.9	5.5	12.7	9.2	5.8
ITE,actual	(%)	46.2	47.1	48.1	46.8	48.8	51.3	45.5	48.1	50.7
ITE,theoretical	(%)	55.9	57.1	58.6	55.9	57.2	58.6	55.8	57.1	58.6
RATIO, actual/theoretical		.827	.825	.821	.837	.853	.874	.816	.843	.866
ENGINE FLOW PARAMETERS										
FUEL FLOW	(kg/hr)	6.4	4.4	2.6	7.9	5.4	3.2	9.8	6.7	4.0
AIR FLOW	(kg/hr)	159.8	137.3	114.0	197.5	170.4	141.6	239.5	207.2	173.6
AIR FUEL RATIO		25.0	31.0	43.8	25.1	31.4	44.3	24.5	31.1	43.8
CHEMICAL AIR FUEL RATIO		26.5	33.3	46.9	26.3	33.1	46.5	25.9	33.2	46.5
EQUIVALENCE RATIO		.5746	.4632	.3281	.5730	.4576	.3246	.5860	.4619	.3287
APPARENT BLOWBY (m**3/hr)		10.2	8.8	6.5	10.0	8.6	6.9	13.6	11.9	9.8
SMOKE OPACITY	(%)	.3	.4	.4	.5	.6	.5	1.2	1.1	1.8
TEMPERATURE PARAMETERS (deg.c)										
COOLANT IN BLOCK		103	103	103	102	103	103	102	102	103
COOLANT OUT BLOCK		105	104	104	105	105	104	105	104	104
COOLANT IN HEAD		103	104	102	102	103	101	102	103	104
COOLANT OUT HEAD		104	104	102	105	104	101	105	104	104
OIL TO COOLER		103	100	96	101	100	100	99	105	105
OIL TO ENGINE		101	99	95	98	99	99	93	102	104
FUEL		34	34	33	38	37	38	38	41	40
INTAKE AT PORT		82	81	81	85	84	85	84	84	82
LFE INLET		15	15	14	22	23	22	23	25	25
EXHAUST PORT		505	404	302	536	430	326	579	464	357
LINER INSIDE #1		165	160	143	185	161	148	186	173	157
LINER INSIDE #2		166	159	143	185	162	149	187	173	157
LINER INSIDE #3		132	126	118	138	129	123	138	132	126
LINER INSIDE #4		135	128	120	141	131	124	140	133	127
LINER INSIDE #5		133	127	120	138	129	124	135	132	128
LINER INSIDE #6		132	127	119	136	128	123	134	131	127
LINER OUTSIDE #7		151	147	134	164	147	137	167	156	143
LINER OUTSIDE #8		150	145	134	162	147	138	164	153	144
LINER OUTSIDE #9		119	115	111	120	116	113	121	118	114
LINER OUTSIDE #10		119	115	111	118	115	112	118	114	113
LINER OUTSIDE #11		123	120	114	122	119	115	121	120	118
LINER OUTSIDE #12		122	118	114	124	119	116	122	120	118
FIRE SURFACE #1		307	267	217	315	273	222	322	277	228
FIRE SURFACE #2		301	263	218	304	265	218	311	267	223
PRESSURE PARAMETERS										
OIL	(kpa)	35.6	36.1	36.8	40.3	40.4	40.4	45.6	43.0	42.9
FUEL	(kpa)	22.7	22.9	22.9	23.7	24.4	25.1	23.0	23.8	24.6
BOOST	(kpa)	6.4	4.2	1.7	7.3	4.9	2.3	8.8	6.1	3.1
EXHAUST	(kpa)	6.4	4.2	1.8	7.2	4.8	2.2	8.8	6.1	3.2
EMISSION PARAMETERS										
PARTICULATES	(g/kw-hr)	.0594	.0834	.1787	.1090	.1169	.3114	.2834	.2208	.5134
BSHC	(g/kw-hr)	.5275	.7657	1.5100	.4084	.8657	1.5110	.3943	.7785	1.7182
BSCO	(g/kw-hr)	1.0957	1.2065	2.6551	1.0216	1.3003	3.0311	2.0323	1.4842	3.7788
BSNOx	(g/kw-hr)	17.538	20.699	22.241	14.596	16.949	16.328	11.065	12.838	12.216
CO2	(%)	8.2	6.5	4.5	8.3	6.5	4.6	8.4	6.5	4.6
O2	(%)	9.4	11.6	14.2	9.2	11.5	14.1	9.1	11.6	14.2
PARTICULATES	(g/ikw-hr)	.0512	.0674	.1209	.0913	.0905	.1972	.2320	.1654	.3083
ISHC	(g/ikw-hr)	.4554	.6183	1.0261	.3419	.6696	.9583	.3227	.5829	1.0306
ISCO	(g/ikw-hr)	.9460	.9742	1.8042	.8553	1.0058	1.9223	1.6635	1.1112	2.2665
ISNOx	(g/ikw-hr)	15.140	16.714	15.114	12.220	13.110	10.355	9.0570	9.6121	7.3270
AMBIENT PARAMETERS										
BARO.PRESSURE	(mm.hg)	745.7	745.5	745.5	744.5	743.6	743.1	742.1	739.1	737.8
RELATIVE HUMIDITY	(%)	13.9	14.5	16.7	19.7	20.1	20.3	21.1	22.7	19.0

****NASA PROJECT 03-8966 ****

TEST #3		74	75	76
RUN NUMBER				
DAY	(julian)	7114	7114	7114
TIME	(military)	1235	1351	15 7
ENGINE HOURS		102.0	103.2	104.4
ENGINE PARAMETERS				
ENGINE SPEED	(rpm)	2004	2002	2002
TORQUE	(N-M)	204.4	136.0	68.5
POWER	(kw)	42.9	28.5	14.4
BSFC	(g/kw-hr)	225.5	234.3	282.6
BMEP	(bar)	10.4	6.9	3.5
BTE	(%)	37.7	36.2	30.0
INDICATED PARAMETERS				
POWER	(ikw)	52.8	38.4	24.3
ISFC	(g/ikw-hr)	183.2	174.0	167.4
IMEP	(bar)	12.8	9.3	5.9
ITE, actual	(%)	46.3	48.8	50.7
ITE, theoretical	(%)	56.0	57.2	58.5
RATIO, actual/theoretical		.827	.853	.867
ENGINE FLOW PARAMETERS				
FUEL FLOW	(kg/hr)	9.7	6.7	4.1
AIR FLOW	(kg/hr)	247.1	210.6	174.2
AIR FUEL RATIO		25.5	31.5	42.9
CHEMICAL AIR FUEL RATIO		26.7	33.2	44.5
EQUIVALENCE RATIO		.5633	.4562	.3352
APPARENT BLOWBY (m**3/hr)		13.2	10.2	9.3
SMOKE OPACITY	(%)	5.4	5.2	5.4
TEMPERATURE PARAMETERS (deg.c)				
COOLANT IN BLOCK		79	79	81
COOLANT OUT BLOCK		83	83	83
COOLANT IN HEAD		78	79	80
COOLANT OUT HEAD		83	82	81
OIL TO COOLER		103	103	103
OIL TO ENGINE		104	104	104
FUEL		43	44	41
INTAKE AT PORT		62	62	60
LFE INLET		27	28	23
EXHAUST PORT		542	443	343
LINER INSIDE #1		165	152	141
LINER INSIDE #2		166	153	142
LINER INSIDE #3		127	121	114
LINER INSIDE #4		129	123	116
LINER INSIDE #5		127	123	118
LINER INSIDE #6		126	122	117
LINER OUTSIDE #7		146	135	126
LINER OUTSIDE #8		143	134	126
LINER OUTSIDE #9		106	103	100
LINER OUTSIDE #10		101	99	96
LINER OUTSIDE #11		111	108	105
LINER OUTSIDE #12		111	108	105
FIRE SURFACE #1		271	237	194
FIRE SURFACE #2		285	248	200
PRESSURE PARAMETERS				
OIL	(kpa)	49.4	49.3	49.2
FUEL	(kpa)	22.7	23.5	24.2
BOOST	(kpa)	8.5	5.6	2.5
EXHAUST	(kpa)	8.3	5.7	2.5
EMISSION PARAMETERS				
PARTICULATES	(g/kw-hr)	.3323	.3205	.7126
BSHC	(g/kw-hr)	.5460	.8474	1.7551
BSCO	(g/kw-hr)	1.8491	1.6452	4.1655
BSNOx	(g/kw-hr)	8.7105	10.160	10.541
CO2	(%)	8.1	6.5	4.8
O2	(%)	9.6	11.7	14.1
PARTICULATES	(g/ikw-hr)	.2698	.2378	.4232
ISHC	(g/ikw-hr)	.4436	.6292	1.0394
ISCO	(g/ikw-hr)	1.5023	1.2214	2.4670
ISNOx	(g/ikw-hr)	7.0772	7.5430	6.2430
AMBIENT PARAMETERS				
BARO.PRESSURE	(mm.hg)	742.6	741.6	741.7
RELATIVE HUMIDITY	(%)	40.1	36.5	65.3

****NASA PROJECT 03-8966 ****

TEST #4	87	88	89	91	92	93	94	95	96
RUN NUMBER									
DAY (julian)	7156	7156	7156	7159	7159	7159	7159	7159	7159
TIME (military)	1136	1236	1345	1125	1237	14 1	1526	1623	1730
ENGINE HOURS	13.6	14.6	15.7	19.6	20.8	22.2	23.4	24.4	25.5
ENGINE PARAMETERS									
ENGINE SPEED (rpm)	1403	1405	1403	1704	1703	1703	2004	2004	2003
TORQUE (N-M)	185.9	127.7	65.4	186.4	127.9	63.3	187.0	124.0	60.8
POWER (kw)	27.3	18.8	9.6	33.3	22.8	11.3	39.3	26.0	12.8
BSFC (g/kw-hr)	241.0	246.9	285.5	238.3	244.2	289.3	247.8	256.6	312.9
BMEP (bar)	9.4	6.5	3.3	9.5	6.5	3.2	9.5	6.3	3.1
BTE (%)	35.2	34.4	29.7	35.6	34.8	29.4	34.3	33.1	27.1
INDICATED PARAMETERS									
POWER (ikw)	32.9	24.3	15.1	41.2	30.7	19.2	49.3	36.1	22.8
ISFC (g/ikw-hr)	200.3	190.6	181.1	192.6	181.5	170.3	197.2	185.0	174.8
IMEP (bar)	11.4	8.4	5.2	11.7	8.7	5.5	11.9	8.7	5.5
ITE,actual (%)	42.4	44.5	46.9	44.1	46.8	49.9	43.1	45.9	48.6
ITE,theoretical (%)	55.7	57.2	58.6	56.0	57.2	58.7	55.8	57.1	58.5
RATIO, actual/theoretical	.760	.779	.800	.788	.818	.850	.772	.804	.830
ENGINE FLOW PARAMETERS									
FUEL FLOW (kg/hr)	6.6	4.6	2.7	7.9	5.6	3.3	9.7	6.7	4.0
AIR FLOW (kg/hr)	161.0	145.0	120.0	200.6	175.7	145.5	238.7	206.3	171.9
AIR FUEL RATIO	24.5	31.3	43.7	25.3	31.5	44.6	24.5	30.9	43.1
CHEMICAL AIR FUEL RATIO	24.0	30.6	42.8	24.9	31.2	43.4	24.6	30.8	42.8
EQUIVALENCE RATIO	.5880	.4600	.3288	.5683	.4561	.3226	.5863	.4655	.3340
APPARENT BLOWBY (m**3/hr)	11.9	10.7	7.9	11.9	10.2	7.4	12.4	10.2	10.7
SMOKE OPACITY (%)	1.7	1.0	.7	1.2	.8	1.4	1.8	1.3	2.0
TEMPERATURE PARAMETERS (deg.c)									
COOLANT IN BLOCK	79	80	80	80	79	80	79	79	80
COOLANT OUT BLOCK	82	82	83	83	82	83	82	82	82
COOLANT IN HEAD	79	80	81	79	80	81	79	80	81
COOLANT OUT HEAD	83	82	82	83	83	82	84	83	82
OIL TO COOLER	100	102	99	102	103	101	103	103	102
OIL TO ENGINE	100	103	100	104	104	101	104	104	104
FUEL	38	42	42	39	41	42	42	42	42
INTAKE AT PORT	82	82	81	82	82	83	84	83	82
LFE INLET	27	28	29	25	25	27	26	26	25
EXHAUST PORT	544	439	336	557	457	353	601	490	378
LINER INSIDE #1	147	133	123	153	138	127	162	145	131
LINER INSIDE #2	148	134	124	154	138	127	164	146	131
LINER INSIDE #3	120	115	109	123	117	111	127	118	113
LINER INSIDE #4	119	113	108	121	115	110	125	117	112
LINER INSIDE #5	121	116	111	123	119	114	127	121	117
LINER INSIDE #6	119	115	110	122	118	113	126	120	116
LINER OUTSIDE #7	129	119	111	133	123	115	140	128	117
LINER OUTSIDE #8	117	110	105	119	111	106	122	113	107
LINER OUTSIDE #9	111	107	102	113	108	104	116	109	105
LINER OUTSIDE #10	108	104	100	110	105	102	112	107	103
LINER OUTSIDE #11	100	98	96	102	99	97	103	99	98
LINER OUTSIDE #12	107	105	101	109	105	103	111	107	105
FIRE SURFACE #1	221	193	161	226	198	165	234	202	171
FIRE SURFACE #2	219	192	162	224	197	166	231	201	171
PRESSURE PARAMETERS									
OIL (kpa)	45.3	44.7	45.5	50.1	49.9	50.5	54.3	54.3	54.6
FUEL (kpa)	23.0	23.2	23.6	23.5	24.4	25.6	22.9	23.8	24.6
BOOST (kpa)	6.7	4.8	2.1	7.4	5.2	2.5	8.7	5.9	2.8
EXHAUST (kpa)	6.9	4.8	2.2	7.7	5.2	2.6	9.0	5.9	2.8
EMISSION PARAMETERS									
PARTICULATES (g/kw-hr)	.2721	.1536	.2389	.2860	.1647	.3357	.5577	.3261	.5701
BSHC (g/kw-hr)	.3500	.6476	1.4221	.3587	.8018	1.4058	.2275	.7647	1.3264
BSCO (g/kw-hr)	3.9190	2.2993	2.9073	2.7308	1.7082	3.0657	2.7112	2.0143	3.7571
BSNOx (g/kw-hr)	13.364	17.239	22.045	12.666	16.627	17.441	9.6530	12.477	12.986
CO2 (%)	9.0	7.0	5.0	8.7	6.9	4.9	8.8	7.0	5.0
O2 (%)	8.2	11.0	13.7	8.7	11.2	13.9	8.6	11.0	13.7
PARTICULATES (g/ikw-hr)	.2259	.1188	.1517	.2311	.1224	.1972	.4432	.2351	.3186
ISHC (g/ikw-hr)	.2910	.5000	.9020	.2899	.5959	.8277	.1810	.5513	.7412
ISCO (g/ikw-hr)	3.2583	1.7753	1.8440	2.2073	1.2695	1.8050	2.1576	1.4522	2.0996
ISNOx (g/ikw-hr)	11.111	13.310	13.983	10.238	12.357	10.269	7.6818	8.9952	7.2570
AMBIENT PARAMETERS									
BARO.PRESSURE (mm.hg)	743.8	743.6	743.4	742.8	742.5	741.6	741.1	740.8	740.6
RELATIVE HUMIDITY (%)	57.3	53.1	47.8	80.5	86.1	72.2	79.4	90.2	84.2

****NASA PROJECT 03-8966 ****

TEST #5				
RUN NUMBER		97	98	99
DAY	(julian)	7160	7160	7160
TIME	(military)	1623	1750	1856
ENGINE HOURS		32.0	33.4	34.5
ENGINE PARAMETERS				
ENGINE SPEED	(rpm)	1402	1700	2001
TORQUE	(N-M)	185.7	185.0	184.6
POWER	(kw)	27.3	32.9	38.7
BSFC	(g/kw-hr)	240.2	241.5	250.4
BMEP	(bar)	9.4	9.4	9.4
BTE	(%)	35.4	35.2	33.9
INDICATED PARAMETERS				
POWER	(ikw)	32.5	40.3	48.8
ISFC	(g/ikw-hr)	201.6	197.2	198.8
IMEP	(bar)	11.2	11.5	11.8
ITE,actual	(%)	42.1	43.0	42.7
ITE,theoretical	(%)	55.8	56.0	55.8
RATIO, actual/theoretical		.755	.769	.766
ENGINE FLOW PARAMETERS				
FUEL FLOW	(kg/hr)	6.5	8.0	9.7
AIR FLOW	(kg/hr)	161.7	201.6	237.8
AIR FUEL RATIO		24.7	25.3	24.5
CHEMICAL AIR FUEL RATIO		23.7	24.7	24.1
EQUIVALENCE RATIO		.5823	.5676	.5863
APPARENT BLOWBY (m**3/hr)		12.8	12.4	11.5
SMOKE OPACITY (%)		1.7	2.0	2.8
TEMPERATURE PARAMETERS (deg.c)				
COOLANT IN BLOCK		117	120	120
COOLANT OUT BLOCK		120	123	122
COOLANT IN HEAD		130	135	136
COOLANT OUT HEAD		134	140	142
OIL TO COOLER		103	103	103
OIL TO ENGINE		104	104	104
FUEL		42	43	44
INTAKE AT PORT		82	83	83
LFE INLET		26	25	26
EXHAUST PORT		560	575	628
LINER INSIDE #1		175	184	191
LINER INSIDE #2		175	185	191
LINER INSIDE #3		140	145	147
LINER INSIDE #4		140	145	146
LINER INSIDE #5		137	141	143
LINER INSIDE #6		136	140	142
LINER OUTSIDE #7		160	167	172
LINER OUTSIDE #8		143	148	147
LINER OUTSIDE #9		135	139	140
LINER OUTSIDE #10		133	137	138
LINER OUTSIDE #11		125	127	127
LINER OUTSIDE #12		127	129	125
FIRE SURFACE #1		313	337	345
FIRE SURFACE #2		307	351	363
PRESSURE PARAMETERS				
OIL	(kpa)	44.0	49.2	53.7
FUEL	(kpa)	22.8	23.9	22.5
BOOST	(kpa)	7.0	7.7	8.9
EXHAUST	(kpa)	6.8	7.6	9.0
EMISSION PARAMETERS				
PARTICULATES	(g/kw-hr)	.2641	.3128	.5230
BSHC	(g/kw-hr)	.2423	.2027	.1571
BSCO	(g/kw-hr)	3.7091	2.9677	2.8028
BSNOx	(g/kw-hr)	13.987	12.442	10.246
CO2	(%)	9.1	8.8	9.0
O2	(%)	8.1	8.6	8.3
PARTICULATES	(g/ikw-hr)	.2223	.2555	.4150
ISHC	(g/ikw-hr)	.2034	.1656	.1247
ISCO	(g/ikw-hr)	3.1134	2.4239	2.2246
ISNOx	(g/ikw-hr)	11.741	10.162	8.1317
AMBIENT PARAMETERS				
BARO.PRESSURE	(mm.hg)	738.4	737.9	738.0
RELATIVE HUMIDITY	(%)	87.7	79.6	79.9

****NASA PROJECT 03-8966 ****

TEST #6			
RUN NUMBER		100	101
DAY	(julian)	7166	7166
TIME	(military)	1323	1414
ENGINE HOURS		38.0	38.8
ENGINE PARAMETERS			
ENGINE SPEED	(rpm)	2001	2001
TORQUE	(N-M)	184.8	123.0
POWER	(kw)	38.7	25.8
BSFC	(g/kw-hr)	251.8	262.2
BMEP	(bar)	9.4	6.3
BTE	(%)	33.7	32.4
INDICATED PARAMETERS			
POWER	(ikw)	49.1	36.2
ISFC	(g/ikw-hr)	198.5	186.8
IMEP	(bar)	11.9	8.8
ITE,actual	(%)	42.8	45.4
ITE,theoretical	(%)	55.8	57.1
RATIO, actual/theoretical		.767	.796
ENGINE FLOW PARAMETERS			
FUEL FLOW	(kg/hr)	9.8	6.8
AIR FLOW	(kg/hr)	240.2	208.5
AIR FUEL RATIO		24.6	30.8
CHEMICAL AIR FUEL RATIO		24.2	30.6
EQUIVALENCE RATIO		.5839	.4665
APPARENT BLOWBY (m**3/hr)		11.1	9.8
SMOKE OPACITY (%)		3.0	1.9
TEMPERATURE PARAMETERS (deg.c)			
COOLANT IN BLOCK		78	79
COOLANT OUT BLOCK		82	82
COOLANT IN HEAD		78	79
COOLANT OUT HEAD		83	83
OIL TO COOLER		103	103
OIL TO ENGINE		104	104
FUEL		47	48
INTAKE AT PORT		61	61
LFE INLET		33	33
EXHAUST PORT		595	479
LINER INSIDE #1		157	142
LINER INSIDE #2		159	143
LINER INSIDE #3		125	117
LINER INSIDE #4		123	116
LINER INSIDE #5		124	119
LINER INSIDE #6		122	117
LINER OUTSIDE #7		136	126
LINER OUTSIDE #8		108	105
LINER OUTSIDE #9		115	109
LINER OUTSIDE #10		108	103
LINER OUTSIDE #11		96	96
LINER OUTSIDE #12		91	90
FIRE SURFACE #1		272	234
FIRE SURFACE #2		281	241
PRESSURE PARAMETERS			
OIL	(kpa)	54.4	54.5
FUEL	(kpa)	23.1	24.0
BOOST	(kpa)	7.9	5.3
EXHAUST	(kpa)	8.0	5.3
EMISSION PARAMETERS			
PARTICULATES	(g/kw-hr)	.5427	.3367
BSHC	(g/kw-hr)	.1807	.6131
BSCO	(g/kw-hr)	2.9807	2.1848
BSNOx	(g/kw-hr)	7.8791	9.8081
CO2	(%)	9.0	7.0
O2	(%)	8.4	11.1
PARTICULATES	(g/ikw-hr)	.4273	.2402
ISHC	(g/ikw-hr)	.1424	.4369
ISCO	(g/ikw-hr)	2.3496	1.5568
ISNOx	(g/ikw-hr)	6.2110	6.9890
AMBIENT PARAMETERS			
BARO.PRESSURE	(mm.hg)	738.2	737.8
RELATIVE HUMIDITY	(%)	46.9	47.0

****NASA PROJECT 03-8966 ****

TEST #7		103	104	114	115	110	111	112
RUN NUMBER		103	104	114	115	110	111	112
DAY	(julian)	7169	7169	7191	7191	7189	7189	7189
TIME	(military)	1317	15 0	1522	1627	1218	1342	15 5
ENGINE HOURS		43.9	45.6	75.8	77.0	66.0	67.4	68.8
ENGINE PARAMETERS								
ENGINE SPEED	(rpm)	1399	1702	1697	1699	2001	2000	1998
TORQUE	(N-M)	188.2	186.3	129.8	64.5	188.1	127.6	63.9
POWER	(kw)	27.6	33.2	23.1	11.5	39.4	26.7	13.4
BSFC	(g/kw-hr)	240.4	241.1	243.5	284.0	248.7	249.6	301.5
BMEP	(bar)	9.6	9.5	6.6	3.3	9.6	6.5	3.2
BTE	(%)	35.3	35.2	34.9	29.9	34.1	34.0	28.2
INDICATED PARAMETERS								
POWER	(ikw)	32.9	40.6	29.9	18.3	48.8	36.1	22.7
ISFC	(g/ikw-hr)	201.2	197.5	187.8	177.8	200.9	184.8	177.3
IMEP	(bar)	11.4	11.6	8.6	5.2	11.8	8.8	5.5
ITE,actual	(%)	42.2	43.0	45.2	47.7	42.3	45.9	47.9
ITE,theoretical	(%)	55.8	55.9	57.2	58.7	55.8	57.1	58.5
RATIO, actual/theoretical		.757	.769	.791	.814	.757	.805	.819
ENGINE FLOW PARAMETERS								
FUEL FLOW	(kg/hr)	6.6	8.0	5.6	3.3	9.8	6.7	4.0
AIR FLOW	(kg/hr)	162.6	200.9	176.3	146.5	241.7	205.9	171.4
AIR FUEL RATIO		24.5	25.1	31.4	44.9	24.6	30.9	42.5
CHEMICAL AIR FUEL RATIO		23.7	24.7	31.6	45.1	24.8	31.0	43.0
EQUIVALENCE RATIO		.5864	.5733	.4585	.3202	.5835	.4659	.3382
APPARENT BLOWBY (m**3/hr)		11.9	11.9	10.7	8.8	11.5	10.7	8.8
SMOKE OPACITY	(%)	1.9	1.8	1.1	1.2	1.9	2.2	2.3
TEMPERATURE PARAMETERS (deg.c)								
COOLANT IN BLOCK		120	121	120	118	119	120	121
COOLANT OUT BLOCK		123	123	122	121	122	123	123
COOLANT IN HEAD		21	23	47	47	38	50	48
COOLANT OUT HEAD		171	180	133	115	207	146	115
OIL TO COOLER		112	117	111	111	120	120	117
OIL TO ENGINE		113	118	112	112	121	121	119
FUEL		44	47	46	47	48	50	49
INTAKE AT PORT		84	83	83	82	82	82	81
LFE INLET		30	31	32	32	29	31	32
EXHAUST PORT		592	601	503	380	649	538	419
LINER INSIDE #1		187	192	179	161	199	184	168
LINER INSIDE #2		188	193	179	162	201	185	169
LINER INSIDE #3		147	150	141	134	152	145	139
LINER INSIDE #4		147	149	140	134	150	144	139
LINER INSIDE #5		143	147	138	134	148	144	139
LINER INSIDE #6		142	145	137	132	146	142	138
LINER OUTSIDE #7		171	174	165	152	177	169	157
LINER OUTSIDE #8		145	147	142	136	145	144	140
LINER OUTSIDE #9		140	139	131	127	136	133	131
LINER OUTSIDE #10		136	134	122	121	123	124	124
LINER OUTSIDE #11		127	127	123	121	124	125	125
LINER OUTSIDE #12		123	123	121	120	120	122	122
FIRE SURFACE #1		464	465	431	349	477	433	353
FIRE SURFACE #2		474	473	449	364	485	448	363
PRESSURE PARAMETERS								
OIL	(kpa)	41.9	46.0	48.0	48.0	50.4	50.5	51.2
FUEL	(kpa)	23.7	23.7	24.7	26.0	22.6	23.4	24.3
BOOST	(kpa)	7.8	8.0	5.6	2.7	9.4	6.3	3.2
EXHAUST	(kpa)	7.8	8.0	5.7	2.6	9.4	6.2	3.3
EMISSION PARAMETERS								
PARTICULATES	(g/kw-hr)	.2971	.4450	.1945	.3593	.5560	.3040	.8016
BSHC	(g/kw-hr)	.2565	.1868	.6164	1.6898	.1909	.4954	1.6077
BSCO	(g/kw-hr)	3.1138	2.7953	1.8129	3.1153	2.5233	2.0351	3.4887
BSNOx	(g/kw-hr)	14.598	12.463	18.568	19.234	10.527	13.880	13.795
CO2	(%)	9.2	8.8	6.8	4.7	8.7	6.9	4.9
O2	(%)	8.1	8.6	11.2	14.0	8.5	11.0	13.7
PARTICULATES	(g/ikw-hr)	.2487	.3639	.1499	.2249	.4497	.2248	.4704
ISHC	(g/ikw-hr)	.2148	.1530	.4754	1.0582	.1543	.3668	.9453
ISCO	(g/ikw-hr)	2.6067	2.2889	1.3981	1.9509	2.0385	1.5068	2.0513
ISNOx	(g/ikw-hr)	12.220	10.206	14.320	12.045	8.5047	10.277	8.1115
AMBIENT PARAMETERS								
BARO.PRESSURE	(mm.hg)	740.3	738.7	739.3	738.7	739.6	738.8	738.1
RELATIVE HUMIDITY	(%)	63.1	59.8	51.5	48.5	66.5	58.4	50.0

****NASA PROJECT 03-8966 ****

TEST #8						
RUN NUMBER		117	118	119	120	121
DAY	(julian)	7195	7195	7195	7195	7195
TIME	(military)	10 1	1155	1319	1420	1528
ENGINE HOURS		82.1	84.0	85.3	86.3	87.5
ENGINE PARAMETERS						
ENGINE SPEED	(rpm)	1399	1699	2001	1999	1999
TORQUE	(N-M)	186.8	181.7	174.5	121.4	60.7
POWER	(kw)	27.4	32.3	36.6	25.4	12.7
BSFC	(g/kw-hr)	240.1	247.6	267.7	264.1	314.4
BMEP	(bar)	9.5	9.2	8.9	6.2	3.1
BTE	(%)	35.4	34.3	31.7	32.1	27.0
INDICATED PARAMETERS						
POWER	(ikw)	32.5	39.4	46.3	35.1	22.4
ISFC	(g/ikw-hr)	202.5	203.3	211.5	191.1	178.3
IMEP	(bar)	11.3	11.2	11.2	8.5	5.4
ITE,actual	(%)	41.9	41.8	40.1	44.4	47.6
ITE,theoretical	(%)	55.8	55.9	55.8	57.1	58.5
RATIO, actual/theoretical		.752	.747	.720	.778	.814
ENGINE FLOW PARAMETERS						
FUEL FLOW	(kg/hr)	6.6	8.0	9.8	6.7	4.0
AIR FLOW	(kg/hr)	161.6	201.2	240.7	207.4	172.1
AIR FUEL RATIO		24.6	25.1	24.6	30.9	43.0
CHEMICAL AIR FUEL RATIO		24.8	25.4	24.9	31.3	43.1
EQUIVALENT RATIO		.5848	.5723	.5852	.4654	.3341
APPARENT BLOWBY (m**3/hr)		13.2	12.4	12.4	10.7	8.8
SMOKE OPACITY	(%)	1.9	2.3	3.4	2.5	4.5
TEMPERATURE PARAMETERS (deg.c)						
COOLANT IN BLOCK		119	117	118	119	120
COOLANT OUT BLOCK		122	121	122	122	122
COOLANT IN HEAD		40	49	47	52	49
COOLANT OUT HEAD		216	210	221	149	118
OIL TO COOLER		112	117	119	119	118
OIL TO ENGINE		113	118	120	121	119
FUEL		43	48	50	51	50
INTAKE AT PORT		82	84	84	83	84
LFE INLET		27	30	31	32	32
EXHAUST PORT		606	616	672	546	425
LINER INSIDE #1		190	192	201	184	167
LINER INSIDE #2		192	194	202	185	167
LINER INSIDE #3		144	146	151	143	138
LINER INSIDE #4		143	146	150	143	138
LINER INSIDE #5		139	143	147	142	138
LINER INSIDE #6		138	141	144	140	136
LINER OUTSIDE #7		173	173	179	168	156
LINER OUTSIDE #8		145	145	146	143	138
LINER OUTSIDE #9		132	133	135	132	130
LINER OUTSIDE #10		121	120	121	121	122
LINER OUTSIDE #11		122	122	123	123	123
LINER OUTSIDE #12		120	119	120	121	121
FIRE SURFACE #1		479	482	483	423	340
FIRE SURFACE #2		485	486	485	429	348
PRESSURE PARAMETERS						
OIL	(kpa)	42.7	46.3	50.3	50.4	50.9
FUEL	(kpa)	23.9	24.0	23.0	24.0	24.8
BOOST	(kpa)	7.4	7.9	9.3	6.3	3.2
EXHAUST	(kpa)	7.6	7.9	9.3	6.1	3.1
EMISSION PARAMETERS						
PARTICULATES	(g/kw-hr)	.4178	.6061	.9114	.6036	1.3855
BSHC	(g/kw-hr)	.2104	.1598	.1181	.3532	1.3532
BSCO	(g/kw-hr)	2.7788	2.7256	2.3163	2.8107	3.5556
BSNOx	(g/kw-hr)	10.931	8.7207	7.0013	8.3732	8.4164
CO2	(%)	8.7	8.5	8.7	6.9	4.9
O2	(%)	8.2	8.8	8.5	11.0	13.7
PARTICULATES	(g/ikw-hr)	.3525	.4971	.7192	.4370	.7826
ISHC	(g/ikw-hr)	.1774	.1312	.0933	.2555	.7672
ISCO	(g/ikw-hr)	2.3433	2.2380	1.8301	2.0337	2.0159
ISNOx	(g/ikw-hr)	9.2183	7.1604	5.5317	6.0584	4.7717
AMBIENT PARAMETERS						
BARO.PRESSURE	(mm.hg)	742.3	742.2	741.8	741.1	740.4
RELATIVE HUMIDITY	(%)	77.0	59.2	58.0	49.8	52.2

****NASA PROJECT 03-8966 ****

TEST #9			
RUN NUMBER		122	123
DAY	(julian)	7196	7196
TIME	(military)	1316	1452
ENGINE HOURS		90.6	92.1
ENGINE HOURS			93.5
ENGINE PARAMETERS			
ENGINE SPEED	(rpm)	1997	1996
TORQUE	(N-M)	188.9	127.6
POWER	(kw)	39.5	26.7
BSFC	(g/kw-hr)	246.9	250.5
BMEP	(bar)	9.6	6.5
BTE	(%)	34.4	33.9
INDICATED PARAMETERS			
POWER	(ikw)	49.0	36.2
ISFC	(g/ikw-hr)	198.9	184.6
IMEP	(bar)	11.9	8.8
ITE, actual	(%)	42.7	46.0
ITE, theoretical	(%)	55.8	57.1
RATIO, actual/theoretical		.766	.806
ENGINE FLOW PARAMETERS			
FUEL FLOW	(kg/hr)	9.8	6.7
AIR FLOW	(kg/hr)	239.4	205.6
AIR FUEL RATIO		24.5	30.7
CHEMICAL AIR FUEL RATIO		24.8	31.0
EQUIVALENCE RATIO		.5861	.4677
APPARENT BLOWBY (m**3/hr)		16.7	10.7
SMOKE OPACITY	(%)	2.1	1.6
TEMPERATURE PARAMETERS (deg.c)			
COOLANT IN BLOCK		118	119
COOLANT OUT BLOCK		122	122
COOLANT IN HEAD		34	52
COOLANT OUT HEAD		192	142
OIL TO COOLER		120	121
OIL TO ENGINE		121	122
FUEL		47	48
INTAKE AT PORT		82	84
LFE INLET		30	30
EXHAUST PORT		646	536
LINER INSIDE #1		200	183
LINER INSIDE #2		201	183
LINER INSIDE #3		152	144
LINER INSIDE #4		151	143
LINER INSIDE #5		148	143
LINER INSIDE #6		146	141
LINER OUTSIDE #7		178	167
LINER OUTSIDE #8		148	143
LINER OUTSIDE #9		134	131
LINER OUTSIDE #10		120	121
LINER OUTSIDE #11		123	123
LINER OUTSIDE #12		120	120
FIRE SURFACE #1		476	427
FIRE SURFACE #2		482	137
PRESSURE PARAMETERS			
OIL	(kpa)	50.2	49.8
FUEL	(kpa)	22.8	23.7
BOOST	(kpa)	9.1	6.2
EXHAUST	(kpa)	9.2	6.2
EMISSION PARAMETERS			
PARTICULATES	(g/kw-hr)	.4917	.2711
BSHC	(g/kw-hr)	.1154	.4348
BSCO	(g/kw-hr)	2.7727	2.0400
BSNOx	(g/kw-hr)	12.485	15.915
CO2	(%)	8.8	7.0
O2	(%)	8.3	10.9
PARTICULATES	(g/ikw-hr)	.3966	.1997
ISHC	(g/ikw-hr)	.0930	.3204
ISCO	(g/ikw-hr)	2.2339	1.5035
ISNOx	(g/ikw-hr)	10.059	11.729
AMBIENT PARAMETERS			
BARO.PRESSURE	(mm.hg)	740.7	740.2
RELATIVE HUMIDITY	(%)	71.8	63.6

****NASA PROJECT 03-8966 ****

IDLE TEST #1,2,4				
RUN NUMBER		62	73	90
DAY	(julian)	7085	7090	7156
TIME	(military)	1731	1815	15 1
ENGINE HOURS		68.8	95.3	16.9
ENGINE PARAMETERS				
ENGINE SPEED	(rpm)	1003	1001	1004
TORQUE	(N-M)	19.4	19.3	16.7
POWER	(kw)	2.0	2.0	1.8
BSFC	(g/kw-hr)	478.6	460.6	543.5
BMEP	(bar)	1.0	1.0	.8
BTE	(%)	17.7	18.4	15.6
INDICATED PARAMETERS				
POWER	(ikw)	4.9	4.6	4.8
ISFC	(g/ikw-hr)	200.8	201.1	198.5
IMEP	(bar)	2.4	2.3	2.3
ITE,actual	(%)	42.3	42.2	42.8
ITE,theoretical	(%)	59.9	59.9	59.9
RATIO, actual/theoretical		.706	.704	.714
ENGINE FLOW PARAMETERS				
FUEL FLOW	(kg/hr)	1.0	.9	1.0
AIR FLOW	(kg/hr)	65.9	65.1	65.7
AIR FUEL RATIO		67.5	69.7	68.8
CHEMICAL AIR FUEL RATIO		74.0	77.6	69.8
EQUIVALENCE RATIO		.2130	.2062	.2089
APPARENT BLOWBY (m**3/hr)		4.5	3.4	6.0
SMOKE OPACITY	(%)	1.8	1.7	.8
TEMPERATURE PARAMETERS (deg.c)				
COOLANT IN BLOCK		79	89	81
COOLANT OUT BLOCK		80	90	82
COOLANT IN HEAD		73	85	81
COOLANT OUT HEAD		72	84	81
OIL TO COOLER		78	84	90
OIL TO ENGINE		77	83	89
FUEL		32	37	40
INTAKE AT PORT		82	82	82
LFE INLET		20	24	29
EXHAUST PORT		196	195	221
LINER INSIDE #1		102	115	106
LINER INSIDE #2		103	116	106
LINER INSIDE #3		92	100	98
LINER INSIDE #4		92	101	97
LINER INSIDE #5		93	101	100
LINER INSIDE #6		93	101	99
LINER OUTSIDE #7		97	108	99
LINER OUTSIDE #8		98	110	96
LINER OUTSIDE #9		87	95	94
LINER OUTSIDE #10		86	94	93
LINER OUTSIDE #11		89	97	91
LINER OUTSIDE #12		89	97	94
FIRE SURFACE #1		138	149	128
FIRE SURFACE #2		140	151	130
PRESSURE PARAMETERS				
OIL	(kpa)	34.1	33.3	40.3
FUEL	(kpa)	21.5	21.8	21.7
BOOST	(kpa)	-.2	-.2	-.2
EXHAUST	(kpa)	.5	.4	.4
EMISSION PARAMETERS				
PARTICULATES	(g/kw-hr)	2.9647	2.1651	2.8264
BSHC	(g/kw-hr)	8.4283	7.4847	7.6460
BSCO	(g/kw-hr)	14.903	13.217	19.214
BSNOx	(g/kw-hr)	47.353	44.655	58.910
CO2	(%)	2.8	2.7	3.0
O2	(%)	16.5	16.6	16.3
PARTICULATES	(g/ikw-hr)	1.2315	.9429	1.0599
ISHC	(g/ikw-hr)	3.5368	3.2679	2.7931
ISCO	(g/ikw-hr)	6.2536	5.7706	7.0192
ISNOx	(g/ikw-hr)	19.871	19.497	21.520
AMBIENT PARAMETERS				
BARO.PRESSURE	(mm.hg)	737.3	737.5	742.7
RELATIVE HUMIDITY	(%)	40.0	23.5	49.5

APPENDIX D
COMBUSTION ANALYSIS SUMMARY

PRECEDING PAGE BLANK NOT FILMED

<u>Test Number</u>		<u>Condition</u>	<u>Run Numbers</u>
1	Baseline Metal:	82°C Coolant, 82°C Intake Air	53 - 61
2	"	104°C Coolant, 82°C Intake Air	64 - 72
3	"	82°C Coolant, 60°C Intake Air	74 - 76
4	Baseline Ceramic:	82°C Coolant, 82°C Intake Air	87 - 96
5	"	104°C Coolant, 82°C Intake Air	97 - 99
6	"	82°C Coolant, 60°C Intake Air	100 - 102
7	Hot Ceramic:	121°C Block Coolant, 82°C Intake Air, Coolant Drained From Head	103 - 112
8	"	Same as No. 7 but with retarded fuel-injection timing	117 - 121
9	"	Same as No. 7 but with advanced fuel-injection timing	122 - 124

PRECEDING PAGE BLANK NOT FILMED

LEGEND

- 1 Run No.
- 2 RPM
- 3 Indicated Power (kw)
- 4 Injection Timing (degrees, 180 = TDC)
- 5 Injection Duration (degrees)
- 6 Point of Ignition (degrees)
- 7 Ignition Delay (degrees)
- 8 Combustion Duration (degrees)
- 9 Total Heat Release [Chr (max) - Chr (ign)] (J)
- 10 Premixed/Total Heat Release Ratio
- 11 Peak Cylinder Pressure (MPa)
- 12 Peak Rate of Pressure Rise (kPa/deg.)
- 13 Angle where Peak Cylinder Pressure Occurs (degrees)
- 14 Angle where Peak Rate of Pressure Rise Occurs (degrees)

1	2	3	4	5	6	7	8	9	10	11	12	13	14
53	1400	30.65	154.0	26.0	165.2	11.2	33.77	4794.	0.147	11.96	610.1	186.0	168.0
54	1400	19.54	154.5	20.0	166.4	11.9	26.12	3215.	0.272	9.79	699.1	184.5	169.5
55	1400	10.03	154.5	9.5	167.1	12.6	21.89	1806.	0.610	7.48	734.3	182.0	171.0
56	1700	36.58	155.0	30.5	166.7	11.7	34.79	4763.	0.112	11.67	510.2	187.0	169.0
57	1700	23.99	155.0	24.5	167.7	12.7	27.81	3292.	0.191	9.84	557.9	186.0	170.5
58	1700	12.50	155.0	12.0	169.5	14.5	23.47	1895.	0.408	7.55	610.6	183.0	172.5
59	2000	44.09	155.5	36.0	168.0	12.5	40.48	4976.	0.088	11.34	481.6	188.0	170.5
60	2000	28.60	155.5	29.5	169.3	13.8	29.68	3381.	0.149	9.57	504.2	187.0	172.0
61	2000	14.89	155.5	14.0	170.4	14.9	26.60	1948.	0.379	7.31	515.6	184.5	174.0
64	1400	29.65	154.5	25.0	165.1	10.6	32.43	4699.	0.155	12.02	637.2	185.5	168.0
65	1400	19.57	154.5	20.0	165.5	11.0	28.01	3295.	0.259	9.88	677.5	184.5	169.0
66	1400	9.93	154.5	9.5	166.8	12.3	21.70	1794.	0.638	7.43	733.7	181.5	171.0
67	1700	35.78	155.0	31.0	166.8	11.8	32.73	4654.	0.108	11.44	485.3	186.5	169.5
68	1700	23.81	155.0	25.0	167.4	12.4	29.14	3309.	0.191	9.79	552.3	186.0	170.5
69	1700	12.17	155.0	12.0	168.3	13.3	25.24	1859.	0.409	7.40	578.4	182.5	172.0
70	2000	43.47	155.0	36.5	168.0	12.5	37.00	4920.	0.075	11.20	449.9	188.0	170.5
71	2000	28.84	156.0	29.5	169.4	13.4	31.13	3434.	0.150	9.58	454.8	187.0	172.0
72	2000	15.31	155.5	14.5	170.6	15.1	27.44	1983.	0.308	7.36	505.9	185.0	173.5
74	2000	47.02	156.0	36.5	168.1	12.1	53.89	5478.	0.001	10.51	481.0	188.0	172.0
75	2000	32.17	156.0	29.5	169.6	13.6	40.42	3656.	0.183	8.85	517.5	187.0	173.5
76	2000	17.73	156.0	13.5	171.6	15.6	34.86	2047.	0.358	6.80	535.4	183.5	175.5
87	1400	30.42	154.5	25.5	165.3	10.8	58.70	4946.	0.154	10.70	585.8	185.0	168.5
88	1400	22.26	154.5	20.5	166.3	11.8	56.66	3641.	0.259	8.97	674.6	184.0	169.5
89	1400	12.37	154.5	10.0	167.5	13.0	62.03	2072.	0.608	6.72	757.4	181.5	171.5
91	1700	37.26	155.0	31.0	166.9	11.9	55.63	5048.	0.130	10.49	494.3	186.5	170.0
92	1700	27.07	155.0	25.0	167.7	12.7	48.26	3635.	0.224	8.86	535.9	185.0	171.0
93	1700	14.64	155.0	12.0	169.7	14.7	50.83	2028.	0.491	6.68	568.7	183.5	173.0
94	2000	44.20	156.0	36.0	168.3	12.3	61.23	5336.	0.074	10.06	431.4	187.5	171.0
95	2000	31.76	156.0	29.5	169.6	13.6	52.44	3781.	0.167	8.46	472.9	186.5	172.5
96	2000	17.38	156.0	14.0	170.9	14.9	58.57	2151.	0.328	6.41	543.5	185.0	174.5
97	1400	29.37	154.5	25.5	164.9	10.3	77.15	4946.	0.119	10.31	513.7	185.0	168.0
98	1700	36.11	155.0	32.0	166.7	11.7	78.79	5147.	0.093	10.05	431.9	186.5	169.5
99	2000	42.86	156.0	36.5	168.2	12.2	77.26	5389.	0.067	9.71	384.0	187.0	171.0
100	2000	43.77	156.0	37.0	169.7	13.7	81.80	5583.	0.099	9.35	474.1	188.0	172.5
101	2000	31.18	156.0	30.0	170.7	14.7	73.32	3887.	0.184	8.06	539.5	186.5	173.5
102	2000	17.41	156.0	14.5	173.1	17.1	61.89	2172.	0.391	6.37	608.6	184.0	176.0
103	1400	30.16	154.5	28.5	164.1	9.6	70.44	5059.	0.087	10.60	445.6	185.5	167.0
104	1700	36.73	155.5	32.5	166.3	10.8	66.21	5130.	0.075	10.16	397.4	186.5	169.0
110	2000	36.99	156.0	39.0	167.9	11.9	83.59	5558.	0.047	9.63	342.7	188.0	170.5
111	2000	25.97	156.0	31.0	168.8	10.8	108.70	3965.	0.078	8.12	328.5	187.0	172.0
112	2000	15.05	156.0	15.0	170.8	12.6	123.70	2432.	0.216	6.24	402.7	185.0	173.5

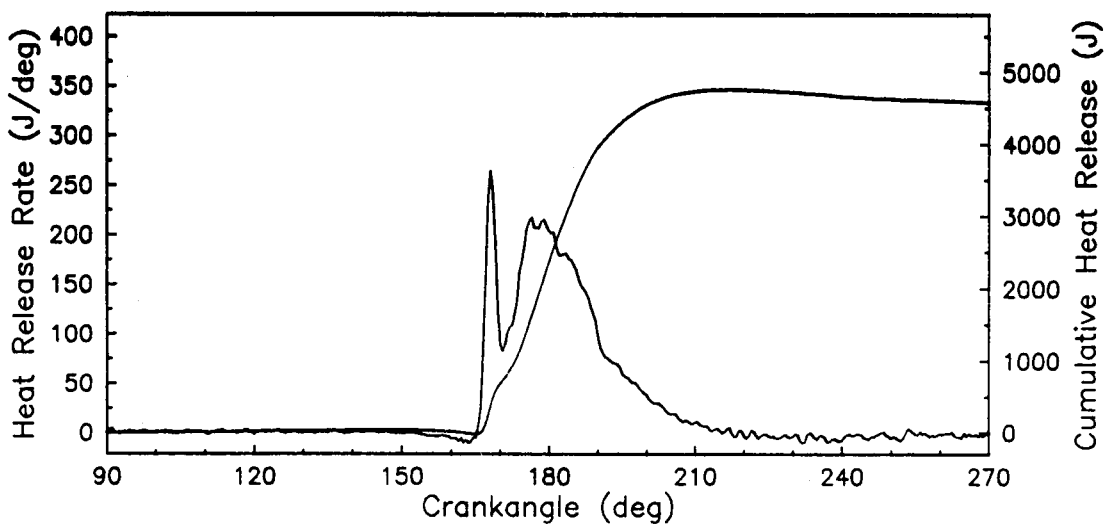
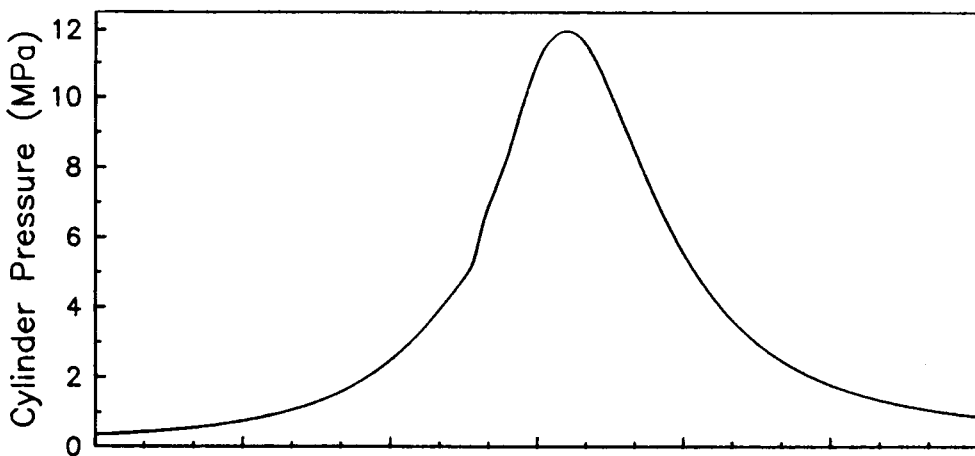
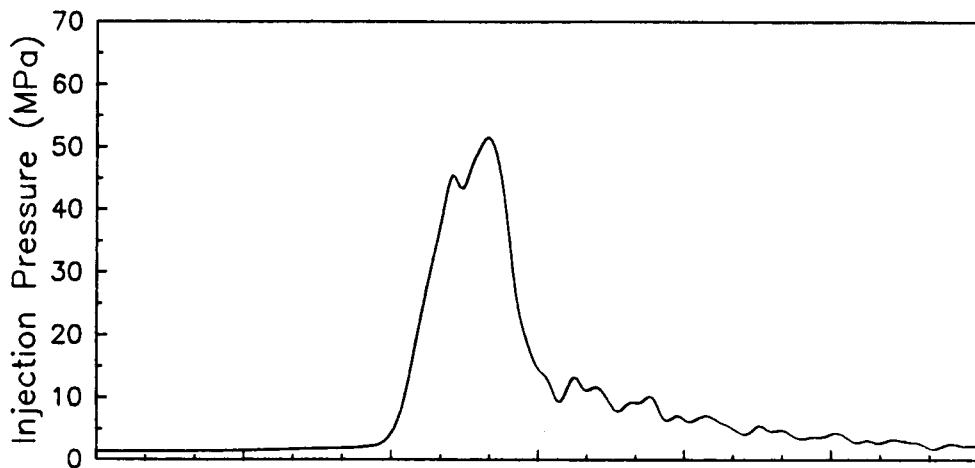
APPENDIX E
HIGH SPEED COMBUSTION PLOTS

PRECEDING PAGE BLANK NOT FILMED

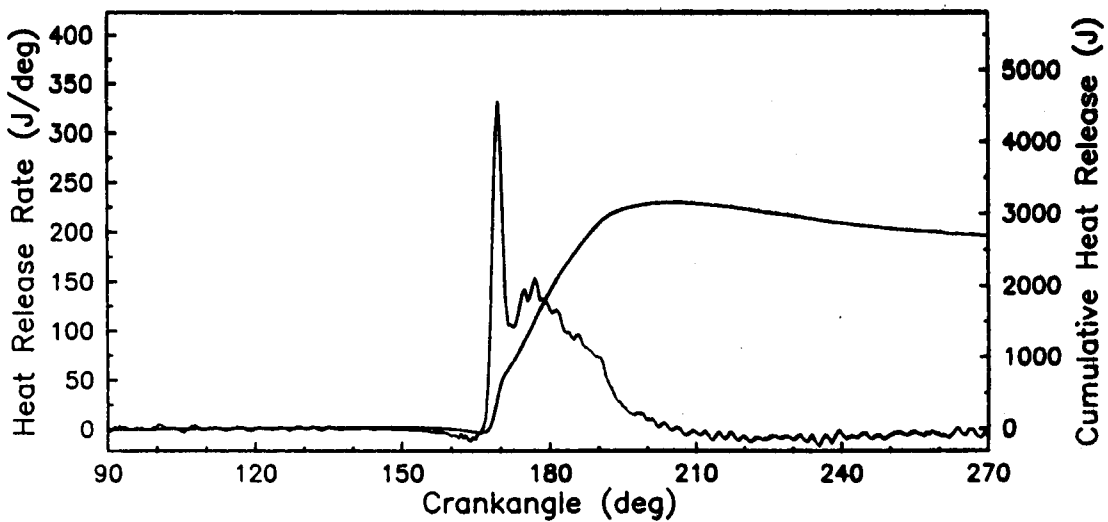
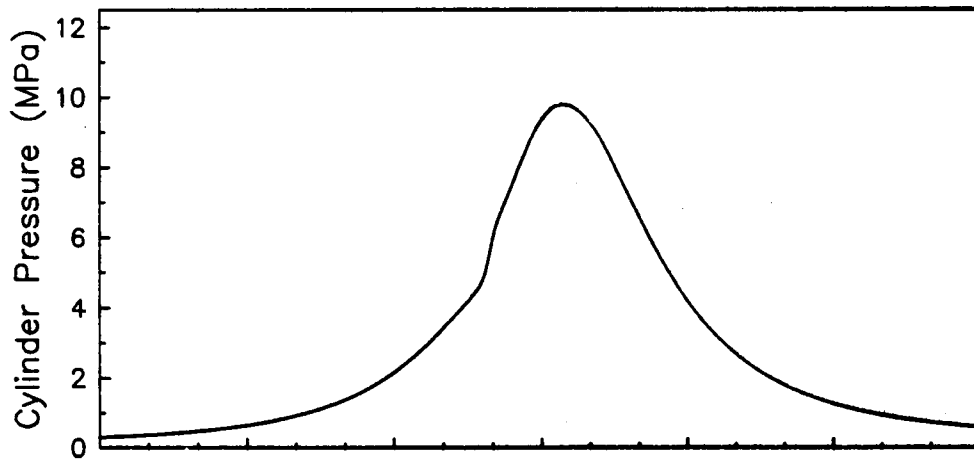
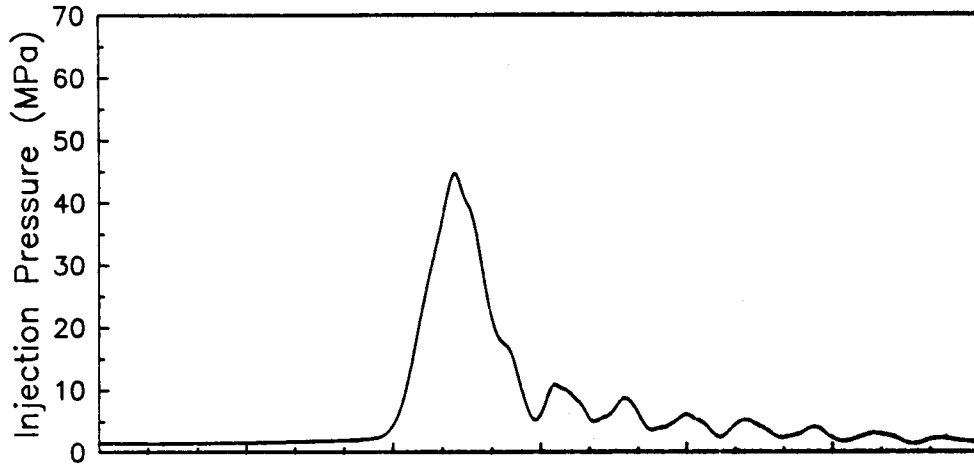
<u>Test Number</u>		<u>Condition</u>	<u>Run Numbers</u>
1	Baseline Metal:	82°C Coolant, 82°C Intake Air	53 - 61
2	"	104°C Coolant, 82°C Intake Air	64 - 72
3	"	82°C Coolant, 60°C Intake Air	74 - 76
4	Baseline Ceramic:	82°C Coolant, 82°C Intake Air	87 - 96
5	"	104°C Coolant, 82°C Intake Air	97 - 99
6	"	82°C Coolant, 60°C Intake Air	100 - 102
7	Hot Ceramic:	121°C Block Coolant, 82°C Intake Air, Coolant Drained From Head	103 - 112
8	"	Same as No. 7 but with retarded fuel-injection timing	117 - 121
9	"	Same as No. 7 but with advanced fuel-injection timing	122 - 124

PRECEDING PAGE BLANK NOT FILMED

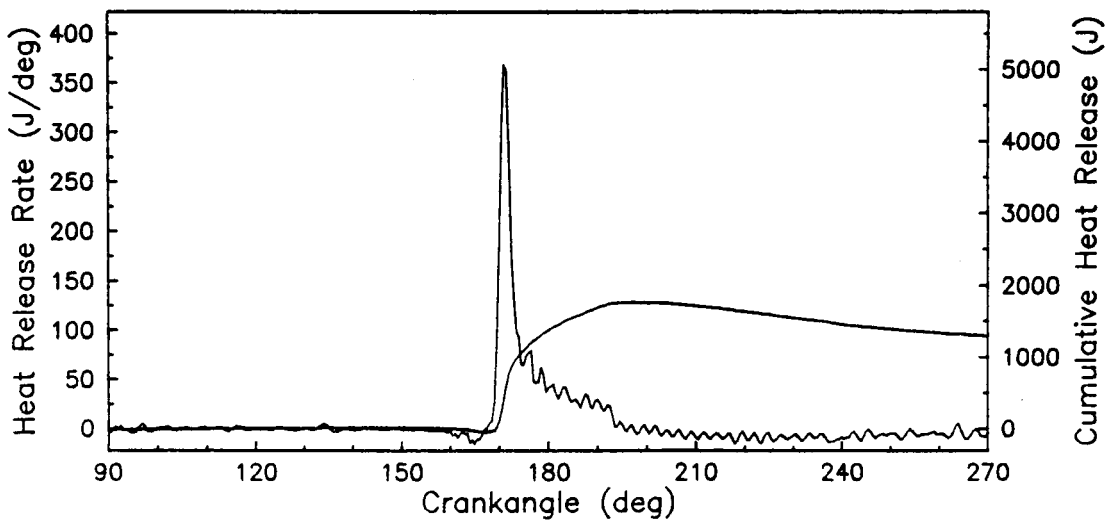
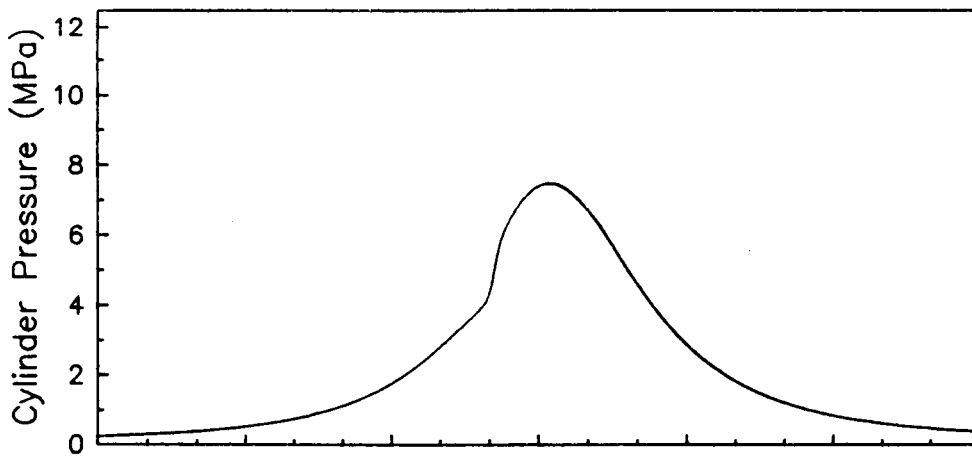
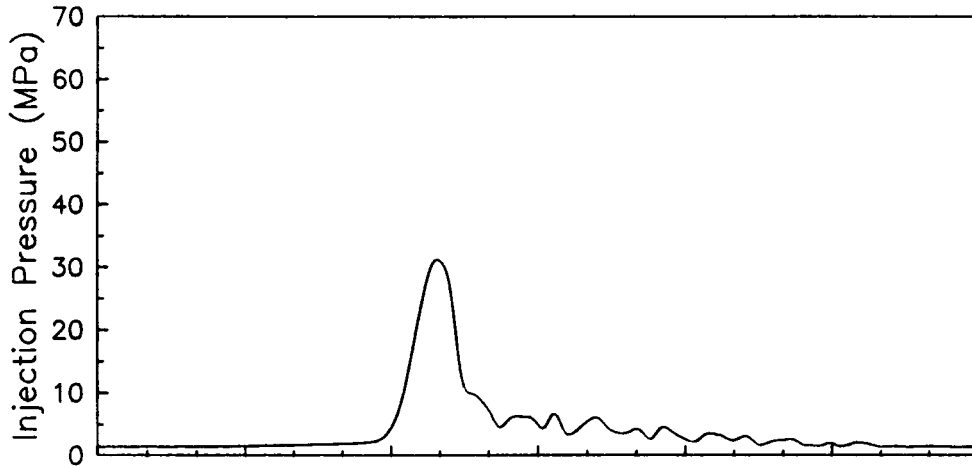
RUN #53, 1400 RPM, 100 % LOAD



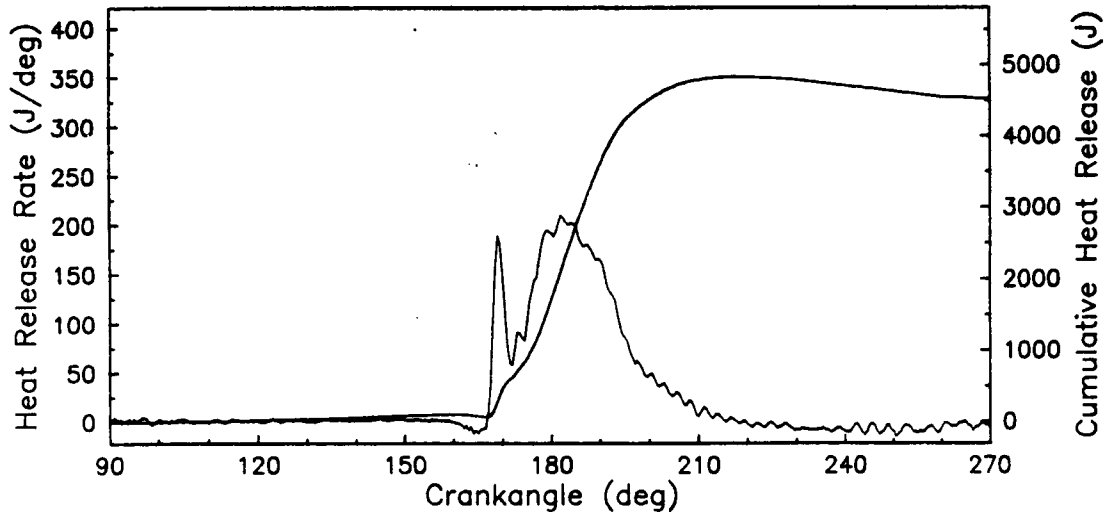
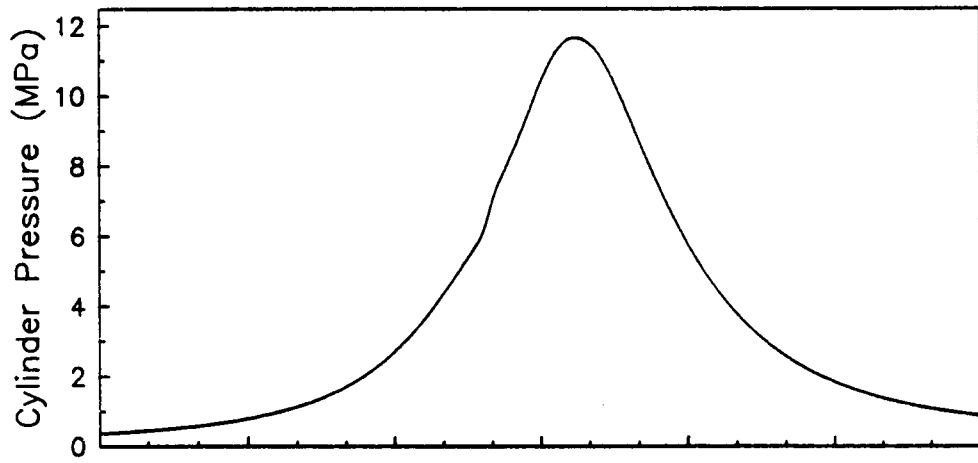
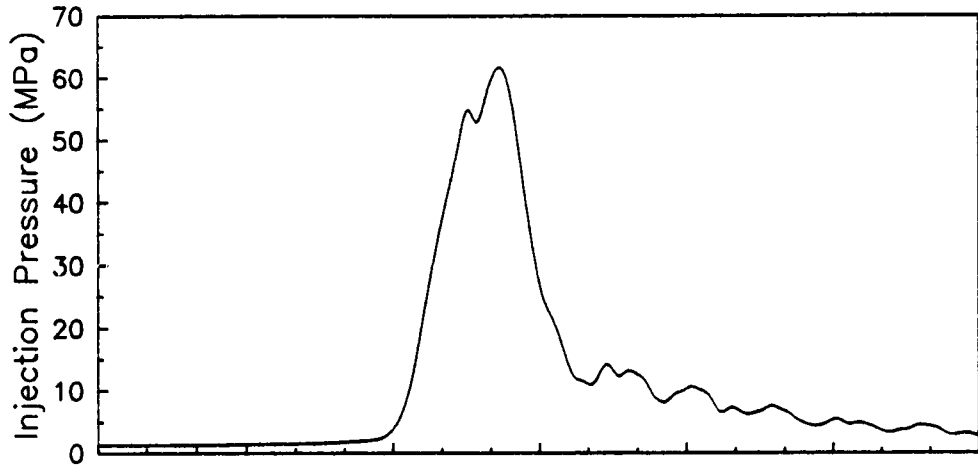
RUN #54, 1400 RPM, 67 % LOAD



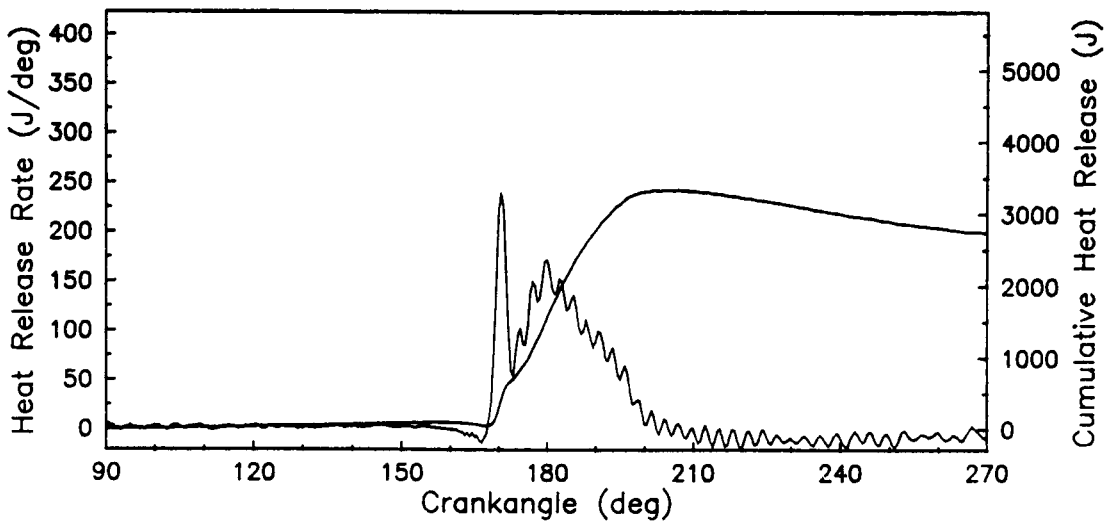
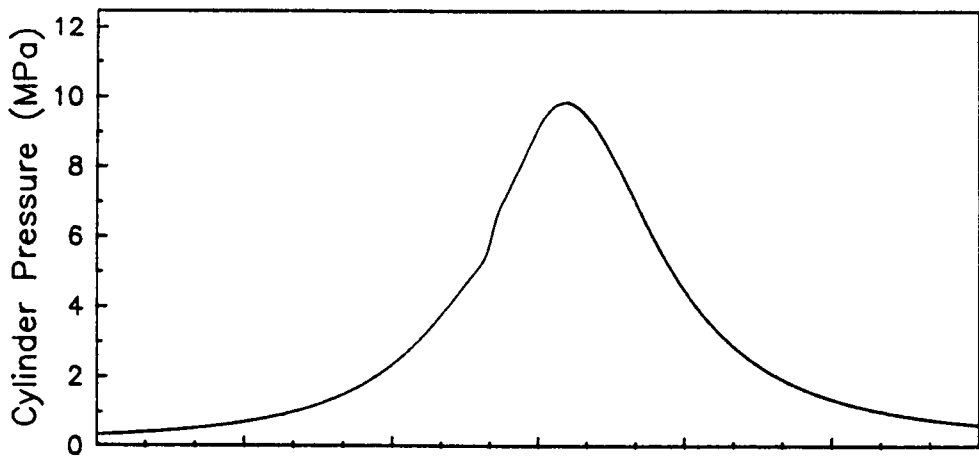
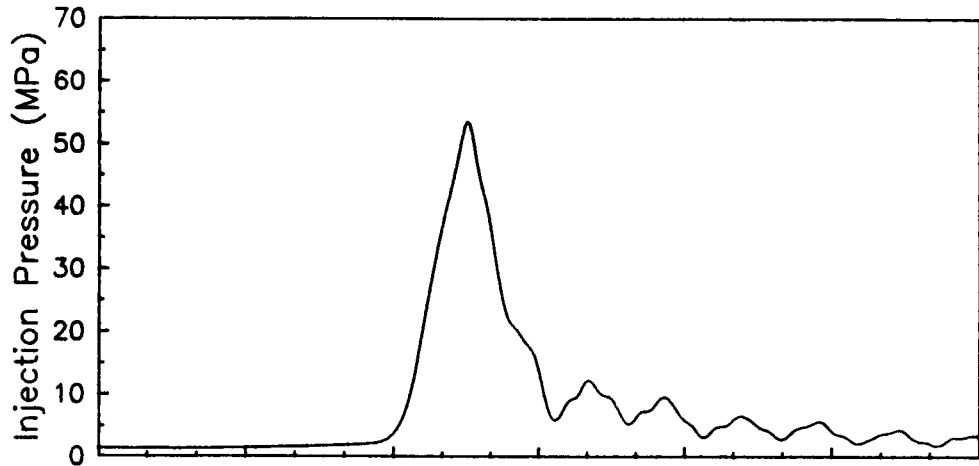
RUN #55, 1400 RPM, 33 % LOAD



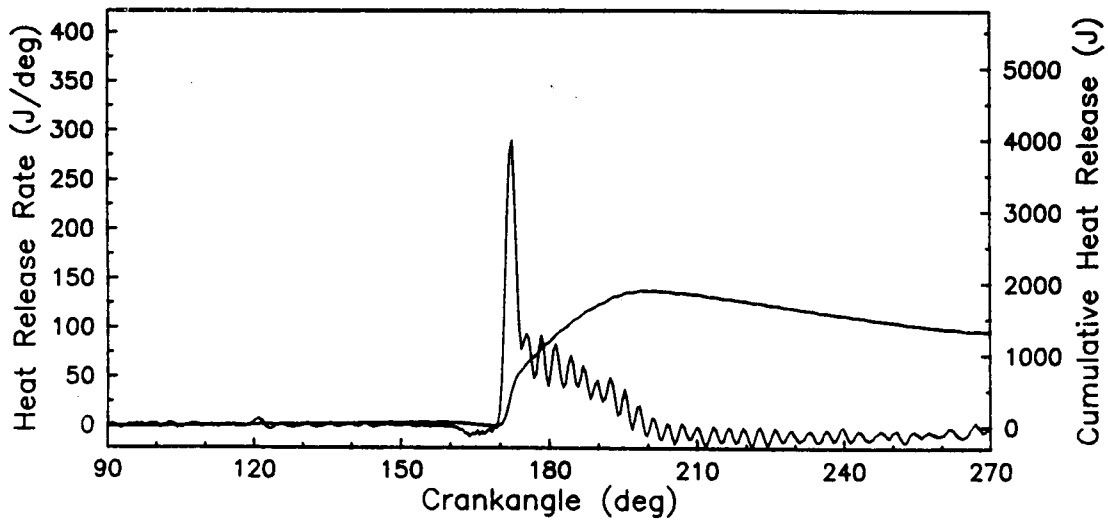
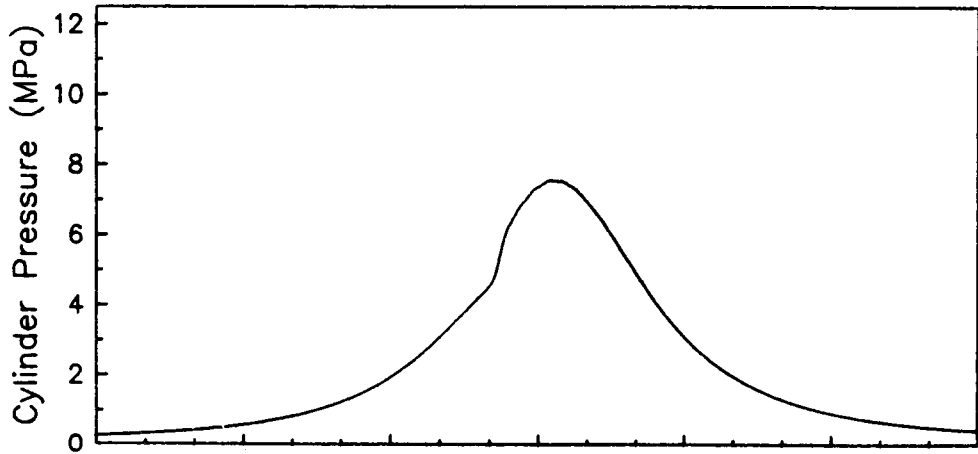
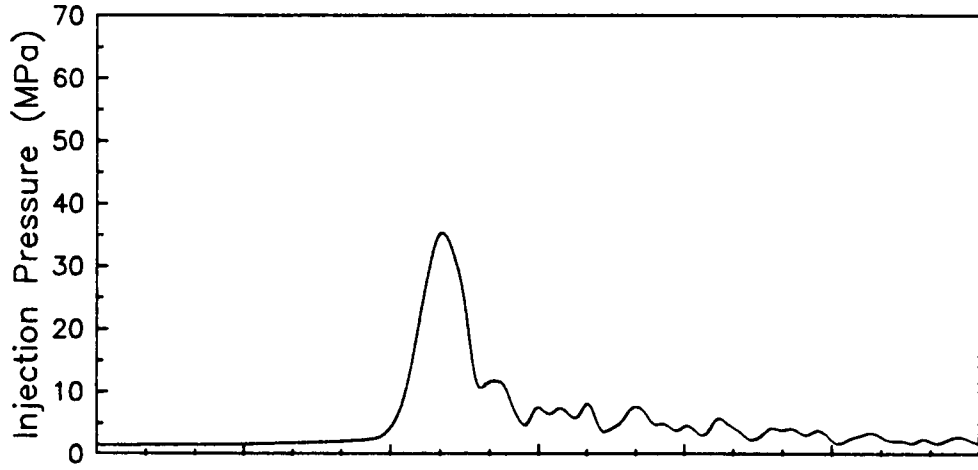
RUN #56, 1700 RPM, 100 % LOAD



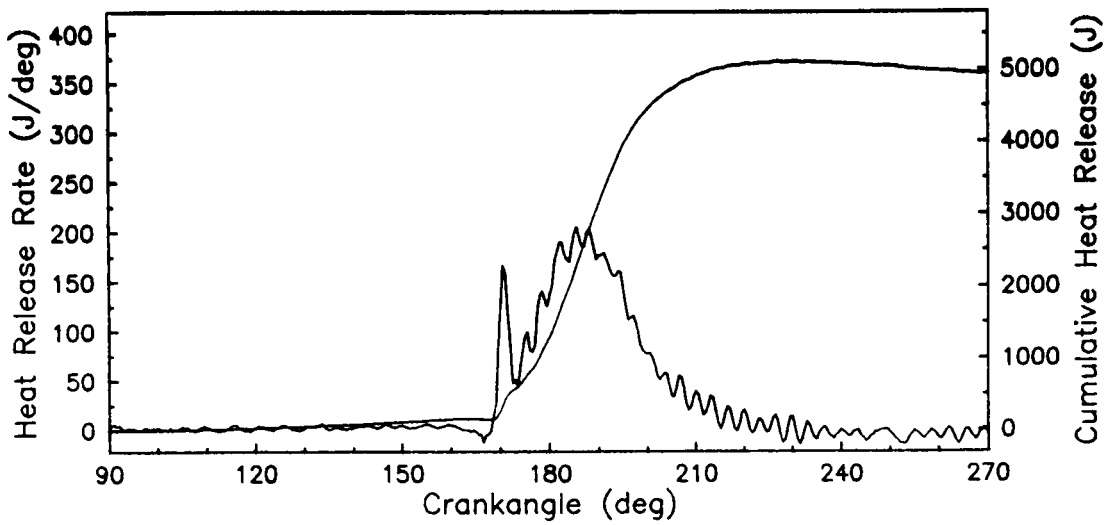
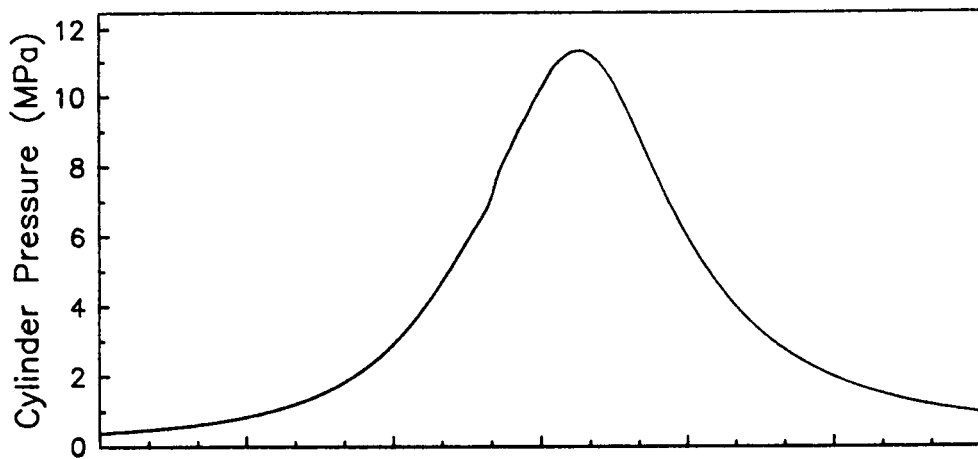
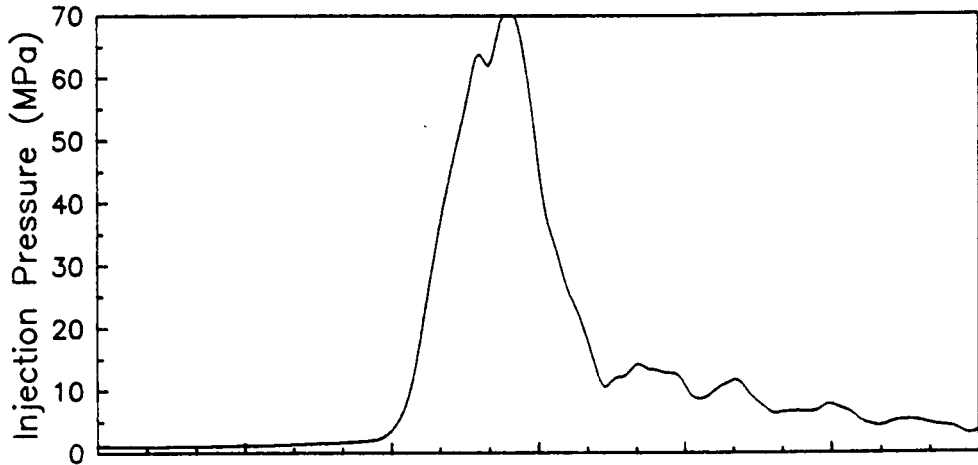
RUN #57, 1700 RPM, 67 % LOAD



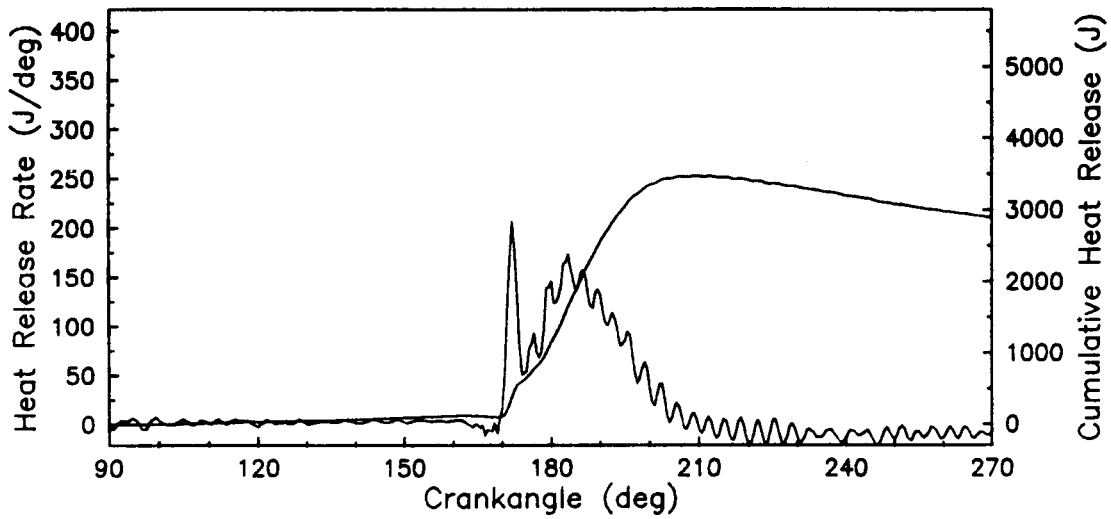
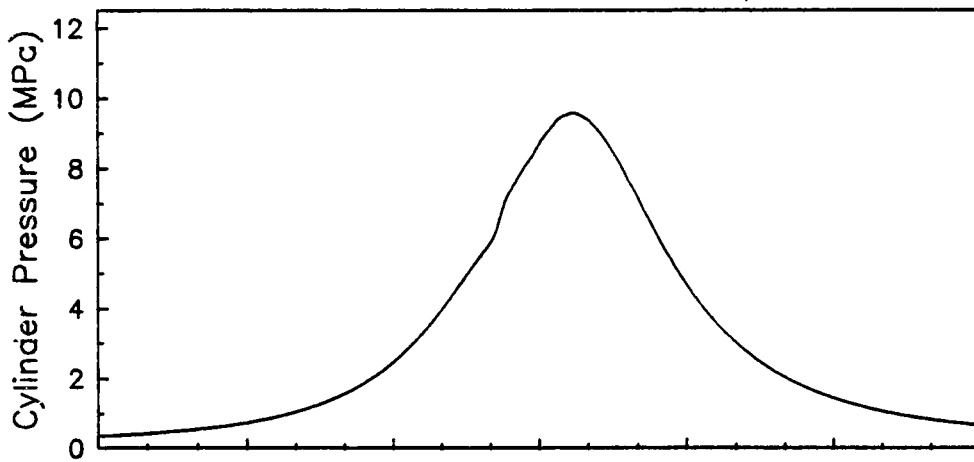
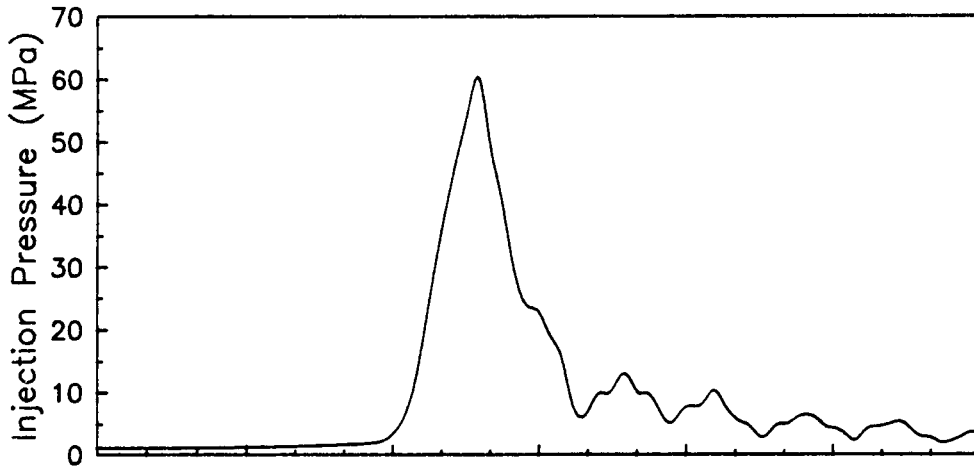
RUN #58, 1700 RPM, 33 % LOAD



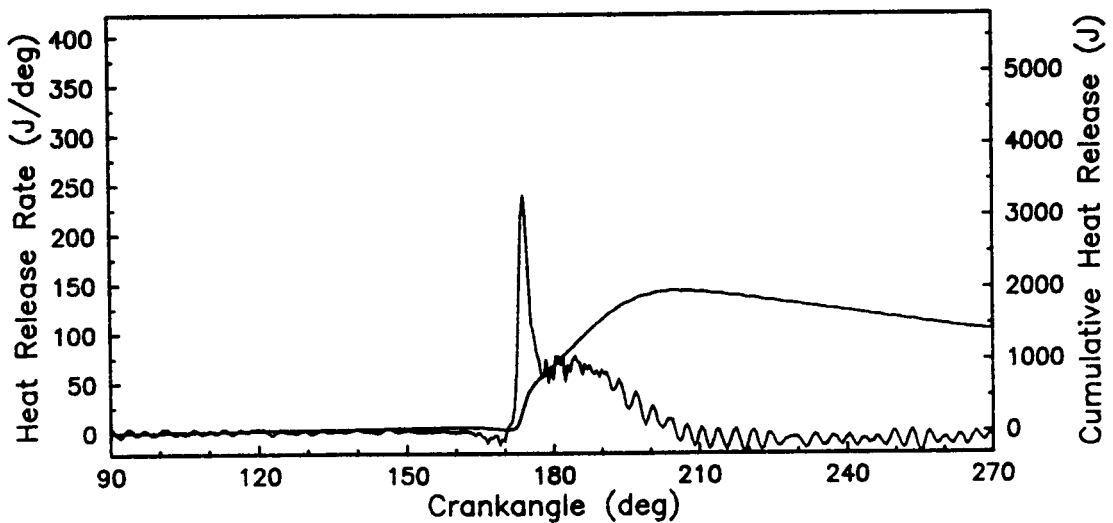
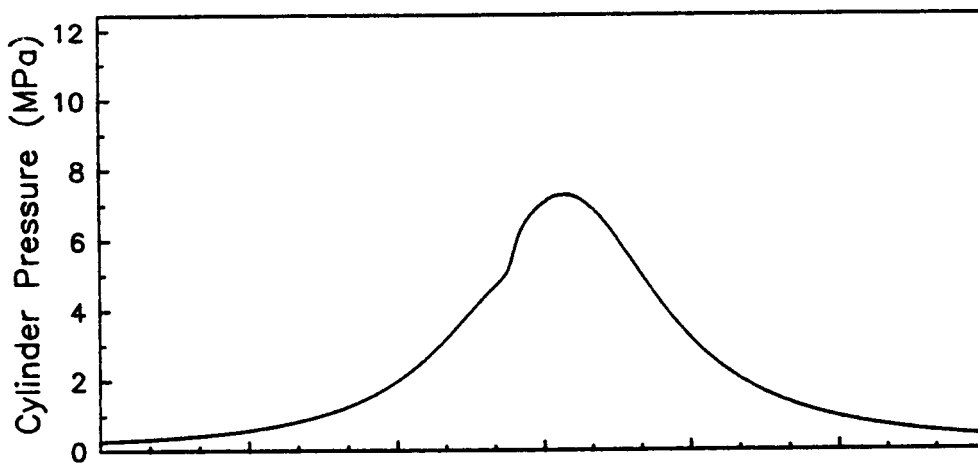
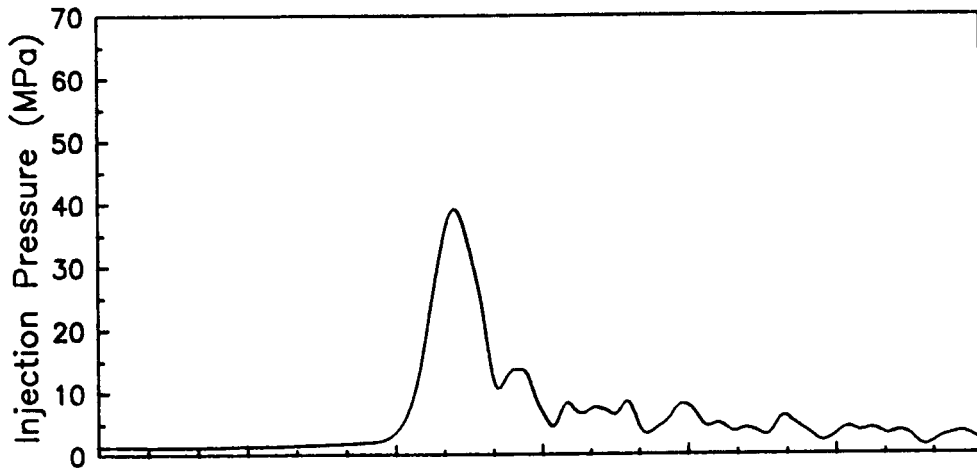
RUN #59, 2000 RPM, 100 % LOAD



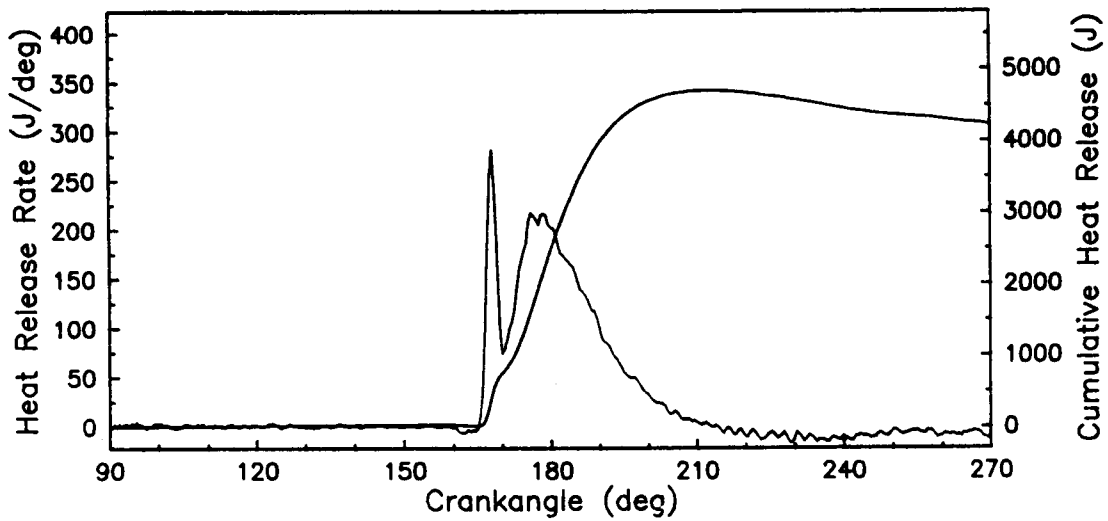
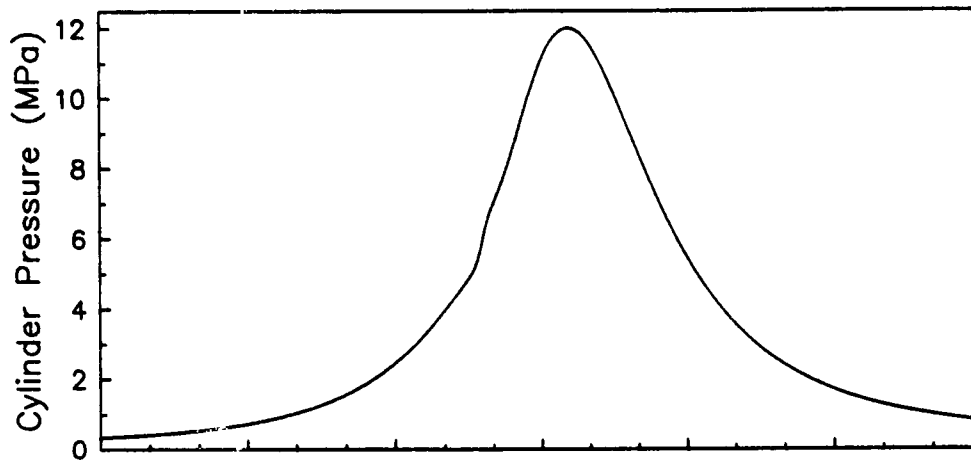
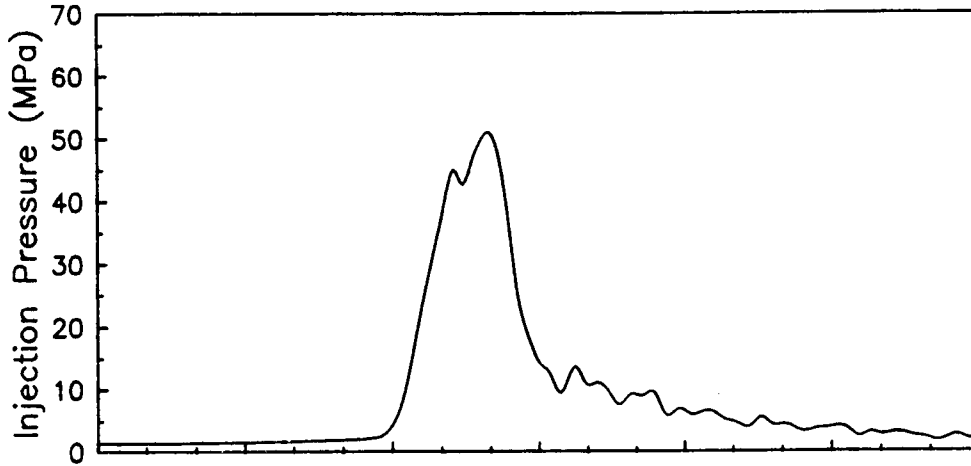
RUN #60, 2000 RPM, 67 % LOAD



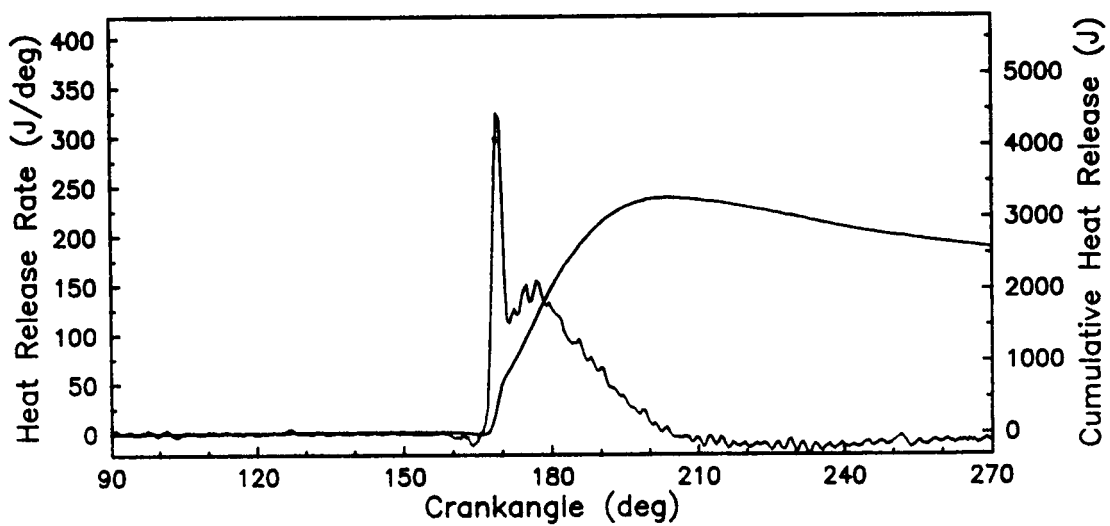
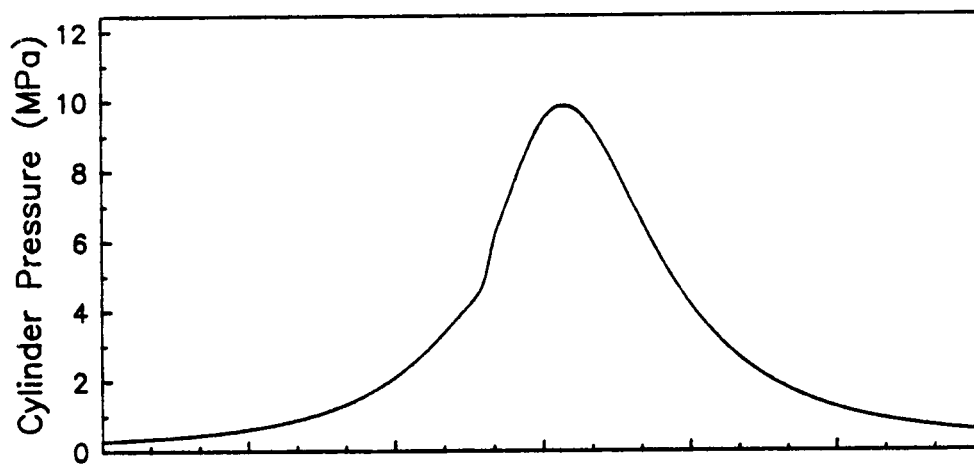
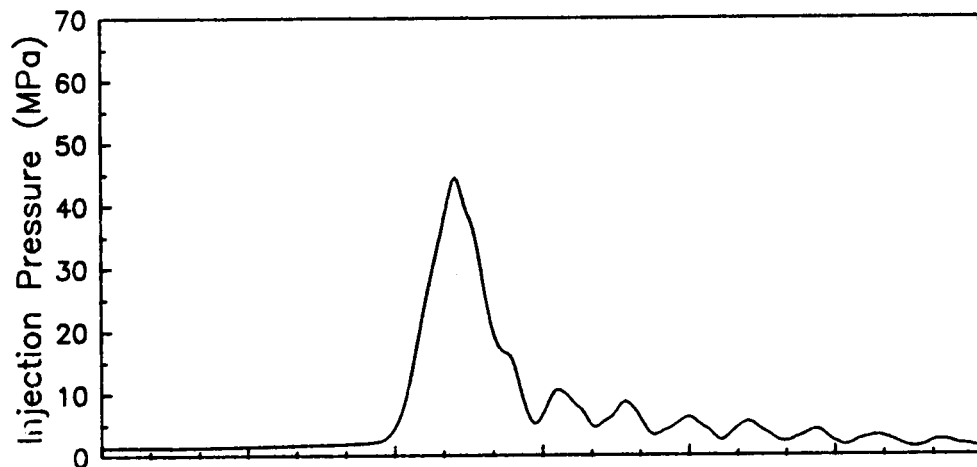
RUN #61, 2000 RPM, 33 % LOAD



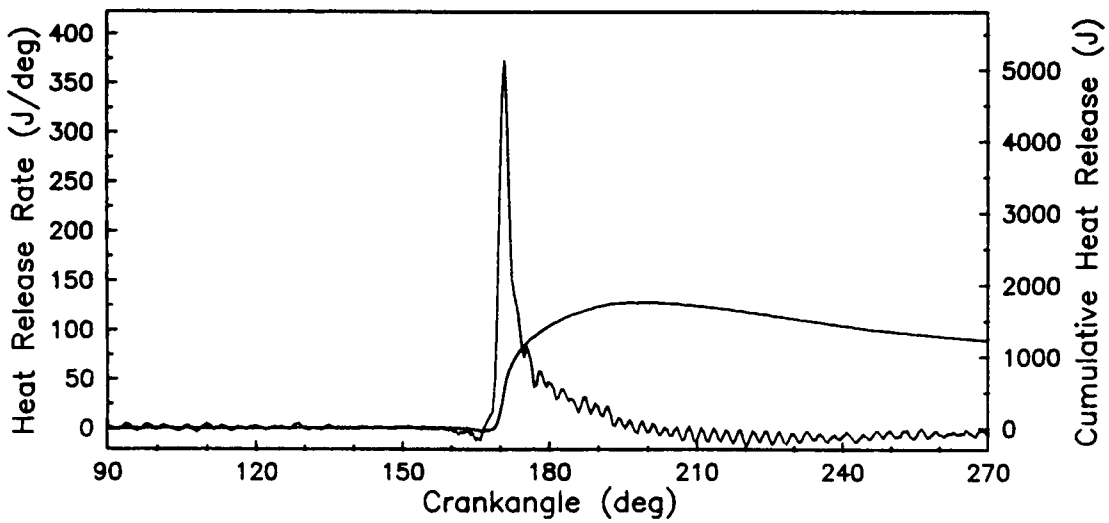
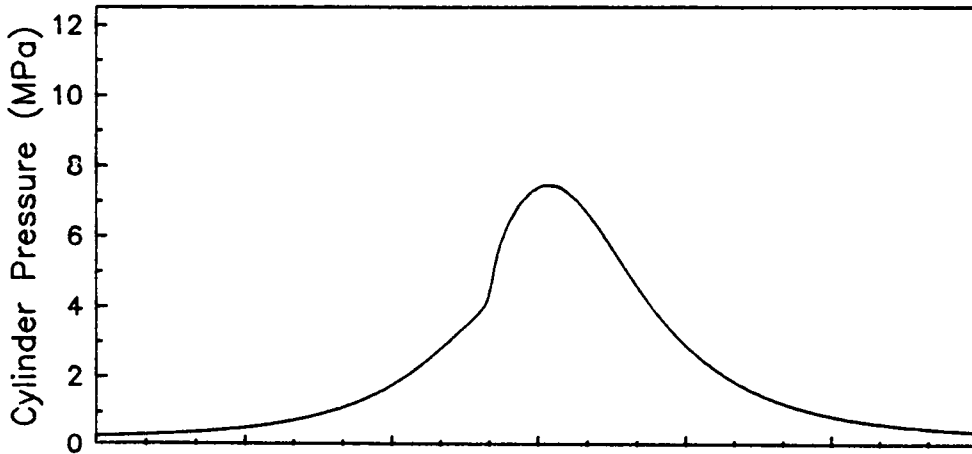
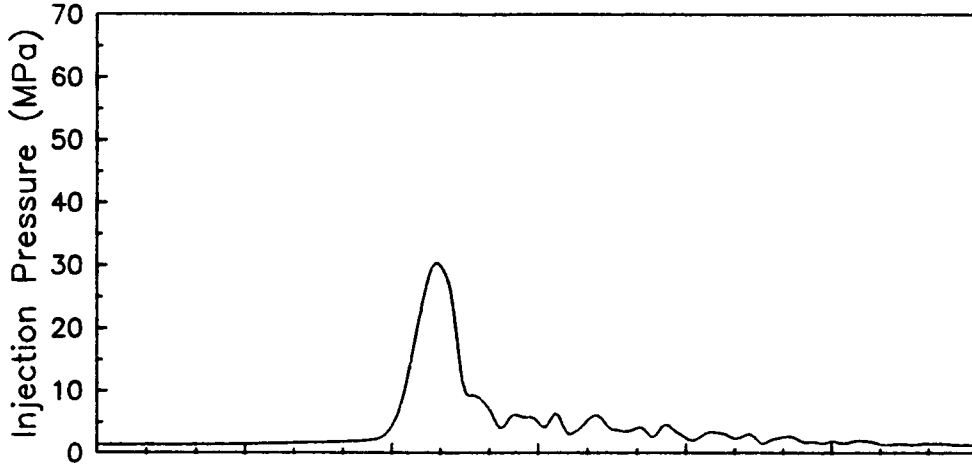
RUN #64, 1400 RPM, 100 % LOAD



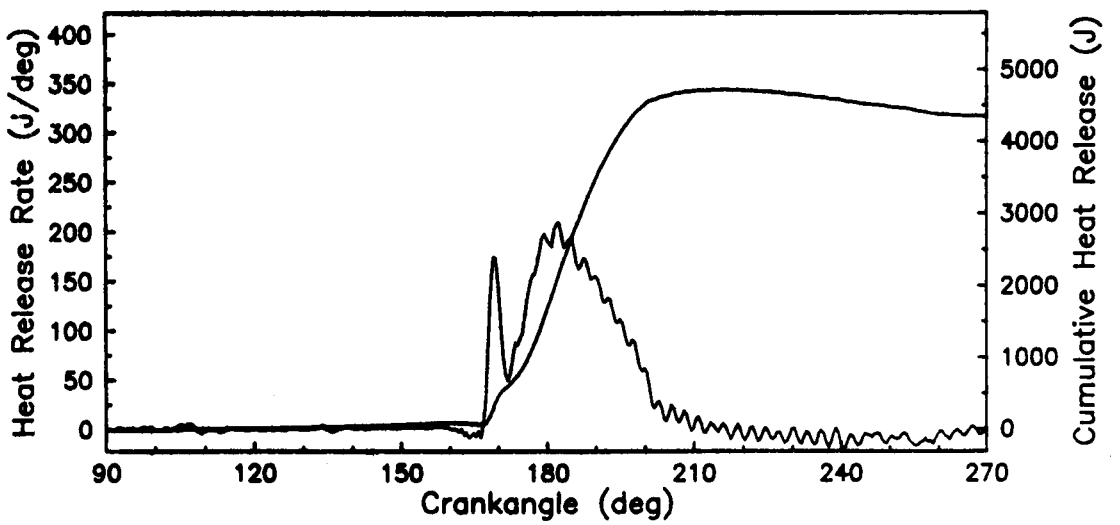
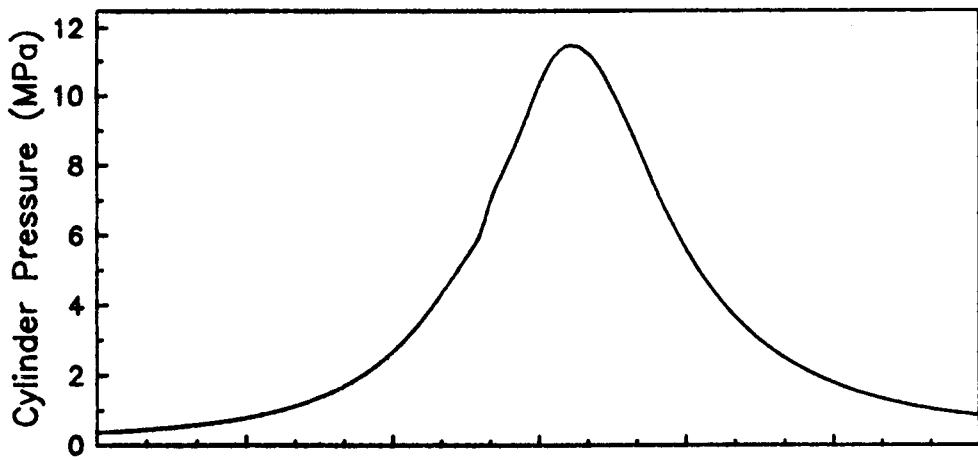
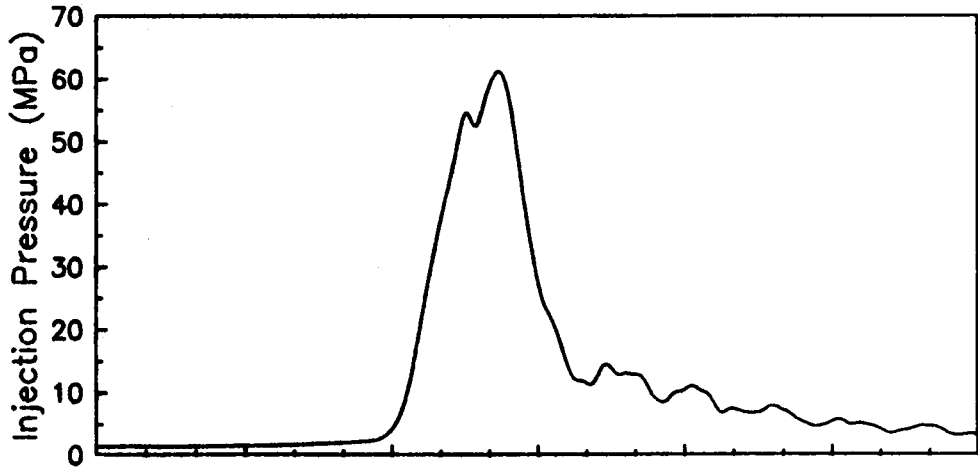
RUN #65, 1400 RPM, 67 % LOAD



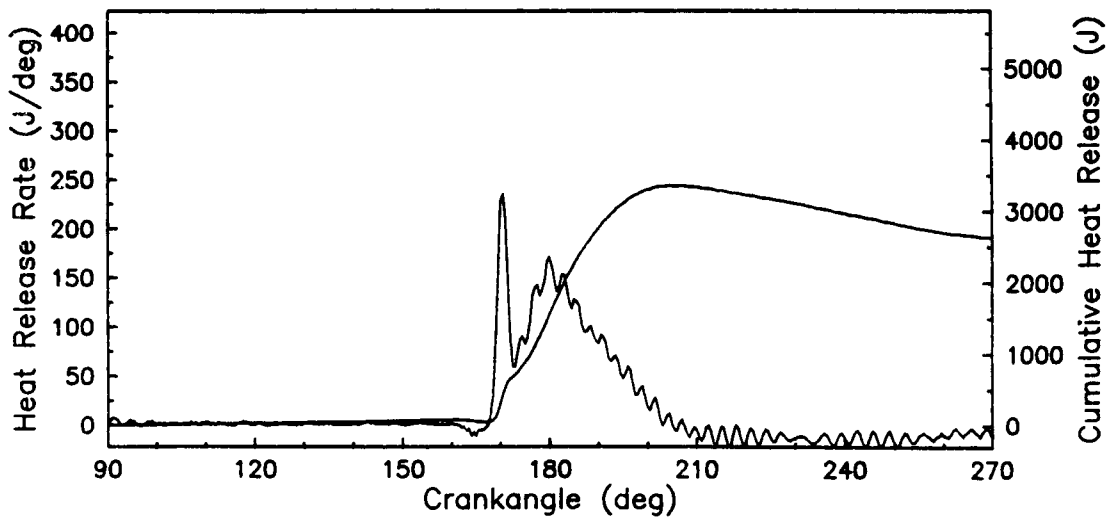
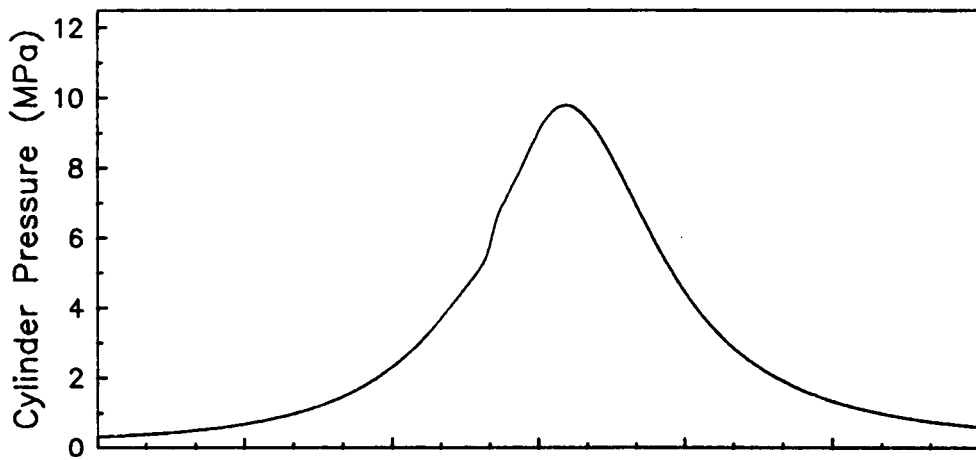
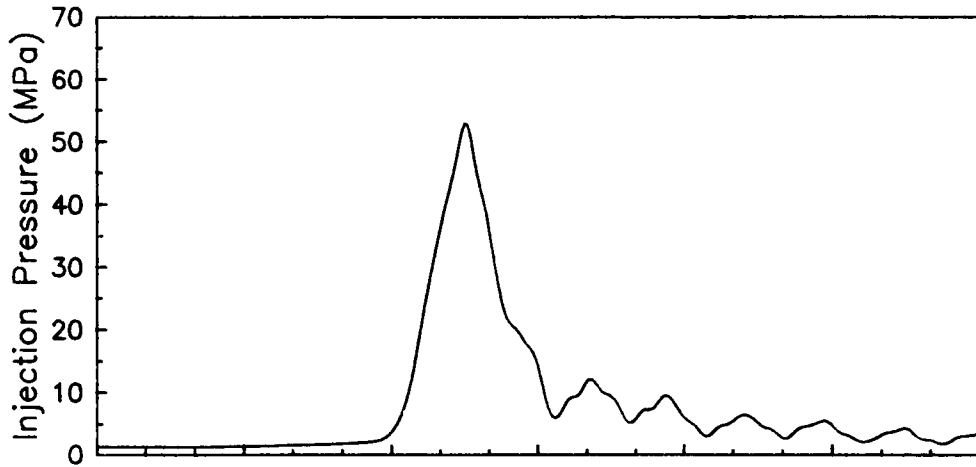
RUN #66, 1400 RPM, 33 % LOAD



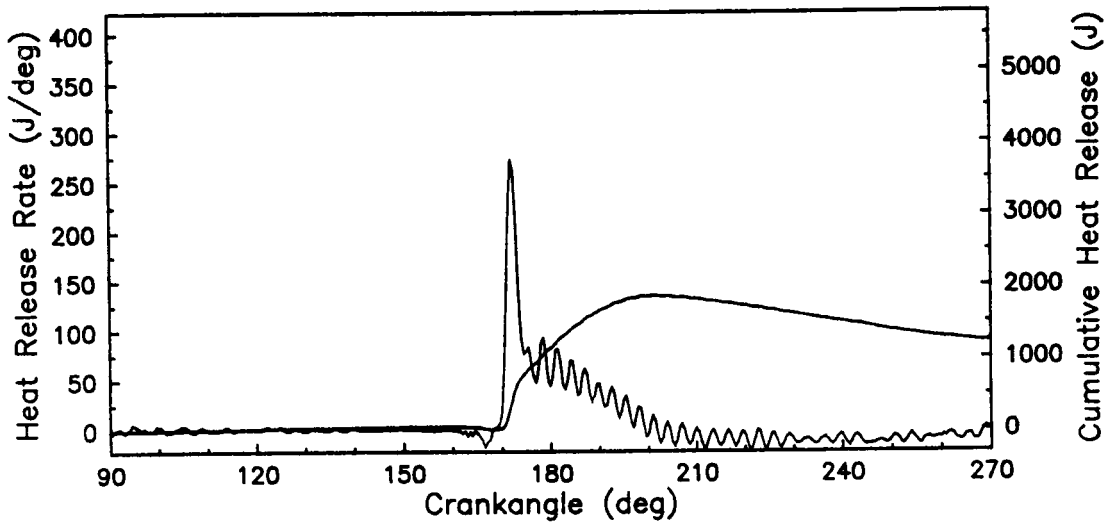
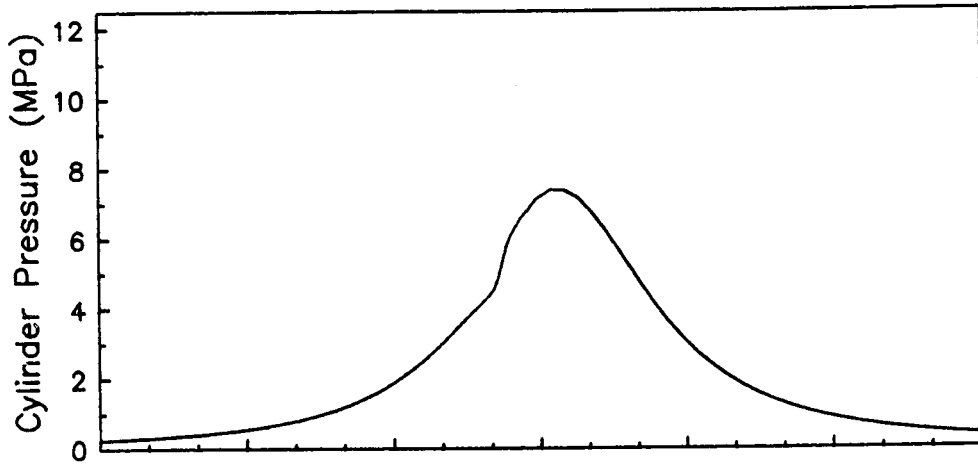
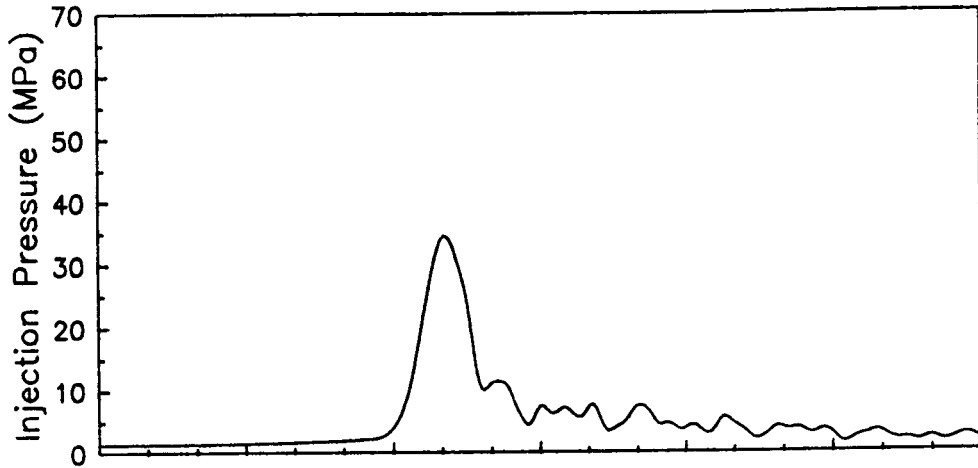
RUN #67, 1700 RPM, 100 % LOAD



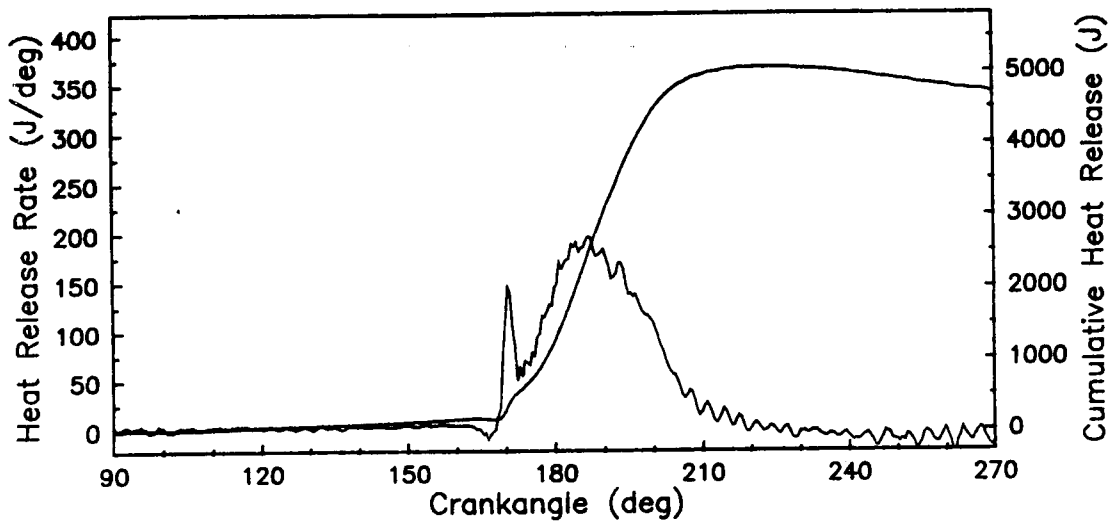
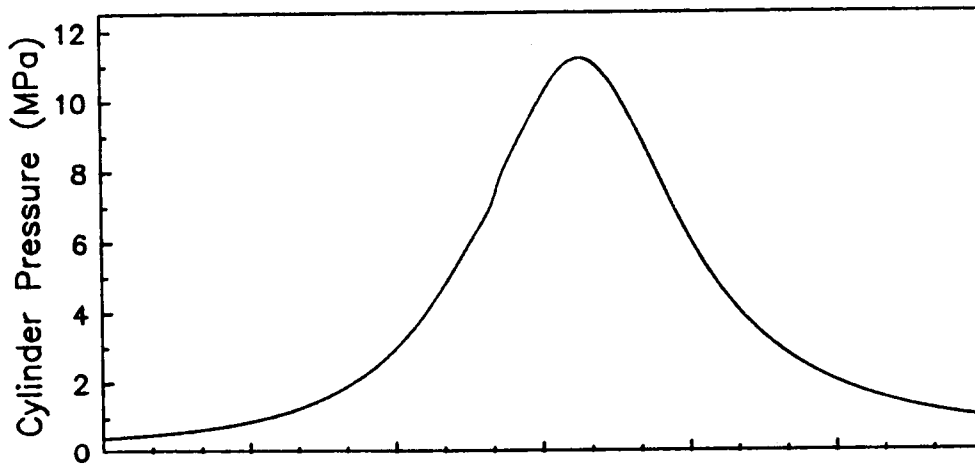
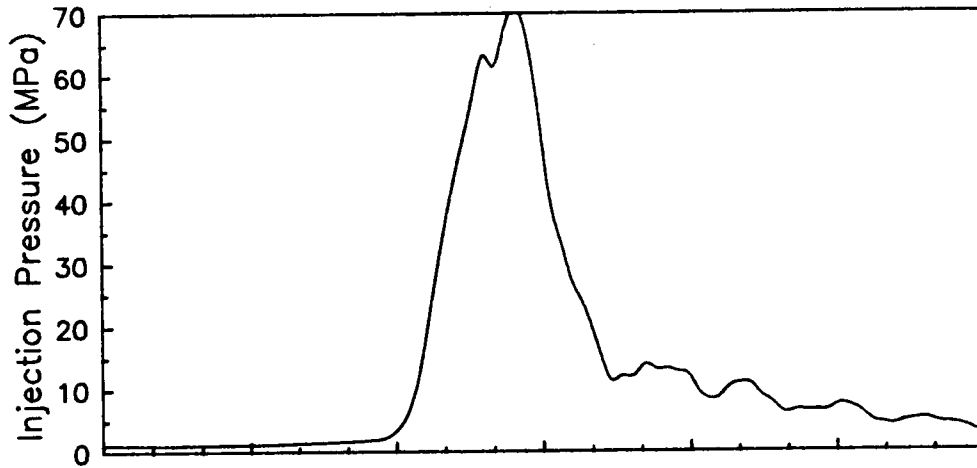
RUN #68, 1700 RPM, 67 % LOAD



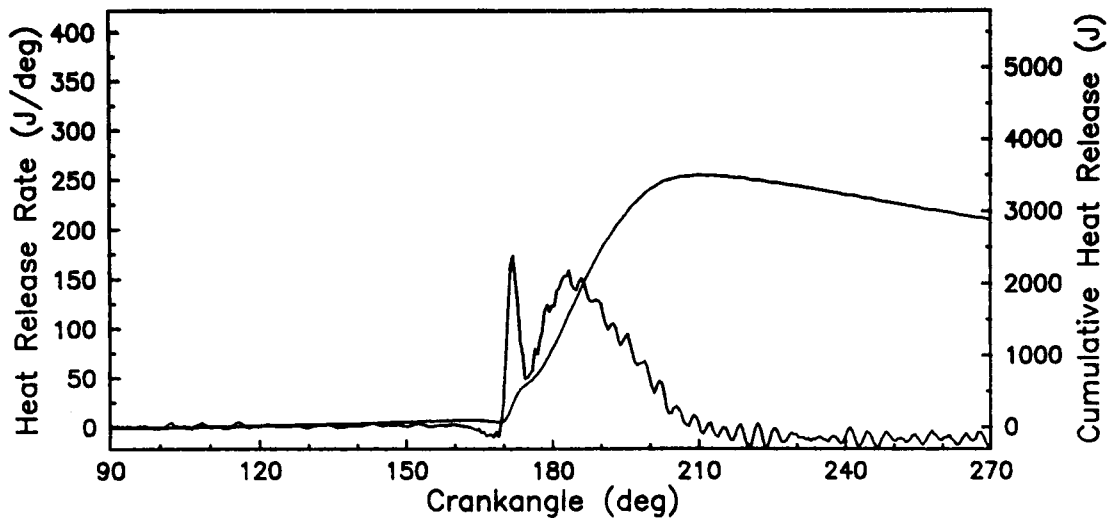
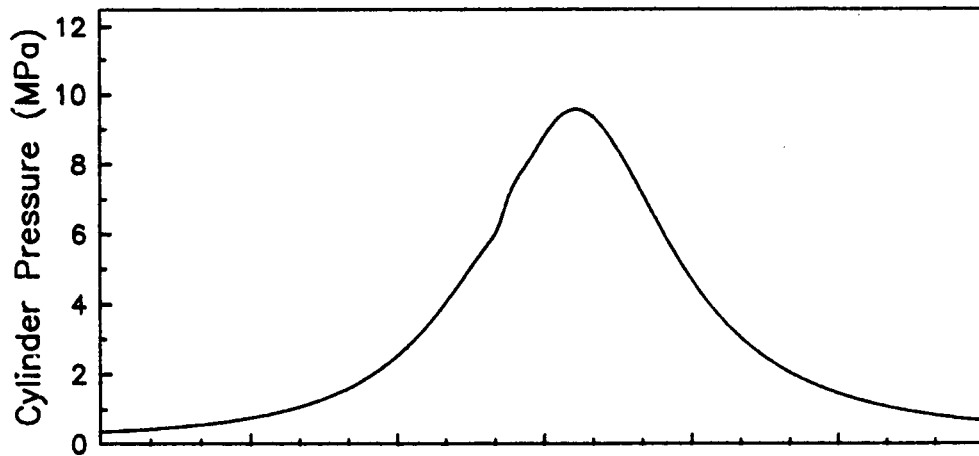
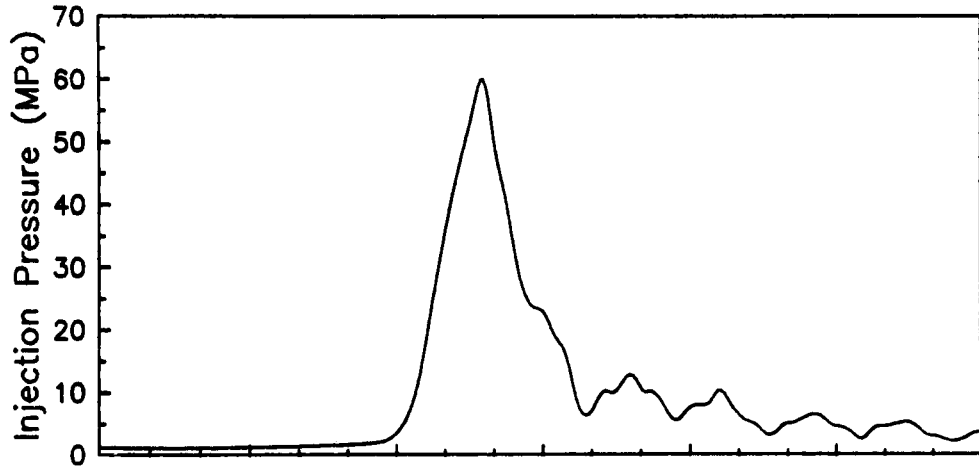
RUN #69, 1700 RPM, 33 % LOAD



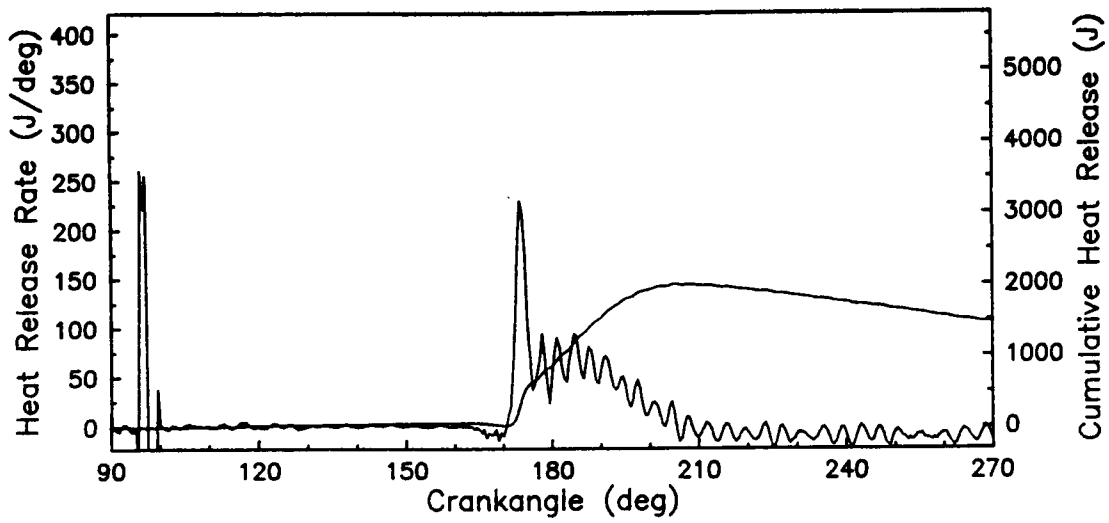
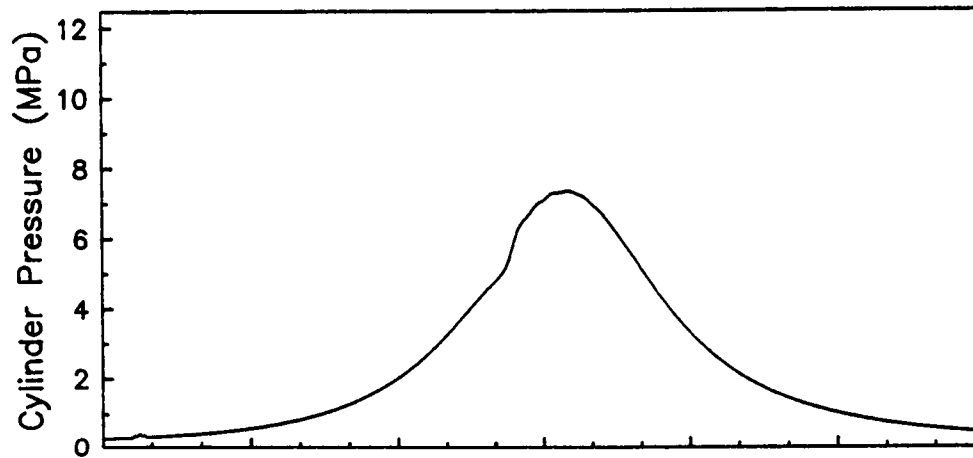
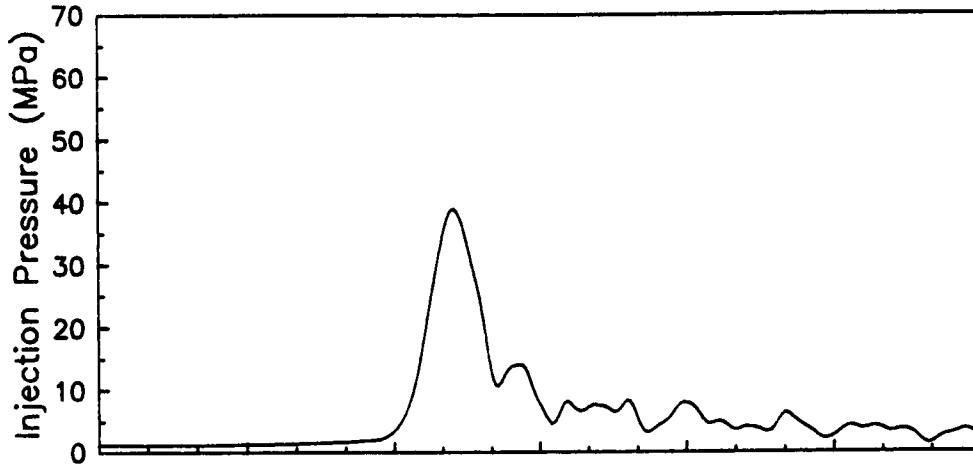
RUN #70, 2000 RPM, 100 % LOAD



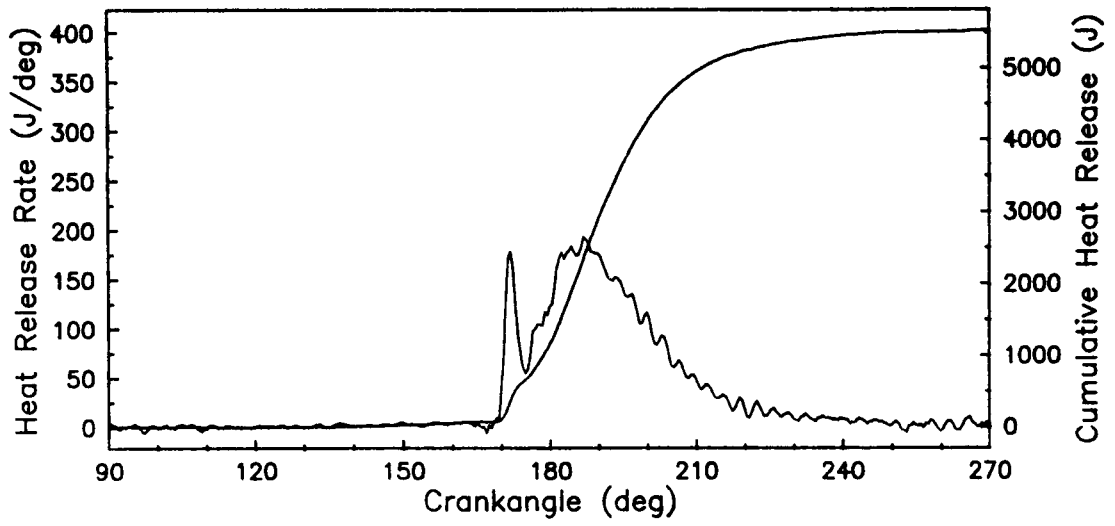
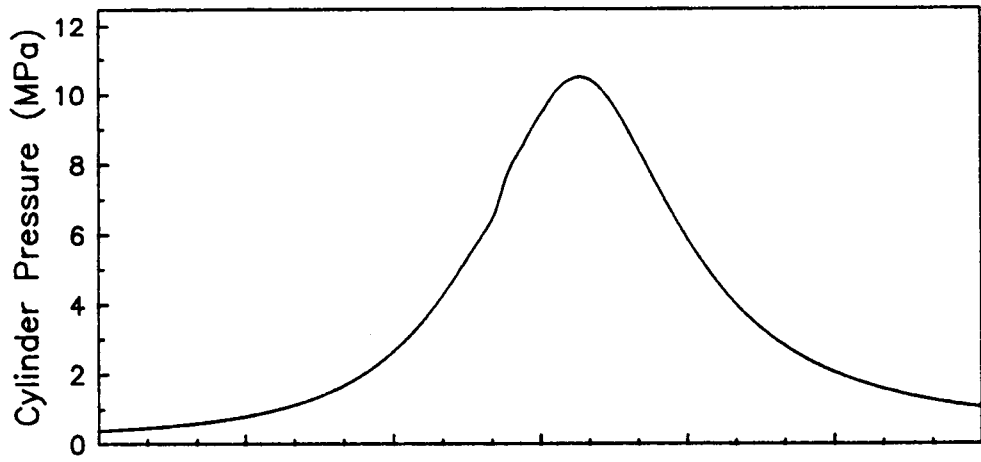
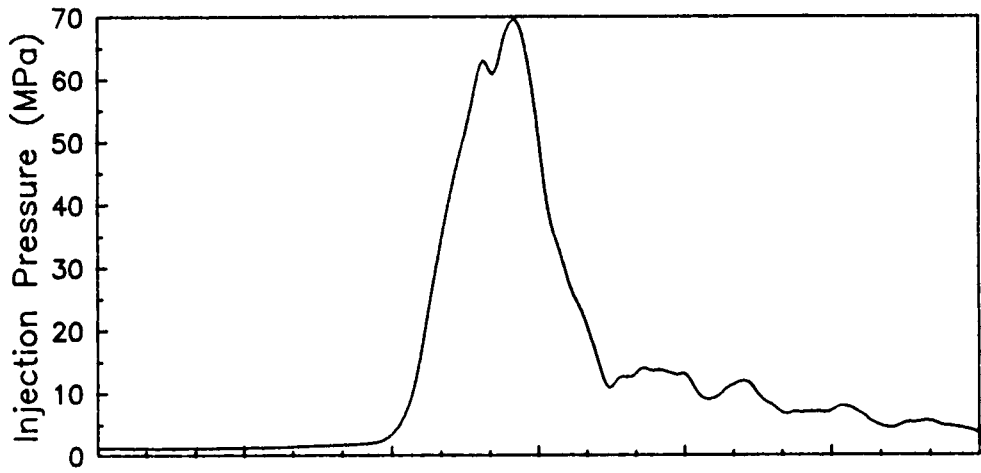
RUN #71, 2000 RPM, 67 % LOAD



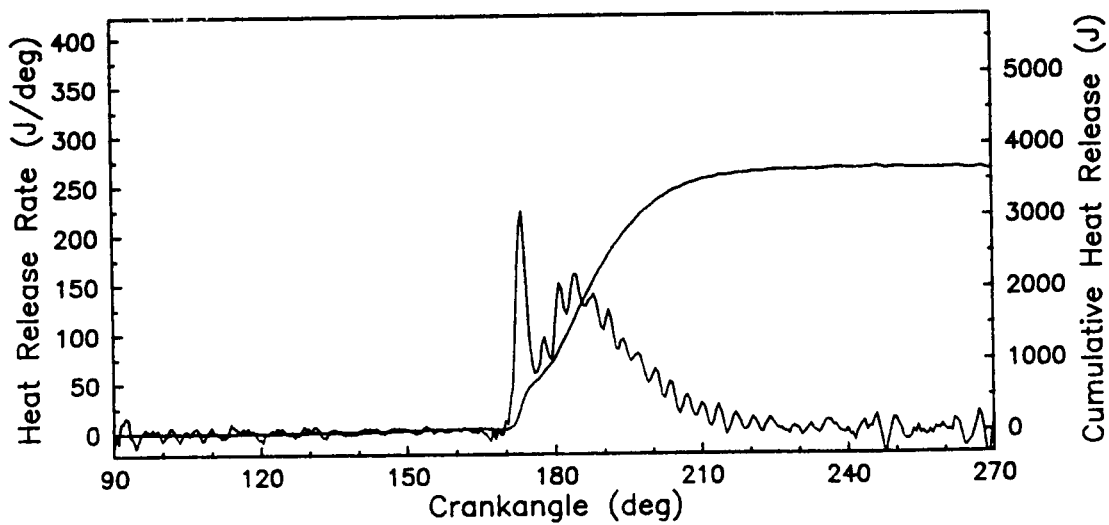
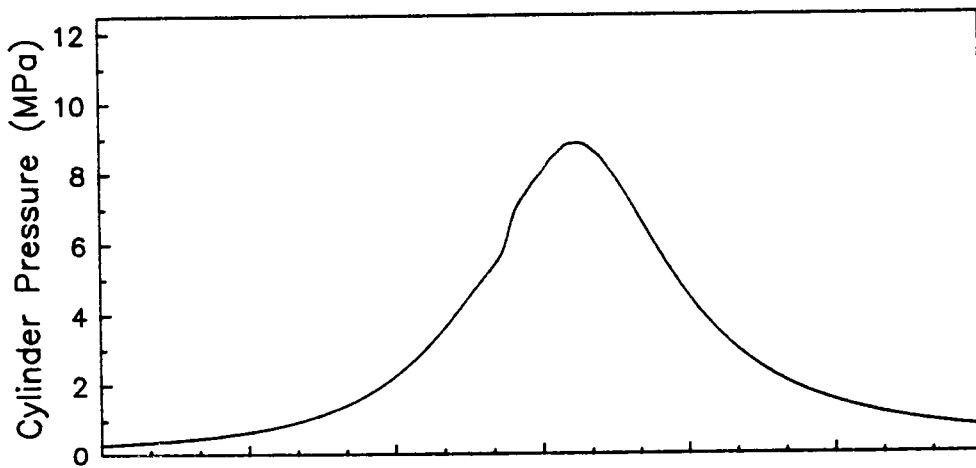
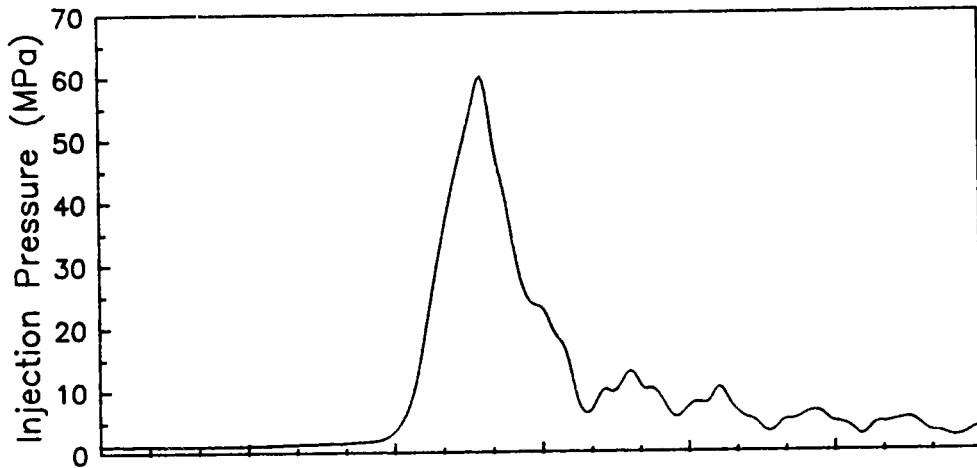
RUN #72, 2000 RPM, 33 % LOAD



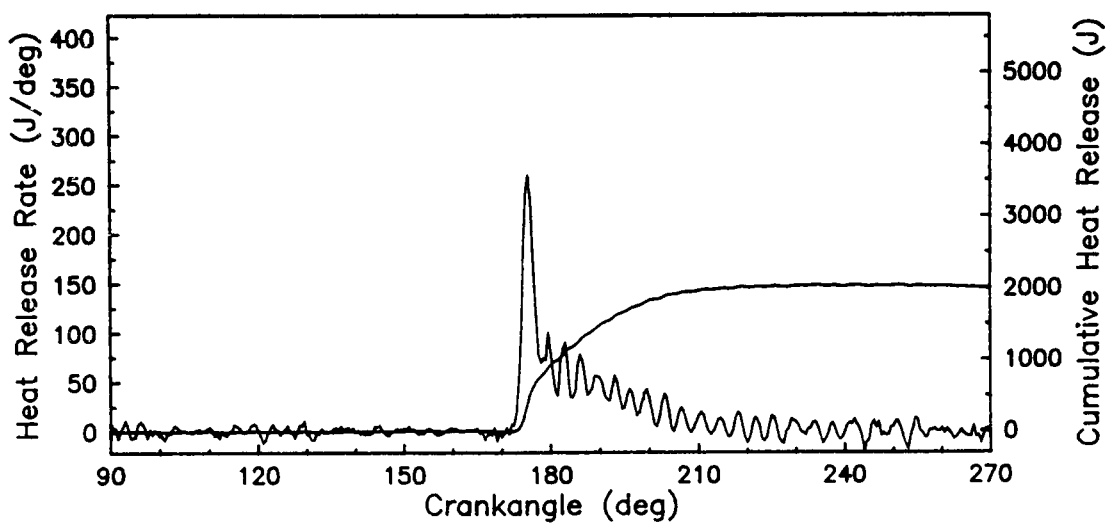
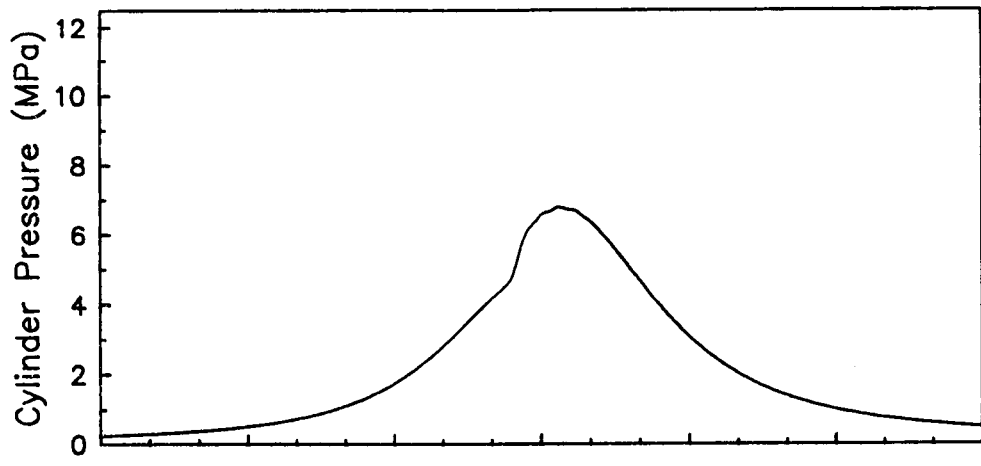
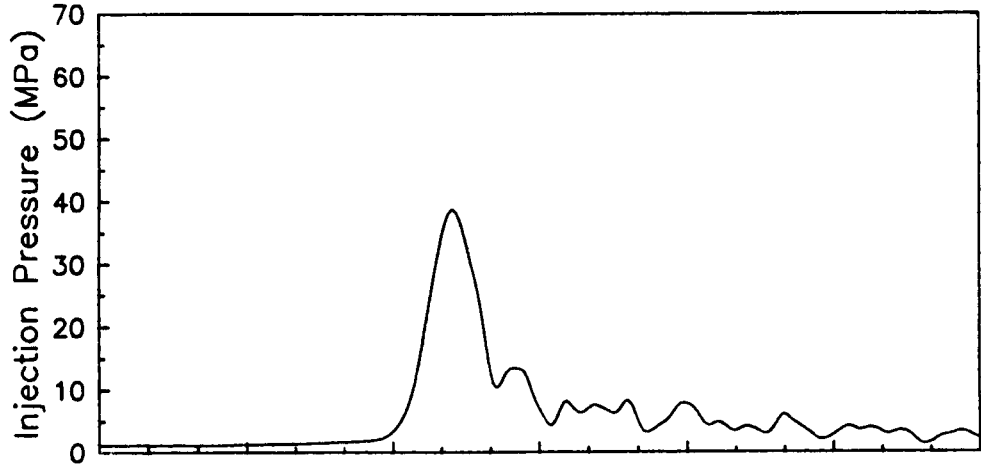
RUN #74, 2000 RPM, 100 % LOAD



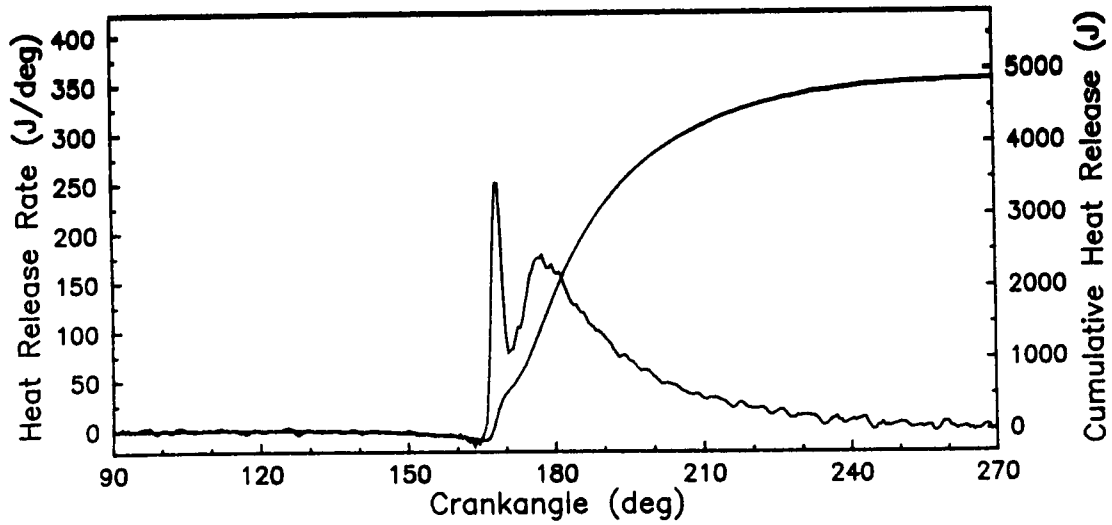
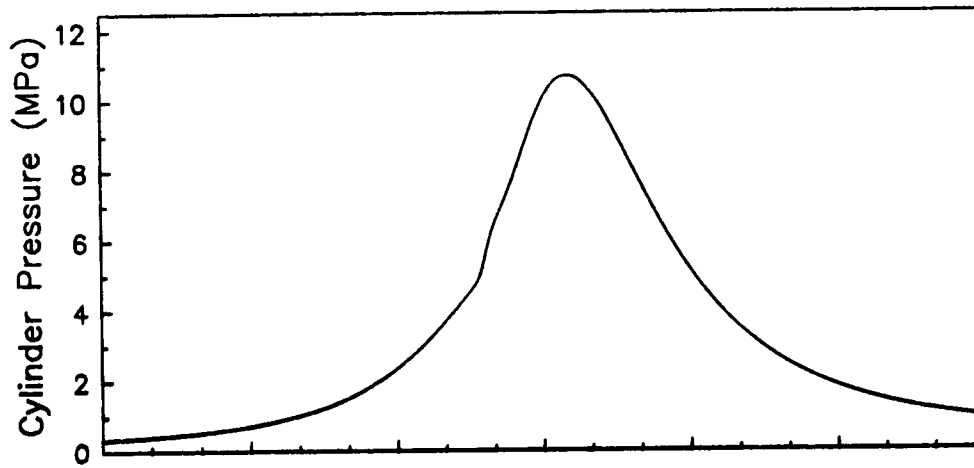
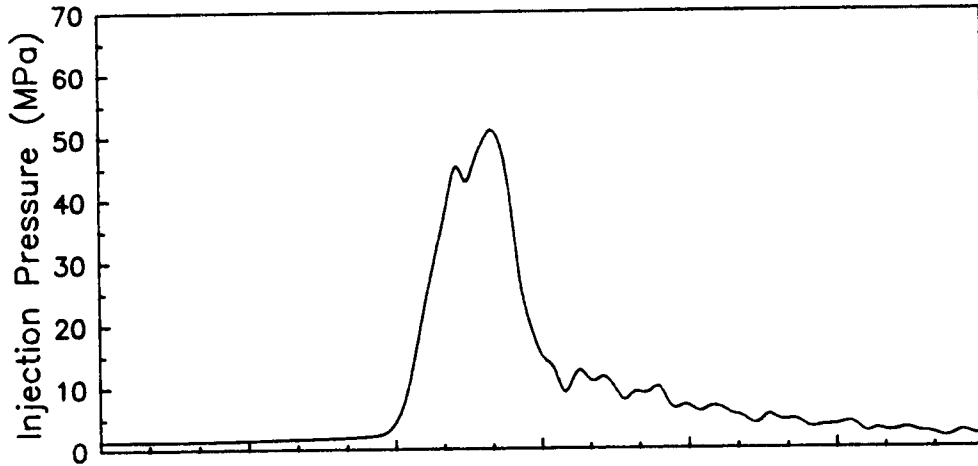
RUN #75, 2000 RPM, 67 % LOAD



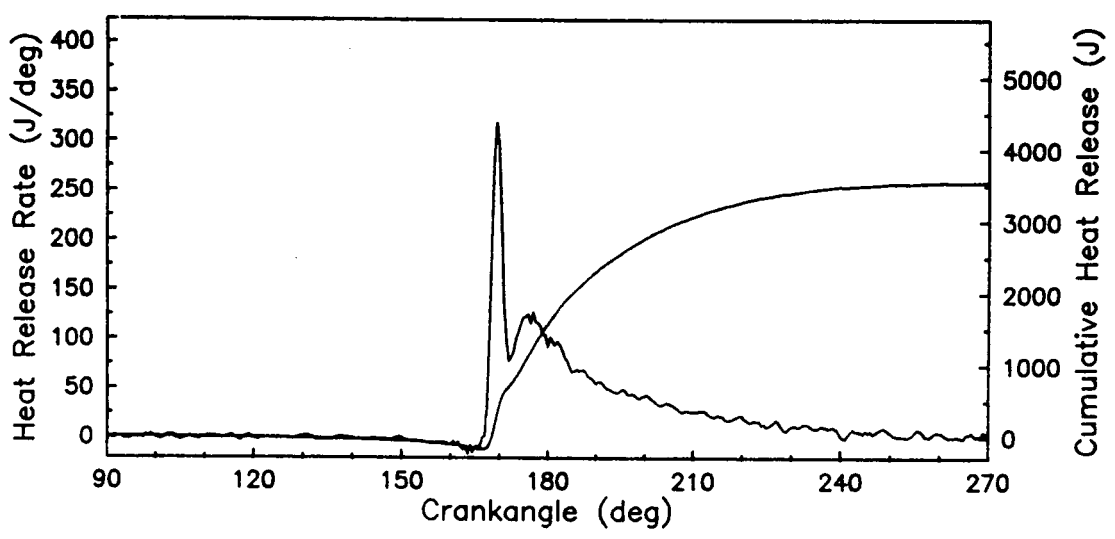
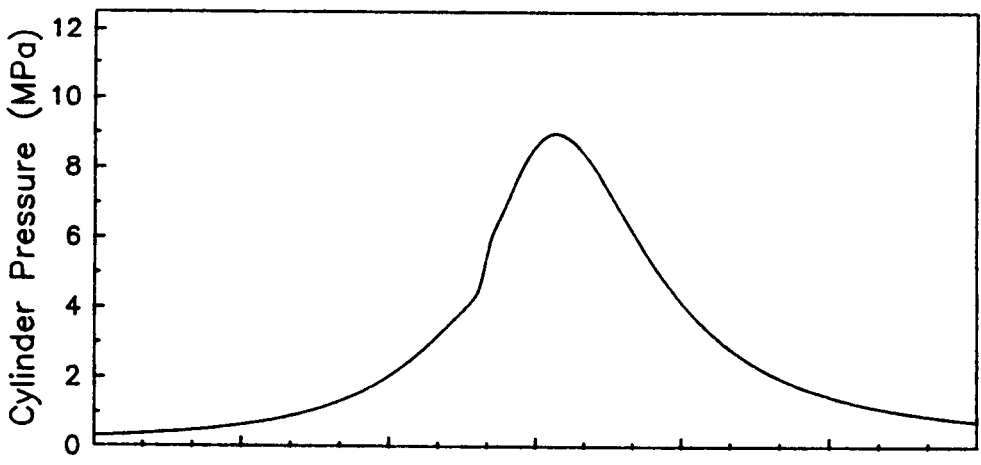
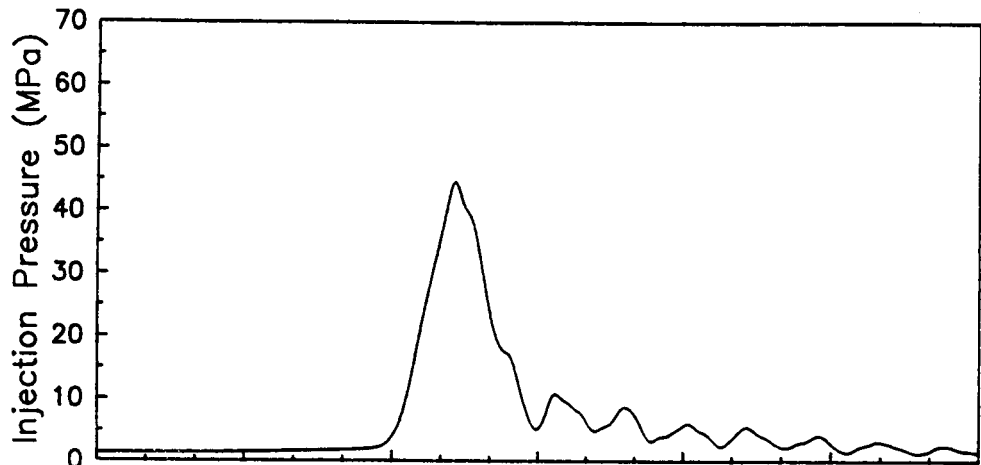
RUN #76, 2000 RPM, 33 % LOAD



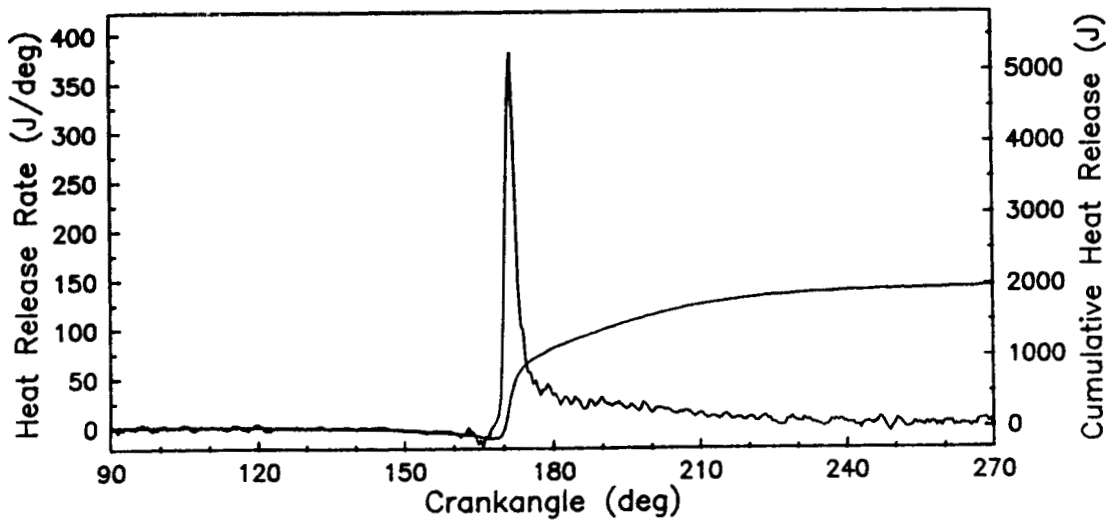
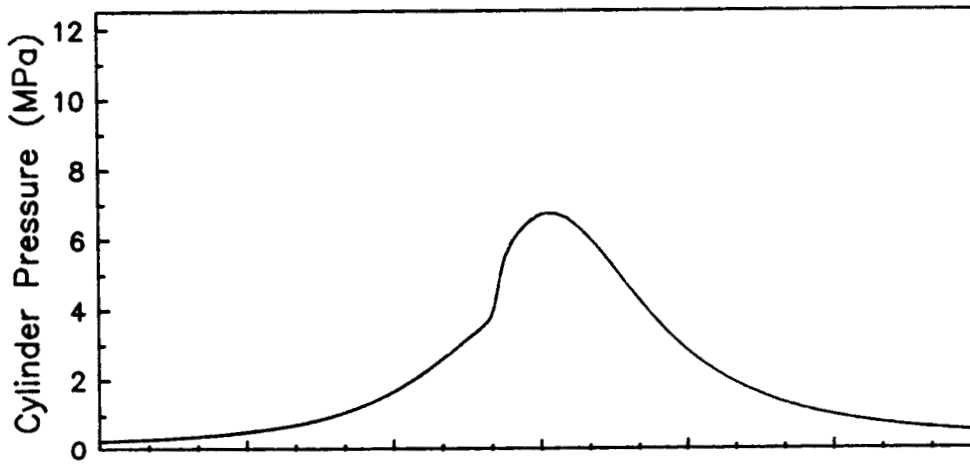
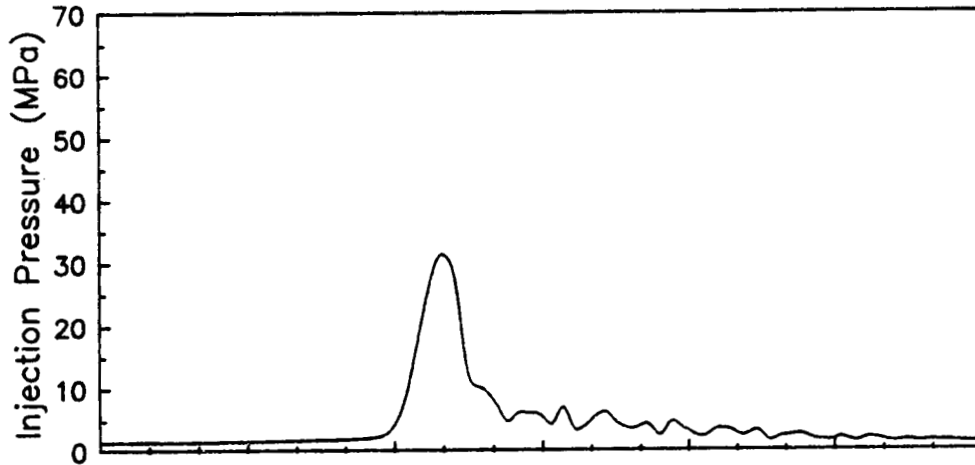
RUN #87, 1400 RPM, 100 % LOAD



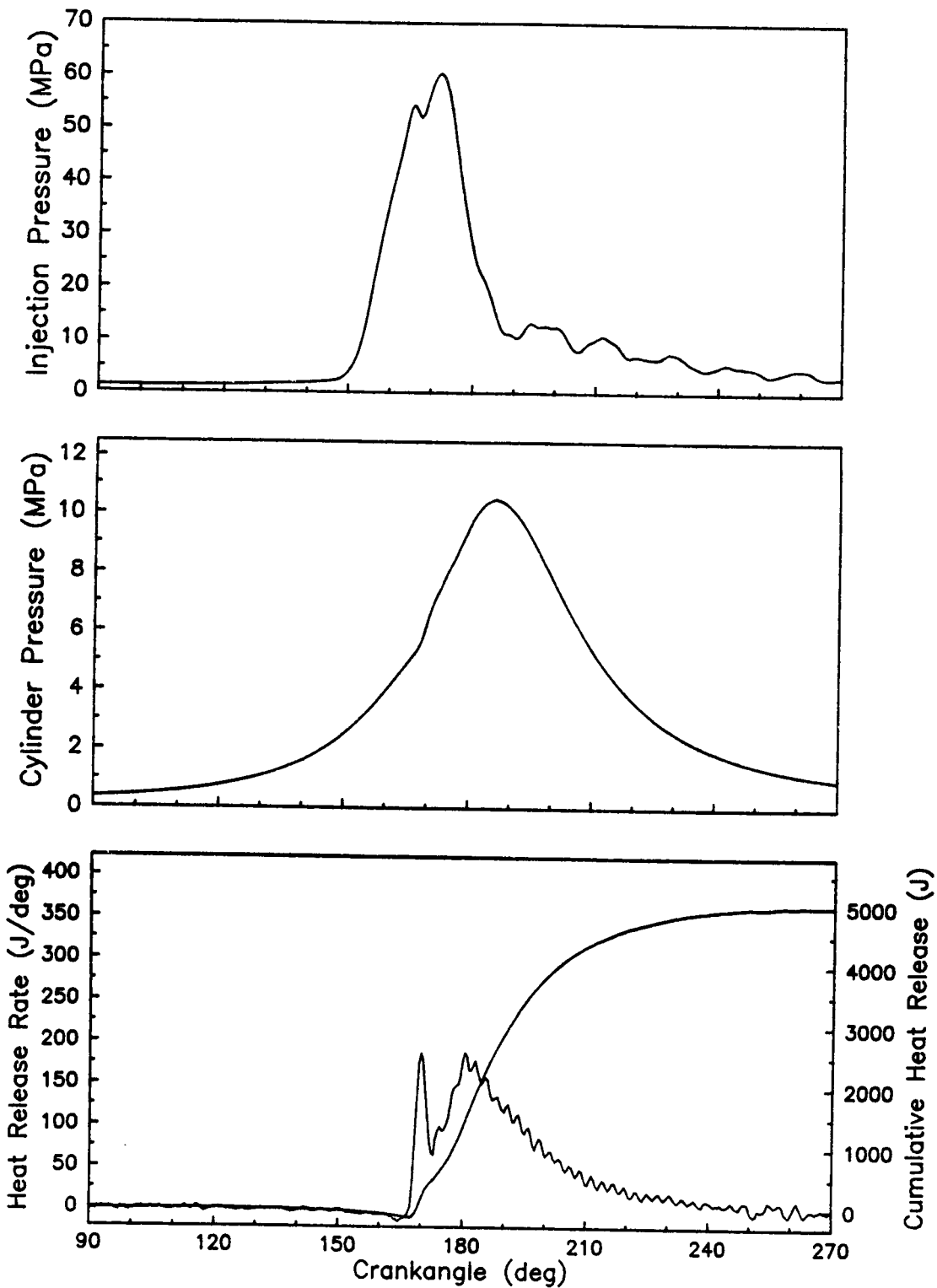
RUN #88, 1400 RPM, 67 % LOAD



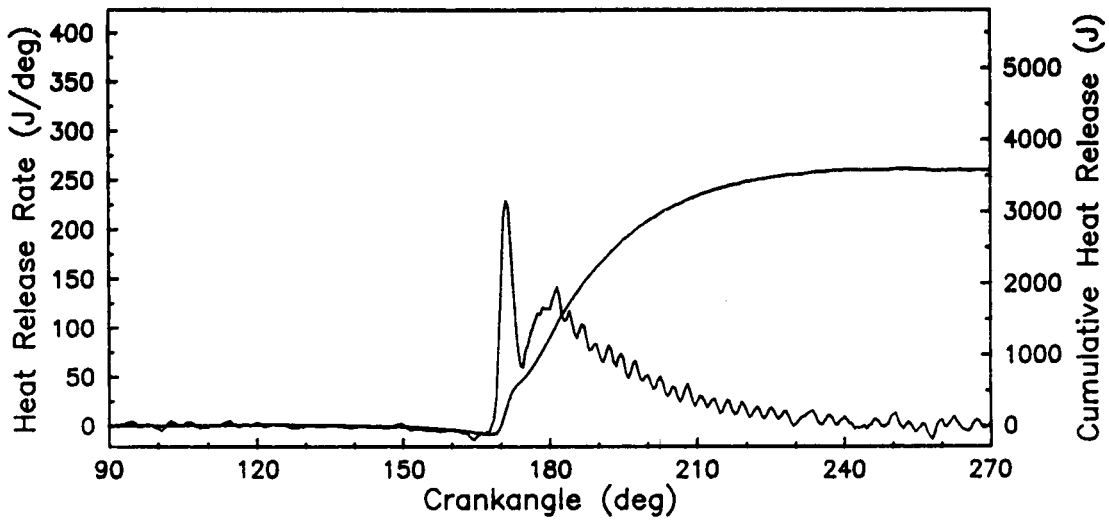
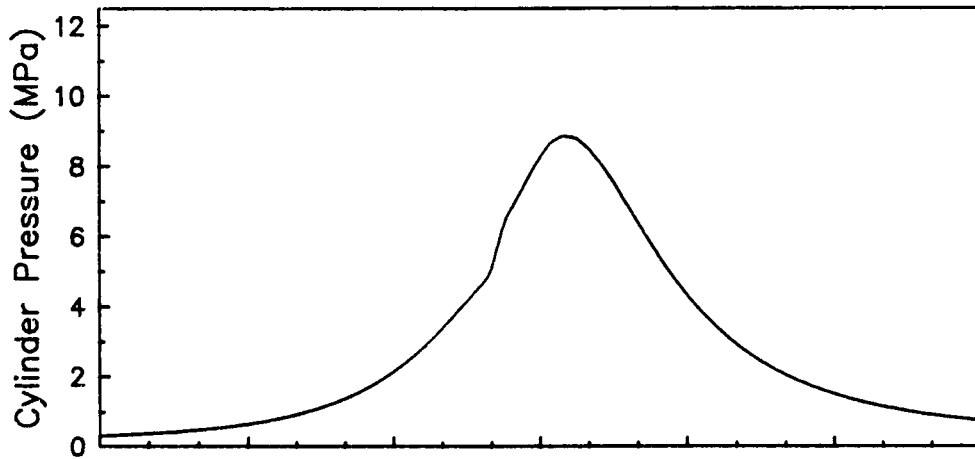
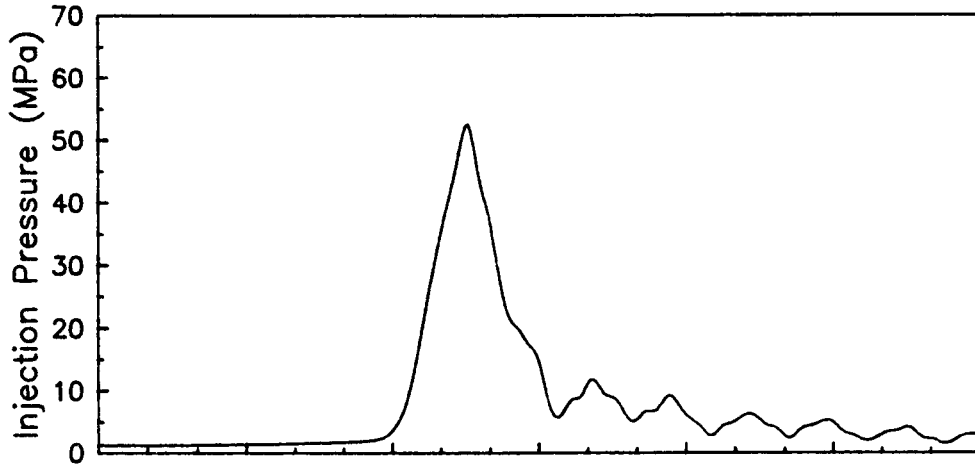
RUN #89, 1400 RPM, 33 % LOAD



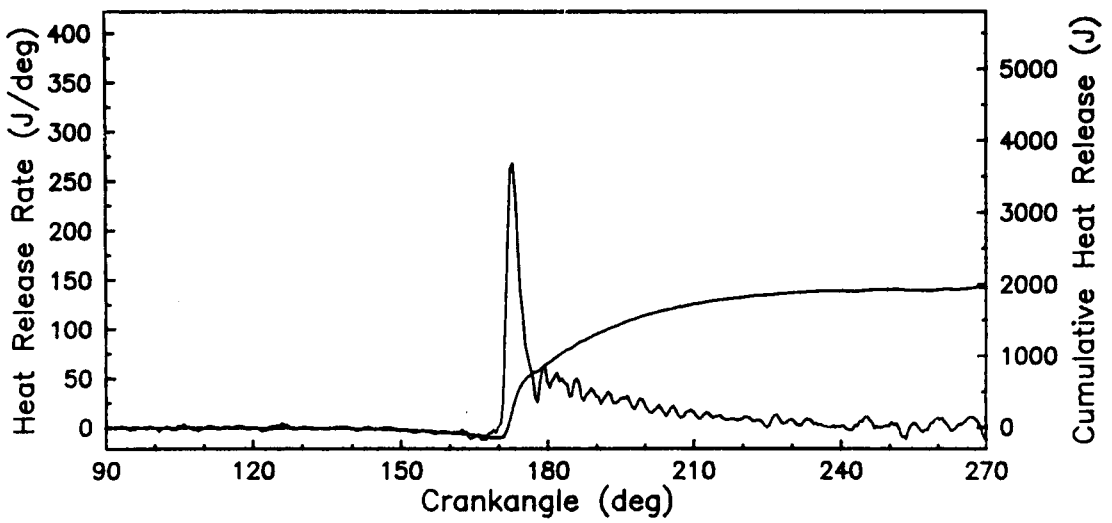
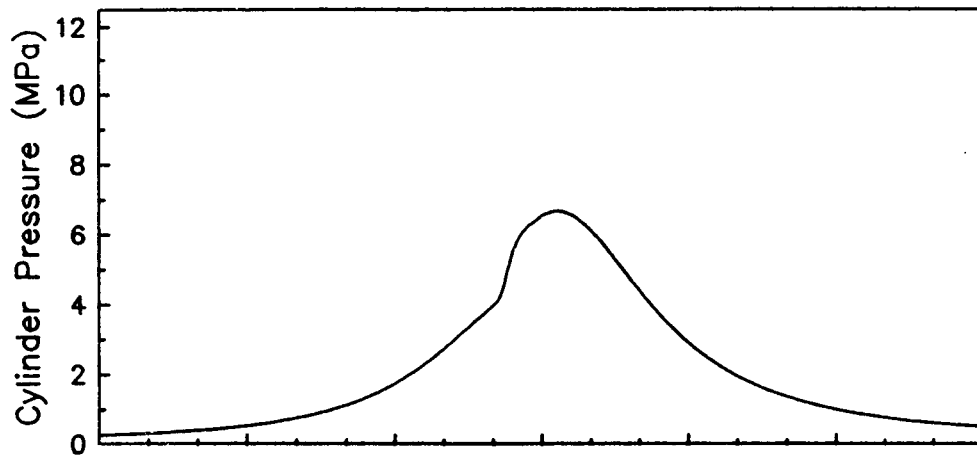
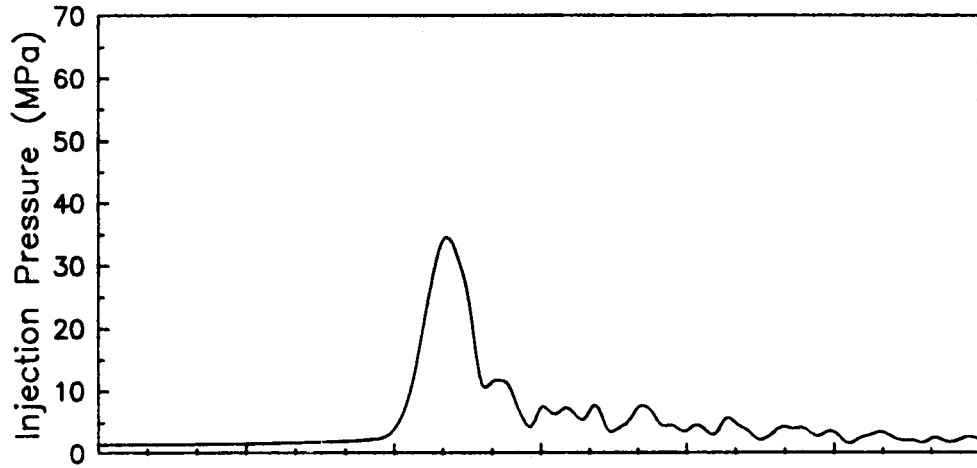
RUN #91, 1700 RPM, 100 % LOAD



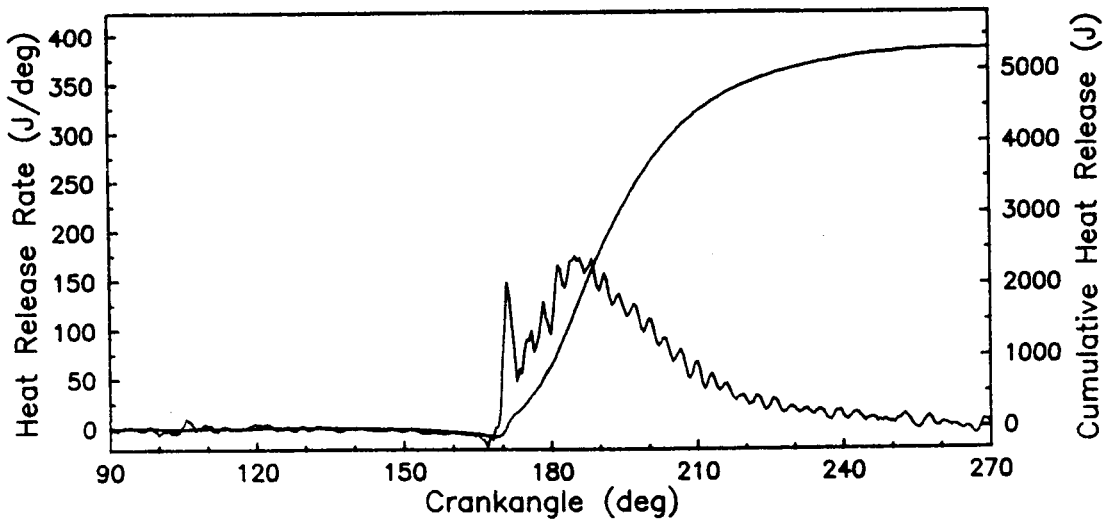
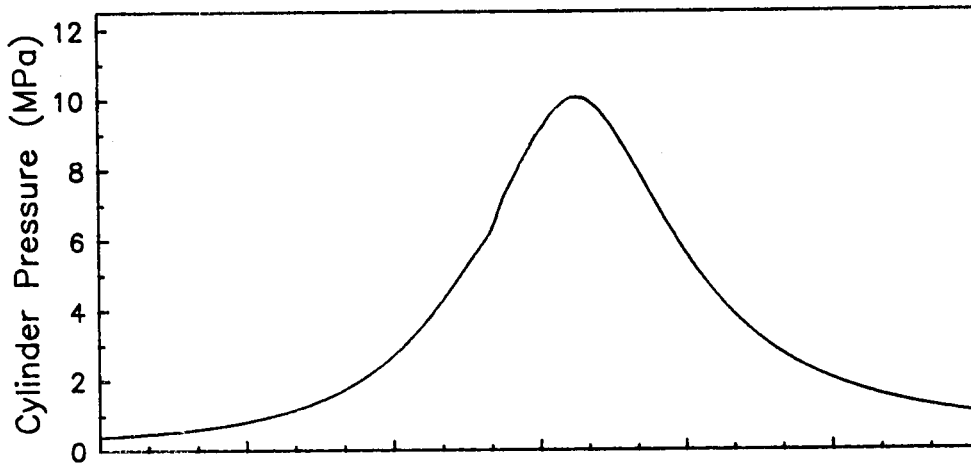
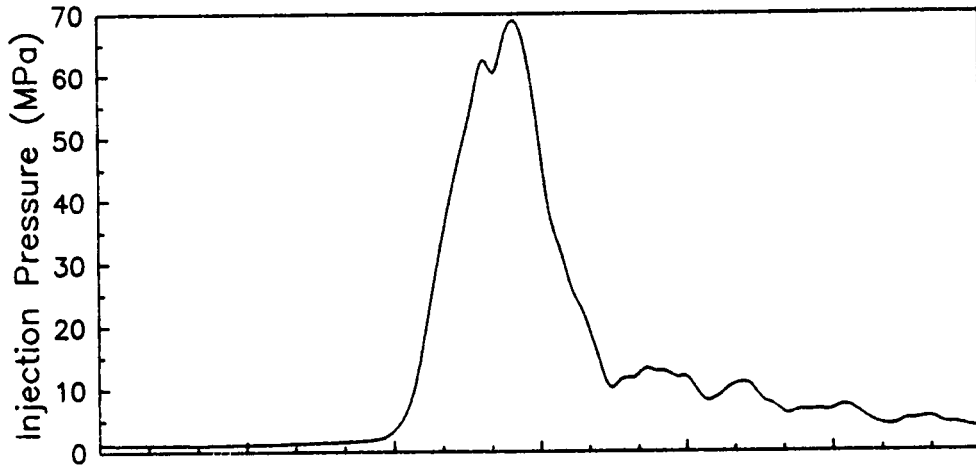
RUN #92, 1700 RPM, 67 % LOAD



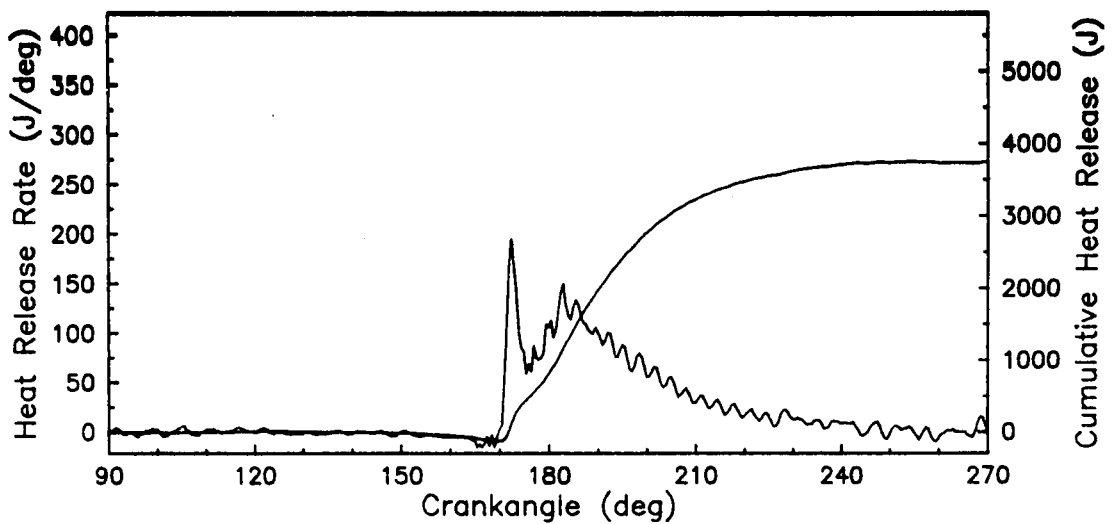
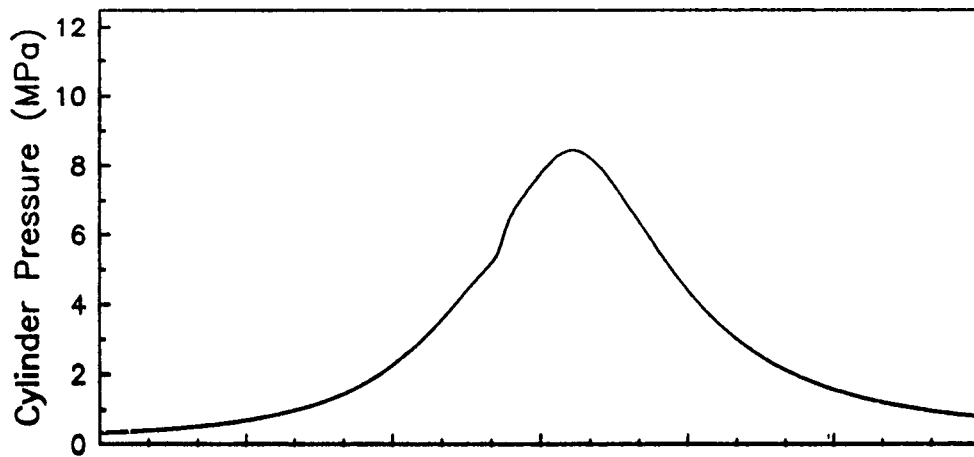
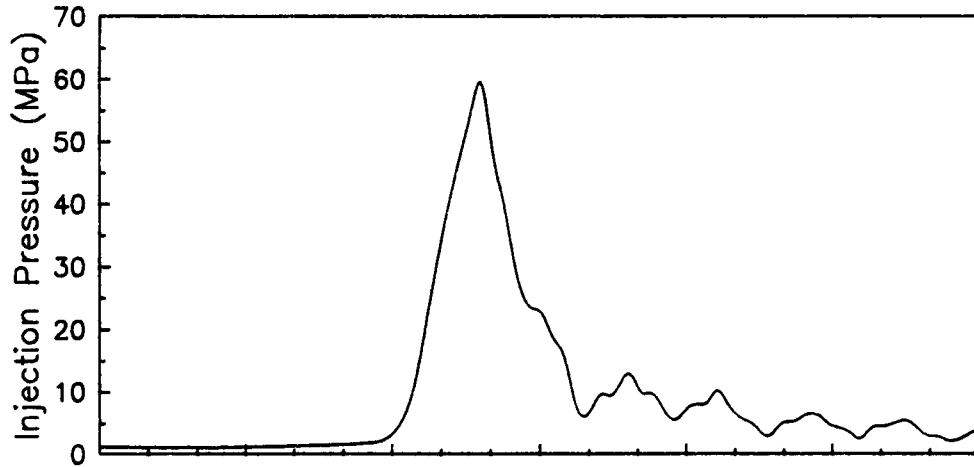
RUN #93, 1700 RPM, 33 % LOAD



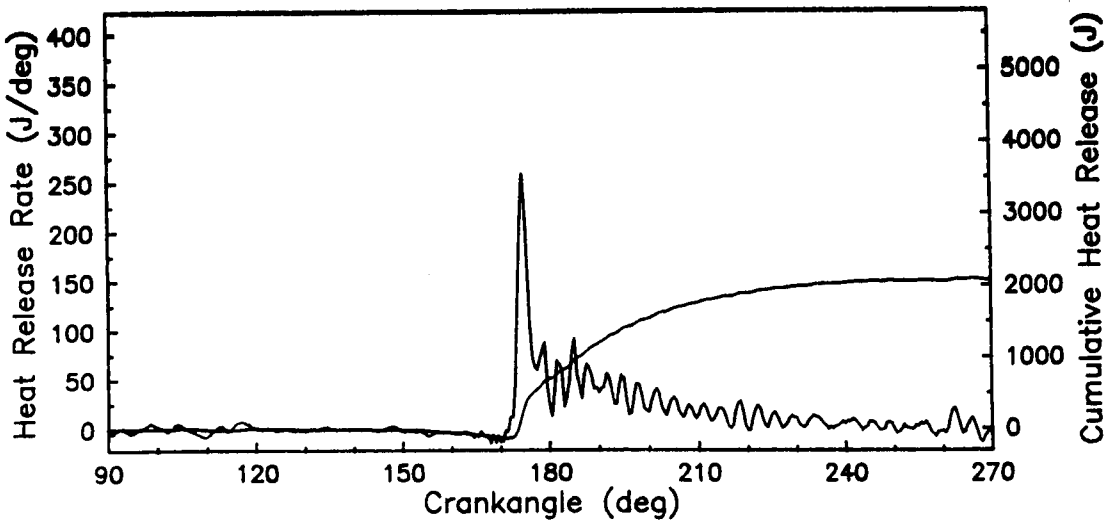
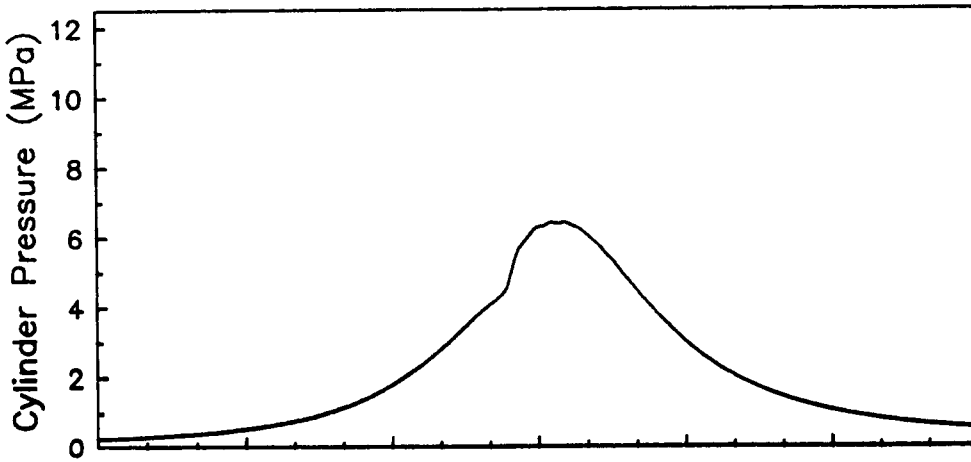
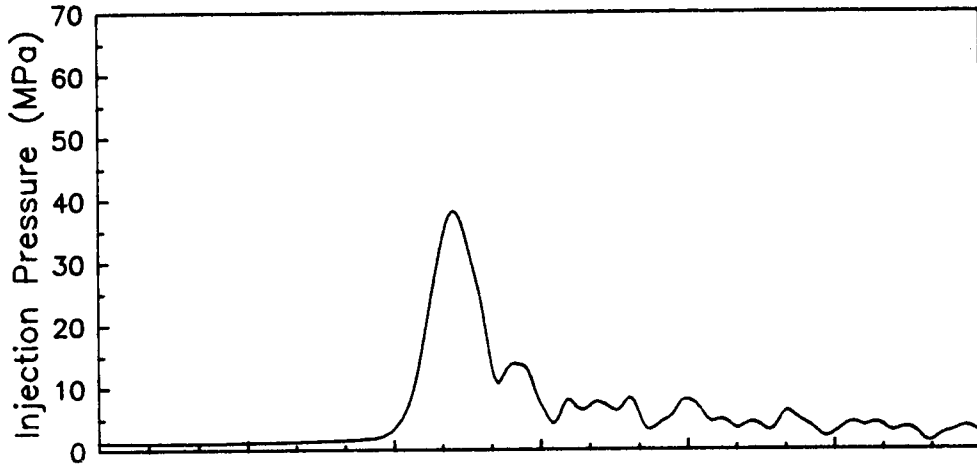
RUN #94, 2000 RPM, 100 % LOAD



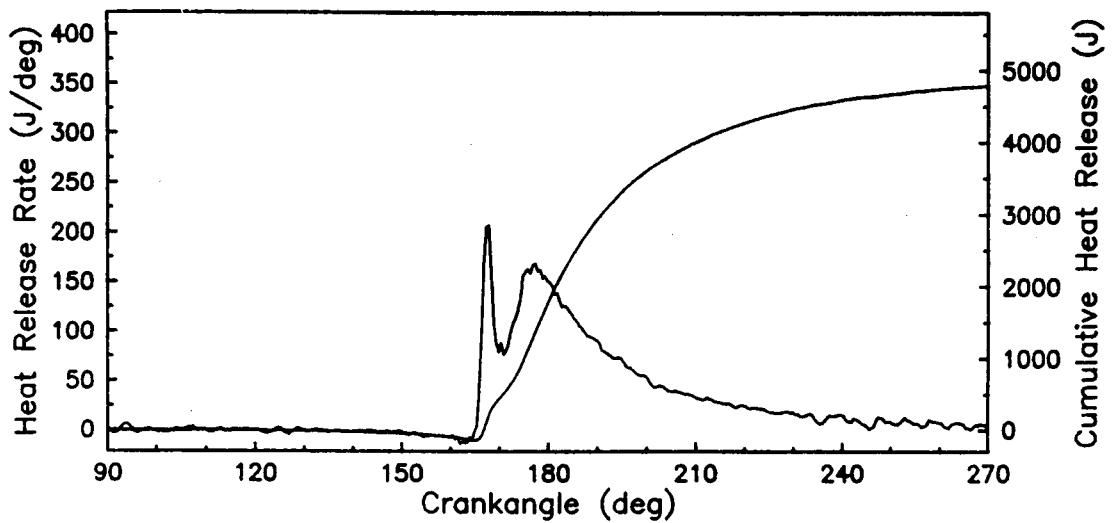
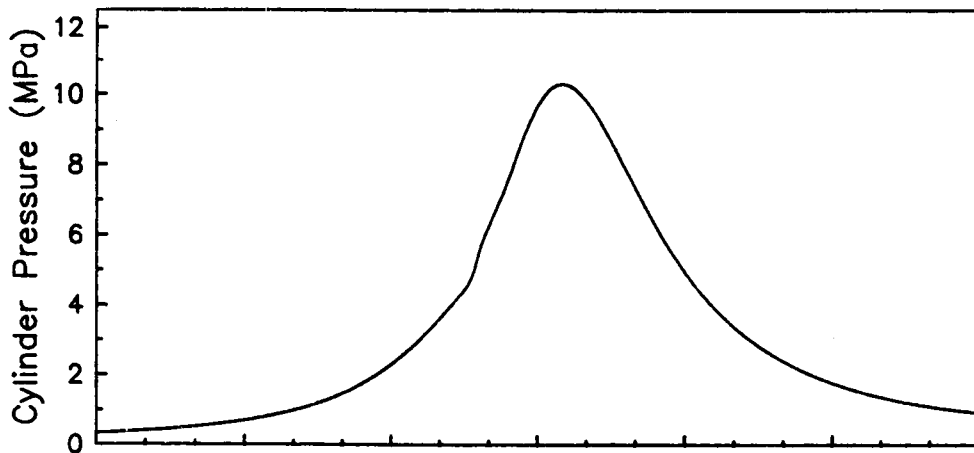
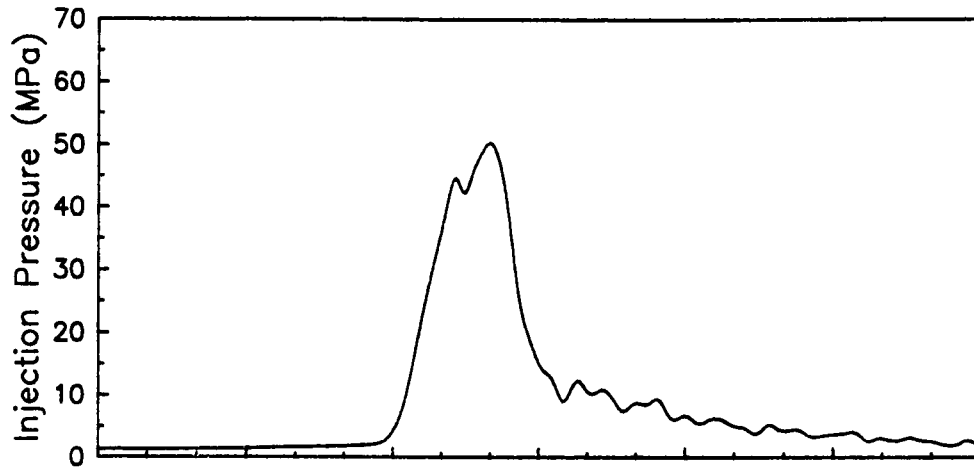
RUN #95, 2000 RPM, 67 % LOAD



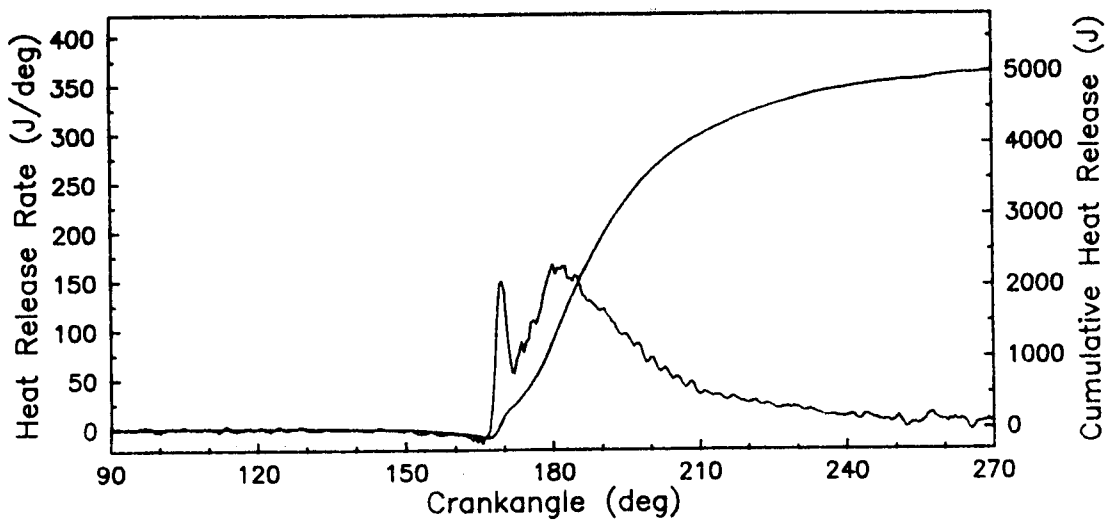
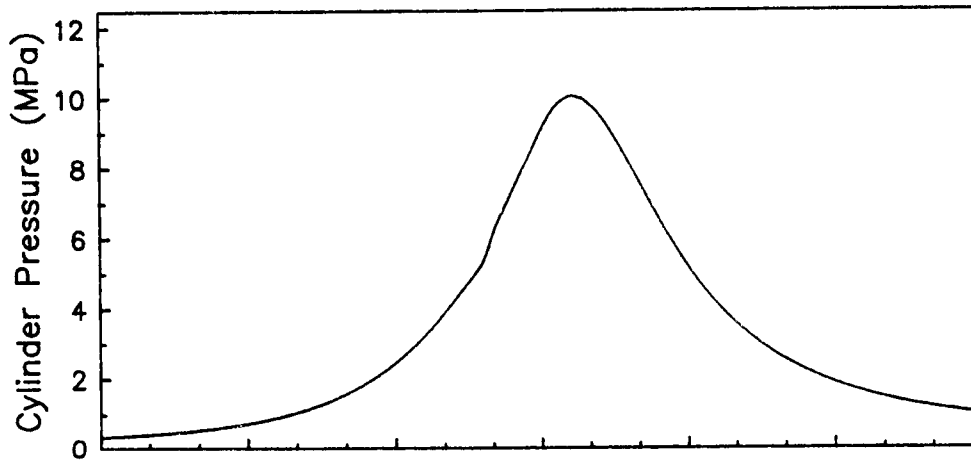
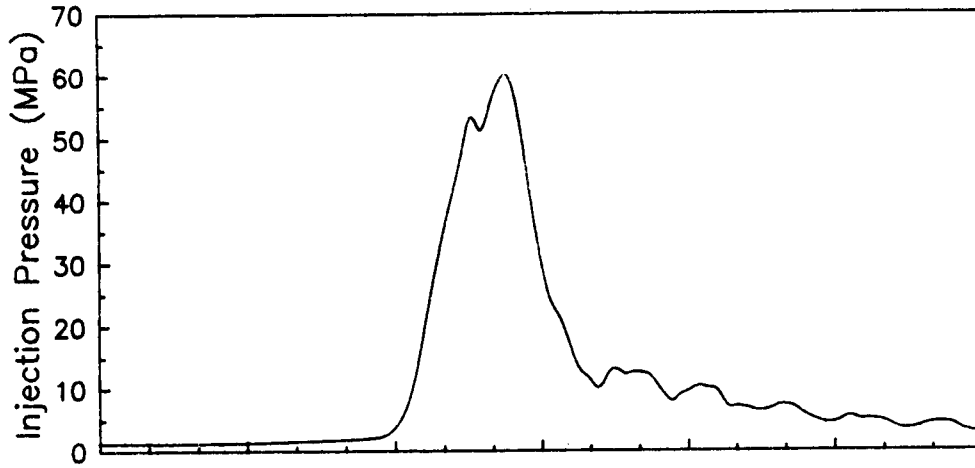
RUN #96, 2000 RPM, 33 % LOAD



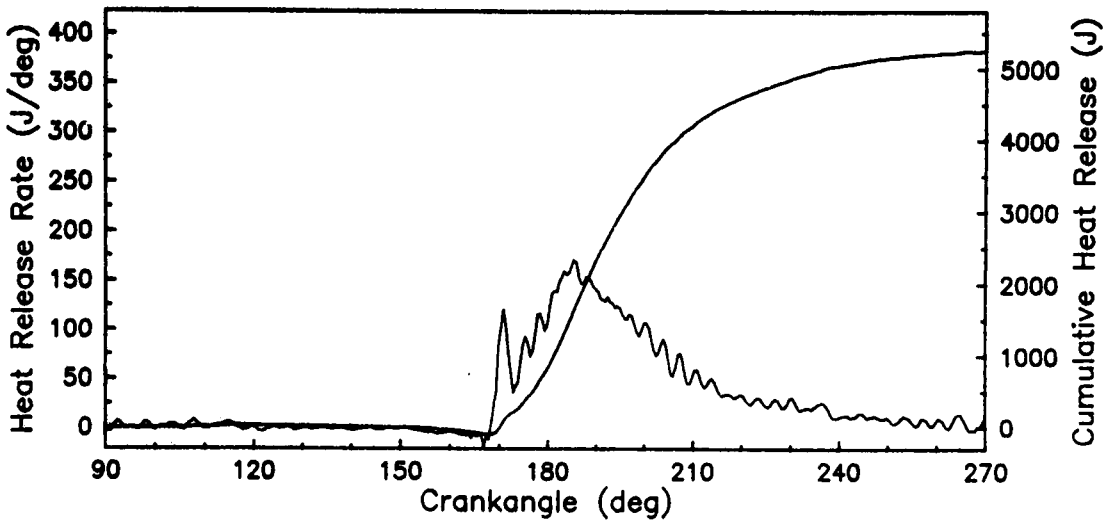
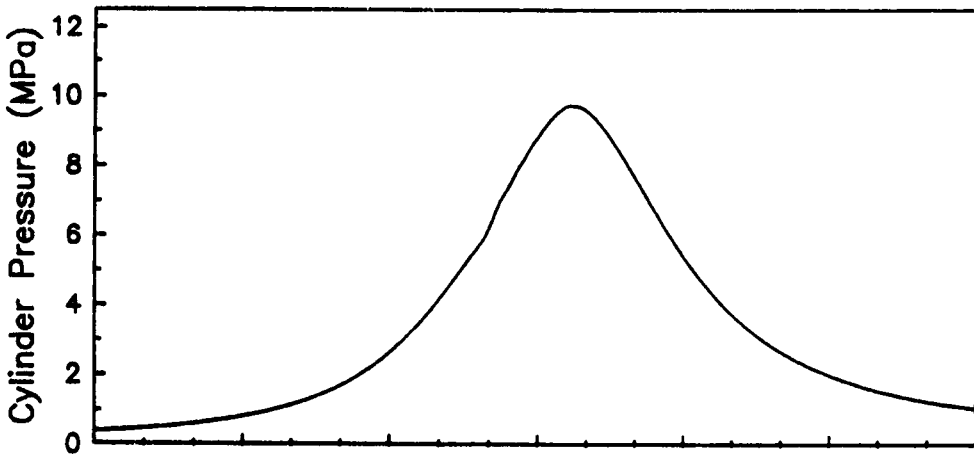
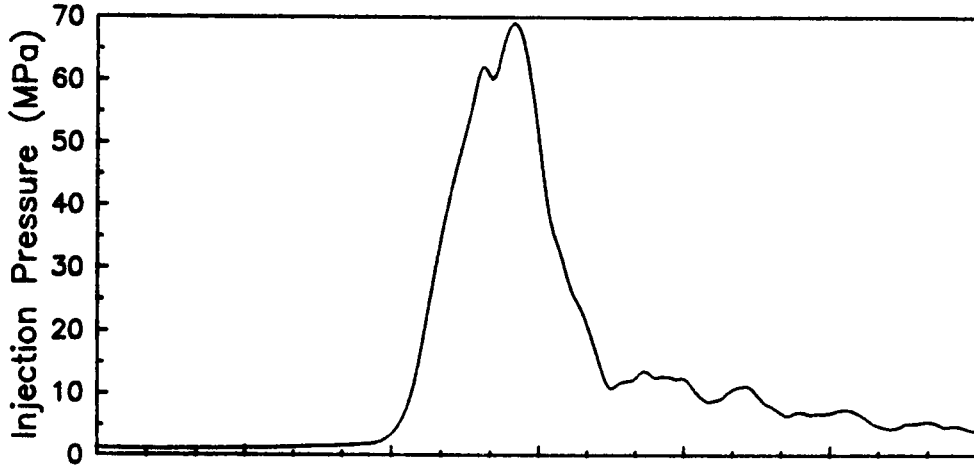
RUN #97, 1400 RPM, 100 % LOAD



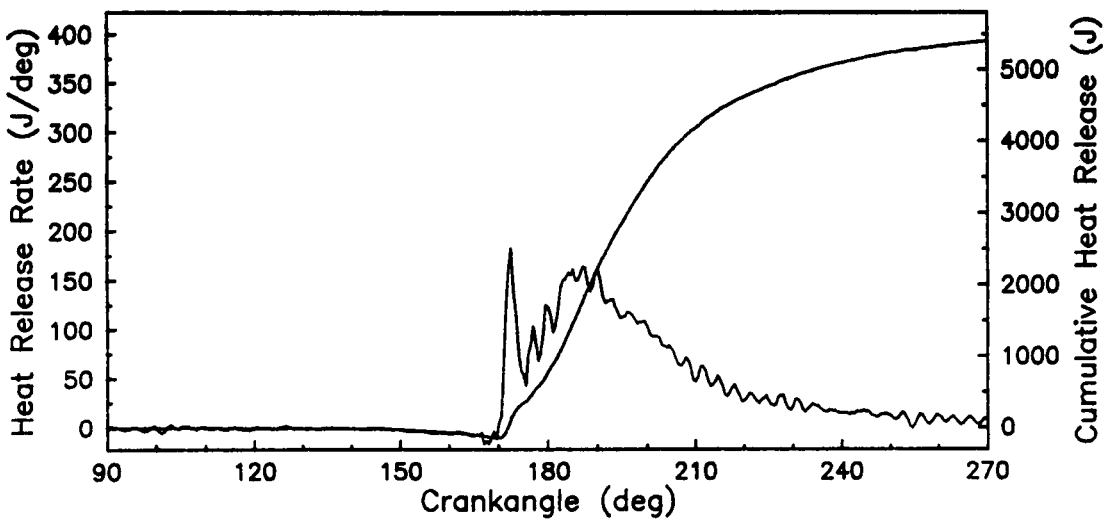
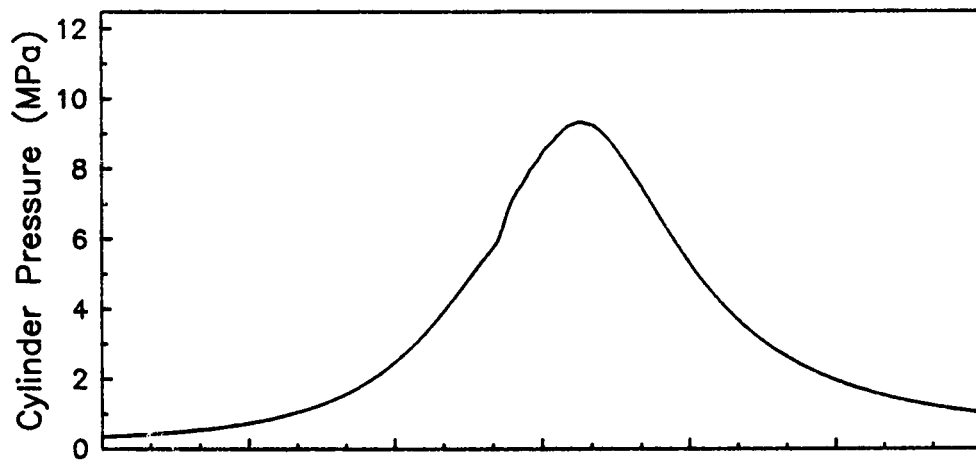
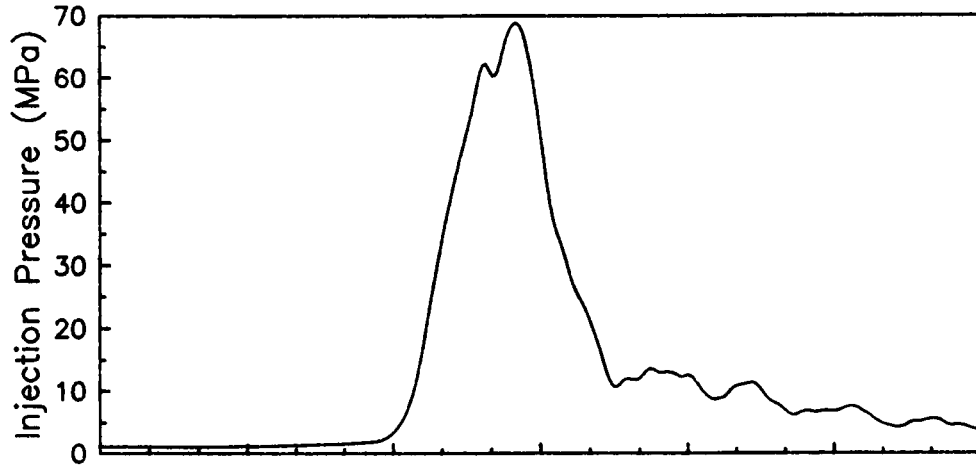
RUN #98, 1700 RPM, 100 % LOAD



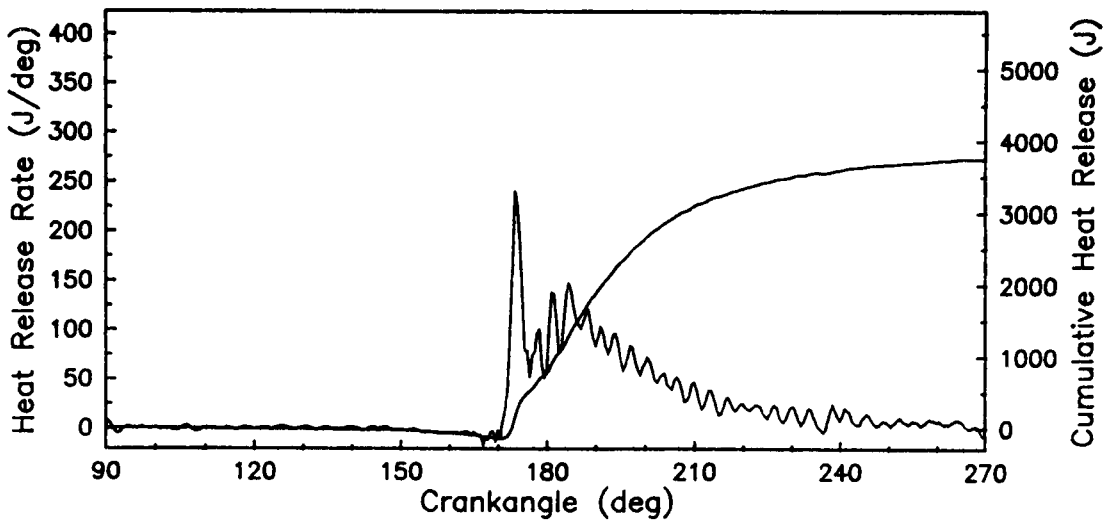
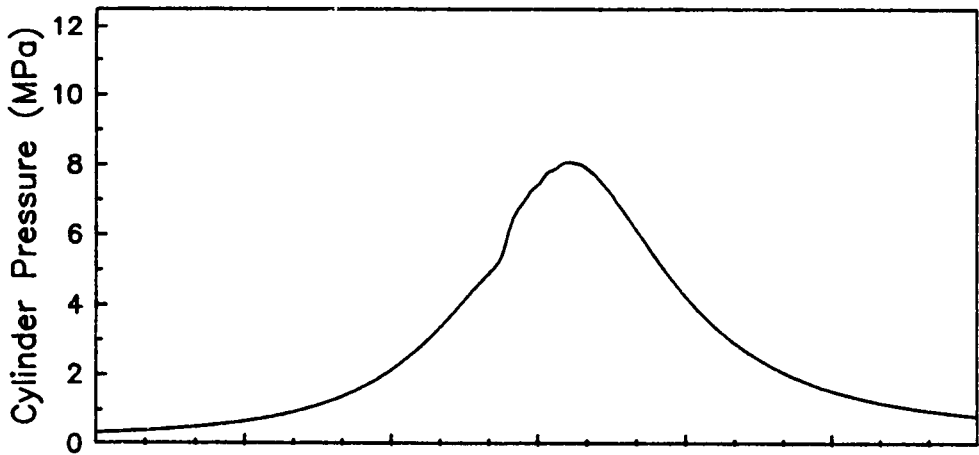
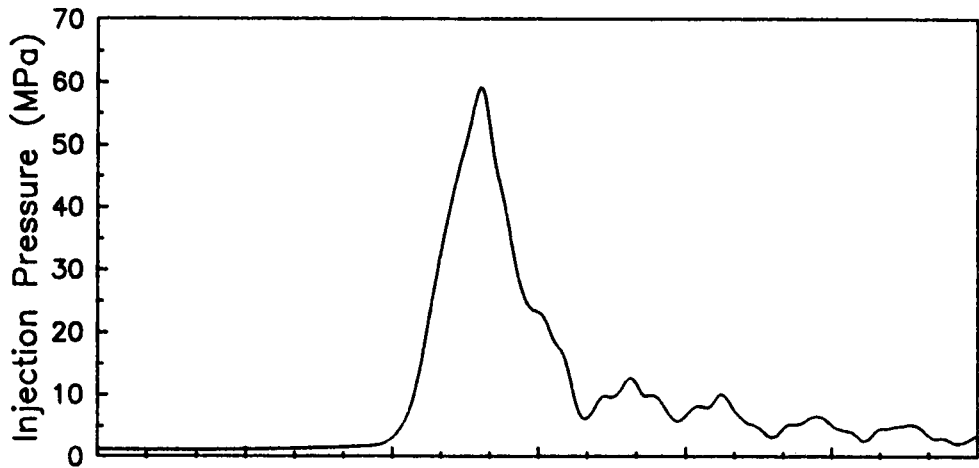
RUN #99, 2000 RPM, 100 % LOAD



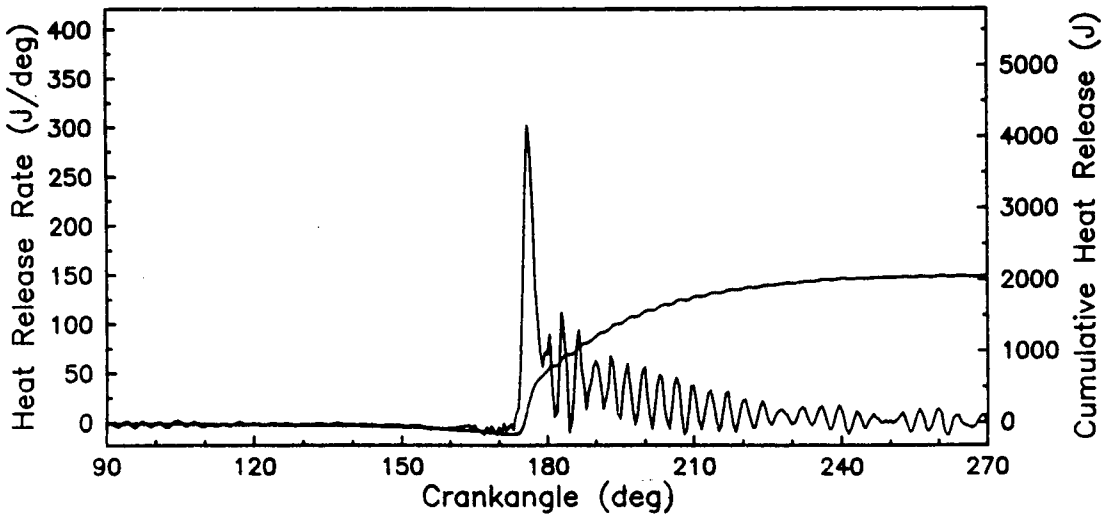
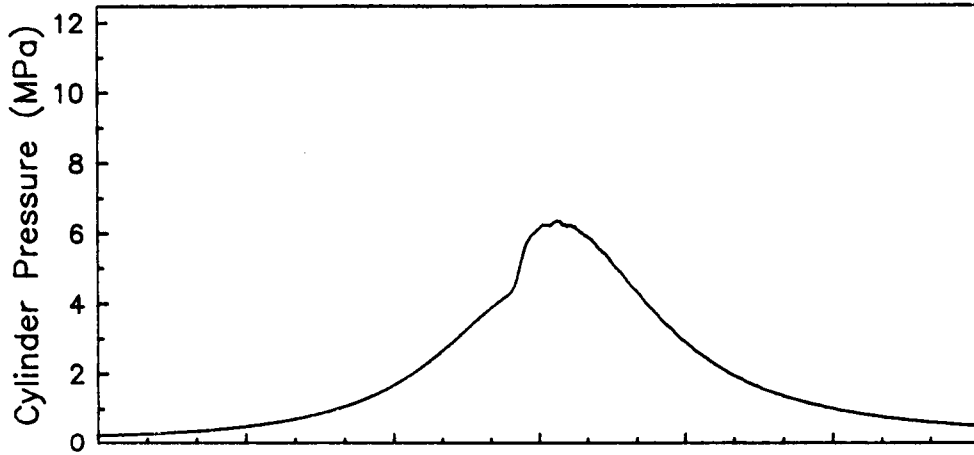
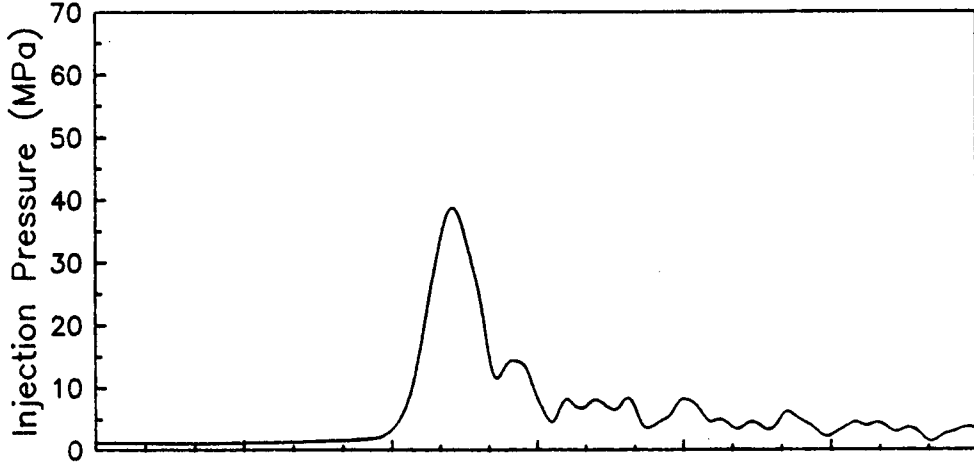
RUN #100, 2000 RPM, 100 % LOAD



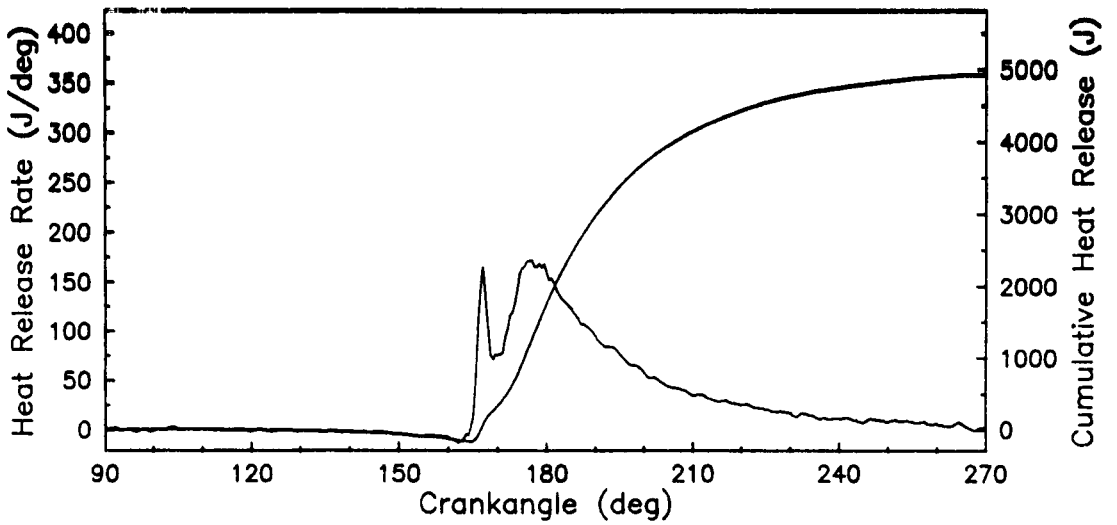
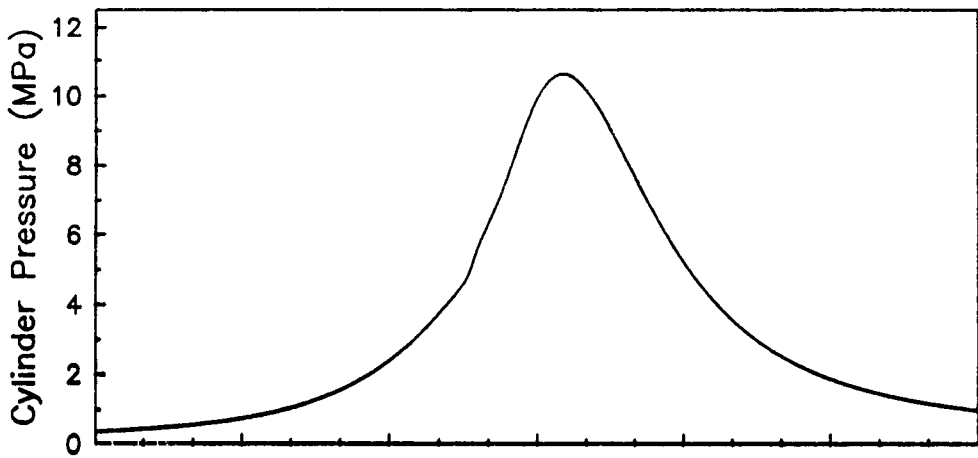
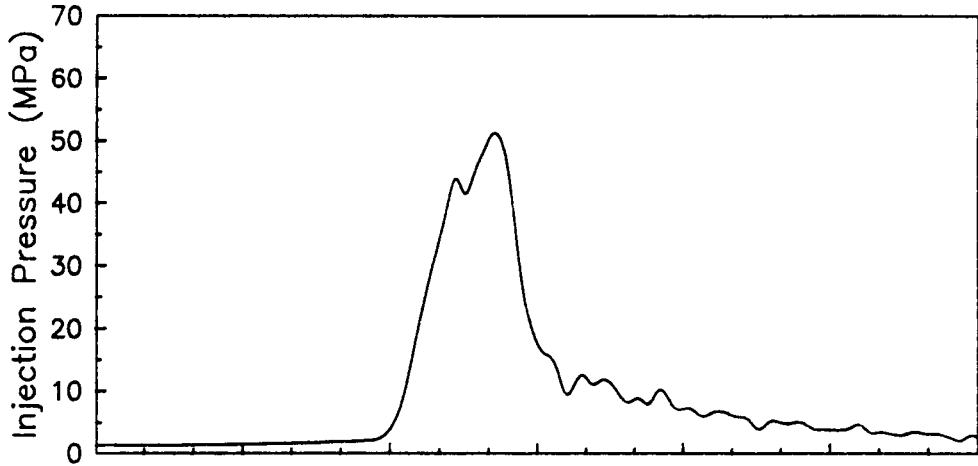
RUN #101, 2000 RPM, 67 % LOAD



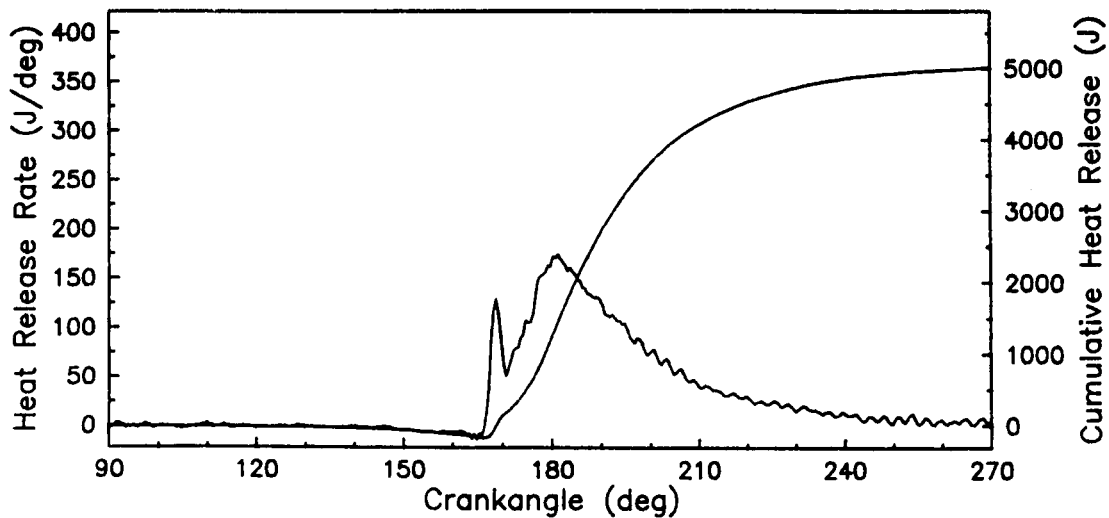
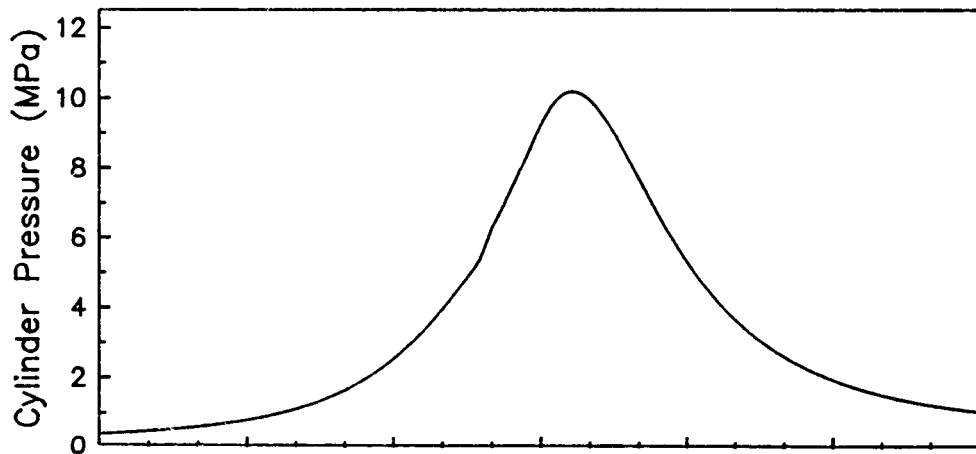
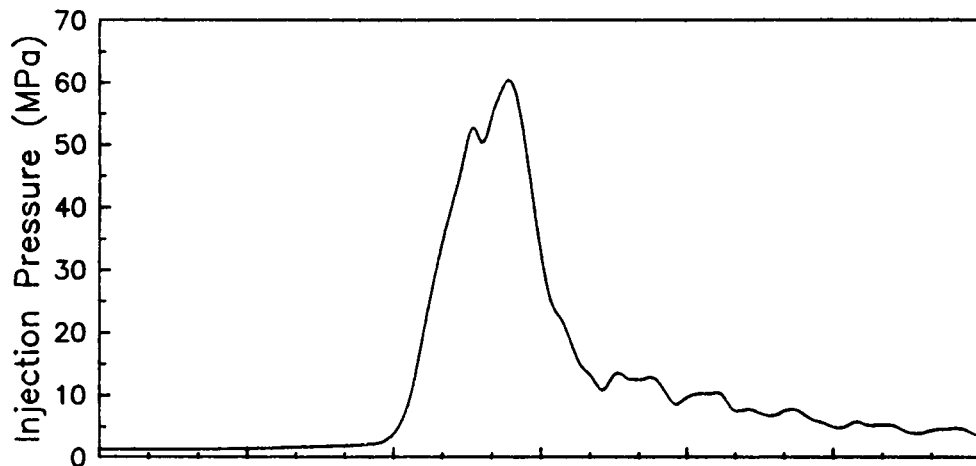
RUN #102, 2000 RPM, 33 % LOAD



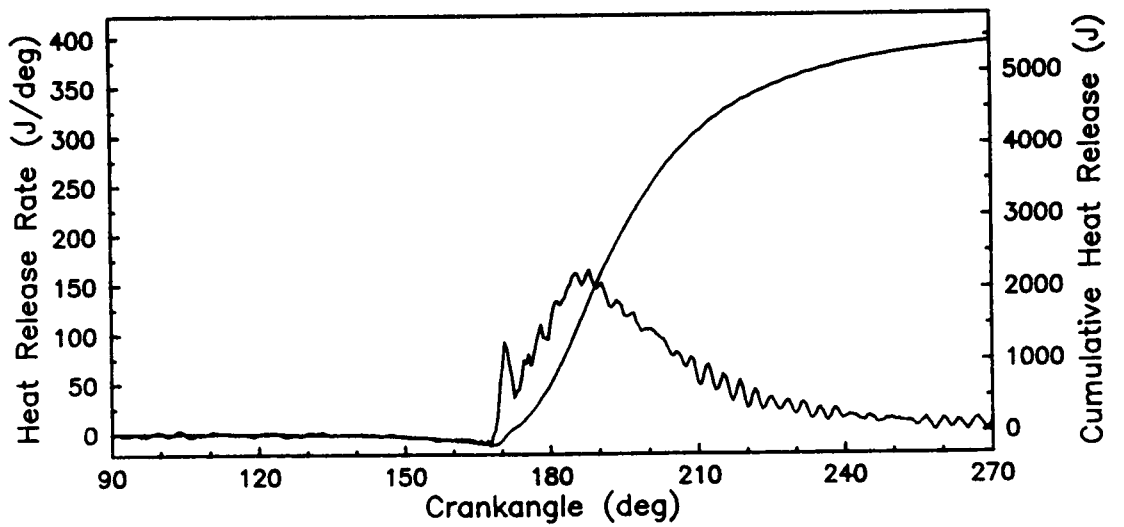
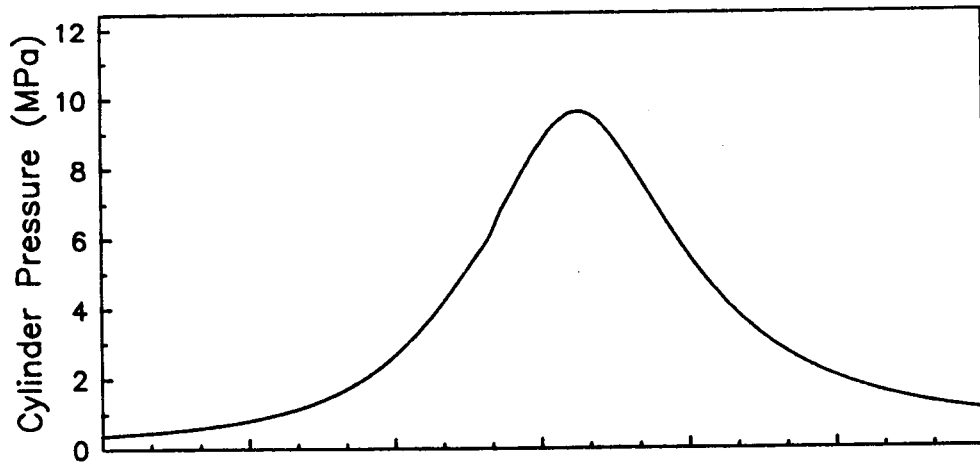
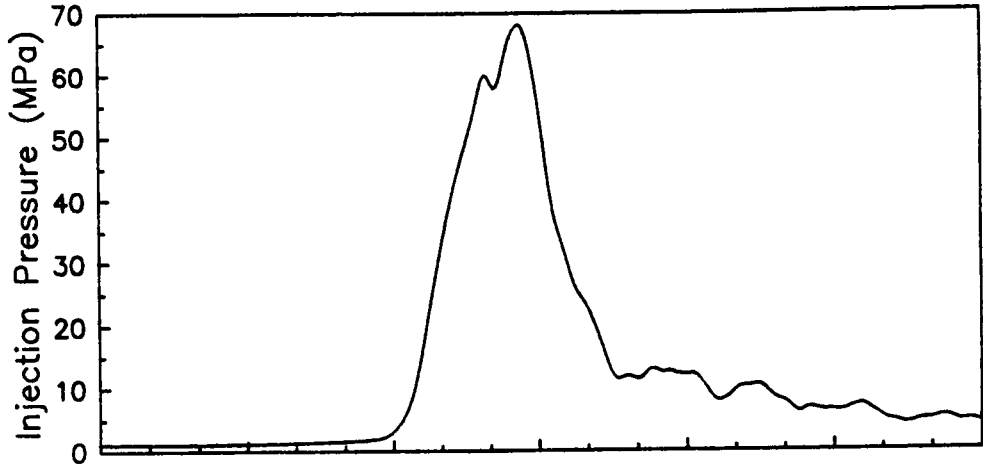
RUN #103, 1400 RPM, 100 % LOAD



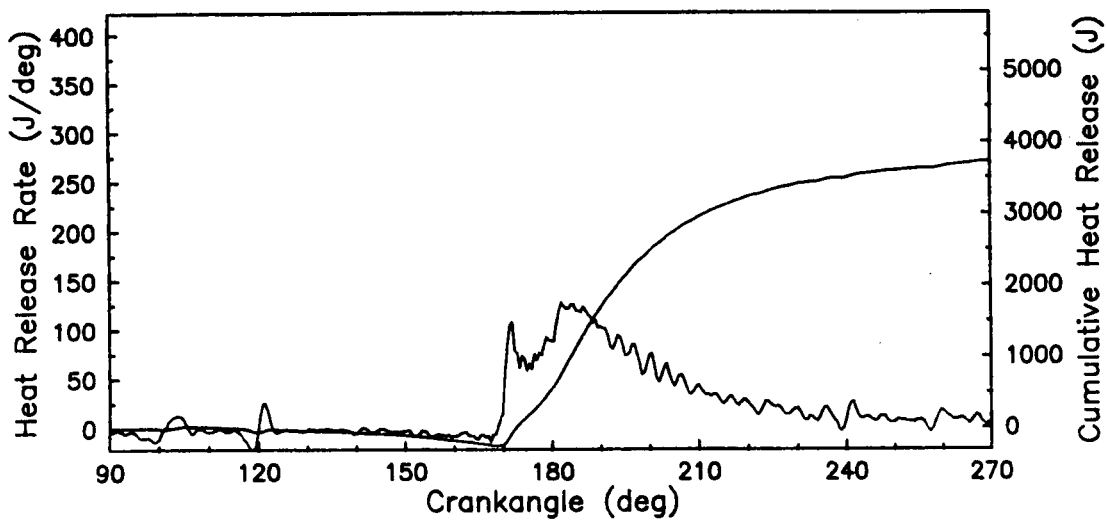
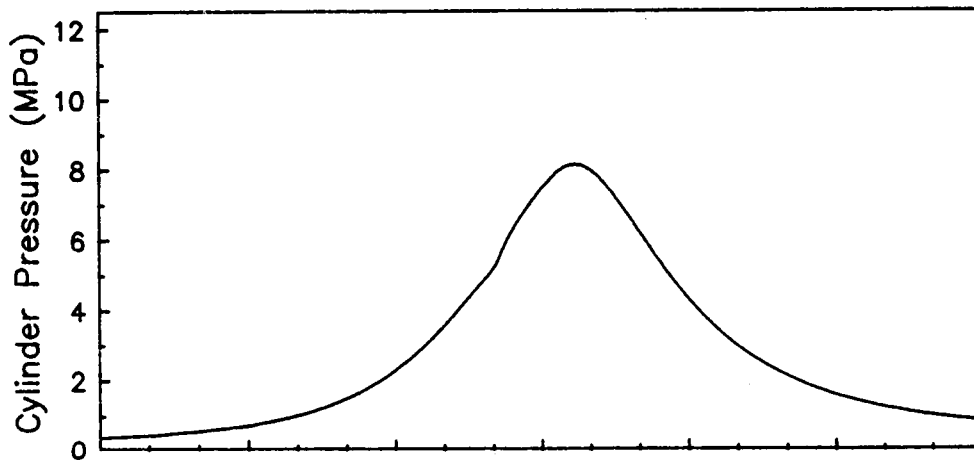
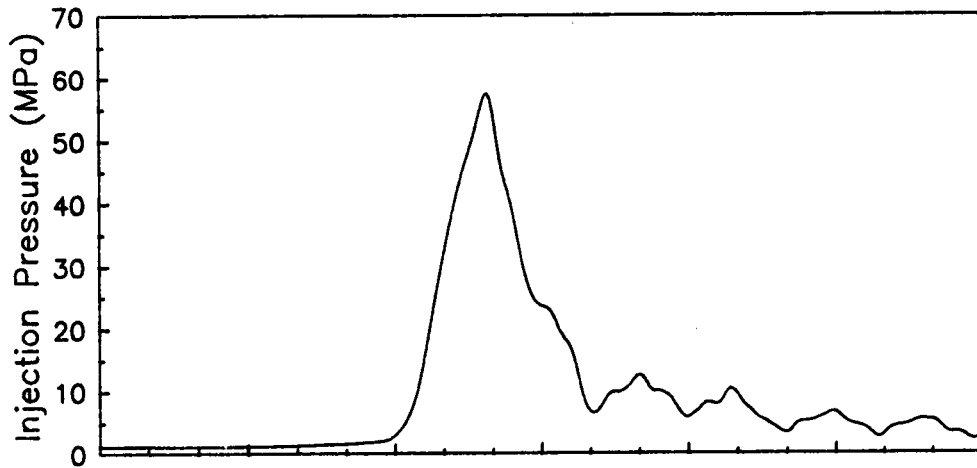
RUN #104, 1700 RPM, 100 % LOAD



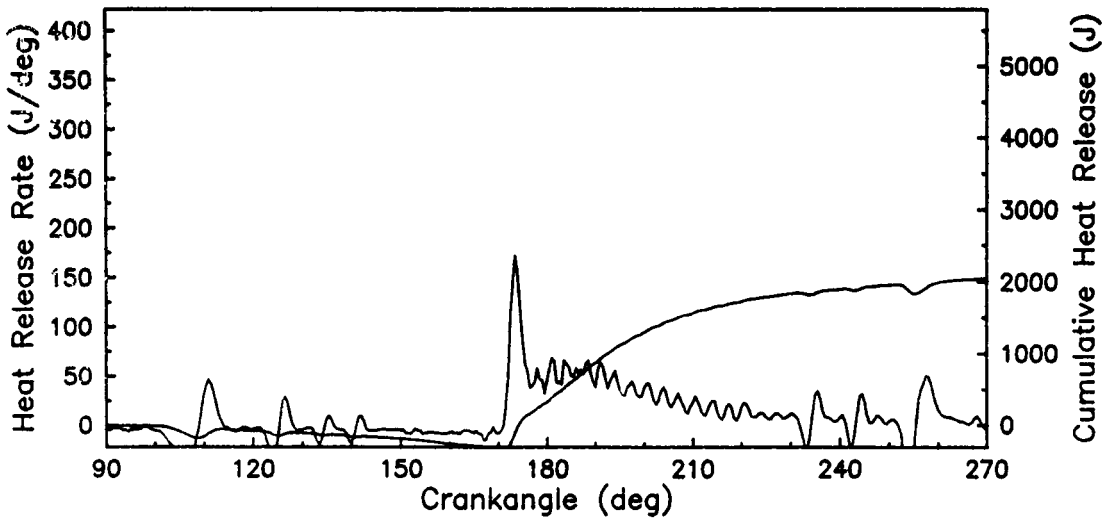
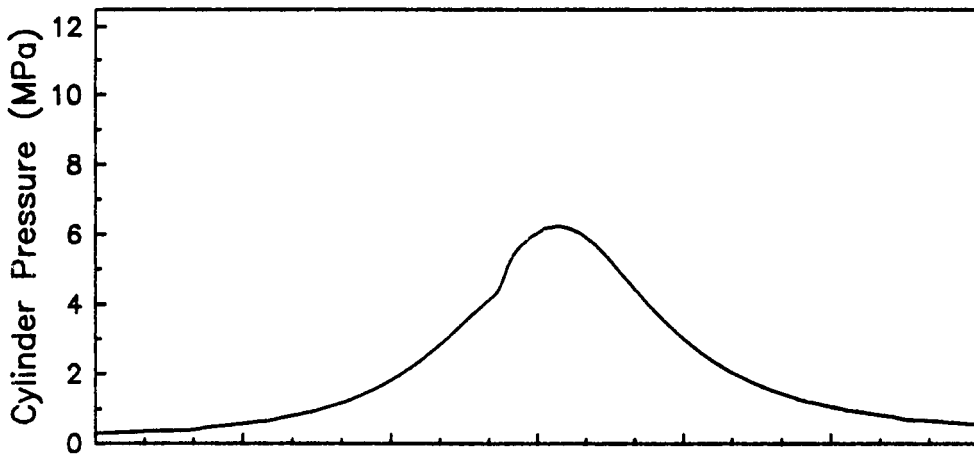
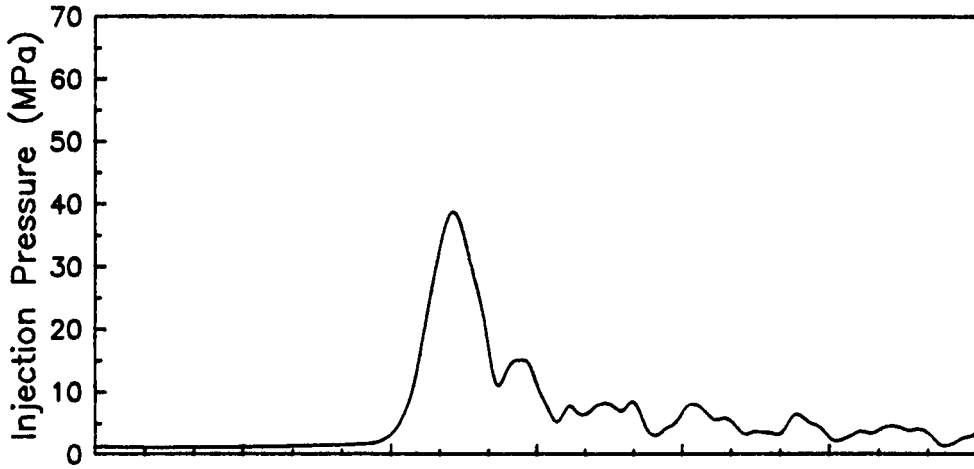
RUN #110, 2000 RPM, 100 % LOAD



RUN #111, 2000 RPM, 67 % LOAD



RUN #112, 2000 RPM, 33 % LOAD





Report Documentation Page

1. Report No. NASA CR-182204 DOE/NASA/0330-3		2. Government Accession No.		3. Recipient's Catalog No.	
4. Title and Subtitle The Effect of Insulated Combustion Chamber Surfaces on Direct-Injected Diesel Engine Performance, Emissions, and Combustion				5. Report Date September 1988	
				6. Performing Organization Code	
7. Author(s) Daniel W. Dickey, Shannon Vinyard, and Rifat Keribar				8. Performing Organization Report No. SwRI-8966	
				10. Work Unit No. 778-34-22	
9. Performing Organization Name and Address Southwest Research Institute 6220 Culebra Rd. San Antonio, Texas, 78284				11. Contract or Grant No. DEN3-330	
				13. Type of Report and Period Covered Contractor Report Final	
12. Sponsoring Agency Name and Address U.S. Department of Energy Office of Vehicle and Engine R&D Washington, D.C. 20545				14. Sponsoring Agency Code	
15. Supplementary Notes Prepared under Interagency Agreement DE-AI01-86CE50162. Project Manager, R.F. Barrows, Propulsion Systems Division, NASA Lewis Research Center, Cleveland, Ohio 44135.					
16. Abstract The combustion chamber of a single-cylinder, direct-injected diesel engine was insulated with ceramic coatings to determine the effect of low heat rejection (LHR) operation on engine performance, emissions, and combustion. In comparison to the baseline cooled engine, the LHR engine had lower thermal efficiency, with higher smoke, particulate, and full load carbon monoxide, emissions. The unburned hydrocarbon emissions were reduced across the load range. The nitrous oxide emissions increased at some part-load conditions and were reduced slightly at full loads. The poor LHR engine performance was attributed to degraded combustion characterized by less premixed burning, lower heat release rates, and longer combustion duration compared to the baseline cooled engine.					
17. Key Words (Suggested by Author(s)) Engine; Diesel; Insulated; Ceramic; Coating; Performance; Emissions; Combustion				18. Distribution Statement Unclassified—Unlimited Subject Category 85 DOE Category UC-96	
19. Security Classif. (of this report) Unclassified		20. Security Classif. (of this page) Unclassified		21. No of pages 178	22. Price* A09